Proceedings of the Second Airborne Imaging Spectrometer Data Analysis Workshop

May 6, 7, 8, 1986

Gregg Vane
Alexander F.H. Goetz
Editors

August 15, 1986

NASA

Proceedings of the Second Airborne Imaging Spectrometer Data Analysis Workshop

May 6, 7, 8, 1986

Gregg Vane
Alexander F.H. Goetz
Editors

August 15, 1986

NASA

CONTENTS

BOTANICAL AND GEOBOTANICAL RESEARCH

ABSTRACT

The Second Airborne Imaging Spectrometer (AIS) Data Analysis Workshop was held at the Jet Propulsion Laboratory on May 6, 7, and 8, 1986. It was attended by 100 people from seven countries. Papers were presented by 24 attendees; summaries of 19 of the papers are published in these Workshop Proceedings. The Second Workshop was divided into three sessions: Calibration, the Atmosphere, and Data Techniques; Geological Research; and Botanical and Geobotanical Research. Because many of the AIS researchers have had an additional year to work with their data, a general advance was seen in the utilization of the data for solving earth science problems. The major conclusions that can be drawn from the Workshop are: (1) Amost everyone now working with AIS data is attempting to take into account in data analysis the effects of the atmosphere and sensor calibration and performance. As a result, information extraction techniques are becoming more sophisticated and effective. (2) The emphasis on work in the geological disciplines is beginning to shift to the application of AIS data for solving geological problems, now that the efficacy of the data for mineral identification has been demonstrated. (3) In the botanical sciences, interpretation of AIS data is becoming more quantitative. Several statistical techniques are under development for extracting the subtle differences in plant spectra in the region of the near infrared and short wavelength infrared. In summary, an overall advance was seen in the ability to effectively utilize the fundamentally new class of data acquired with imaging spectrometers. There was also a general feeling at the Workshop however, that much work remains to be done in remote sensing research before the maximum potential of these data for solving earth science problems is realized.

FOREWORD

In the text and figure captions of several papers in the Proceedings, reference is made to color slides in a pocket at the end of the Proceedings. These 35 millimeter slides are color versions of the referenced black and white figures within the Proceedings. A limited number of copies was printed with the color slides included.

INTRODUCTION TO THE PROCEEDINGS OF THE SECOND AIRBORNE IMAGING SPECTROMETER (AIS) DATA ANALYSIS WORKSHOP

GREGG VANE, Jet Propulsion Laboratory, California Institute of Technology, Pasadena, California

ABSTRACT

An overview of the Second AIS Data Analysis Workshop is presented and each of the 19 papers from the Workshop published in the Proceedings is briefly summarized. AIS program activities during the past year are summarized, and a description of the new AIS-2 is given. Finally, a discussion of AIS data quality is presented which includes the effects of vertical striping, horizontal striping and second order overlap.

WORKSHOP OVERVIEW AND SUMMARY OF CONTRIBUTED PAPERS

The Second AIS Data Analysis Workshop, which was held at JPL on May 6, 7, and 8, 1986, was attended by one hundred scientists from six countries in addition to the United States. Twenty-four papers were presented of which nineteen are represented in these Proceedings. Much of the work presented at the second workshop was in a preliminary state last year at the first workshop; a significant advance was seen in the maturity of research in high spectral resolution remote sensing at this workshop. Research in three broad areas was presented at JPL this year: in calibration, the atmosphere, data problems and techniques, in geological research, and in botanical and geobotanical research. From the papers in these Proceedings and those presented at the workshop, it is clear that most AIS researchers are taking an active interest in calibration and in understanding sensor performance. Several papers deal with these issues in considerable detail, and as a result, the value and limitations of AIS data are becoming better understood. It is also clear that the geological community is making good progress in moving from material identification to the application of mineral identification to geological problems. The vegetation community is also making progress in utilizing high spectral resolution data. At the first AIS Data Analysis Workshop, emphasis was on visually inspecting spectral reflectance curves for their information content; at the second workshop several researchers reported on more quantitative techniques being developed to gain access to the information. Following is a more detailed summary of the material that is presented in these Proceedings in the three broad areas above.

Calibration, The Atmosphere, Data Problems and Techniques

The Airborne Imaging Spectrometer is an experimental test bed not only for infrared area array detectors, but in essence for all aspects of high spectral resolution remote sensing, from sensor design and operation through all phases of data handling and information extraction. One of the major objectives of the Imaging Spectrometer Program at JPL in operating AIS as extensively as it has been operated has been to enlist the science community in helping to assess the quality of AIS data, as well as to help in devising the best techniques for extracting the maximum information from the data. There is much work to be done in these areas requiring more than the capabilities of any one single organization. The work reported on in the Calibration, Atmosphere, Data Problems and Techniques Session of the Workshop represents a valuable and significant first step in what will undoubtedly be an on-going process for several years to come.

The session began with a paper by Tucker and Vane describing the optical alignment of the AIS detector array and the radiometric calibration of the instrument, which at present is a spectral relative rather than absolute calibration. In the area of data preprocessing, Roberts et al. have explored four techniques for compensating for the effects of decreasing solar irradiance at longer wavelengths and for the effects of atmospheric absorptions. These are the log residual, the least upper bound residual, the flat field correction, and calibration using field reflectance measurements. The field reflectance calibration was superior overall, while the log residual technique was useful for scenes not containing a dominant cover type. The least upper bound residual technique was found to be effective in heavily vegetated areas.

Conel et al. have been working to develop a method of atmospheric correction for major absorbers using the AIS data themselves. In their paper the radiometric calibration of AIS is discussed as well as the impact of the second order radiation contamination beyond the 1.5 micron region. Cocks and Green also discuss the order overlap problem, as well as the effects of horizontal striping in the data. Examples of each effect are presented. A technique for removing the effects of horizontal striping is described by Huntington et al., who also suggest one approach to minimizing the effects of second order overlap on data interpretation. Kruse and Clark present results of their work with atmospheric water absorption features centered at 2.17 and 2.20 microns which under some circumstances can lead to erroneous conclusions about surface mineralogy. Examples of the effect of superimposing the atmospheric spectrum on mineral spectra are shown. Finally, Hlavka discusses a notch filter applied to the Fourier transform of AIS imagery to remove the noise caused by vertical and horizontal striping in the AIS data.

Geological Research

The geology section of the Proceedings begins with a paper by Mustard and Pieters who have determined the spatial distribution and relative abundance of

clays, gypsum and serpentine associated with the channels and dispersed components of kimberlite and blocks of country rocks at the Moses Rock Diatreme, Utah. Data calibration and information extraction techniques are discussed also. Lyon reports that while 1985 AIS data over the Yerington, Nevada test site appear to be noiser than a 1984 data set, O-H absorption bands for sericite and/or kaolinite can be identified at the correct wavelength. Wavelength calibration techniques using two water and two carbon dioxide absorption features were used. Feldman and Taranik have extended work from the previous year by acquiring field and lab spectra and performing x-ray diffraction analysis on field samples from the Hot Creek Range, Nevada. Using these, the AIS data and Spectral Analysis Manager (SPAM), the efficacy of a spectral matching algorithm was tested for separating kaolinite, montmorillonite and illite. The approach is shown to be more effective with AIS data than using the location of absorption minima alone.

Hutsinpiller and Taranik have identified areas of strong clay alteration at Virginia City, Nevada, that can be mapped with AIS data as being zones of kaolinitic, illitic and sericitic alteration. The effects of mineral mixing within a pixel and the spectral contribution of vegetation are also addressed. Huntington et al. present preliminary results of their work in mineral absorption spectra extraction from AIS data over the Mary Kathleen Uranium Mine in Queensland. Because of the higher concentration of vegetation in the area than is normally found in the southwestern US, the second order overlap problem is more serious in the Australian data. Techniques that attempt to model this effect, used with the log residual analytical technique, are shown to be effective in recovering spectra that exhibit characteristics expected of clays, carbonates, amphibole and epidote. Kruse et al. present the results of a technique using Munsell color transformations to reduce the dimensionality of AIS data to a single color composite image that successfully allows the limestone and dolomite roof pendants and sericite-illite and other clay minerals to be mapped in the quartz monzonite stock in the Grapevine Mountains of California and Nevada. Field and lab studies verify the mineralogical distributions mapped from the AIS data. Krohn discusses the nature of ammonium-bearing minerals at Ivanhoe Hot Springs, Nevada, and shows preliminary results from AIS data collected over the area. The AIS flight line missed the intended target by 500 meters and vegetation in the scene presents a problem for information extraction; hence spectra characteristic of ammonium minerals such as Buddingtonite have not yet been observed in the AIS Ivanhoe data.

Botanical and Geobotanical Research

Spanner and Peterson report spectral variations in the 1.4 to 1.8 micron region that are thought to relate to biological diferences between several forest stands near Fairbanks, Alaska, overflown with AIS. The data were filtered with the technique discussed by Hlavka and flat field corrected using portions of the AIS flight lines that crossed an airport runway and a road. Green and Arvidson discuss work done with Thematic Mapper (TM) and AIS data from the deciduous

oak-hickory forests in southern Missouri. High reflectance in TM band 4 over xeric forests as compared to mesic forests was confirmed with AIS data in the same approximate spectral region. Their preliminary analysis of AIS data, however, does not indicate the presence of more information in that spectral region than found in TM band 4. Milton et al. have taken a preliminary look at AIS data over Pilot Mountain, North Carolina, and found spectral variations in the region between the 1.4 and 1.9 micron water bands related to vegetation cover types. Work is under way to improve data calibration and normalization, to allow a better study to be made of these spectral variations.

Wood and Beck find a consistent relationship between AIS spectral response and plant tissue chemistry in a freshwater wetland in central California. An increase in trace element concentration in the plant tissue was found to correspond with an increase in spectral reflectance in the 1.5 to 1.7 micron region. Ustin et al. report from their work with AIS data in the Owens Valley, California, that shadows cast by vegetation canopies have a major impact on broad spectral reflectance under conditions of low canopy cover, especially for xeric shrub communities. Mesic communities with high vegetation density exhibit greater variations in spectral signature in the near and short wavelength infrared than do sparse xeric communities of shrubs. Murray et al. conclude from a preliminary Principal Factor Analysis (PFA) of AIS data from an area with two sagebrush species and montmorillonitic and volcanic soils that much information is available for material discrimination. As many as six factors in the PFA were identified as significant in contributing to the spectral structure observed in the 1.5 to 1.8 micron region.

AIS PROGRAM ACTIVITIES IN 1985 AND 1986

There has been a wide range of activities on the AIS program this past year at JPL. In addition to data collection, preprocessing and dissemination, there has been on-going work to improve the spectral relative calibration of the instrument, efforts have been increased to assess data quality, and an improved version of AIS was designed and built which incorporates a new 64 by 64 element detector area array and also incorporates several other improvements that will enhance data quality. The issue of data quality will be addressed later in the Introduction to the Proceedings; AIS calibration is covered in the paper by Tucker and Vane following the Introduction.

AIS Flight Operations

In terms of data collected, the past flight season was the most successful of the three years that AIS has been in operation. Data were collected for every approved investigator, and in almost all cases, along the desired flight lines and under the desired conditions. The success of the season is due primarily to the professionalism of the Ames C-130 operations staff and to generally good weather conditions. Approximately 50 test sites were flown in the US, including sites in Alaska and Hawaii, and another 60 test sites were flown in Australia. In Appendix

3, a complete list is given of all the test sites that have been flown with AIS between December 1982 and April 1986. Figure 1 shows the geographical distribution of the US test sites. In the summer of 1986, a major European deployment with the C-130 will take place. AIS data will be collected over German forests suffering from acid rain damage, over Austrian forests where heavy metal stress has been identified, and over the major volcanos of southern Italy. In the US, flights are planned in the northeastern forests of Vermont and New Hampshire, and in the southwestern states. AIS will be retired from its active role in data collecting at the end of the season.

Several improvements were made in data preprocessing during the past year and new subroutines were added to the SPAM software. Data turnaround times were very slow, however, due to continuing problems with the aging PDP-11 computer used in the AIS decommutation facility at JPL. In January, the transition was begun in shifting the decommutation of the AIS high density tapes to Ames, where a more modern and efficient facility exists to handle remote sensing data collected by the Ames sensors. Transition of this function to Ames was completed in May and the decommutated tapes are now sent routinely to JPL for logging, archival and retrieval processing on the AVIRIS VAX 11-780 computer. The preprocessed data are sent to investigators from JPL as in the past.

Instrument Improvements

The original AIS, which operated with a prototype 32 by 32 element mercury cadmium telluride (HgCdTe) area detector array, was completely rebuilt during the past winter to incorporate a prototype 64 by 64 element HgCdTe array, which is the next step in the development of detectors which will be used for the Shuttle Imaging Spectrometer Experiment (SISEX). Both arrays were made by Rockwell International Science Center as part of an ongoing detector development program at JPL. The new instrument, called AIS-2 to distinguish it from its ancestor, has the capability to image a swath that is 64 rather than 32 pixels wide. One hundred twenty-eight spectral bands are acquired with two steps of the diffraction grating rather than four in AIS-1, which allows 16 lines per second to be acquired rather than 12, while still allowing a greater integration time for improved signal-to-noise performance. AIS-2 incorporates new foreoptics (but the same spectrometer optics) which have a wider field of view to take advantage of the 64 pixel swath width capability. The modulation transfer function (MTF) of the foreoptics had be relaxed somewhat in order to the fit the new foreoptics into the same instrument housing. Thus while the swath width has been doubled, the effective instantaneous field of view (IFOV) has been degraded. See Table 1 for a comparison of AIS-1 and AIS-2.

The two most significant improvements to instrument performance relate to the new signal chain electronics and to the inclusion of switchable order blocking filters. The new electronics include additional shielding from the rest of the instrument (the digital and analog electronics are connected now by opto-isolators, for example), so electronic signal chain noise is much lower. The instrument is
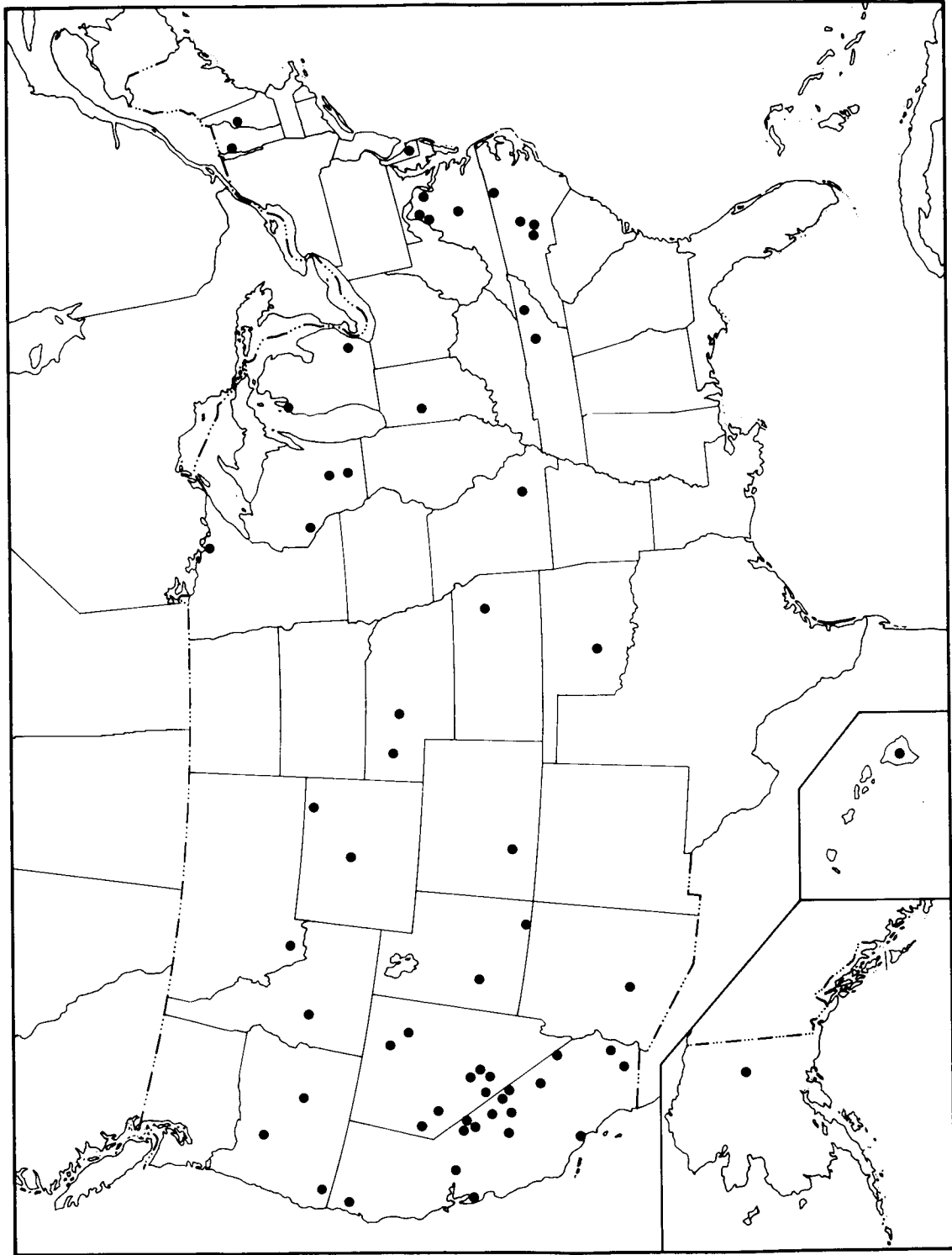
FIGURE 1. Geographical locations of AIS test sites covered from December 1982 through April 1986.

also more effectively isolated electrically from the aircraft, which has always been a major source of noise in the flight data. The other signal chain improvement allows the full 12 bits of digitized data to be recorded on the high density tape, rather than a selectable 8 bits with AIS-1. The switchable blocking filters were installed to avoid the problem of second order overlap at wavelengths beyond 1.6 microns. This problem with AIS-1 is discussed further in the following section of the Introduction. The transmission curves for the two blocking filters are shown in Figure 2. The choice of filter is programmed into the microcomputer which controls AIS-2 so that when the instrument operator specifies the operating mode ("tree" or "rock"), a stepper motor automatically moves the correct filter into position at the entrance to the foreoptics.

Table 1. Comparison of AIS-1 and AIS-2 Performance Parameters

Parameter	AIS-1	AIS-2
IFOV (mrad)	1.91	2.05
Ground IFOV (m, at 6 km altitude)	11.4	12.3
FOV (degrees)	3.7	7.3
Swath Width (m, at 6 km altitude)	365	787
Spectral Sampling Interval (nm)	9.3	10.6
Data Rate (kbps)	394	1,670
Spectral Sampling:		
"Tree" Mode (microns)	0.9-2.1[a]	0.8-1.6[b]
"Rock" Mode (microns)	1.2-2.4[a]	1.2-2.4[c]

[a] Region beyond 1.6 microns contaminated with second order radiation. See text.
[b] An additional approximately 40 spectral bands are taken beyond 1.6 microns, but they contain second order radiation.
[c] An additional approximately 10 spectral bands are taken beyond 2.4 microns, but they contain second order radiation.

AIS DATA QUALITY

Although some impressive results have been achieved with AIS, the quality of the data has not been as high as an instrument of this type is potentially capable of producing. Calculations show that an instrument such as AIS, which is based on infrared area detector array technology, should have a signal-to-noise ratio (SNR) in excess of 100:1 in the 2.2 micron region for a scene albedo of 0.5. Under these conditions, SNRs have been measured from AIS-1 in the range of 10:1 to 40:1,
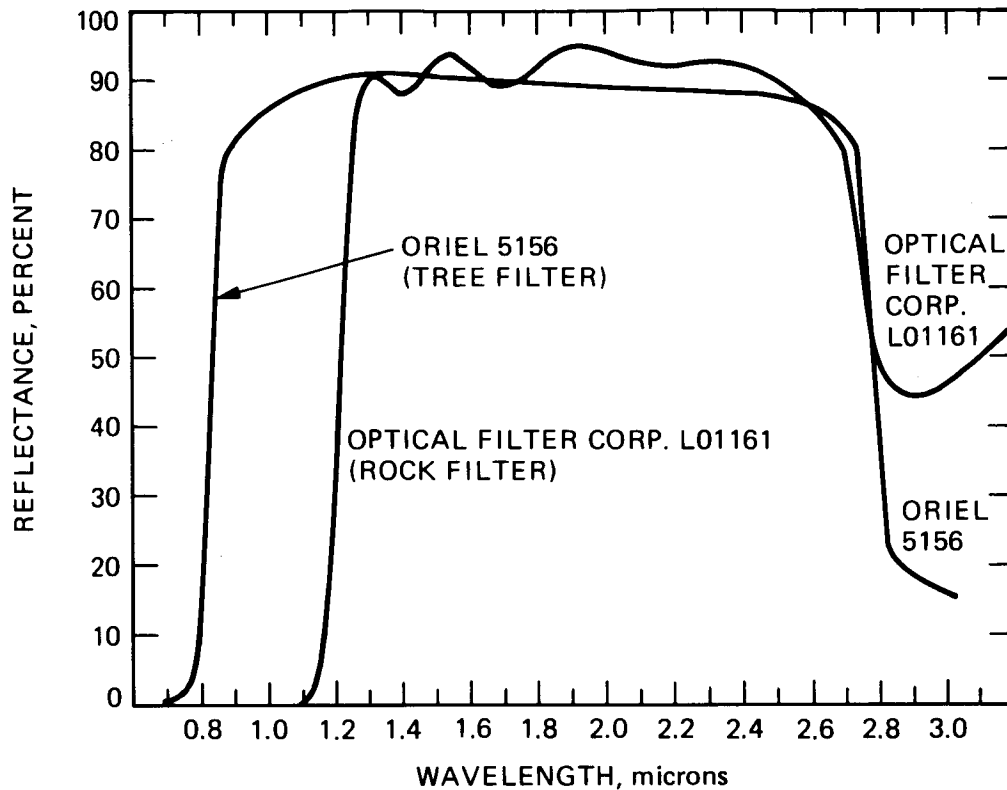
FIGURE 2.   AIS-2 blocking filter transmission curves.

depending on the data set. It is thought that most of the discrepancy between observed and predicted SNR performance in AIS-1 was due to signal chain noise and to instrument/aircraft ground loops. Both of these problems were addressed in the design of AIS-2. Another class of noise is related to the detector itself. If, for example, the response of the detector changes between calibrations, data will appear noisy (in the case of AIS, it will be vertically stripped) because the detector response equalization was not adequte during the radiometric correction operation. In addition to electronic and detector noise, there are sources of noise that are related to the mechanical and optical qualities of the sensor. The effects of these sources of noise are not seen in the typical signal-to-noise ratio, but they do affect data quality nevertheless by degrading the purity of the signal in a given pixel. AIS-1 suffered from two such noise sources which will be discussed below: "horizontal striping," which degrades the spectral resolution of the sensor, and second order overlap, which contaminates the spectral signal by mixing light from two different wavelengths.

Vertical Striping

Shown in Figure 3 are raw AIS data from Cuprite, Nevada, which have not been processed in any way. The data were collected on September 23, 1985, in

8
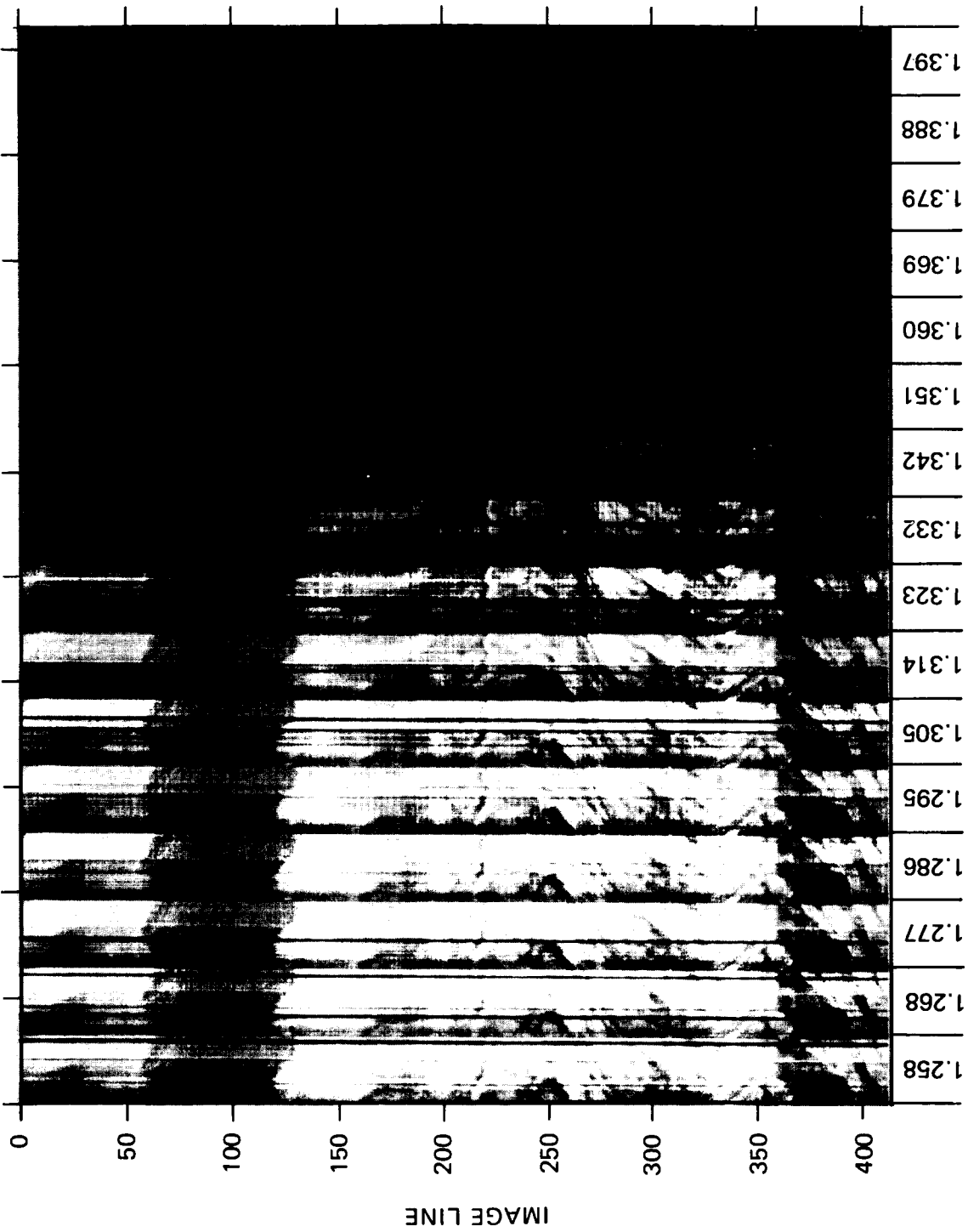
FIGURE 3. 16 channels of raw, uncorrected AIS-1 data over Cuprite, Nevada, September 23, 1985.

rock scan mode; shown are 16 of the 128 spectral images, starting at 1.258 microns and ending at 1.397 microns, inside the 1.4 micron water absorption band. The top 60 lines of the figure (south on the ground) are alluvium with medium albedo, followed by another 60 lines of alluvium of lower albedo. Kaolinite Hill begins at about line 120; its center is the bright spot at about line 145. Below line 200, the effects of aircraft roll are obvious as the C-130 drifted off the flight line. A number of other features stand out in this raw image: the transition into the 1.4 micron water band beginning at about 1.323 microns and the associated scene attenuation, the pronounced vertical striping in the individual images, some of which are bright but most of which are dark, and the horizontal striping that is most obvious in the transition zone going into the water band. Horizontal striping will be discussed later. The vertical striping is due to nonuniformity in the response of the individual detector elements in the 32 by 32 element area array. In the extreme case, the black vertical lines are due to detector elements that are dead, i.e., which do not respond to light at all. The bright stripes are due to detector elements that are more responsive than their neighbors.

The purpose of radiometric correction during AIS data preprocessing is to remove the effects of detector response nonuniformity by multiplying the response of each individual detector element by a wavelength-dependent quantity determined during instrument calibration (see Tucker and Vane), which in effect is a normalizing factor. In the case of the black stripes which are due to dead detector elements, the gap in spectral coverage at that position on the detector array is interpolated across by averaging the radiometrically corrected values of the detector outputs on either side of the dead detector element. This is done in the spectral dimension of the detector array. The results of the radiometric correction to Figure 3 are shown in Figure 4. The first five or so images appear to be clean, the next few show both dark and light vertical striping (as well as horizontal striping). The residual vertical striping is thought to be due to a change in instrument performance after the calibration file was constructed in the lab, before installation in the airplane. The most likely cause is time-varying detector response, although it is possible that the noisy electronic environment of the C-130 could be having an effect, too.

To remove the remaining vertical striping, there are several options. One can normalize to a portion of the scene with known reflectance which is spatially uniform across the AIS image. Such an area occurs in the Cuprite data between lines 65 and 115. Another approach is to do a log residual correction to the data (see Roberts et al., these Proceedings). Both these techniques have been used at JPL, as well as the others discussed by Roberts et al., but since many AIS test sites do not contain a spatially uniform area of known spectral reflectance, a log residual correction was applied to these Cuprite data to illustrate the efficacy of this correction technique. The result is shown in Figure 5, which has been stretched differently than the preceding two figures to make the residual noise more obvious. In fact, the vertical noise is gone in Figure 5, leaving only the horizontal striping which will now be discussed.
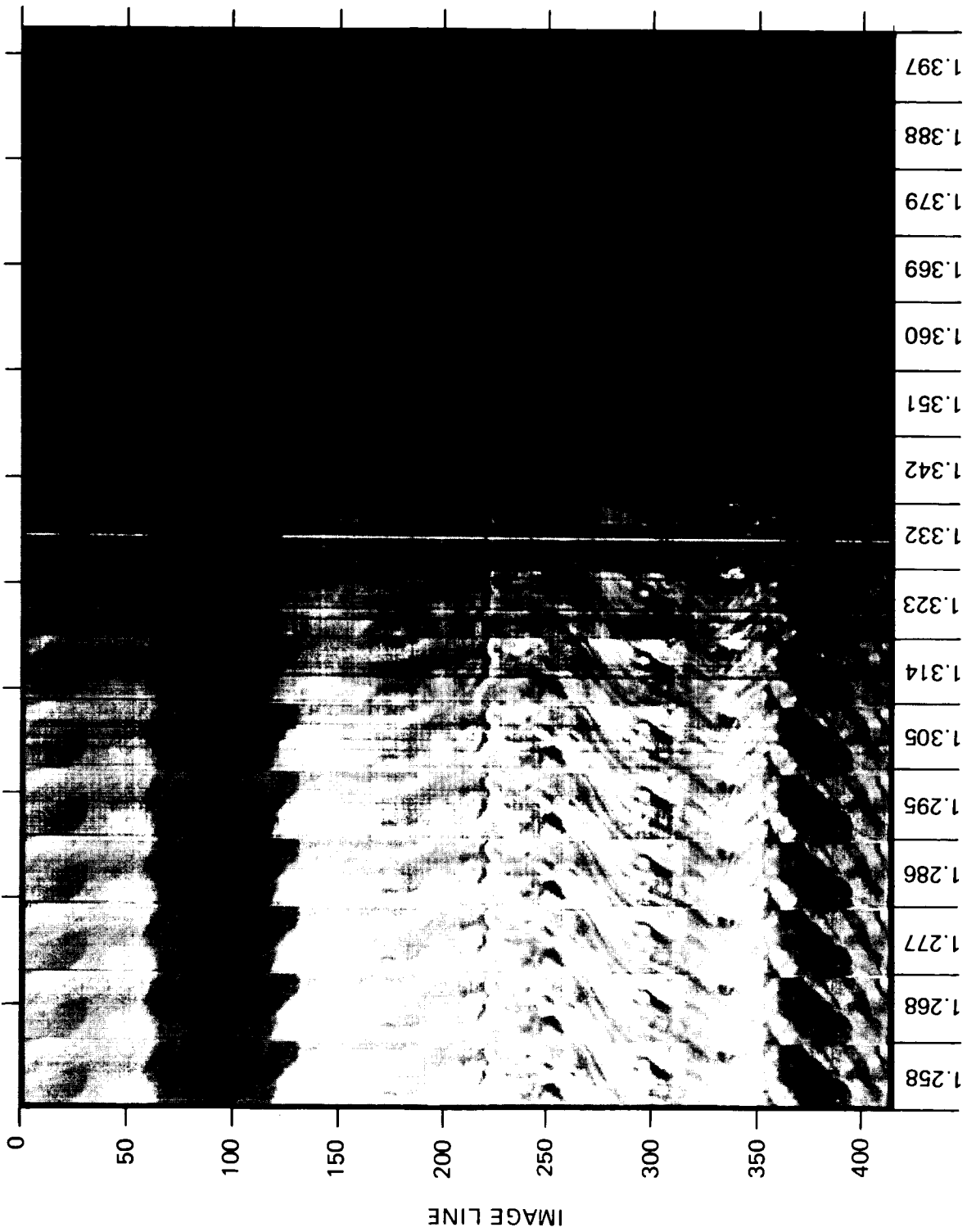
FIGURE 4.   Radiometrically corrected AIS-1 Cuprite data.
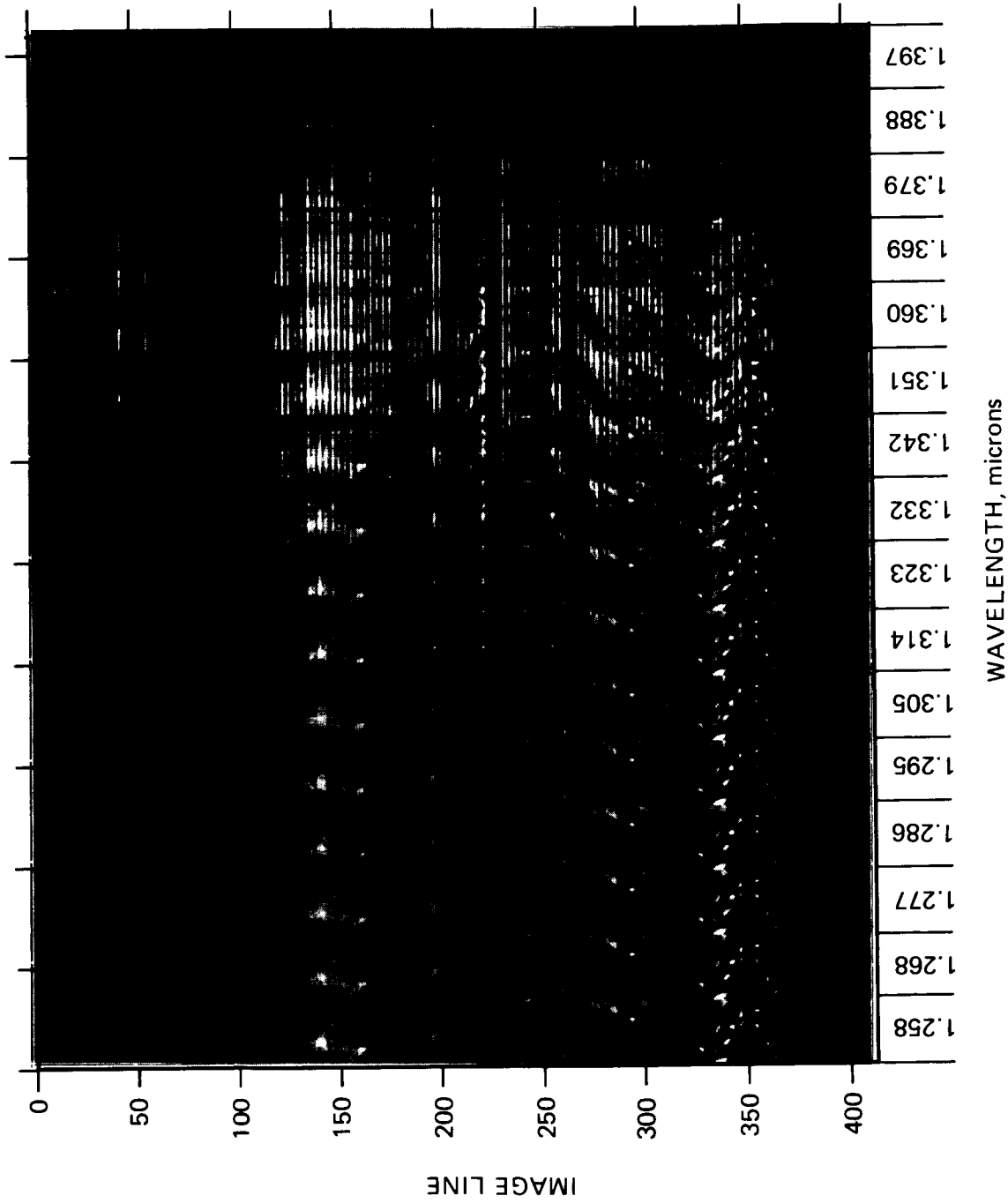
FIGURE 5. AIS-1 Cuprite data with log residual correction.

12

Horizontal Striping

If one looks at the horizontal striping that occurs in various spectral bands throughout the 128 bands collected by AIS, the distribution at first appears to be random. On closer inspection, it appears to be most frequently associated with the edges of the 1.4 and 1.9 micron water absorption bands. This observation led Cocks and Green (these Proceedings) to speculate that the horizontal striping was due to wobble in the grating drive which steps the diffraction grating through its various positions, resulting in successive scan lines being sampled at longer or shorter wavelengths than they should be. If this were the case, the effect would be most pronounced at the edges of the water bands where reflectance is most rapidly changing, which is what is observed.

Two additional pieces of information from AIS-2 have become available since Cocks and Green advanced their theory, however. During the checkout flight of AIS-2 it was noted by the instrument operator that (1) the small amount of vignetting introduced by the new foreoptics (which results in a 50 percent attenuation of the first and last cross-track pixels) shifted position at about the same rate as the horizontal striping occurred, i.e., every few scan lines, and (2) the position sensor on the grating drive indicated that the grating was returning to the same position throughout the scan line to a precision well in excess of that which would cause horizontal striping. The conclusion: horizontal striping is caused by the detector array vibrating around at the focal plane of the spectrometer. The cause was a poorly designed dewar cold finger on which the detector is mounted. The cold finger is mounted to the liquid nitrogen reservoir in such a way that it was free to resonate at the frequency induced into the instrument by the aircraft. To fix the problem, the detector end of the cold finger was immobilized with a spider mount connected to the dewar nose piece. The subsequent test flight of AIS-2 with this modification showed no horizontal striping.

While the cause of horizontal striping has been removed from AIS-2, the effects remain in AIS-1 data. Cocks and Green give an excellent description of the spectral manifestations of horizontal striping and Huntington et al. describe a technique they have developed to remove the spectral effects without degrading the data. However, there is still a spatial effect since the detector array in AIS-1 was moving in the spatial dimension as well as in the spectral. This results in a degrade instrument IFOV, which is no longer diffraction limited. It will probably turn out after further analysis that the effective IFOVs of AIS-1 and AIS-2 are similar, for while it was not possible to build diffraction limited foreoptics to fit into the available instrument volume of the old AIS-1 housing, AIS-2 has a very rigid detector array mount and hence no horizontal striping occurs in the data.

Contamination from Spectral Order Overlap

The final effect to be discussed here which has a negative impact on the quality of AIS-1 data is that of contamination from second order light falling on the detector. The effect is shown conceptually in Figure 6. Unlike prisms, gratings disperse light
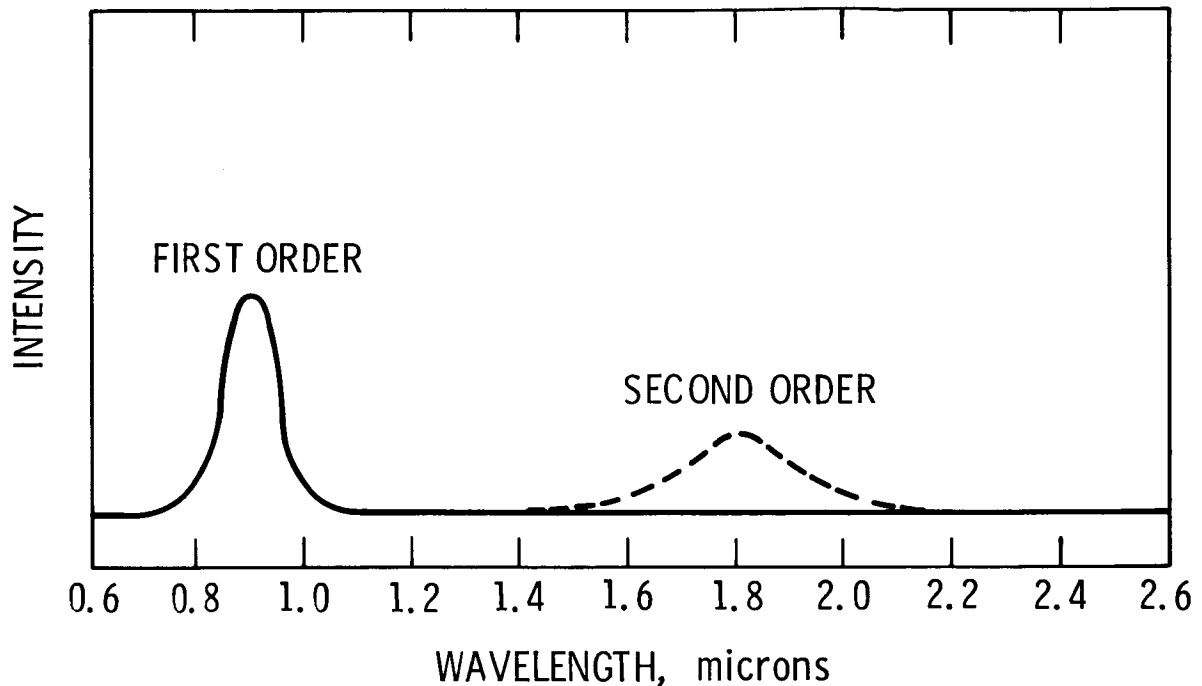
FIGURE 6. The effect of second order overlap in a grating spectrometer.

in many orders. First order light which appears at one wavelength appears again in second order at twice the wavelength, in third order at three times the wavelength, and so on. In the figure a situation is shown in which light at a wavelength of 0.9 microns passes through the spectrometer. Its second order appears at the position where first order radiation of wavelength 1.8 microns falls, at an intensity which depends on the grating efficiency in second order. Thus, if the spectrometer is allowed to pass light of wavelength 0.9 microns, then the signal at 1.8 microns will be the sum of the second order light at 0.9 microns plus whatever first order light at 1.8 microns is passing through the spectrometer. The only way to have light that is purely 1.8 microns in wavelength falling at that position in a grating spectrometer is to place a blocking filter in front of the spectrometer which rejects all radiation short of 0.9 microns.

In an early version of AIS, a blocking filter was used which rejected all radiation short of 1.2 microns in order to keep the spectral region from 1.2 to 2.4 microns uncontaminated by light of second or higher orders. In an attempt to accommodate the needs of the botanists for access to the near infrared plateau starting at 0.8 microns, the original blocking filter was replaced with one that only rejected light short of 0.8 microns. This was done in late 1983, and was done with the knowledge that some contamination would occur at 1.6 microns and beyond. A calculation was made of the magnitude of the contamination by extrapolating from 4 points on the grating efficiency curve in first order (which was the only information available on the grating) to estimate the efficiency of the grating in second order. The calculation indicated that only a few percent (10 percent or less) of contamination would occur, which seemed an acceptable level. An experiment

was done with a monochromator to measure the amount of contamination and the result appeared to confirm the calculation. Unfortunately, the calculation was incorrect, as was the measured value. The monochromator used in the experiment had been damaged, and this was not discovered until a year later. Now that the actual grating efficiency in second order has been measured by the manufacturer and AIS-1 data which were gathered since the change in blocking filters have been analyzed, it is apparent that the second order contamination is several tens of percent rather than less than ten percent.

The impact of the contamination depends on the scene and on the observer's perspective. Obviously for those who are interested primarily in the 0.8 to 1.6 micron region, the impact is positive since the region short of 1.2 microns would not have been available these past two years. For those interested in the region beyond 1.6 microns, the impact of the contamination from shorter wavelengths depends on the scene intensity at the shorter wavelengths and the amount of structure in the spectral reflectance at those wavelengths. In the southwestern US, for example, in areas with very little vegetation, the typical effect of the contamination is to add what is essentially a dc signal to the longer wavelengths, which has little or no impact on the spectral structure there. However, vegetation is highly reflective at the shorter wavelengths so scenes containing much vegetation can be expected to show a much larger contamination at the longer wavelengths. This is the case at many of the Australian test sites; Huntington et al. are developing techniques to remove the effects by modeling the contribution expected at the longer wavelengths from the high vegetation reflectance at the shorter wavelengths.

Figure 7 shows second order contamination in the AIS-1 Cuprite data set discussed earlier in this Introduction to the Proceedings. Shown is a spectrum from a 3 by 3 pixel area centered on Kaolinite Hill. The second order contribution to the 1.8 micron water absorption feature can be clearly seen: the reflectance values in that region should be zero but in fact are about 60 percent of the total signal level, which has been normalized. Note, however, that the double absorption feature at 2.2 microns is still quite clear, as it has been in all AIS-1 data over Kaolinite Hill. In the Cuprite setting, the second order contamination has not affected the ability to do direct mineral identification.

Thus, data collected with AIS-1 will continue to be useful in spite of their various shortcomings. In many cases, additional work will be required to extract the information that lies hidden in the data, while in others the second order contamination will be found to have minimal effect. However, even in the latter case the investigator should be cautioned to remember that second order radiation is present. AIS-2 has been designed to avoid this and the other problems discussed above (as of course have AVIRIS and SISEX). Each of these instruments will still have its own "personality," as do all such complex sensors. It remains incumbent upon all investigators who work with data from any sensor to learn as much about the sensor as possible, and to approach the interpretation of data with alert and open minds.
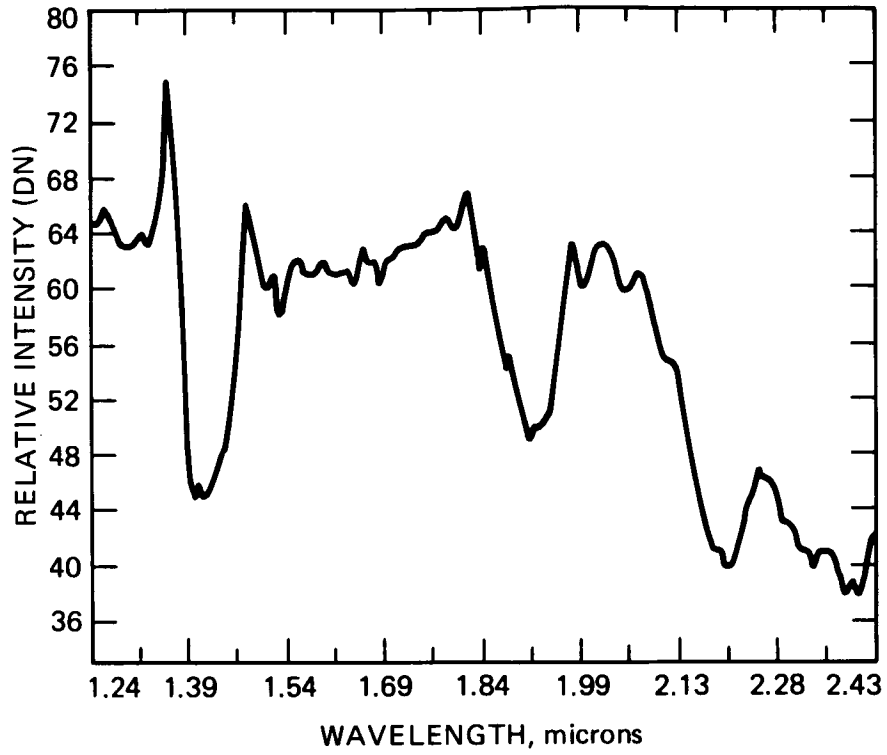
AIS-1 IMAGE
AT 1.24 microns

FIGURE 7. Spectrum of a 3 by 3 pixel area centered on Kaolinite Hill, Cuprite; AIS-1 data set from September 23, 1985. Data have been corrected with the log residual technique.

16

RADIOMETRIC CALIBRATION OF THE AIRBORNE IMAGING SPECTROMETER

DEANNE TUCKER and GREGG VANE, Jet Propulsion Laboratory, Pasadena, California

ABSTRACT

The spectral and radiometric calibration of the Airborne Imaging Spectrometer is described.

INTRODUCTION

Several laboratory calibration tests have been developed for the Airborne Imaging Spectrometer (AIS). The goals of these tests are to 1) adjust the physical alignment of the detector within the optical system and set the spectral endpoints, and 2) produce a calibration file of multipliers which equalizes the relative responses of each of the detector elements in the entire two-dimensional array. Tests are also performed as part of an ongoing effort to provide absolute radiometric calibration. This paper describes the tests and discusses the merits and limitations of each.

TECHNIQUE

Spectral Alignment. The detector is mounted inside a dewar which is mounted to the optical head of the instrument. This dewar can be positioned in the spectrometer focal plane to align the detector with respect to the spectrally dispersed image.

A monochromator and broadband lamp are used to provide illumination of one spectral channel (approximately 10 nm) on the detector array. The monochromator is calibrated using the visible emission lines from a mercury vapor pen-ray lamp. Since this monochromator has no order blocking filters, the higher orders of these visible lines are used to calibrate in the infrared.

The AIS dewar is rotated until the line of illumination falls squarely on the detector. The dewar is adjusted side-to-side to place the detector close to the desired position within the spectrum and to minimize any vignetting. The wavelength endpoints are set by adjusting resistors and potentiometers in the grating drive circuit. The wavelength end points are determined by measuring the wavelengths which center the illumination on the first and last row of the detector. The spectral sampling interval is a calculated quantity determined by dividing the difference between the two edge wavelengths by 31 for AIS-1 and 63 for AIS-2 (there are N-1 increments from pixel 1 to pixel N).

The accuracy of this method is limited in two ways. The repeat accuracy associated with exactly centering the spectral line on a pixel is about 5 to 10 nm, or just under one spectral bandwidth. Also, the center wavelength which AIS receives depends on the viewing geometry somewhat, since in order to get enough signal from the monochromator into the instrument, a spectral band wider than 10 nm is used. The monochromator optics require the light source to be tilted away from the center axis in order to

maximize the signal. Changing the incident angle will alter the exit angle of a particular wavelength.

The combination of these factors induces an uncertainty of about two spectral channels. Results from several experiments comparing these measured spectral endpoints with endpoints determined from observing the carbon dioxide or water absorption features or other known spectral features in AIS data have indicated as much as a two band difference.

A krypton pen-ray lamp has been used both in the lab and as an in-flight calibrator. This gas has emission lines in the AIS spectral region. However, the convolution of the lamp with the instrument response produces a spectrum whose lines are not necessarily sharp. In AIS-1 the grating "jitter" smeared the lines considerably making it difficult to assign wavelengths to the observed emission lines. The krypton data for AIS-1 is most useful as a monitor of calibration stability rather than as an abso-lute calibration standard. The grating jitter has been eliminated for AIS-2 and the krypton spectra are much cleaner.

Laboratory calibrations before and after the Australia/Hawaii de-ployment in October 1985, differ by about one spectral band, which is well within the measurement accuracy. Comparison of two sets of in-flight krypton lamp spectra show that no measurable shift in the calibration occured.

DETECTOR RESPONSE EQUALIZATION

Although the quantum efficiency of the mercury cadmium telluride detector drops to near zero beyond 2.6 microns, a thermal contribution to the signal at warm temperatures has been detected. As a consequence, the detector pixel response equalization tests are performed with AIS inside a cooled thermal chamber. The test is repeated at several temperatures, bracketing actual flight temperatures.

As a source of uniform radiance, a standard laboratory flat field illumination source (light cannon) is used. Two projector lamps are mount-ed inside a housing which has a hemisphere at the rear and a cone on the front. The inside of this housing is painted with Kodak white reflectance paint. On the front of the cone are two diffuse pieces of water-free quartz.

The light cannon radiance is calibrated using an Optronics Labora-tories spectroradiometer. A cooled lead sulfide detector is used in order to calibrate out to 2.5 microns. First, the spectroradiometer response is calibrated in units of irradiance (Watts/square cm - nm) viewing a second-ary calibration standard lamp whose irradiance is known to within one to two percent. Second, the light cannon is calibrated also in units of irradiance with the calibrated spectroradiometer. Radiance units can be obtained by multiplying the irradiance curve by a constant which depends on the geometry of the system. Equipment is currently being purchased to enable us to perform a radiance calibration directly.

The AIS optics are placed in the thermal chamber. A flat fold mirror projects the AIS slit through a hole cut through the side of the chamber and onto the 11" diameter diffuser plate of the light cannon. Assuming the radiance of the light cannon is uniform throughout the region viewed, variations in digital number output among the detector pixels will be due to detector response variations as well as any off-axis effects from the optical system. For a radiance level approximately equal to flight levels, multipliers are generated for each pixel to equalize their signal levels. These values are then applied to flight data. For any particular scene, the value of each pixel is adjusted by its multiplier.

Data are taken at ten different radiance levels by adjusting the light cannon iris. A neutral density filter is placed over the AIS entrance window such that the detector just saturates when the iris is at the full open position. For each pixel, a light transfer curve is generated by plotting signal against wavelength at a relative light level. For AIS-1 the curves depart enough from a linear relationship to warrant using a piecewise linear fit to the data. Multipliers are generated from a data set which is at typical flight intensities. When the target intensities are at different levels from this laboratory data set, the corrected value for a particular pixel is obtained by a piece-wise linear fit to its light transfer curve.

The above procedure eliminates most of the striping seen in raw images; however, some striping remains. One factor which may contribute is the nonuniformity of the light cannon surface. Ideally, the radiance of the light cannon should be uniform across the surface of the diffuser plates. The uniformity has recently been measured with a broad-band spot photometer, sensitive to visible wavelengths. A thirty percent decrease in brightness was observed from center to edge. The nonuniformity will alter the radiance level depending on which portion of the surface an instrument is viewing. However, it should not alter the spectral shape of the radiance curve. The relative calibration seems quite constant with time. AIS is out of focus at the distances used for calibration which should minimize the effect of nonuniformity of the light cannon output. Efforts are under way to improve the light cannon performance.

A more likely cause for the residual striping is in the detector itself. If the detector array's properties vary with time or environment, striping will result. If, for example, there is a small change in detector responsivity after the instrument has been calibrated in the lab, the application of the lab-derived multipliers will not completely equalize the output of each detector element in the array. The only way to overcome this situation with AIS is to use an inflight calibration taken at the same time as the data. Many investigators have successfully used regions of the flight line which are spatially uniform and have a known spectral reflectance to take out the effects of the detector variation as well as some of the atmospheric effects.

PERFORMANCE EVALUATION

There is an on-going effort at JPL to determine instrument performance characteristics such as the signal-to-noise ratio. One method to determine these parameters is to image pure rock samples under solar illumination.

This is done under flight temperature conditions by enclosing the instrument optics in a styrofoam box and purging with cold nitrogen gas. Data from kaolinite, montmorillonite, halon, gypsum, alunite, aphrosiderite, and calcite have been acquired. One such data set gives a signal-to-noise ratio of about ten-to-one for AIS-1. This low number is most likely due to the electronic signal chain noise. Much of this noise has been removed from AIS-2. Hence the performance of the instrument should be considerably improved.

FUTURE PROJECTS

Several activities are under way to further improve the calibration of AIS. Halon targets are being made at the lab to provide a spatially uniform and spectral known surface which will be illuminated both with sunlight and with calibrated lamps of sufficient intensity to approximate an AIS scene. An integrating sphere is also being purchased which will have a uniform radiance across a 16-inch diameter output port. Although this will be part of the calibration equipment for AVIRIS, it will be used for a check on AIS calibration at the end of 1986. Finally, improvements are being made in onboard spectral alignment calibration. Because pen-ray lamps frequently contain impurities which results in unidentifiable extraneous emission lines, the use of rare earth filters such as holmium oxide and praseodymium is being investigated. These materials have broad but deep absorption features throughout the visible and short wavelength infrared, and when used in conjunction with a stable broad band light source, should provide a more accurate means of assessing spectral alignment in flight.

COMPARISON OF VARIOUS TECHNIQUES FOR CALIBRATION OF AIS DATA

DAR A. ROBERTS, Stanford University, USA; YASUSHI YAMAGUCHI, Geological Survey of Japan, Japan; RONALD J.P. LYON, Stanford University, USA

ABSTRACT

The Airborne Imaging Spectrometer (AIS) samples a region which is strongly influenced by decreasing solar irradiance at longer wavelengths and strong atmospheric absorptions. Four techniques, the Log Residual, the Least Upper Bound Residual, the Flat Field Correction and calibration using field reflectance measurements were investigated as a means for removing these two features. Of the four techniques field reflectance calibration proved to be superior in terms of noise and normalization. Of the other three techniques, the Log Residual was superior when applied to areas which did not contain one dominant cover type. In heavily vegetated areas, the Log Residual proved to be ineffective. After removing anomalously bright data values, the Least Upper Bound Residual proved to be almost as effective as the Log Residual in sparsely vegetated areas and much more effective in heavily vegetated areas. Of all the techniques, the Flat Field Correction was the noisiest.

INTRODUCTION

The Airborne Imaging Spectrometer (AIS) samples a spectral region which is severely affected by two factors, decreased solar irradiance at longer wavelengths and wavelength specific atmospheric absorptions, such as the 1400 and 1900 nm water absorptions. These factors result in a reduced brightness and dynamic range in data collected in these regions, an undesirable characteristic with regards to data interpretation for geological or botanical purposes.

The purpose of this study was to investigate a number of techniques which have the potential for removing atmospheric and solar effects from the data. Four techniques were investigated. These have been divided by the authors into two groups, statistically based techniques which derive various parameters from the data and use them in the normalization process, and physically based techniques which utilize some physical/spectral property derived from the AIS data or from spectra collected in the field to standardize the data to some known physical quantity. The study was conducted in the vicinity of the town of

Yerington and the adjacent Singatze Range, located approximately 50 miles south of Reno, Nevada. Five flight lines of data in the "rock mode" (1200 to 2400 nm) were acquired on July 25, 1984. The five flights, flights 407 to 411, were acquired over a variety of targets ranging from hydrothermally altered areas and mine dumps to alfalfa fields. Two areas, one located in a hydrothermally altered area on flight 407, and one located on flight 411 in a region dominated by alfalfa, were selected for comparison of the four techniques.

STATISTICALLY BASED METHODS

The statistically based techniques are the Log Residual and the Least Upper Bound Residual (Green and Craig, 1985). The Log Residual is based upon the following multiplicative relationship:

$$DN_{s\lambda} = T_s R_{s\lambda} I_\lambda \tag{1}$$

Where $DN_{s\lambda}$ = Radiance, equal to the digital number value for each channel at each pixel in the data, T_s = a topographic factor which takes into account brightness differences due to slope orientation, $R_{s\lambda}$ = Reflectance for each channel at each pixel in the image and I_λ = Average irradiance throughout the image.

Equation (1) is divided by a number of logarithmic averages derived from the data, and rearranged to give the following equation:

$$LOG(R_{s\lambda}) = LOG(DN_{s\lambda}) - AVG(LOG_\lambda) - AVG(LOG_s) \tag{2}$$

The average logarithmic spectrum is derived by summing the logarithmic values for each channel, then dividing these sums by the total number of samples in the image. The topographic factor is calculated by summing the logarithmic values for the 128 channels at each pixel, then dividing this sum by 128.

The Least Upper Bound Residual differs from the Log Residual in only one area. Instead of the average logarithmic spectrum, the maximum spectrum is used. The equation is as follows:

$$DN_{s\lambda} = T_s R_{s\lambda} LUB_\lambda \tag{3}$$

Where LUB_λ = the maximum real brightness value for each of the 128 channels. Like equation (1) this equation can be rearranged:

$$LOG(R_{s\lambda}) = LOG(DN_{s\lambda}) - LOG(MAX_\lambda) - AVG(LOG_s) \tag{4}$$

Both the Log Residual and Least Upper Bound Residual values had one more value added to them. This value was called the image average and was equal to the average logarithmic value for every sample and channel in the image. This value was employed as a means of normalizing each flight line.

PHYSICALLY BASED METHODS

The physically based techniques employed are the Flat Field Correction as defined by the Jet Propulsion Laboratory and Field Reflectance Calibration.

The Flat Field Correction is based upon locating a pixel or a number of pixels in the imagery which are spectrally flat. This spectrum is then divided into every pixel in the flight using the following equation:

$$R_{s\lambda} = DN_{s\lambda}/F_{\lambda}$$

(5)

Where F_{λ} = a spectrally flat 128 channel spectrum.

Reflectance calibration is based upon locating a number of homogeneous, unvegetated targets in the AIS data. Field spectra are measured at each site in an attempt to characterize the spectral reflectance of the target. Next, reflectance, determined in the field, is compared to the digital number response measured by the AIS. Theoretically, there should be a strong linear relationship between these two values. By comparing field reflectance for a number of targets to thier corresponding response measured by the AIS the following equation can be derived:

$$R_{s\lambda} = DN_{s\lambda} slope_{\lambda} + intercept_{\lambda}$$

(6)

Where $slope_{\lambda}$ = the slope of the best-fit equation and $intercept_{\lambda}$ = the intercept of this equation. These constants can be applied to the digital number value for each channel at each pixel to calculate a corresponding percent reflectance value.

Four calibration targets were located in the AIS data. These targets consisted of the Yerington Mine dump (at 4300 feet on flight 410), the Bluestone Mine dump (at 4300 feet on flight 407), a sparsely vegetated tuff (at 5200 feet on flight 407) and a patch of pavement (at 4300 feet on flight 411).

Six to thirteen spectral measurements were made at each site using a GER IRIS spectroradiometer which collects 820 channels of data between the 400 and 2500 nm region at a spectral resolution of 2 to 4 nm. The spectra were collected between 10:00 A.M. and 3:00 P.M.. All spectra were standardized to a barium sulfate plate. The number of spectra collected varied depending upon the homogeneity of the target which was assessed visually at the time of collection. Six were collected over the pavement and the Bluestone Mine dumps. Thirteen were collected over the tuff. Nine were collected over the Yerington Mine dumps. In all cases, spectra were collected randomly in an effort to best characterize the target.

Field spectra were converted to percent reflectance by dividing the radiance measurement of the target by the radiance value for the barium sulfate plate which was measured simultaneously. Next, spikes, present in the field spectra in the 1400 and 1900 nm regions were removed by interpolating across the spike, usually a

region 4 to 8 nm wide. Despiked field spectra were averaged producing a single spectrum for each target, modeling the pixel response for that target. Finally, the modeled spectra were convolved to the 9.6 nm AIS spectral equivalent using a gaussian filter transfer function.

Raw data values were extracted from the AIS imagery over the four calibration targets. Between 5 and 19 pixels were extracted for each target and averaged. Next, the averaged pixel value was plotted against the averaged, convolved field spectra. Least squares regression was used to produce a best fit line. The R^2 values ranged from as low as .874 to as high as .992. The average R^2 value was around .95. The slope and intercept of the best fit lines were used to convert each AIS channel to "percent reflectance" (Table 1).

Table 1. Airborne Imaging Spectrometer channel information

CHANNEL	WAVELENGTH (um.)	REGRESSION EQUATION	R^2	CHANNEL	WAVELENGTH (um.)	REGRESSION EQUATION	R^2
1	1.135	.0195x -6.91	.970	65	1.728	.0448x -13.47	.978
2	1.144	.0164x -5.89	.967	66	1.737	.0457x -12.01	.977
3	1.153	.0149x -4.49	.974	67	1.746	.0476x -10.46	.975
4	1.162	.0152x -5.84	.976	68	1.755	.0566x -12.10	.969
5	1.172	.0146x -4.31	.973	69	1.765	.0696x -13.55	.970
6	1.181	.0146x -4.34	.972	70	1.774	.0983x -19.31	.970
7	1.190	.0143x -3.98	.971	71	1.783	.1527x -29.82	.972
8	1.199	.0137x -3.60	.973	72	1.793	.1788x -29.77	.958
9	1.208	.0134x -2.76	.973	73	1.802	.1837x -26.08	.945
10	1.218	.0139x -3.57	.962	74	1.811	.2016x -31.81	.976
11	1.227	.0149x -3.93	.969	75	1.820	.2092x -31.72	.959
12	1.236	.0162x -4.27	.970	76	1.830	.2161x -28.70	.946
13	1.245	.0161x -3.72	.967	77	1.839	.2691x -35.21	.932
14	1.254	.0162x -3.81	.967	78	1.848	.3049x -38.25	.930
15	1.264	.0164x -4.44	.966	79	1.858	.3006x -34.78	.925
16	1.273	.0179x -4.97	.976	80	1.867	.2895x -33.09	.937
17	1.282	.0189x -4.88	.969	81	1.876	.2538x -26.54	.932
18	1.291	.0224x -6.50	.966	82	1.885	.2759x -33.78	.942
19	1.301	.0268x -8.11	.965	83	1.895	.2146x -22.31	.903
20	1.310	.0363x -12.46	.973	84	1.904	.2100x -24.73	.938
21	1.319	.0576x -19.54	.960	85	1.913	.1538x -15.10	.904
22	1.328	.1034x -29.69	.952	86	1.923	.1398x -14.39	.913
23	1.337	.1755x -47.65	.952	87	1.932	.1203x -10.57	.918
24	1.347	.2098x -55.52	.903	88	1.941	.1011x -6.23	.903
25	1.356	.1997x -52.07	.896	89	1.950	.0858x -5.06	.914
26	1.365	.2097x -50.66	.874	90	1.960	.0777x -4.39	.910
27	1.374	.2383x -61.28	.923	91	1.969	.0858x -6.68	.923
28	1.383	.2192x -53.83	.934	92	1.976	.0994x -7.26	.908
29	1.393	.1848x -42.65	.913	93	1.988	.0990x -5.23	.908
30	1.402	.1508x -32.21	.974	94	1.997	.0849x -4.03	.930
31	1.411	.1180x -24.10	.945	95	2.006	.0741x -4.66	.936
32	1.420	.0827x -18.75	.930	96	2.016	.0743x -6.27	.951
33	1.432	.0766x -13.12	.908	97	2.028	.0812x -4.74	.948
34	1.442	.0720x -14.15	.933	98	2.037	.0825x -4.90	.946
35	1.451	.0606x -10.80	.946	99	2.046	.0823x -4.87	.956
36	1.460	.0531x -10.20	.956	100	2.055	.0852x -7.23	.962
37	1.469	.0396x -5.82	.948	101	2.065	.0800x -5.07	.962
38	1.479	.0327x -4.26	.950	102	2.074	.0769x -5.11	.966
39	1.488	.0288x -3.53	.958	103	2.083	.0783x -5.98	.965
40	1.497	.0274x -4.08	.963	104	2.093	.0786x -6.07	.967
41	1.506	.0271x -4.93	.966	105	2.102	.0796x -6.62	.964
42	1.516	.0281x -6.85	.965	106	2.111	.0804x -6.84	.970
43	1.525	.0279x -6.19	.966	107	2.121	.0823x -6.56	.968
44	1.534	.0292x -7.29	.966	108	2.130	.0859x -7.18	.965
45	1.543	.0302x -7.93	.963	109	2.139	.0896x -8.30	.967
46	1.553	.0304x -7.10	.959	110	2.149	.0922x -8.76	.964
47	1.562	.0306x -6.63	.966	111	2.158	.0951x -8.83	.965
48	1.571	.0322x -8.03	.967	112	2.167	.0958x -8.13	.946
49	1.581	.0314x -6.90	.967	113	2.177	.0962x -9.06	.956
50	1.590	.0331x -8.59	.963	114	2.186	.1024x -11.24	.963
51	1.599	.0327x -8.33	.969	115	2.195	.0962x -8.74	.950
52	1.608	.0332x -8.85	.972	116	2.205	.1004x -9.26	.961
53	1.618	.0346x -9.57	.973	117	2.214	.1120x -19.31	.938
54	1.627	.0351x -9.93	.979	118	2.223	.1137x -9.10	.942
55	1.636	.0363x -10.99	.977	119	2.232	.1175x -9.31	.932
56	1.645	.0369x -11.59	.978	120	2.242	.1204x -9.21	.936
57	1.655	.0367x -11.52	.978	121	2.251	.1228x -9.66	.924
58	1.664	.0371x -11.42	.978	122	2.260	.1255x -9.10	.929
59	1.673	.0383x -12.76	.983	123	2.270	.1303x -10.23	.950
60	1.682	.0390x -12.96	.984	124	2.279	.1346x -10.65	.945
61	1.692	.0410x -14.02	.984	125	2.288	.1436x -12.82	.945
62	1.701	.0436x -15.19	.988	126	2.298	.1474x -12.82	.967
63	1.710	.0450x -15.20	.986	127	2.307	.1593x -15.22	.964
64	1.728	.0479x -16.37	.992	128	2.316	.1679x -14.75	.963

Channel wavelengths determined using 1.96, 2.01 and 2.06 CO_2 absorption features and maximum H_2O absorptions at 1.379 and 1.87 (Goldberg, 1954)

RESULTS FOR UNVEGETATED TARGETS

Figure 1 shows an uncorrected, unprocessed AIS spectrum extracted from flight 407 in an area which is hydrothermally altered. Though, unverified on the ground, this pixel has been interpretated as containing kaolinite. The two most notable features in this spectral plot are the strong absorptions in the 1400 and 1900 nm regions and the decreased brightness at longer wavelengths; no definitive clay absorption features are evident.

Figures 2 and 3 show the results of the Log Residual and Least Upper Bound Residual for the same location. Figure 2 has several notable features. First, both the atmospheric absorption features and solar irradiance have been normalized. Second, mineral absorption features have been markedly accentuated; the resulting spectrum looks like a kaolinite spectrum. Finally, the resulting spectrum is relatively noise free and easy to interpret.

Figure 3 demonstrates that the Least Upper Bound Residual process was not as effective. In this plot, solar irradiance has been normalized and atmospheric absorption partially normalized. However, mineral absorption features are not as evident and the resulting spectrum is very noisy.
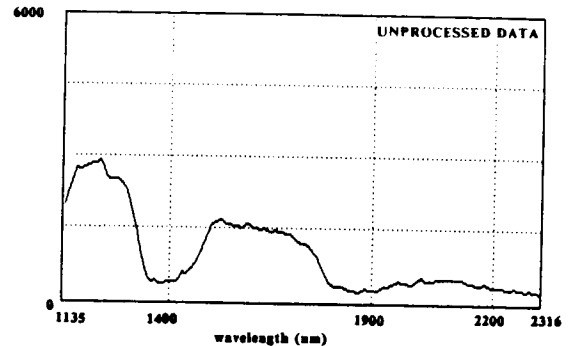
Fig. 1. Uncorrected AIS spectrum Hydrothermal alteration
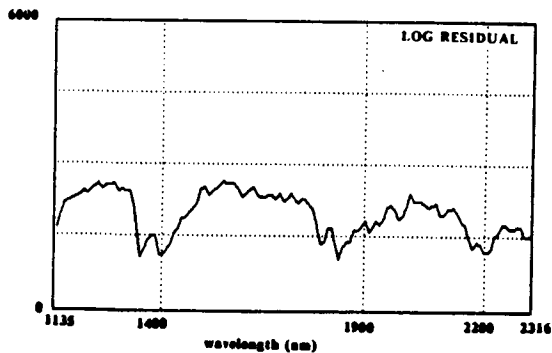
Fig. 2. Log Residual spectrum Hydrothermal alteration
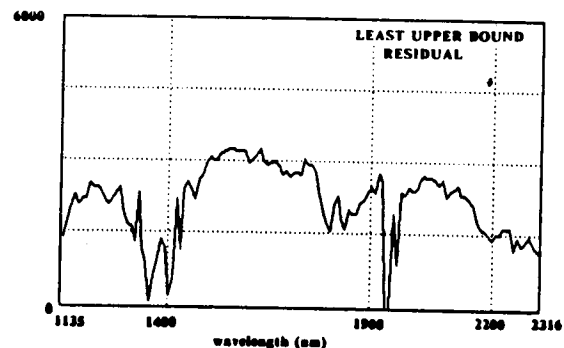
Fig. 3. Least Upper Bound Residual spectrum, Hydrothermal alteration

Many of the problems in the Least Upper Bound Residual spectrum do not accurately reflect the utility of this technique. The noise, and poor resolution of mineral absorption features are the result of anomalously high AIS data values which do not reflect the true maximum value for each channel. In order to solve this problem, it became evident that these anomalous data values had to be removed from the data set before using the Least Upper Bound Residual technique.

In order to remove these anomalous data values two filtering

techniques were employed. The first technique is based upon removing all data values brighter or darker than a select percentile. A .01 percentile value was chosen empirically. Based upon this technique, all data values darker than the first percentile or brighter than the 99th percentile were assigned the average brightness value for that channel, calculated from the data confined by these two bounds.

The second filtering technique was based upon anomalously large changes in brightness in the down-track direction. These anomalous data values were located by comparing digital numbers in one cross-track line to digital numbers in the previous cross-track line. Two threshold values, one for pixels brighter than 1500 dn, and one for pixels darker than 1500 were selected empirically. The threshold values used on this data set were 1600 in bright areas and 600 in darker areas. The average brightness for that channel was assigned to a pixel if the absolute difference from one line to the next was greater than the threshold value. The resulting Log Residual and Least Upper Bound Residual spectra are presented in figures 4 and 5.
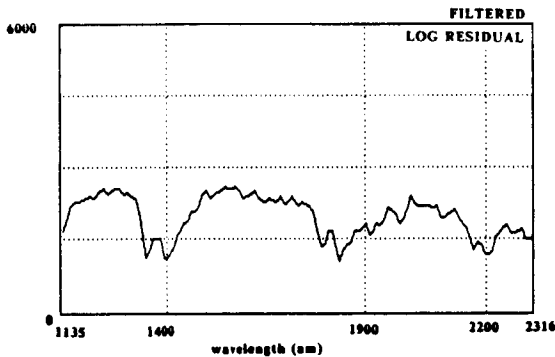
Fig. 4. Filtered Log Residual
spectrum, Hydrothermal
alteration
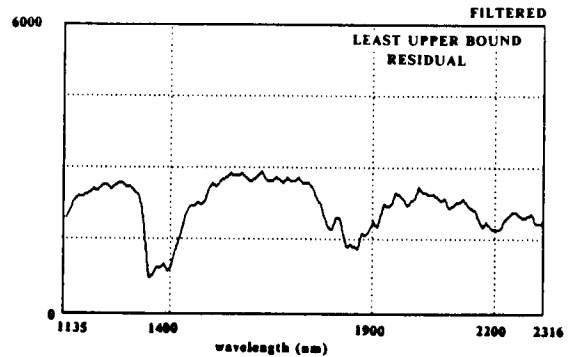
Fig. 5. Filtered Least Upper Bound
Residual spectrum
Hydrothermal alteration

Comparing figure 2 to figure 4, it is evident that filtering did not result in any marked improvement in the Log Residual spectrum. However, comparing figures 3 and 5, a very marked improvement is shown. The filtered Least Upper Bound Residual spectrum is almost as good as the Log Residual spectrum in terms of showing mineral absorption features and in terms of noise. However, though the Least Upper Bound Residual has been improved, there are some problems with the filtering process. Visual display of the entire AIS flight demonstrated that a number of bright, non anomalous pixels were removed, suggesting that a 99th percentile was too extreme.

Figure 6 shows the resulting Flat Field spectrum for this same area. Like the other two techniques, the Flat Field Correction successfully normalized solar irradiance. However, some atmospheric absorption is still evident in the 1400 and 1900 nm regions. In addition, the resulting spectrum is not as easy to interpret as the Log Residual and is much noisier.

Figure 7 shows the percent reflectance spectrum for this same area. Both solar irradiance and atmospheric absorption have been

normalized. In addition, the resulting spectrum is very smooth. However, mineral absorption features are not as pronounced as they are in the Log Residual and Least Upper Bound Residual spectra.
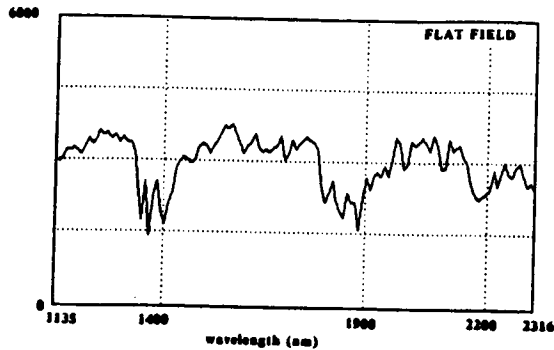
Fig. 6.   Flat Field corrected spectrum, Hydrothermal alteration
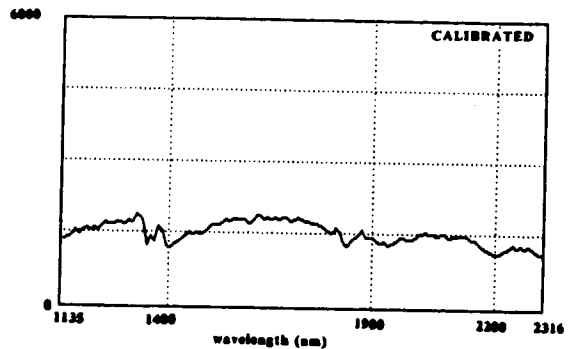
Fig. 7.   Reflectance calibrated spectrum, Hydrothermal alteration

RESULTS FOR VEGETATED TARGETS

Figure 8 shows an unprocessed spectrum of alfalfa located on flight 411. Comparison to figure 1 demonstrates that there are some noticeable differences between the two, especially in the 1200 and 1500 nm regions. However, at wavelengths longer than 1600 nm, the differences are not strongly evident.
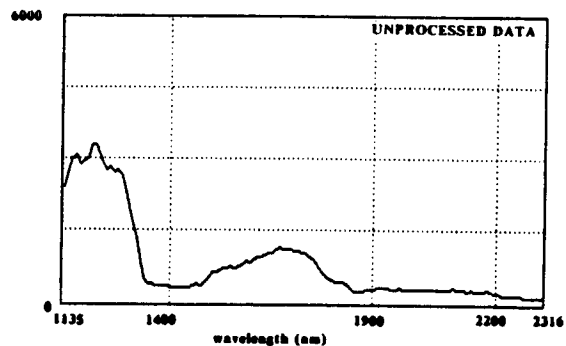
Fig. 8.   Uncorrected AIS spectrum Alfalfa

Figures 9 and 10 show the Log Residual and Least Upper Bound Residual results for this same area. Once again solar irradiance and atmospheric absorption have been partially to completely normalized. In addition, though unusually shaped, the Log Residual spectrum for the alfalfa is relatively noise free. The Least Upper Bound Residual, on the otherhand,is extremely noisy.
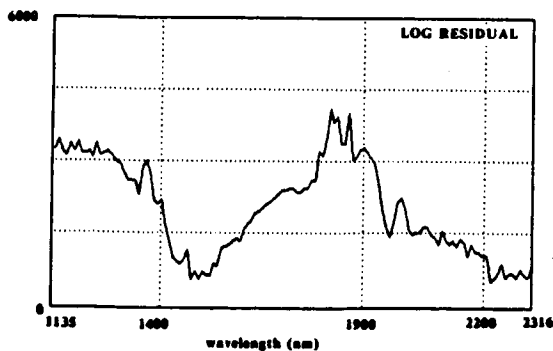
Fig. 9.   Log Residual spectrum Alfalfa
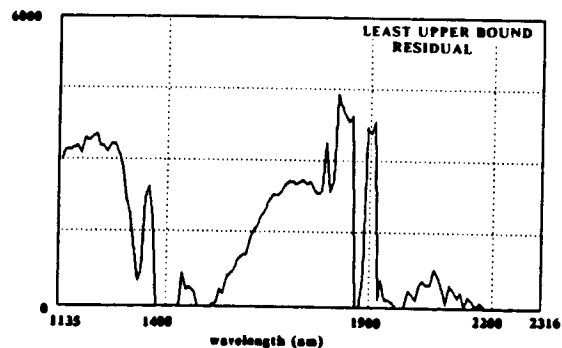
Fig. 10. Least Upper Bound Residual spectrum, Alfalfa

Figures 11 and 12 show the Log Residual and Least Upper Bound Residual spectra resulting from filtered AIS data (97.5 percentile, threshold values of 1600 and 500). Once more the only marked improvement occurs in the Least Upper Bound Residual.
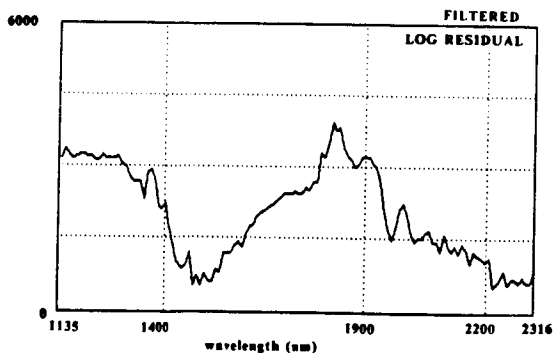
Fig. 11. Filtered Log Residual spectrum, Alfalfa
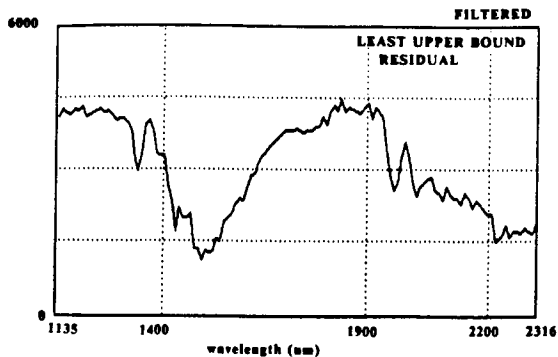
Fig. 12. Filtered Least Upper Bound Residual spectrum, Alfalfa

Analysis of an unvegetated area located along flight 411 demonstrates a major problem with the Log Residual when it is applied to heavily vegetated flight lines. Figure 13 shows the Log Residual spectrum for an area containing stubble or plowed soil. Comparison of figure 13 to figure 11 demonstrates that figure 13 is the mirror image of figure 11. This is a product of the average logarithmic spectrum which is utilized in the Log Residual process. Along flight 411, the average logarithmic spectrum is strongly influenced by alfalfa. Therefore, any surface feature which is not alfalfa will show departures from this average spectrum, resulting in a mirror image.
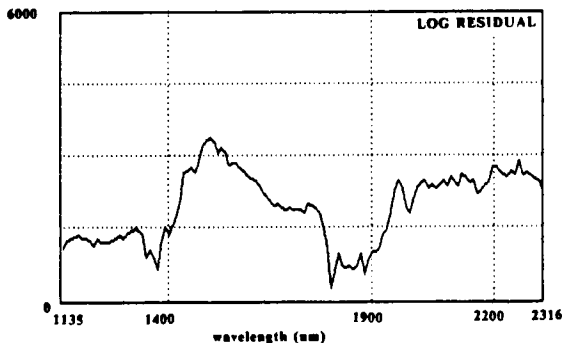
Fig. 13. Log Residual spectrum unvegetated area

Figure 14 shows the Flat Field corrected spectrum for the same area of alfalfa. Both solar irradiance and atmospheric absorption appear to be normalized. In addition, the resulting spectrum is relatively noise free. Finally, the spectral shape is unusual for vegetation, though very similar to the result obtained using the previously mentioned statistically based techniques.

Figure 15 shows the result obtained using field spectra as a means for calibrating the AIS data. Of the four techniques, this result shows the best normalization and has the least amount of noise. In addition, like the spectra produced by the Log Residual, Least Upper Bound Residual and the Flat Field Correction, this spectrum does not have a typical shape for vegetation.
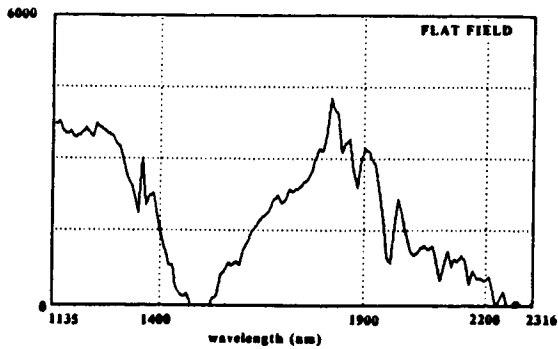
Fig. 14. Flat Field corrected
spectrum, Alfalfa
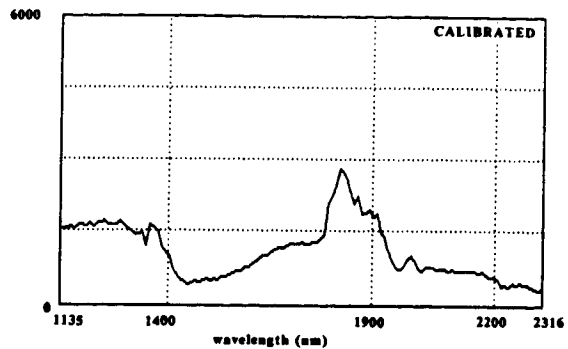
Fig. 15. Reflectance calibrated
spectrum, Alfalfa

The unusual shape of the vegetation may have resulted from the processing techniques which were employed, or originated in the AIS data. The fact that this spectral shape is present in all four processed spectra suggests that the problem may be in the unprocessed AIS data. In order to investigate this possibility, uncorrected AIS pixels were extracted from the alfalfa and compared to the uncorrected AIS values for the pavement which was measured in the field and found to be approximately 24 percent reflective. The results showed that the uncorrected AIS values for alfalfa were up to twice as large as the values for pavement in the 1800 to 2000 nm region. A typical vegetation spectrum should be darker than pavement in this region. It was concluded that the problem was in the original AIS data.

A number of possible explanations, including possible atmospheric problems were considered. In light of recent findings at the Jet Propulsion Laboratory, the most likely explanation is second order overlap from the shorter 800 to 1200 nm regions (G. Vane, verbal communication). The Airborne Imaging Spectrometer contains a blocking filter designed to block all wavelengths of light shorter than 800 nm. Thus, light in the 800 to 1200 nm range may add to the 1600 to 2400 nm regions in the form of a second order contribution. This phenomenon would be particularly bad for vegetated areas because vegetation is strongly reflective in the 800 to 1200 nm region and vegetation is strongly absorbent in the 1800 to 1900 nm region. Based upon the results obtained in the unvegetated area, this is not a marked problem where vegetation cover is low. Furthermore, second order overlap is not a problem in unvegetated pixels located in heavily vegetated flight lines if the data is calibrated using field reflectance measurements; the second order contribution is incorporated into the best-fit line established between percent reflectance measurements and uncorrected AIS digital numbers.

SUMMARY

The results of this study suggest a number of strategies for image processing of data with a large number of spectral dimensions. Of the four techniques investigated, calibration using field spectra was the best. However, difficulties in selecting calibration sites, instrumental requirements and the number of

hours required to measure the spectra make this technique impractical from an exploration point of view. In addition, it is not always possible, or desireable, to collect field measurements prior to analyzing the data. Therefore, it is necessary to consider other processing techniques which are not field intensive or difficult to employ. Of the other three techniques investigated, the Log Residual proved to be superior in areas which did not contain a dominant cover type. The Least Upper Bound Residual, after careful filtering of the data to remove anomalous data values, proved to be almost as useful as the Log Residual in these areas. In addition, in an area dominantly composed of one cover type, the filtered Least Upper Bound Residual proved to be very successful, whereas the Log Residual was ineffective in these areas. Of these three techniques, the Flat Field Correction proved to be the noisiest and least effective. However, the Flat Field has an advantage over the Least Upper Bound Residual and the Log Residual in that this technique has some physical basis, and thus the results may be related back to what is occurring on the ground.

REFERENCES

Green, A.A., Craig, M.D., Analysis of aircraft spectrometer data with logarithmic residuals; Proceedings of the Airborne Imaging Spectrometer Data Analysis Workshop, April 8,9,10, 1985, Gregg Vane and Alexander F.H. Goetz editors, Jet Propulsion Laboratory, California Institute of Technology, Pasadena, CA, pp. 111-119

Goldberg, L., 1954, The Absorption Spectrum of the Atmosphere; The Earth as a Planet, G.P. Kuiper editor, University of Chicago Press, Chicago, Il, pp. 434-490

ANALYSIS OF AIS RADIOMETRY WITH EMPHASIS ON DETERMINATION OF ATMOSPHERIC PROPERTIES AND SURFACE REFLECTANCE

J. E. CONEL, S. ADAMS, R. E. ALLEY, G. HOOVER, and S. SCHULTZ, Jet Propulsion Laboratory, California Institute of Technology, Pasadena, California

ABSTRACT

Airborne Imaging Spectrometer data from Mono Lake, California, were studied in order to establish spectral radiance of test areas under solar illumination. The objective is to provide a method of atmospheric correction for major absorbers from the spectrometer data themselves. Crucial to the analysis is radiometric calibration of the instrument. Good agreement is found between calculated and measured radiances for uniform surface targets (beaches), but simulations of atmospheric properties with LOWTRAN lead to unreasonably low values of atmospheric precipitable water. Absorptions from carbon dioxide are not detected in the AIS data, but are strongly present in the LOWTRAN model. The apparent low contrast of all atmospheric absorption bands leads to a study of contamination from overlapping spectral orders in the AIS data. The suspected contamination is shown unambiguously to be present beyond approximately 1500 nm and consists of an extra radiance term including atmospheric bands from the $\lambda/2$ wavelength interval. The magnitude of such contamination remains uncertain pending determination of second-order efficiencies of the grating used. The spectral band filling at 1400 nm cannot be accounted for by order mixing because of the 800-nm blocking filter used. A rigorous removal of the unwanted spectral contamination does not seem possible for any data taken in the rock mode. Rough estimates for tree-mode observations might be pieced together if a suitable after-the-fact radiometric calibration of the instrument can be formulated.

INTRODUCTION

The Airborne Imaging Spectrometer (AIS) is an instrument with sufficient spectral resolution (approximately 9.5 nm) to recover most geologic and geobotanical surface spectral reflectance features. AIS can also provide data for analyzing important atmospheric absorption bands from water and carbon dioxide. Use of the full potential of AIS measurements for surface investigations throughout the spectral interval of observation (900 to 2400 nm) requires accurate compensation for atmospheric effects. The principal sources are gaseous absorptions, but at shorter wavelengths some aerosol scattering may be encountered.

This paper discusses the absolute radiometric characteristics of the AIS data based on laboratory calibration measurements and field observations. An absolute calibration implies that source radiance may be deduced from instrumental output, in this case raw counts from the AIS. For a detailed discussion of the actual laboratory calibration procedures, see Tucker (1984). We investigated the atmospheric problem on an absolute basis because both atmospheric and surface parameters can be derived from simple theory; the numbers obtained can be compared directly with field observations. The absolute approach also requires a rigorous understanding of the actual radiometry of the system and identifies the problem areas that should be addressed in subsequent instrument designs. Three recommendations emerged from the studies: (1) the instrument should be calibrated radiometrically, (2) blocking filters should be included in the optical train to prevent overlapping spectral orders at infrared wavelengths, and (3) wavelength calibration should be done on board to allow channel assignment fixing on a pixel-by-pixel basis for actual flight data.

METHODS OF CALIBRATION

The AIS is an aircraft-mounted system and is thus immersed within the atmosphere. This complication is usually ignored, however, and the radiance I_{ij} seen by the nadir-looking instrument is assumed to be given by

$$I_{ij} = P_{ij} + T_{ij}R_{ij} \qquad (1)$$

where the subscripts refer to image line i and sample j, P_{ij} is the path radiance, T_{ij} is proportional to atmospheric transmittance of diffuse downward plus direct components, and R_{ij} is the surface Lambertian reflectance. All quantities in Eq. (1) are functions of wavelength and, in the most general case, position. If the atmosphere is assumed to be horizontally homogeneous and the elevation variation over the site "small," then the path radiance and transmittance functions can be taken independently of position (equal, say, to P and T, respectively), and Eq. (1) takes the form

$$I_{ij} = P + TR_{ij} \qquad (2)$$

At infrared wavelengths 1200 nm and beyond, the path radiance is often negligible, and Eq. (2) reduces approximately to $I_{ij} = TR_{ij}$.

Probably the simplest method of estimating the function T at each wavelength, requiring only manipulation of the image data themselves, is to form the average of I_{ij} over portions of the scene to secure $\bar{I} = TR$, where

$$\bar{I} = \left(\sum_{i=1}^{M} \sum_{j=1}^{N} I_{ij} \right) / MN \qquad (3)$$

(and a similar definition for $\bar{R}$) in which M is the number of lines and N is the number of samples. Thus

$$I_{ij}/\bar{I} = R_{ij}/\bar{R} \qquad (4)$$

and estimates of the surface reflectance are obtained independently of the transmittance T and scaled according to the average reflectance $\bar{R}$. For Thematic Mapper (TM) data, the average reflectance is not independent of wavelength, even when averages are taken over millions of pixels. However, the ratio in Eq. (4) may still be useful for isolating specific features in R_{ij} apart from the atmosphere. The question of structure in such reflectance averages needs to be investigated at a spectral resolution of 10 nm. Solomon (1984) and Green and Craig (1985) have discussed atmospheric corrections based on the scene average method.

Notice in the above discussion that radiances rather than scanner response (digital number or DN) have been used. For a sufficiently small range of input energy, the instrument response is nearly a linear function of input energy (see below), i.e., DN = A + BI, where A is the dark current response and B is a gain factor, both of which vary from detector to detector. The constants A and B are determined observationally, and the dark current response is corrected for in the raw data. If the constants B are assumed to be approximately equal for all detectors, then forming the ratio in Eq. (4) roughly compensates for instrumental response as well.

When it is possible to employ field measurements of surface reflectance, regression plots of the reflectance vs scanner response can be used on a strictly empirical basis to recover ground reflectance. This method has often been used and is discussed by Conel et al. (1985, 1986) and Paylor et al. (1985) for Landsat IV observations. An example of such plots for AIS data over the Mono Lake test site, California (Conel, 1985), is shown in Figure 1. If scanner counts are converted to radiance using radiometric calibration data, then slope and intercept values obtained from the regression lines provide numerical values for the path radiance and transmittance functions. These functions can then be solved on simple atmospheric models to provide estimates of atmospheric optical depth and single scattering albedo (Conel et al., 1986; Paylor et al., 1985).

The principal assumption involved in applying Eq. (1) to the problems discussed is that the radiances I_{ij} are actually derivable from the AIS measurements. The subsequent discussion examines this problem.

SUMMARY OF RADIOMETRIC CALIBRATION PROCEDURE FOR AIS

The AIS calibration (Tucker, 1984) is performed with a standard laboratory flat-field illumination source (light cannon) whose spectral radiance is measured between 750 and 2500 nm with an Optronics Laboratories spectroradiometer. The spectroradiometer is, in turn, calibrated with a National Bureau of Standards standard irradiance source. The AIS, mounted in a temperature-controlled chamber, is calibrated at operating temperature. The standard source, reflected in a mirror, is
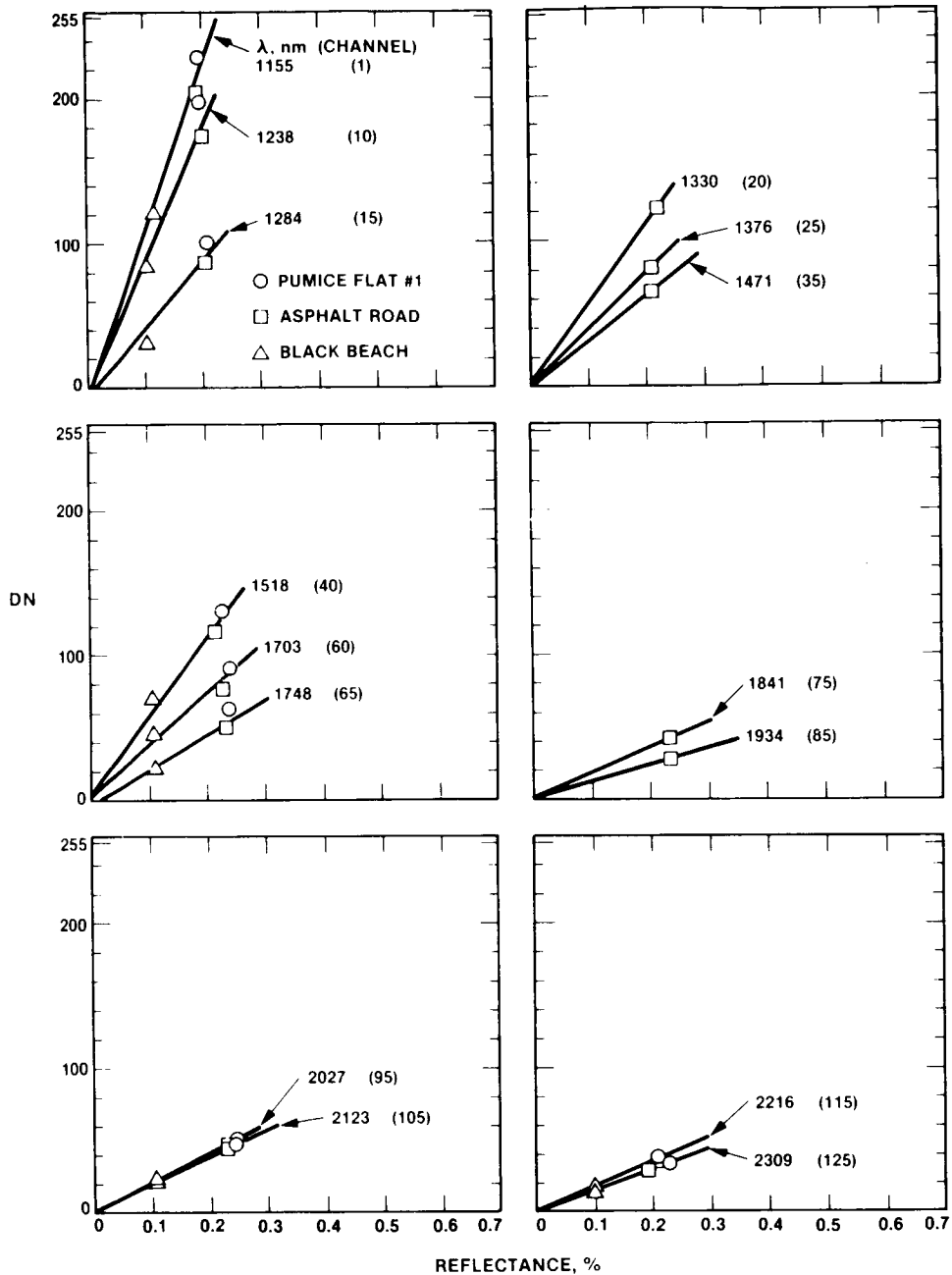
Fig. 1.   Examples of empirical calibration curves for the Mono Lake
test site, October 31, 1984. All lines pass through the ori-
gin consistent with observation of zero radiance (to at least
one part in 4100) over Mono Lake where surface reflectance is
zero.

viewed through a neutral density filter (transmittance = 0.32 to 0.35
over the spectral interval 900 to 2500 nm). An iris diaphram mounted
internally to the light cannon provides variable illumination to the
instrument and is used to construct curves of the instrument response
as a function of illumination.   There are 4096 instrument response
curves, each curve representing one 32 x 32 array detector in each of

four grating positions. Examples of such light transfer curves are shown in Figure 2, in which raw instrument output in digital counts is plotted as a function of the fraction of maximum light cannon energy at each wavelength. In all cases, the instrument dark current response is

FRACTION OF MAXIMUM LIGHT CANNON RADIANCE
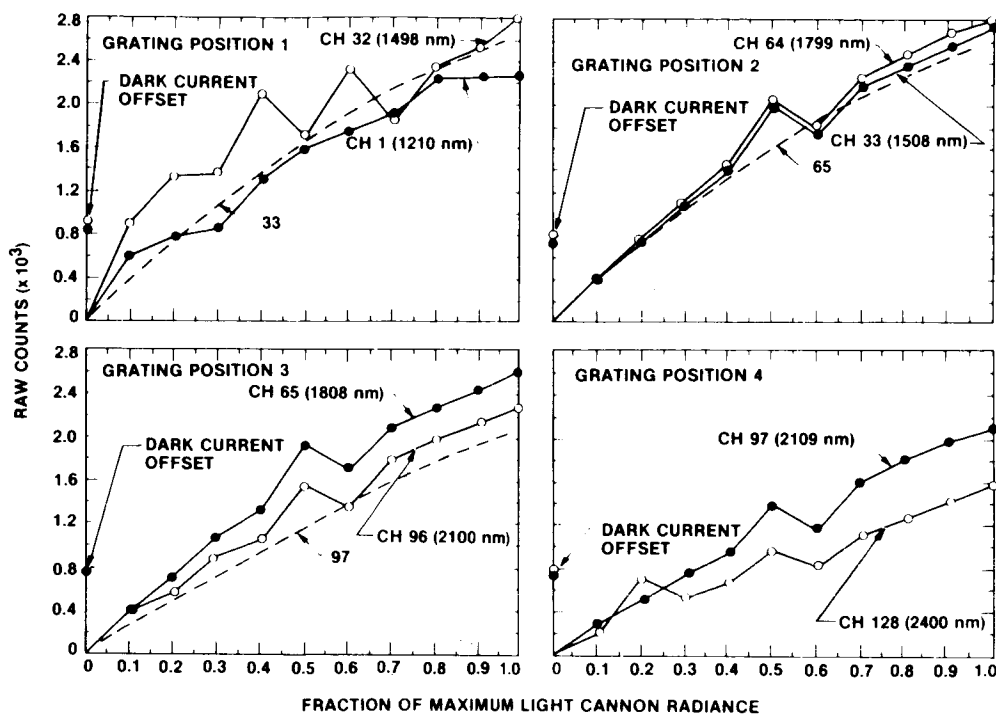
Fig. 2. Examples of relative calibration curves used for conversion of raw digital counts to radiance. Dashed lines in panels for grating positions 1, 2, and 3 represent response of next highest channel.

indicated on the ordinate of each graph and has been subtracted from the output at each iris setting. These light transfer curves (obtained on October 11, 1984) were accepted as representing the radiometric response of the AIS for the data subsequently acquired on October 31, 1984. These calibration data show several important characteristics:

(1) Except for grating position 2, the instrument response varies with the channel. For example, in grating position 1 the response of channel 1 is reasonably smooth, but in channel 32 grating position 1 assumes a jagged sawtooth shape for ordinate values greater than about 1300 counts (500 raw counts is equivalent to approximately 10% ground reflectance over the wavelength interval represented).

(2) For all grating positions, the response demonstrates a sawtooth variation in the abscissa interval 0.4 to 0.7. This behavior may represent missettings of the iris diaphragm rather than mechanical malfunction of the instrument. Except for channels in grating position 1, a smooth extrapolation of the curves over the interval would seem justified.

35

(3)   The instrument response varies abruptly between channel 32 (last channel of grating position 1) and channel 33 (first channel of grating position 2). This behavior has peculiar consequences. Converting spectra from raw counts to radiance introduces a discontinuity in the radiance spectrum at that wavelength representing the boundary between grating positions 1 and 2.

(4)   The instrument response in grating position 1--representing the highest radiance values--is nonlinear.

CONVERSION OF THE RAW COUNT SPECTRUM TO RADIANCE

Mono Lake, in eastern central California, is a large, saline water body whose northern shoreline is a series of wide, uniformly bright and dark contiguous beaches composed of evaporite deposits (trona) and basaltic lag gravel. The basaltic gravels are almost completely barren of vegetation. The spectral reflectance (10 to 15%) is a monotonous, nearly constant function of wavelength in the visible and near infrared. Except where these beach deposits are wetted by springs, absorption bands near 1400 and 1900 nm (representative of OH or HOH) are absent. Both wet and dry gravel beach sites were studied. Detailed computations for a wet beach are presented here. A dry beach example is shown in a LOWTRAN atmospheric simulation described below. Figure 3 gives the raw count spectrum of the wet beach target as a function of channel number. Intervals corresponding to each grating position are indicated. The conversion from raw counts to radiance was accomplished by hand on a point-by-point basis using the instrument response curves
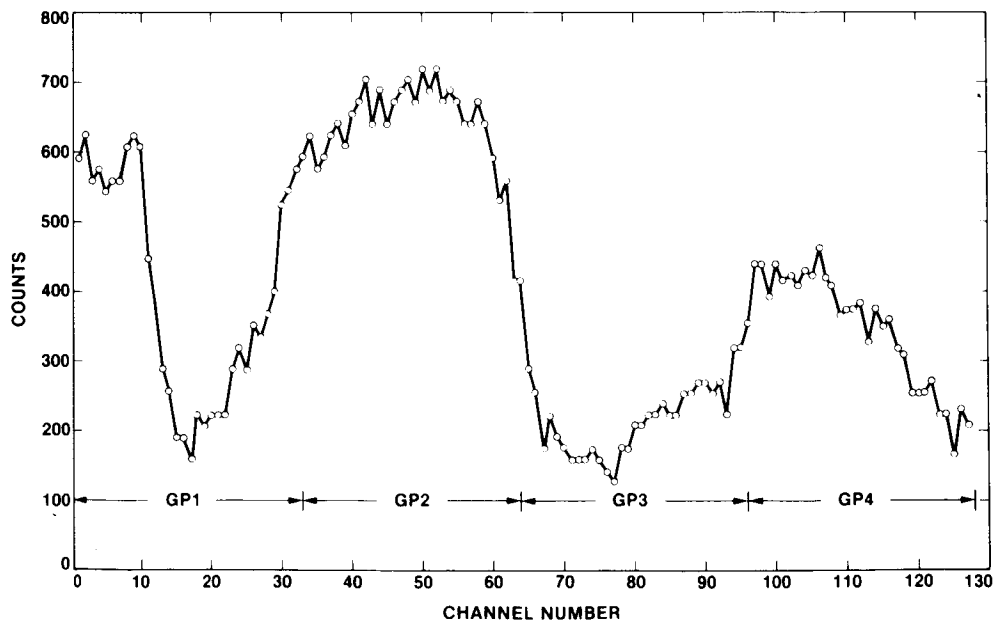
Fig. 3.   Raw count spectrum of (wet) black beach #1 site, Mono Lake, for October 31, 1984.

36

and light cannon radiance values from the October 11, 1984 calibration run. The result of this conversion is shown in Figure 4, where, as described above, the transformation to radiance units introduces a prominent discontinuity between grating positions 1 and 2. An addi-
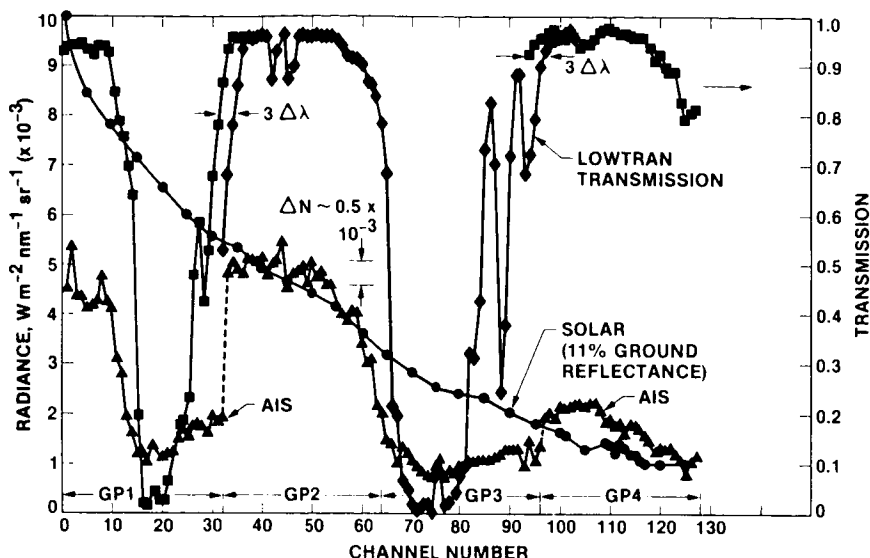
Fig. 4. The "absolute" radiance spectrum of black beach #1 site derived from the raw count spectrum of Figure 3, using laboratory-determined light transfer calibration equations and measured light cannon spectral radiance distribution. The spectrum is calibrated in wavelength by comparison with LOWTRAN transmission spectrum of the atmosphere and is compared to the solar energy expected for zero air mass, solar elevation of 33 deg, and surface reflectance of 11%, as determined by field observation. Solar irradiance data from Arvesen et al. (1969).

tional small discontinuity also appears between grating positions 3 and 4, corresponding to a difference in slope between the light transfer curves of channels 96 and 97. These discontinuities provide evidence that the radiometric calibration is imperfect. The noise level in the data is estimated to be 0.0005 $Wm^{-2}nm^{-1}sr^{-1}$ for a signal/noise ratio of approximately 10 on a single pixel basis.

To provide a wavelength calibration for this spectrum, a LOWTRAN 6 simulation of the one-way atmospheric transmission spectrum for the standard mid-latitude winter model was used, degraded to the spectral resolution of the AIS. Matching the AIS and LOWTRAN spectra on a wavelength basis is uncertain because of noise in the AIS data, but sufficient spectral features representing prominent carbon dioxide and water absorptions were present and recognizable to secure a tentative match. Reconciling the wavelength positions between AIS and the LOWTRAN spectra required shifting the spectrum of the second grating position three resolution elements to a shorter wavelength with respect to the first position. A similar displacement was required for the fourth grating position with respect to the third. The assignment of wavelength to channel number for these flight data is thus secured by reference to the LOWTRAN spectrum.

To provide a tentative check on the absolute energy scale obtained from the laboratory calibration, a comparison was made between the AIS spectrum and the solar spectrum expected for zero air mass after reflection from the surface. The expected solar radiance is $I_{\odot} = F_{\odot}\mu_0 R$ where $\pi F_{\odot}$ is the solar irradiance, μ_0 is the cosine of the solar zenith angle (57 degrees for the October 31, 1984 observations), and R is the surface reflectance. The seasonally adjusted solar curve for measured average 11% ground reflectance is shown as solid circles in Figure 4, where the solar irradiance data of Arvesen et al. (1969) have been used. The apparent agreement between these energy scales is good; in fact, a match between the spectra at 1592 nm in grating position 2 (where the atmospheric transmittance reaches 96% for the real atmosphere) can be achieved by changing the ground reflectance to 12%, an upward adjustment in the surface-measured value of 1%, i.e., 10% of itself.

While good agreement can apparently be achieved between energy scales for the AIS and solar spectra in grating positions 2 and 3, important discrepancies remain. The most significant is in grating position 1, illustrated in Figure 5. Agreement between the AIS and
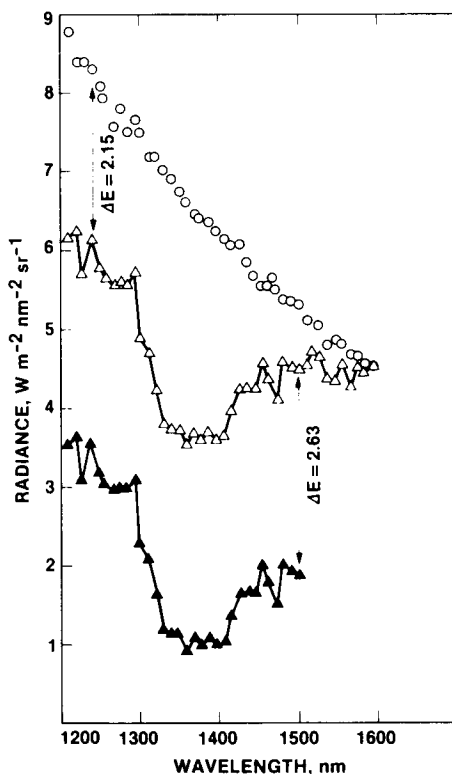
Fig. 5. The apparent spectrum of 1400-nm water band in grating position 1 for black beach #1 site. Solid triangles represent spectrum calculated from the instrument light transfer curves and light cannon spectral radiance data. Open triangles represent arbitrary upward adjustment of 2.62 radiance units to obtain continuity between spectral segments of the first and second grating positions. Open circles represent solar spectrum for 12% ground reflectance. Solar irradiance data from Arvesen et al. (1969).

38

solar scales can be obtained by arbitrarily adjusting the AIS curve upward in one of two ways. In the first method, the scale is translated vertically by adding 2.6 $Wm^{-2}nm^{-1}sr^{-1}$ to the AIS spectrum, thereby producing continuity between grating positions 2 and 3. This leaves a discrepancy of 2.15 $Wm^{-2}nm^{-1}sr^{-1}$ between the solar and measured spectra at 1245 nm where the atmospheric transmission is also high (approximately 94%). In the second method, the AIS and solar spectra are made approximately equal at 1245 nm by adding 2.15 $Wm^{-2}nm^{-1}sr^{-1}$ to the scale. This produces an AIS spectrum protruding above the solar spectrum for wavelengths longer than approximately 1425 nm. These discrepancies are not removed by assuming a shift of the spectrum between grating positions in the steeply rising wing of the water band because a horizontal translation of the AIS spectrum by a few resolution elements is insufficient to produce agreement with the solar radiance curve in the 1245-nm region. These two sets of results in the first grating position appear to be irreconcilable and the responsivity equations evolved by the laboratory calibration must be in error.

LOWTRAN SIMULATIONS WITH THE 1900-nm WATER BAND

Despite uncertainties in the accuracy of radiance values generated using the suspect responsivities and in the wavelength calibration of these spectra, the agreement between calculated curves and the solar spectral radiance scale encouraged us to compare the precipitable water and carbon dioxide estimates based on AIS data and those described by the LOWTRAN atmospheric model. If a close match between aircraft-observed and model spectra could be achieved, a simple way of eliminating atmospheric absorption effects from the observed spectra might be available.

We initially worked with the standard LOWTRAN mid-latitude winter model, specified for the October 31, 1984 overflight conditions. These calculations were carried out in two steps. First, the solar radiance incident on the surface of the Mono Lake beach site at an elevation of 2 km was computed for the day and solar elevation. Second, the zenith-directed radiance reflected from the surface and arriving at the instrument (elevation 7.62 km) was computed. The observed AIS spectrum from a dry basaltic beach gravel (black beach #3 site) was used for the comparison. Results of the simulations are shown in Figure 6. The top panel (Figure 6a) shows that the standard model, which is estimated to contain 0.74 cm of precipitable water (see Figure 5-13 of LaRocca, 1978), produces total absorption in the band center. The prominent carbon dioxide bands near 1960 and 2000 nm are unobserved in the AIS data. An approximate match in band depth between model and observation in Figure 6(b) was produced by decreasing the path-precipitable water by a factor of 20 (0.037 pr cm). However, the reduction in water absorption produces a distinct gap between these spectra in the 1750- and 1830-nm interval and increased the prominent carbon dioxide bands. Altogether the fit is considered unsatisfactory, and the amount of water absorber required in the reduced model seems physically unrealistic.
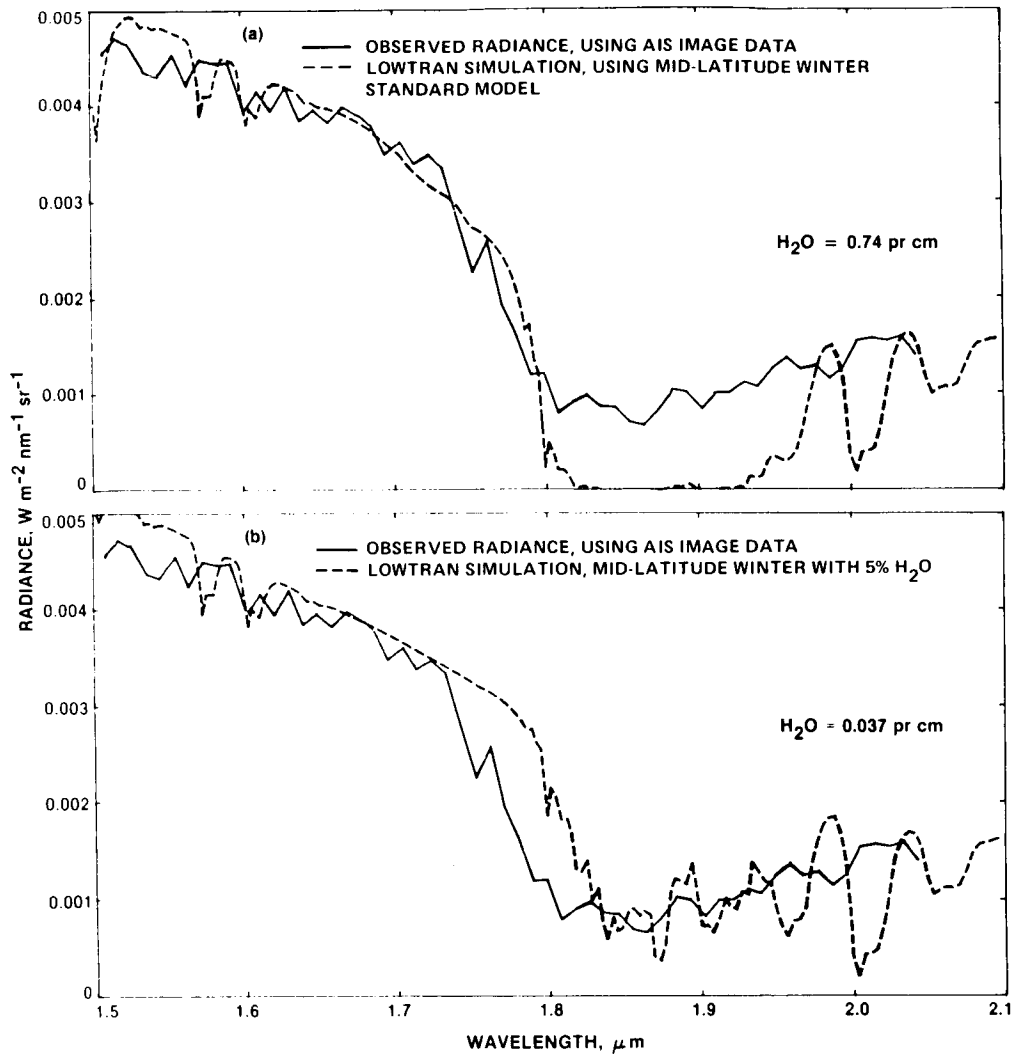
Fig. 6. Observed AIS radiance for the dry black beach #3 site with radiance from LOWTRAN simulation: (a) for the standard mid-latitude winter model; (b) for 5% of the precipitable water present in the standard mid-latitude winter model.

This observation leads us to suspect the existence of spectral contamination. Loss of contrast in the water absorption bands could be caused by mixing or smearing one part of the spectrum with another. This could arise (1) from light scattering by the grating, (2) from light leaks in the spectrometer, or (3) in mixing between the different orders of diffraction by the grating. Below we investigate item (3). For items (1) and (2), independent investigations will be required. Thus, scattering by the grating results from random surface irregularities introduced in the ruling process. This contributes to a broadening of the instrument profile (Dravins, 1978), a filling in of spectral lines, and a lowering of the adjacent continuum. Quantitative evaluation of this possibility, which would be expected to operate across all of the observed spectrum, must await measurements of line broadening on the actual grating used.

40

INFLUENCE OF OVERLAPPING ORDERS IN THE DIFFRACTION GRATING SPECTRA

The problem of overlapping orders is present in the AIS spectral data of grating positions 2, 3, and 4 because the blocking filter used transmits all light with wavelengths longer than about 800 nm. For example, if light of two different wavelengths λ_1 and λ_2 is incident normally upon a grating, the angles corresponding to the principal maxima of diffraction are given by

$$\sin \Theta_1 = m\lambda_1/2d$$

and   (5)

$$\sin \Theta_2 = m\lambda_2/2d$$

where Θ_1 corresponds to the m-th principal maximum for λ_1 and Θ_2 to the corresponding maximum for λ_2 (Ditchburn, 1958). Factor d is grating groove spacing. This equation indicates that the spectra of various orders overlap wherever

$$m_1\lambda_1 = m_2\lambda_2$$ (6)

where m_1 and m_2 are integers. Thus, for example, light of 1800 nm in the first order is diffracted at the same angle as light of 900 nm in the second order. To secure separation of various orders, blocking filters are customarily used to restrict the range of wavelengths received by the instrument. To estimate the possible radiometric and spectral consequences of such spectral order overlapping, grating efficiency calculations using scalar diffraction theory (Madden and Strong, 1958, in Strong, 1958; Bottma, 1981) have been performed for the AIS grating parameters and angles of incidence appropriate for each grating position (Vane et al., 1983). The efficiencies as a function of wavelength for the first and second orders according to these two approximations are given in Figure 7. Both treatments give similar results, but the Madden-Strong efficiencies are in general greater. The effective blaze wavelength where grating efficiency is maximum is 1580 nm by the Madden-Strong formula and 1570+ nm by the Bottma approximation. Both values agree with that given in Vane et al. (1983). In addition, the grating efficiency in the first order is roughly 50% of the maximum at wavelengths of 2/3 and 3/2 of the blaze wavelength, corresponding to a rule of thumb for blazed gratings (Loewen, 1980). Particularly significant is the fact that the calculated efficiency of the grating for the second order is comparable to that for the first in the critical spectral region.

The Madden-Strong efficiency calculations have been used together with the blocking filter transmission function and LOWTRAN simulations of incident irradiance appropriate to the Mono Lake experiment to compute theoretical spectra expected as a consequence of overlapping orders. Experimental tests using the standard light cannon source and special filters have been made in a further attempt to isolate possible effects arising from this source.

The theoretical spectra are computed approximately by assuming (for given instrument throughput) that the energy arriving at the detector

41
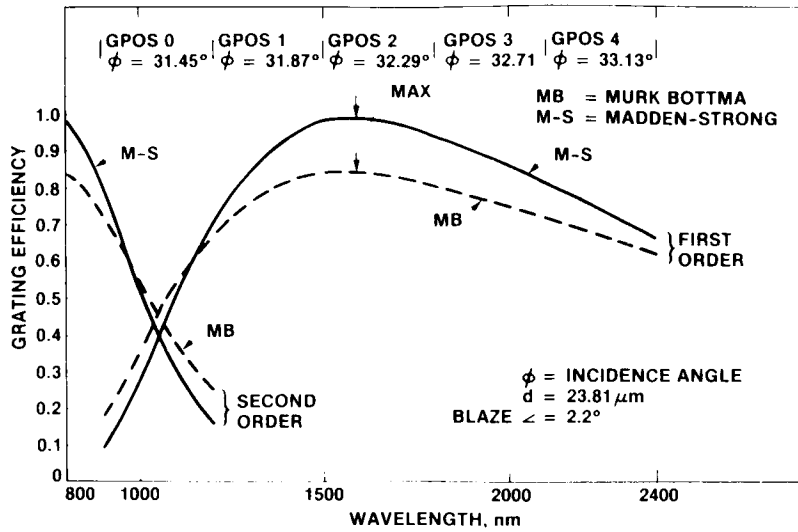
Fig. 7.   Grating efficiencies for first and second orders calculated
          by the Madden–Strong (1958) and Bottma (1981) approxi-
          mations.   Groove spacing = 23.81 μm, blaze angle = 2.2 deg,
          effective blaze wavelength = 1.58 μm (Vane et al., 1983).

at a given diffraction angle consists of contributions from the first-
and second–order diffracted light. Analytically this is

$$Counts = KA\Omega r_s [I(\lambda)T(\lambda)E(\lambda)Q(\lambda)d\lambda$$

$$+ I(\lambda/2)T(\lambda/2)E(\lambda/2)Q(\lambda/2)d(\lambda/2)] \tag{7}$$

where

A	=	area of the entrance aperture
Ω	=	solid angle of detector subtended at the grating
$I(\lambda)$	=	radiance incident at wavelength λ in order one
$I(\lambda/2)$	=	radiance incident at wavelength λ in order two
$T(\lambda)$	=	transmission of blocking filter at wavelength in order one
$E(\lambda)$	=	efficiency of the grating at wavelength in order one
$d\lambda$	=	spectral width of the sample
K	=	proportionality constant between energy input and digital counts
r_s	=	lumped reflection coefficient for optical elements, assumed independent of wavelength
$Q(\lambda)$	=	quantum efficiency of HgCdTe detector wavelength λ

In Eq. (7), as indicated in the definitions, the designation $\lambda/2$ refers to an appropriate quantity in the second order. From the grating equation, the relationship between $d\lambda$ and the spectral order is given by

$$md\lambda = \cos \psi d\psi \qquad (8)$$

where ψ is the angle of diffraction. Since ψ and $d\psi$ remain fixed between orders, the spectral sample width in the second order ($m = 2$), $d(\lambda/2)$ is equal to $d\lambda/2$, i.e., one-half the spectral sample width in the first order.

The average function $Q(\lambda)$ over a 64 x 64 HgCdTe detector array has been used in the calculations since no measurements were available of the quantum efficiency for the actual AIS detector used. This function was measured at discrete wavelengths using broad passband filters (V. Wright, personal communication, 1986) and is shown in Figure 8. For purposes of calculation, a linear variation of Q with wavelength has been assumed.
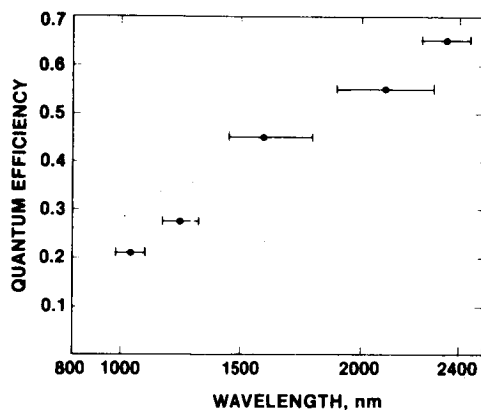
Fig. 8. Quantum efficiency of HgCdTe detector IS #17 used in second-generation AIS, representing average value over the 64 x 64 detector array. Horizontal bars represent filter passbands. Data courtesy of V. Wright (April 1986).

The relative contributions of the first order and the first order + second order spectra based on Eq. (7) for the LOWTRAN simulation are given in Figure 9 and are compared there to a plot of the actual incident irradiance. The influence of any second-order contribution to the spectrum is sharply limited to wavelengths beyond 1600 nm by the presence of the blocking filter. An additional interesting consequence of the overlap is the appearance in the center of the 1900-nm water band of another atmospheric water absorption feature actually located at 950 nm. The water band at 1125 nm appears in the unblocked spectrum at 2250 nm. None of the original atmospheric bands present between 1600 and 2400 nm are filled in by the presence of second-order light. These and later calculations show the second-order contribution at its extreme because the efficiency calculations assume an ideal grating whose properties are probably not matched in practice.

To investigate further the overlap problem, calibration experiments were performed with the light cannon using a test filter, the transmis-

43
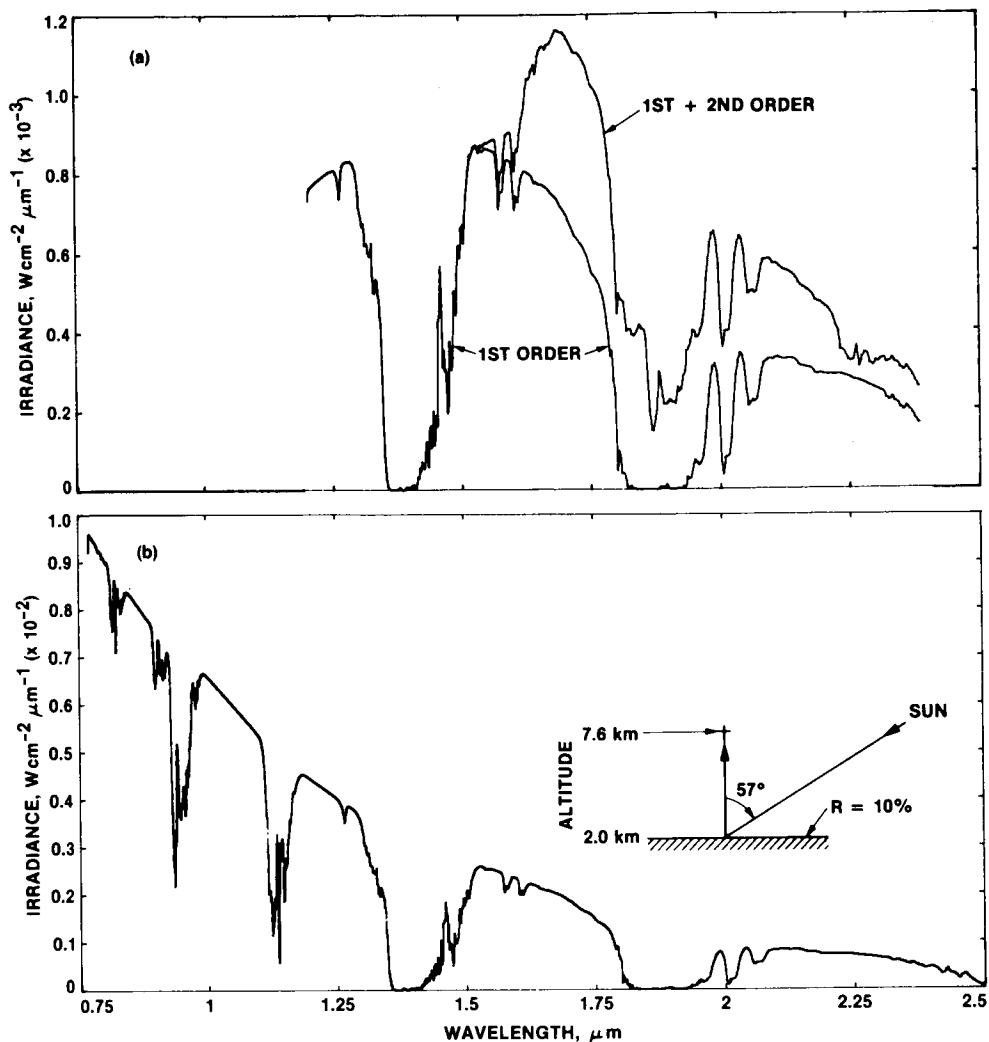
Fig. 9.   Results of LOWTRAN calculations: (a) computed AIS spectra
for mid-latitude winter model and incident irradiance of
(b).   Top curve represents contributions of first +
second-order spectra, bottom curve represents first-order-
alone spectrum; (b) solar irradiance incidence at the AIS
from the October 31, 1984 Mono Lake simulation.

sion function of which is given in Figure 10.   The maximum transmission
is almost 80% at 900 nm and falls abruptly to 5% at 1200 nm.   The
throughput is constant to 1800 nm, and thereafter rises almost linearly
to 55% at 2400 nm.   This filter does not isolate completely the first-
from second-order spectral contributions; however, the falloff of light
cannon energy with wavelength is sufficiently steep so that the con-
tribution of first-order light through the filter beyond 2000 nm is
small compared with that from the second-order light originating from
the spectral region short of 1200 nm.   The test for second-order light
is decisive, despite this contamination.   The assumed light cannon
irradiance distribution is shown in Figure 11.

44
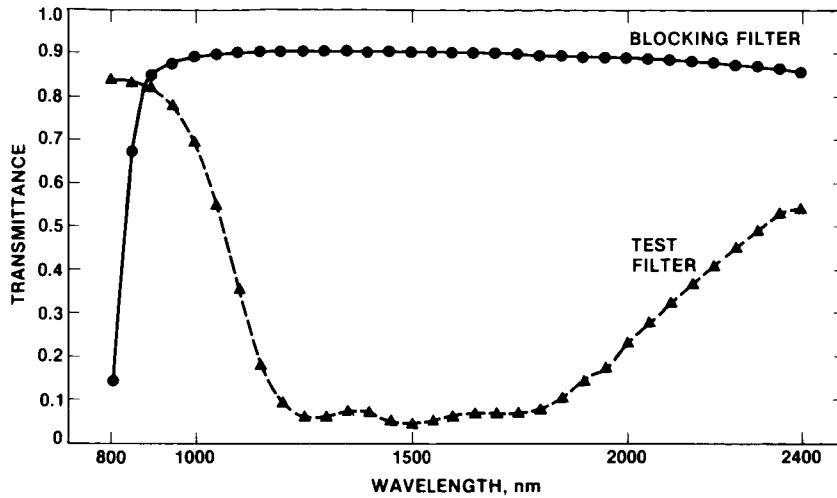
Fig. 10. Transmittances of the AIS blocking and test filters.
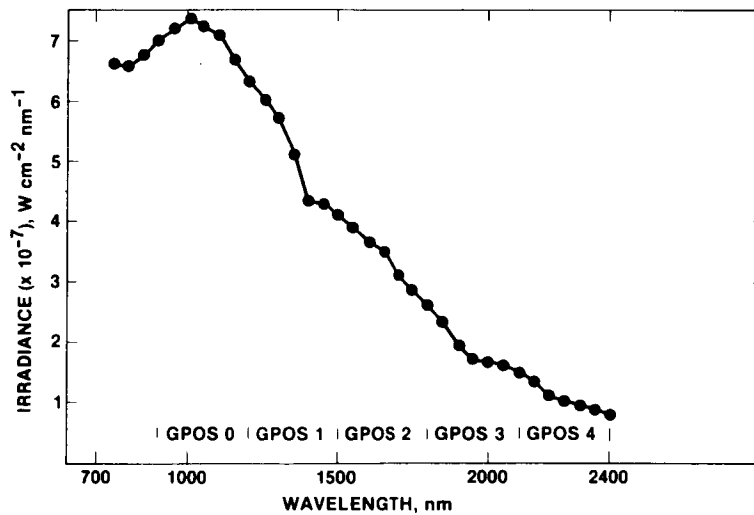
Fig. 11. Assumed light cannon spectral irradiance distribution.

The computed relationships are shown in Figure 12 where the irradiance expected for first order and for first + second-order contributions are depicted separately. As before, the spectral intervals represented by the zeroth and first grating positions (900 to 1500 nm) are uncontaminated by higher orders. The first-order spectrum alone contains peaks at 1050, 1350, and 1650 nm, and rises slowly to a plateau between 2100 and 2400 nm, with a small minimum at 2200 nm. All of these features result from the test filter transmittance or from the light cannon spectral radiance distribution. The calculated first + second-order spectrum is identical to that of the first-order spectrum alone below 1500 nm, but rises beyond that wavelength to a plateau between 1700 and 2000 nm. Thereafter, the combined spectrum falls to a value near the first order by itself at 2400 nm. The combined spectrum is roughly three times that of the first order alone, and the peak radiance at 1900 nm is 30% or so greater than that at 1050 nm.
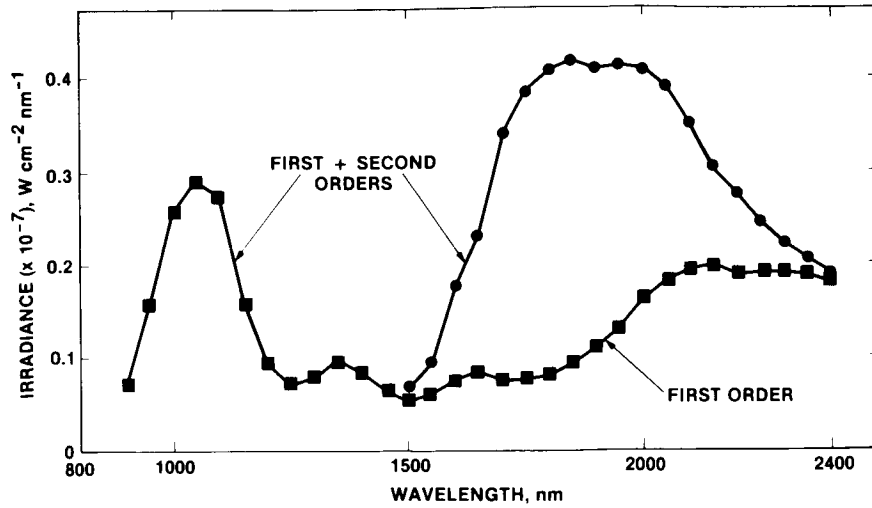
Fig. 12. Calculated spectra for first-order-alone and first + second-order contributions for the test filter transmittance of Figure 10, and the light cannon spectral irradiance distribution of Figure 11.

The experimentally determined AIS response for the test filter and light cannon source averaged over all detectors is given in Figure 13. This spectrum has broad peaks near 1000, 1350, 1800, 2000, and 2250 nm, and sharp peaks at both ends and near the midpoint of the spectral range for each grating position. In grating position 2, the observed spectrum rises beyond 1500 nm through the series of broad and sharp peaks mentioned. The broad maximum centered near 2000 nm is equivalent in height to that at 1000 nm.
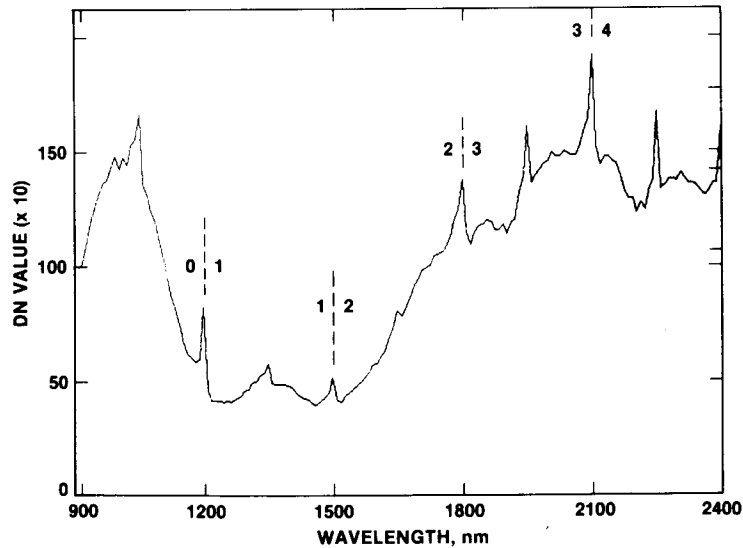
Fig. 13. Raw AIS spectrum obtained for light cannon illumination and the test filter of Figure 10. Sharp peaks indicate boundaries of spectral regions for various grating positions. Wavelength scale is approximate.

To facilitate comparison between the calculated and measured results, these spectra are compared in Figure 14 by normalizing the two at the maximum near 1000 nm. This also required a 36-nm shift in the
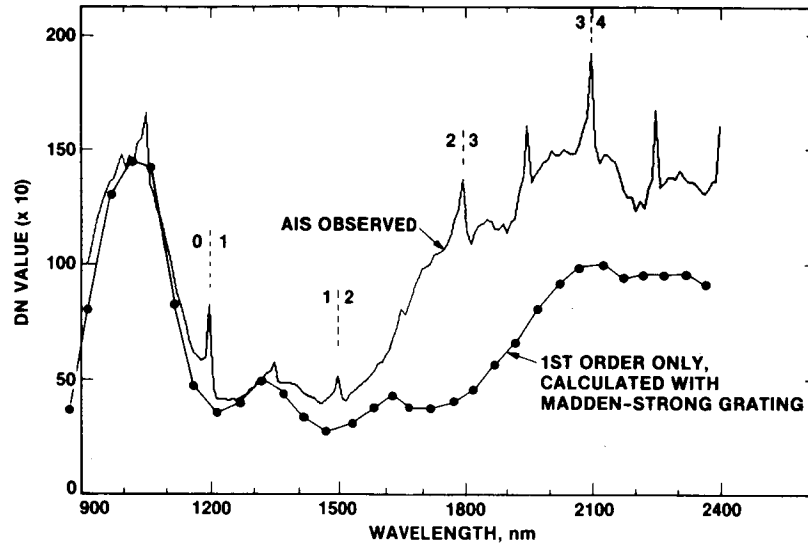
Fig. 14. Comparison of measured and calculated AIS spectra for test filter with light cannon illumination. Spectra are normalized at the maximum near 1000 nm, and the calculated curve shifted 36 nm to the secure agreement of the wavelength scales.

computed curve to shorter wavelengths. The agreement between these two results is good out to 1600 nm, at which point the experimental curve assumes 50 to 100% higher values than the observed one, which is the result expected from the contamination. The calculated curve is an optimum case because the grating efficiency assumed is the maximum efficiency expected. Since the real grating has a lower efficiency, using its values would lower the first-order-alone curve relative to the first + second-order curve. Thus, the contamination is probably greater in magnitude than depicted here. Better comparisons between calculated and measured results will be possible when the calculations are carried out using efficiencies for the actual grating and detector used.

ANALYSIS OF INSTRUMENT RESPONSE CURVES

The AIS response curves, examples of which are given in Figure 2, plot scanner response in digital counts vs the fraction of light cannon radiance present at a given wavelength in each resolution element. As part of the radiometric adjustment of these data to remove variations in responsivity between detectors, a flat-field normalization derived from assumed uniform illumination of the detector array is applied; the responsivity values for detectors in the spatial direction are all rescaled to a constant value, and the wavelength direction is rescaled according to the wavelength distribution of light cannon radiance (Science Investigators Guide to AIS data, 1985). For example, if the value

of light cannon spectral radiance in the first channel (λ_1) is arbitrarily assigned the value 2500 digital counts, the spectral radiance in the n-th channel is $2500[L(\lambda_n)/L(\lambda_1)]$, where $L(\lambda)$ represents light cannon irradiance. For the next two channels the values obtained are $2500 \times 0.987 = 2468$ (λ_2) and $2500 \times 0.977 = 2422$ (λ_3) and so on. If the AIS system is linear, the responsivity $\Gamma(\lambda)$ is defined by the equation

$$V(\lambda) = \Gamma(\lambda)I(\lambda) \tag{9}$$

where $V(\lambda)$ is instrument output in counts (or volts) and $I(\lambda)$ is the incident radiance. The responsivity can be determined from one light cannon observation, which is assumed to be bright enough to encompass the entire range expected from natural targets. Γ is then determined from

$$\Gamma = V_{max}/I_{max} \tag{10}$$

where the subscript max indicates light cannon values. The value of Γ adjusted for the relative spectral radiance of the light cannon is

$$\Gamma_{adj} = \{2500(V_{max}/I_{max})[L(\lambda)/L(\lambda_1)]\} \tag{11}$$

The normalized instrumental output is

$$V_{adj} = \Gamma'_{adj}[I(\lambda)/I_{max}(\lambda)] \tag{12}$$

where $\Gamma'_{adj} = \Gamma_{adj}I_{max}(\lambda)$. The calibration data of Figure 2 are plotted according to Eq. (12). As indicated in Eq. (7), the responsivity $\Gamma(\lambda)$ is proportional to $T(\lambda)E(\lambda)Q(\lambda)$. $T(\lambda)$ and $E(\lambda)$ are roughly comparable between orders, while $Q(\lambda)$ varies by a factor of seven between 800 and 2400 nm. The dominant variation in Γ is thus from the variation in $Q(\lambda)$.

In grating position 2 where second-order diffracted energy is present, the expression 2 takes on the more complicated form

$$V(\lambda) = \Gamma(\lambda)I(\lambda) + \Gamma(\lambda/2)I(\lambda/2) \tag{13}$$

and the incident flux is comprised of two components $I(\lambda) + I(\lambda/2)$, where the magnitude of these two terms is comparable. If the system response were linear, it would again be given by an equation like (9), but in this instance with an apparent value of the responsivity Γ_* given by

$$\Gamma_*(\lambda) = \Gamma(\lambda)I(\lambda)/[I(\lambda) + I(\lambda/2)] + \Gamma(\lambda/2)I(\lambda/2)/[I(\lambda) + I(\lambda/2)] \tag{14}$$

a weighted sum of first- and second-order contributions. The functional dependence of Γ with λ, described above, determines that in general $\Gamma_* < \Gamma$. An apparent decrease in responsivity between first and second grating positions would be sufficient to introduce discontinuities into radiance curves produced from raw count spectra if such spectra were themselves continuous between grating positions.

In addition, a subtler problem must also exist with the calibration curves of Figure 2 themselves. Consider the curves for channels 1 and

32 (first grating position). The relative falloff in light cannon radiance between channels 1 and 32 is $1 - 1648/2500 = 0.34$, but the relative response of channel 32 is 20% higher, not lower, than for channel 1. The correct relative relationship is shown for the same detectors in grating positions 3 and 4. For grating position 2, the response curves are essentially the same. This reversal of position cannot therefore arise from nonuniformity of illumination during the tests or from spurious detector response. Without further details of the test procedure, it is difficult to provide an explanation.

We conclude that the spectral discontinuities observed arise from abrupt jumps in the apparent response between grating positions 1 and 2. This behavior can result from the presence of contamination by second-order light in the second grating position (not a good explanation between 1500 and 1600 nm) or from a spurious calibration test. All of these puzzling details must be resolved before the AIS calibration can be understood.

COMPENSATION FOR SPECTRAL CONTAMINATION FROM THE SECOND-ORDER DIFFRACTION

The AIS atmospheric compensation procedures described earlier all require explicit measurement of the radiances I_{ij} of Eq. (1). If second-order diffracted energy is present in the spectrum, then the instrumental radiance measured is comprised of two terms I_{ij}' and I_{ij}'', representing the first- and second-order contributions. These separate terms each represent atmospheric and surface contributions at λ and $\lambda/2$ approximately in accordance with Eqs. (1) or (2), combined according to Eq. 7. Thus, to remove the second-order contribution, and assuming the relevant instrumental characteristics are known, the surface and atmospheric properties between 800 and 1200 nm are required. In the short wavelength mode of scanner operation (the tree mode), the uncontaminated spectrum between 900 and 1200 nm is taken, and corrections to the longer wavelength (1800 nm and beyond) may be possible. In the long wavelength mode (the rock mode), the spectral interval of observation is 1200 to 2400 nm, and no rigorous correction of the longer wavelength data is possible.

SUMMARY AND DISCUSSION

We studied AIS data for a few pixels from the Mono Lake test site in California in order to establish the absolute spectral radiance of the targets under solar illumination. The ultimate objective of the work is to provide a method of atmospheric correction using the spectral content of the AIS data themselves. We used actual measurements of the surface reflectance to aid in the work. Crucial to this analysis and to other calibration procedures as well is radiometric calibration of the instrument. We studied the calibration procedure and used the response curves provided from laboratory calibrations to calculate "absolute" radiance spectra throughout the 1200- to 2400-nm interval. We find reasonable agreement between the radiance values observed and those calculated for the site assuming zero air mass for the spectral interval 1500 to 2400 nm, but the derived spectrum is 60% or so too low

in the first grating position. Based on the reasonable radiometric comparisons obtained in the 1900-nm region, we used LOWTRAN to simulate the atmospheric transmission observed. In general, the agreement is unsatisfactory. The best match model requires a reduction by a factor of 20 of the precipitable water, which then produces an unsatisfactory match in the 1700-nm wing of the water band. Prominent carbon dioxide absorptions present in the simulation are unobserved in the AIS data. These considerations lead to the study of overlapping spectral orders in the AIS data. The possibility of serious contamination of the first-order spectrum beyond 1600 nm from second-order diffracted light between 800 and 1200 nm is introduced by transmission through the blocking filter, which begins transmission at 800 nm. Lacking actual measurements of the efficiency of the grating used, we calculated efficiencies for the first and second orders of a hypothetical grating with the groove spacing and blaze angle of the actual grating. The efficiencies for first and second order are comparable. Approximate theoretical spectra were calculated using (1) LOWTRAN simulations and (2) laboratory light cannon runs with special filters designed to isolate approximately the 800- to 1220-nm spectral contribution. The LOWTRAN simulations show a strong contribution of second-order light in the first-order spectrum between about 1600 and 2400 nm. In addition to enhanced energy, atmospheric water absorption bands present at 950 and 1125 nm appear in the spectrum at 1900 and 2250 nm. The laboratory light cannon simulation with test filter established the presence of second-order light in the raw spectrum, but unexplained discrepancies remain between the calculated and observed spectra.

The decalibration procedure involving normalization of the raw digital count spectra to the scaled light cannon energy profile may effectively disguise the presence of the second-order energy in all AIS spectral data subjected to this process. The discrepancies may re-emerge only when absolute spectra are calculated using the experimental light transfer curves and may manifest themselves as strong discontinuities particularly between grating positions 1 and 2. The calculated spectra were examined for evidence of the expected extraneous water band contributions, but no such bands have been identified that are distinct from atmospheric or solar absorptions in this region. The lack of discernible bands is not surprising because (1) the prominent atmospheric carbon dioxide bands are somehow suppressed in the data (perhaps by the flat field transform), (2) the signal/noise ratio is low, and (3) the actual wavelength calibration and resolution of the spectra are uncertain.

REFERENCES

Airborne Imaging Spectrometer: Science Investigators Guide to AIS data, 1985, Jet Propulsion Laboratory, Pasadena, CA.

Arvesen, J. C., R. N. Griffin, Jr., B. D. Pearson, Jr., 1969, Determination of extraterrestrial solar spectral irradiance from a research aircraft, Appl. Opt., 8(11), 2215-2232.

Bottma, Murk, 1981, Echelle efficiencies: Theory and experiment: Comment, Appl. Opt., 20(4), 528-529.

Conel, J. E., 1985, Calibration of AIS data using ground-based reflectance measurements (Abstract), Proceedings of the Airborne Imaging Spectrometer Data Analysis Workshop, JPL Publication 85-41, Jet Propulsion Laboratory, Pasadena, CA, 84-85.

Conel, J. E., H. R. Lang, E. D. Paylor, and R. E. Alley, 1985, Preliminary spectral and geologic analysis of Landsat-4 Thematic Mapper Data, Wind River Basin area, Wyoming, IEEE Trans. on Geoscience and Remote Sensing, GE-23(4), 562-573.

Conel, J. E., H. R. Lang, and E. D. Paylor, 1986, Derivation of Surface Reflectance and Atmospheric Properties From Landsat IV Thematic Mapper Data, Jet Propulsion Laboratory, Pasadena, CA (in preparation).

Ditchburn, R. W., 1958, Light, Interscience, New York.

Dravins, D., 1978, High-dispersion astronomical spectroscopy with holographic and ruled diffraction gratings, Appl. Opt., 17(3), 404-414.

Green, A. A., and M. D. Craig, 1985, Analysis of aircraft spectrometer data with logarithmic residuals, Proceedings of the Airborne Imaging Spectrometer Data Analysis Workshop, JPL Publication 85-41, Jet Propulsion Laboratory, Pasadena, CA, 111-119.

LaRocca, A. J., 1978, Atmospheric absorption, Chap. 5, in The Infrared Handbook, W. L. Wolfe and G. J. Zissis, eds., Environmental Research Institute of Michigan, Ann Arbor, MI.

Loewen, E. G., 1980, A review of ruled diffraction gratings, The Industry and Systems Purchasing Directory, 1980, B-327-B-331.

Madden, R. P., and John Strong, 1958, Diffraction gratings, Appendix P, in Strong, J., Concepts of Classical Optics, W. H. Freeman and Co., San Francisco, CA, 597-615.

Paylor, E. D., M. J. Abrams, J. E. Conel, A. B. Kahle, and H. R. Lang, 1985, Performance Evaluation and Geologic Utility of Landsat-4 Thematic Mapper Data, JPL Publication 85-66, Jet Propulsion Laboratory, Pasadena, CA.

Solomon, J. E., 1984, Thoughts on atmospheric "corrections" for AIS imagery, JPL IOM IAS: 384-84-JES102ed (JPL Internal Document), Jet Propulsion Laboratory, Pasadena, CA.

Tucker, D., 1984, AIS calibration report (unpublished JPL Internal Document), Jet Propulsion Laboratory, Pasadena, CA.

Vane, G., A. F. H. Goetz, and J. B. Wellman, 1983, Airborne Imaging Spectrometer: A new tool for remote sensing, Proc. IEEE 1983 Int'l Geoscience and Remote Sensing Symp., IEEE Cat. No. 83CH1837-4, I-1-I-15.

AIRBORNE SPECTRORADIOMETRY : THE APPLICATION OF AIS DATA TO DETECTING SUBTLE MINERAL ABSORPTION FEATURES

TERRY D.COCKS and ANDY A.GREEN, CSIRO DIVISION OF MINERAL PHYSICS AND MINERALOGY, NORTH RYDE, NSW, AUSTRALIA

ABSTRACT

Analysis of AIS data acquired in Australia has revealed a number of operational problems. Horizontal striping in AIS imagery and spectral distortions due to order overlap have been investigated. Horizontal striping, caused by grating position errors can be removed with little or no effect on spectral details. Order overlap remains a problem that seriously compromises identification of subtle mineral absorption features within AIS spectra. A spectrometric model of the AIS has been developed to assist in identifiing spurious spectral features, and will be used in efforts to restore the spectral integrity of the data.

INTRODUCTION

Prior to the AIS mission, some recent research had been conducted into the application of high-spectral-resolution remote sensing in the short-wave infrared (SWIR) to geological remote sensing in Australia. This work showed that, in many cases, mineralogically important absorption features are appreciably weaker in the Australian environment than in the western USA, where the bulk of the AIS data has been acquired to date. The inclusion of the AIS in the C-130 instrument package that came to Australia in October, 1985 provided an opportunity to assess its performance in an environment where weathering and significant vegetation cover place stringent demands on the radiometric sensitivity and spectral integrity of airborne instrumentation.

Over the last four years we have conducted a number of airborne spectroradiometer surveys over selected Australian sites using spectroradiometers from GER (Geophysical Environment Research,Inc New York) and CSIRO. In general, the mineral absorption features used to identify the surface material are not apparent in the raw, surface-radiance spectra. As an example,Figure 1 presents raw radiance spectra (curves A and B) from a flight line at Kambalda, Western Australia, as recorded by the GER spectroradiometer. Here spectra A and B are, respectively, from terrain with little specific mineral content and from terrain containing appreciable amounts of talc . Both curves are dominated by the absorption features of atmospheric water vapour and carbon dioxide, and there is no obvious difference in the radiance spectra.

The inability to distinguish absorption features in

radiance spectra led to the development of the logarithmic residual analysis technique (Green and Craig, 1985).This technique removes multiplicative spectral effects common to the whole flight line (e.g. atmospheric absorption, solar irradiance and detector responsivity), and produces reflectance spectra, that are normalised by the flight line average reflectance spectrum. Figures 1C and 1D illustrate the respective results of a log residual analysis on Figures 1A and 1B, with Figure 1D now showing the talc spectral signature. The log. residual approach has been shown to be a powerful technique for analysis of highly correlated data, such as is normally encountered in the SWIR. The very fact that log residuals successfully isolate subtle absorption features led us rapidly to suspect the spectral integrity of the AIS data, and eventually led us to the second-order overlap problem discussed below. Apart from order overlap, other problems with AIS data include vertical and horizontal image striping, and calibration artifacts. In this paper we limit our discussions to horizontal striping and order overlap. All data presented here were acquired with the AIS operating in the 'rock scan' mode, giving a nominal wavelength range of 1.2-2.4 um.

HORIZONTAL STRIPING -- GRATING WOBBLE

One of the more obvious AIS image defects is horizontal striping. Usually it appears worse at shorter wavelengths; some bands may show little or no striping even under a severe contrast stretch. We suggest that this effect is caused by grating wobble, i.e there exists some random error in the precise location of the grating as it cycles through each of the four positions. Figure 2 (Slide 1) presents the typical appearance of this striping in bands 11 and 29, both within the first grating position. Figure 3 shows a 128-channel spectrum from column 16 of the image. If the grating were positioned such that it diffracted a slightly longer wavelength onto each detector element than it did in the previous cycle, then the signal from channel 11 would be lower and the signal from channel 29 higher than in the previous image line. Thus, we expect the brightness of the stripes in the band 11 and band 29 images to be anti-correlated. This is in fact the case, as shown in Figure 2 (Slide 1). For bands that occur at wavelengths with small spectral radiance gradients, the striping is not so apparent. It also appears as though the striping is worse in the first grating position , probably enhanced by some flyback effect.

The magnitude of the line-to-line grating shift was estimated by fitting a low order polynomial to the cross correlation of successive spectra (limited to channels of the first grating position) for a given cross-track pixel or image column. An example of such estimated shifts for column 8 is shown in Figure 4, where the standard deviation of the

shifts over 400 image lines is 0.65 channels (equivalent to about 6nm). One would also expect the estimated shifts to be independent of the image column selected. Thus the solid dots in Figure 4 show the estimates for column 16. It can be seen that there is excellent correlation with the estimates of column 8,in both magnitude and direction.

The removal of horizontal striping in a manner that took into account its physical cause would involve determining the wavelength shift, at each grating position, for each image line, followed by the required correction obtained from a knowledge of the spectral radiance gradient at each wavelength. As this approach is likely to be very cumbersome we applied a procedure developed to remove aperiodic striping from airborne-line scanner imagery. The correction algorithm, referred to as DMEAN is described by Huntington et. al. (this issue). The procedure has been shown to remove most evidence of horizontal striping without having measureable impact on the spectral integrity of the data. Channel-shift estimation was performed on this corrected data with results shown in Figure 3B. The standard deviation of the estimated shifts in this case was 0.1,a value probably near the limit of resolution for the estimation algorithm. Because horizontal striping is due to a mechanical problem in the AIS, the magnitude of the grating position errors will to some extent depend on the vibration experienced by the aircraft during data acquisition. It may be greater or smaller than the values presented here.

SPECTRAL DISTORTIONS FROM ORDER OVERLAP

Initial analysis of the AIS data involved computing log. residuals on a flight line of 128-channel spectra for a given image column. Figure 5 (Slide 2) presents the results of this analysis. The first column (labelled RADIANCE) is a density-sliced image of the raw radiance spectra,with wavelength increasing left to right from 1.23 um to 2.42 um and flight line spectrum number increasing down the image. Comparison of Figure 5 (Slide 2) and the spectrum of Figure 6 affords ready identification of various spectral regions represented in the spectra images (e.g. the location of atmospheric water vapour and CO_2 bands).A density-sliced representaion of the log. residual spectra appears in column 2 (labelled RAW LR ALL),in which blue represents wavelength regions where the surface reflectance at that part of the flight line is lower than the average flight line reflectance, and vice versa for red. Absorption bands due to a particular mineral usually show up as blue regions located at wavelengths characteristic to that mineral, allowing unique identification of the surface material. The dominant spectral patterns in Figure 5 (Slide 2, column 2) are associated with broad wavelength intervals of the water vapour bands and the atmospheric windows at 1.6 um and 2.2

um. The red or blue colour of the water vapour band is highly correlated with the surface albedo. Few, or no localised, narrow absorption features are apparent in the 2.2 um window, the region of prime interest for geological applications of high-resolution spectroscopy. This atypical behaviour of the log. residual spectra was diagnosed as being due to some unexplained error signal. In the water vapour bands where the signal level is naturally low, such a spurious signal could well predominate, and would cause the log. residuals to behave as in Figure 5. A repetition of the analysis using only channels 1-14, 26-64 and 77-128 (Figure 6, hatched regions) produced log. residual spectra shown in Figure 5, column 3 (labelled RAW LR W). Now the dominance of the water vapour bands has been removed and we begin to see what appear to be more typical mineral absorption bands. One also notices the blue stripes in channels 1-14 and 26-32, caused by the aforementioned grating-wobble-induced horizontal striping. If the log. residuals are computed after destriping by program DMEAN, the striping in the log. residual images effectively disappears without any influence on other spectral features (Figure 5, column 4).

However, two problems still remain in the log. residual spectra. Firstly, we can see evidence of the CO2 bands in the log. residual spectra. Secondly, many of the absorption features occur at wavelengths inconsistent with what is known of the terrain being observed (see Huntington et al.,this issue). Examination of the published AIS optical designs revealed an error in the selection of a cutoff wavelength for the blocking filter, allowing radiation from shorter wavelengths to contaminate the AIS spectra at wavelengths greater than about 1.6 um. Because this shorter wavelength radiation is added into the spectra and varies with the surface reflectance , it cannot be removed by the log. residual process and will generate artificial absorption features.

To estimate the magnitude of the shorter wavelength contamination, we developed a simple spectroradiometric model of the AIS. The grating equation states that, for given angles of incidence and diffraction, radiation is diffracted in the first order at one wavelength, and in the second order at one-half that wavelength. For the grating used in the AIS, the ratio of first to second order diffraction efficiencies is near unity, leading to the possibility of comparable signal levels from both orders. To avoid contamination of the first-order spectrum by second-order (or higher) radiation, one usually incorporates in the optical train a filter that blocks all radiation with wavelengths less than one-half the longest wavelength in the first-order spectrum. For the AIS operating in the 'rock' scan mode, this cutoff wavelength should be near 1.2 um, not 0.8 um as was the case during much of the operational life of AIS to date.

The spectroradiometric model was developed to examine spectral aspects of the AIS, not its absolute radiometry. Hence the detector responsivity has been normalised to unity at 2.4 um, and geometrical factors, such as solid-angle field-of-view have been neglected. Figure 7 shows the spectral details of the solar irradiance (A), atmospheric transmission (B), grating efficiency (C), blocking filter transmission (D) and detector responsivity (E) over wavelengths of the first and second orders. Each pair of curves has been plotted on the same vertical scale to illustrate the relative contributions to the resultant, recorded spectrum. Curves A,B,C,D and E were multiplied and scaled to account for first and second order bandwidths, to produce the AIS spectral response to a 100% reflector (F). The recorded spectrum is then the sum of the first and second order responses as shown in Figure 8. The spectral distortion predicted with this model can be seen to be significant for all wavelengths greater than 1.6 um. Contaminated spectra can be easily recognised by the filling in of the 1.9 um water band, a step-like feature on the side of the water band at about 1.82 um, and by a broad feature centred on 2.28 um (due to the atmospheric water band at about 1.14 um). The second-order leakage is also present during calibration hence the magnitudes of some of these features may be somewhat masked in the data delivered to users. However, sample spectra published in the 1985 AIS workshop proceedings (e.g. pages 77 and 131) do show features similar to those in Figure 8. The strength of the 2.28 um feature will be dependent on the atmospheric water vapour content at the time of measurement, and on the reflectance of the terrain at 1.14 um.

The spectroradiometric model has also been used with representative surface materials. Figures 9 and 10 show, respectively, the computed responses for green vegetation and for kaolinite. The reflectance of vegetation is characterised by a high value on the near-infrared plateau, and a relatively low value in the SWIR resulting in an AIS spectrum dominated by second-order leakage from a wavelength of about 1.8 um. For any terrain containing appreciable amounts of vegetation, the distortions will render analysis procedures such as log. residuals of little value. The computed response to kaolinite shows that, in the contaminated spectrum, the depth of the characteristic 2.2 um clay absorption band in the radiance spectrum is greatly reduced by second-order leakage. It should be noted that the kaolinite spectrum used here was from a laboratory sample. Actual field spectra of minerals are likely to have less prominent features, further aggravating the problem of detecting subtle, but mineralogically significant, absorption bands.

SUMMARY

The analysis of AIS data described above has shown that horizontal striping can be removed without degradation of the spectral information. However, the order overlap problem is far more serious and may render useless data collected in some environments . The paper by Huntington et. al. (this issue) discusses one method of minimising the influence of second-order leakage. Other methods such as using NS001 imagery in conjunction with the spectroradiometric model, should be further investigated. However, the AIS will not realise its true potential in the detection of subtle absorption features until the blocking filter problem is rectified in the AIS itself.

ACKNOWLEDGEMENTS

REFERENCES

Green, A.A. and Craig,M.D (1985). Analysis of Aircraft Spectrometer Data with Logarithmic Residuals. Proceedings of the Airborne Imaging Spectrometer Data Analysis Workshop, April 8-10, 1985. JPL Publication 85-41, p.111-119.

Huntington,J.F., Green, A.A., Craig, M.D., Cocks,T.D., 1986. Preliminary Geological Investigation of AIS Data at Mary Kathleen, Queensland, Australia. Proceedings of the Second Airborne Imaging Spectrometer Data Analysis Workshop, May 6-8, 1986 (this issue).
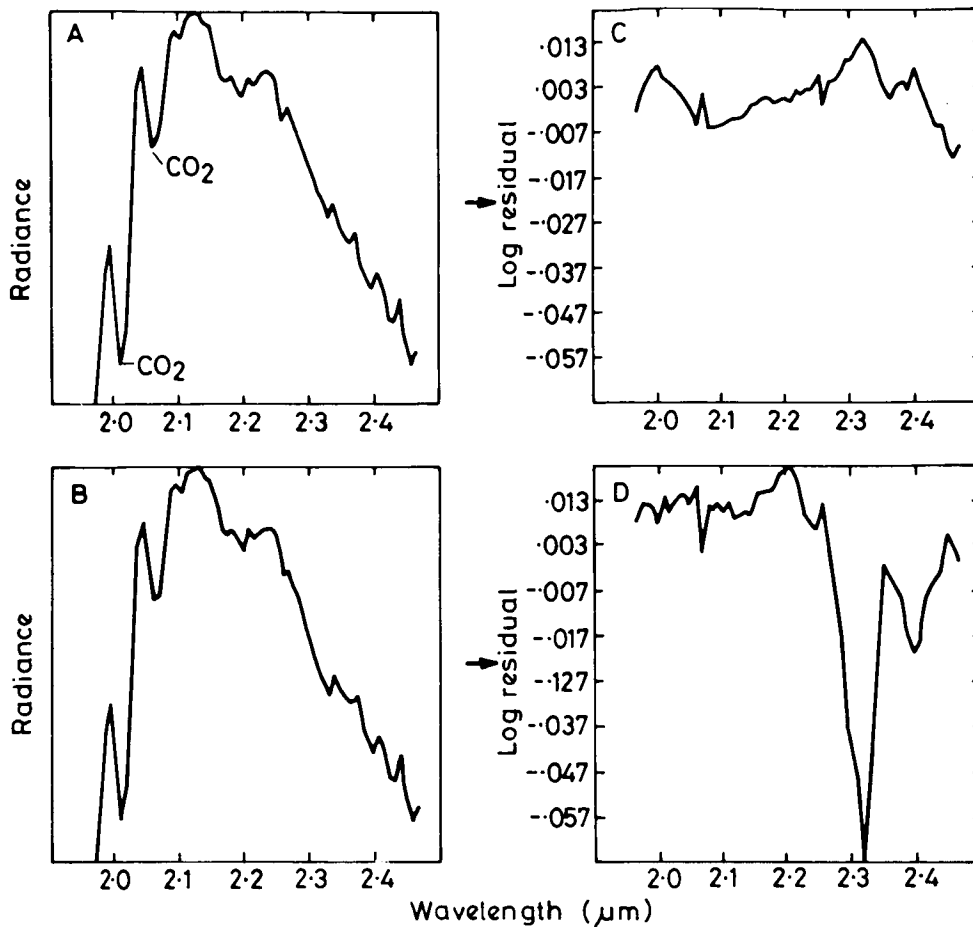
Figure 1.   Surface radiance spectra (A and B) recorded by the
GER airborne spectroradiometer, with the corresponding
log. residual spectra (C and D).
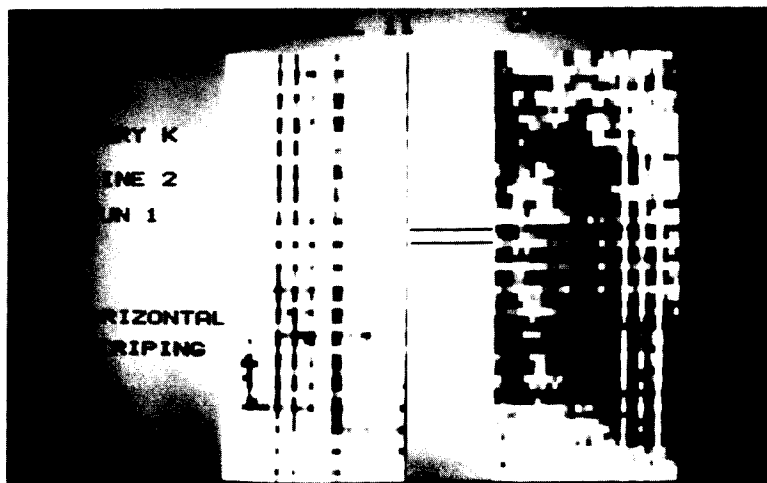
Figure 2. AIS imagery in bands 11 and 29, showing
horizontal striping. (See color slide number 1
in the back cover pocket of this publication.)

58
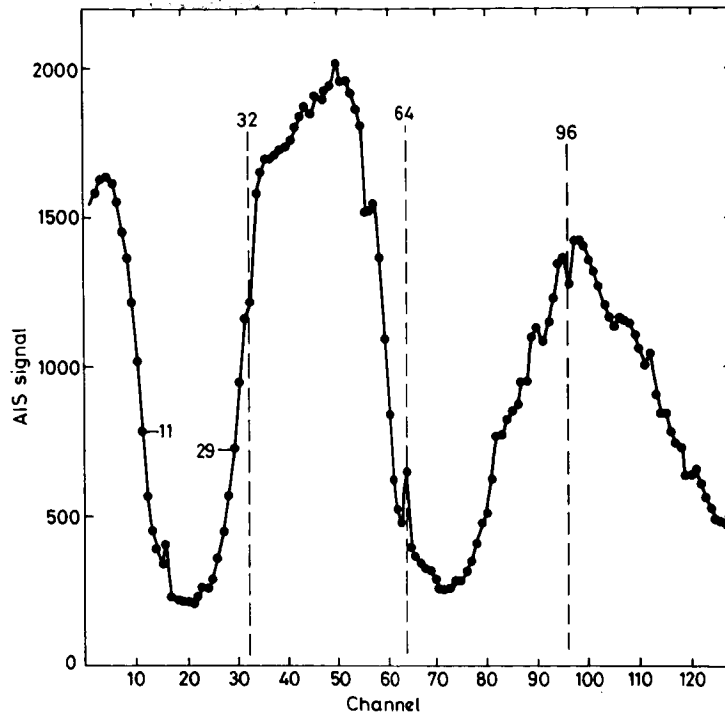
Figure 3. A flight line average radiance spectrum
recorded in the 'rock' scan mode, showing
grating position boundaries in channels 32, 64
and 96.
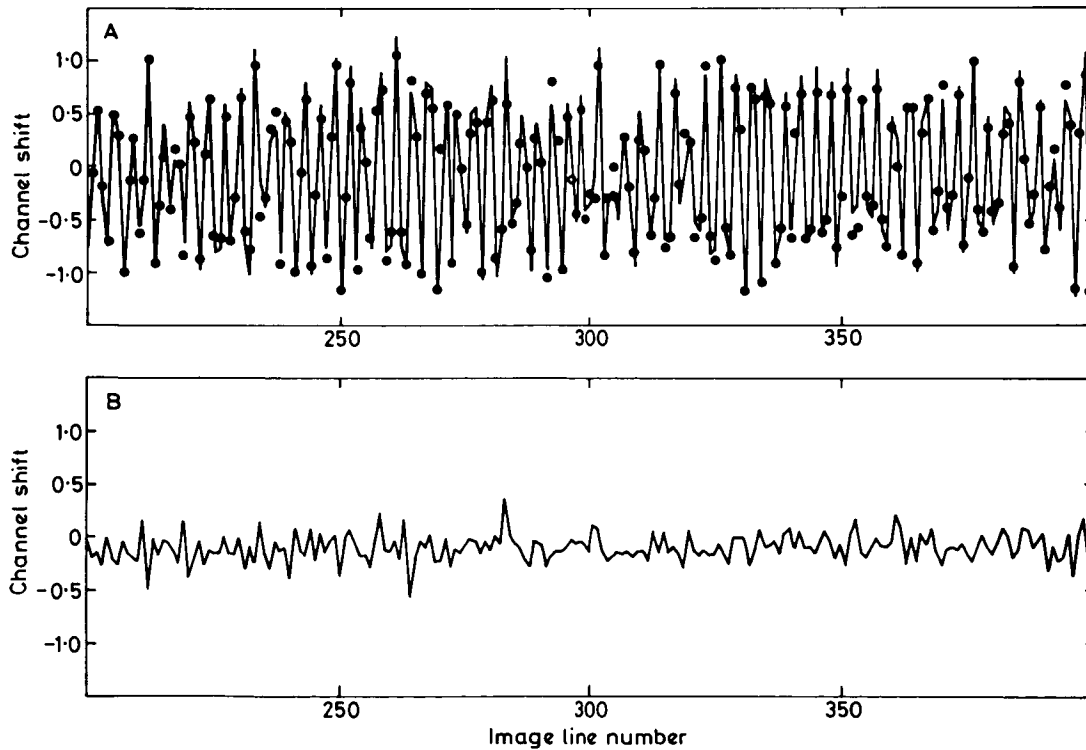
Figure 4. A. Estimated channel shifts induced by grating wobble at
wavelengths in the first grating position, for image columns 8
(line) and 24 (dots). B. Estimated channel shifts for column
8 after application of the destriping algorithm, DMEAN.
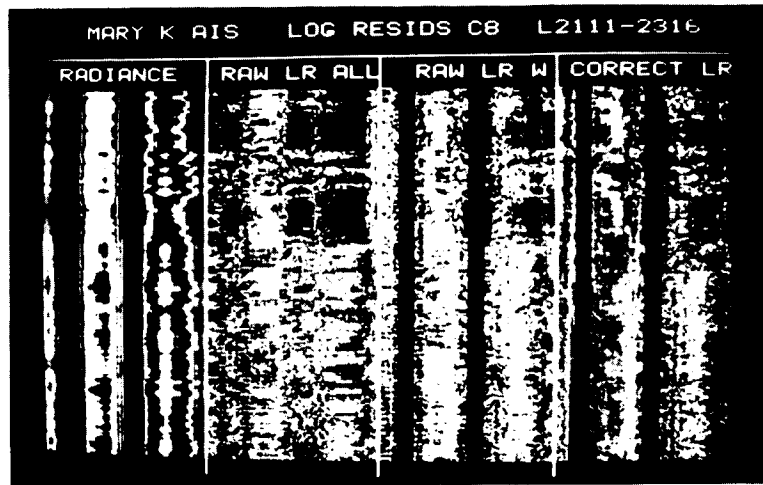
Figure 5. Density-sliced radiance and log. Residual
spectra for a variety of processing conditions.
(See color slide number 2 in the back cover pocket
of this publication.)
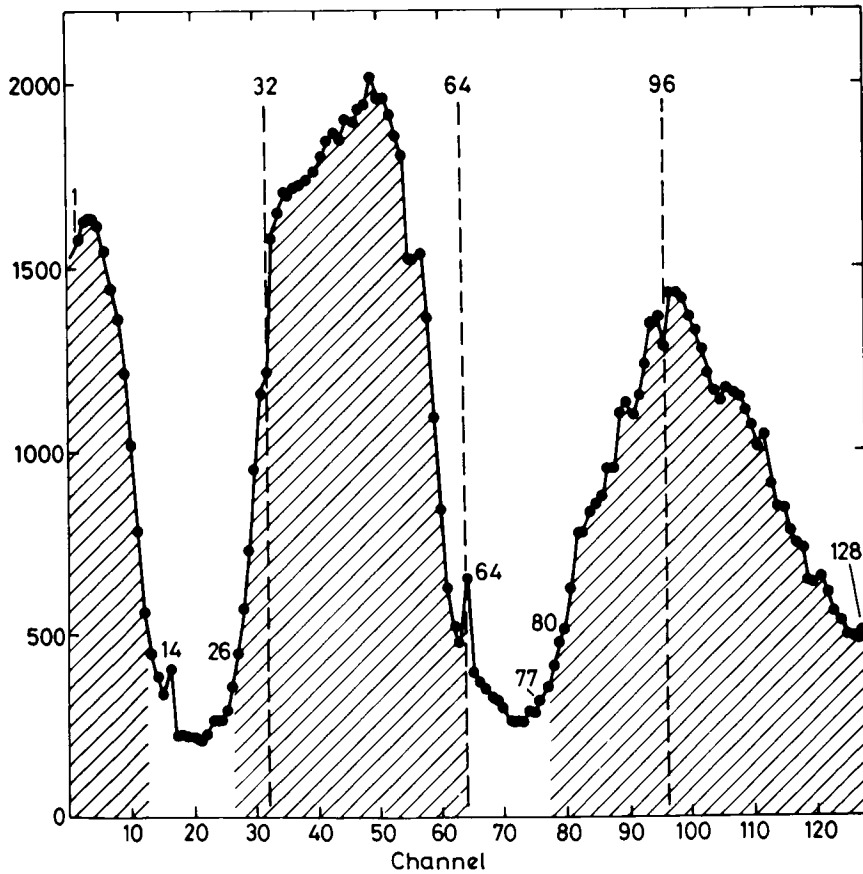
Figure 6. Flight line average radiance spectrum, showing hatched
regions used in a log. residual analysis that excluded water-vapour
band minima.

60
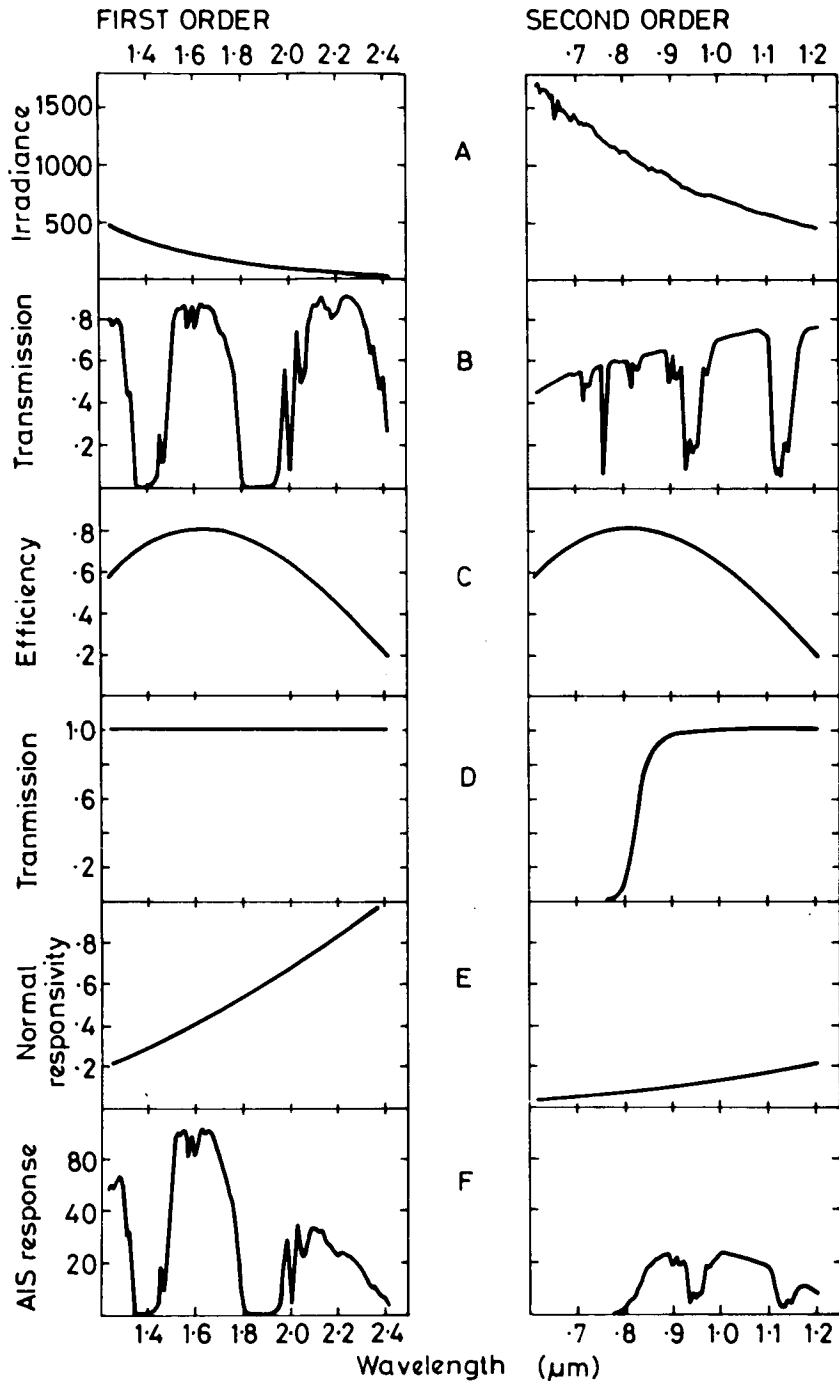
Figure 7. Components of the AIS spectroradiometric model used to assess spectral distortion from second-order leakage. A. Solar irradiance, B. Atmospheric transmission, C. Grating efficiency, D. Blocking filter transmission, E. Detector responsivity, F. Computed response.

61

RESPONSE TO 100 % REFLECTOR
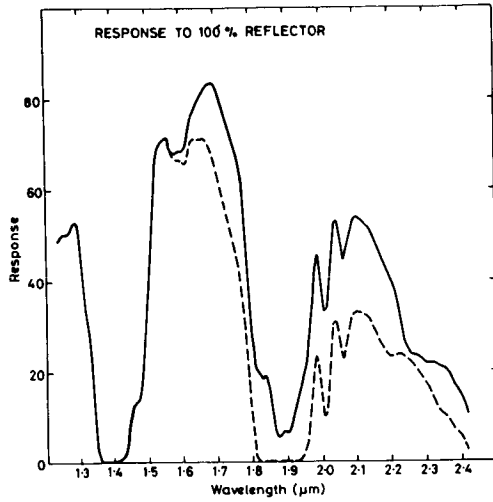
Figure 8. Computed AIS response to a 100% reflector. Solid line shows combined first and second-order response. Dashed line shows first order response.

RESPONSE TO VEGETATION
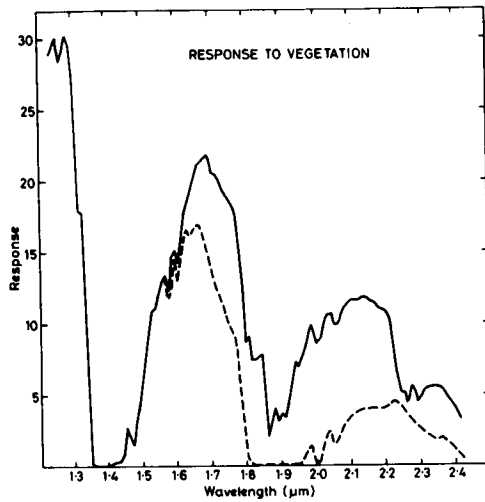
Figure 9. Computed AIS response to green vegetation, presented in the format above.

RESPONSE TO KAOLINITE
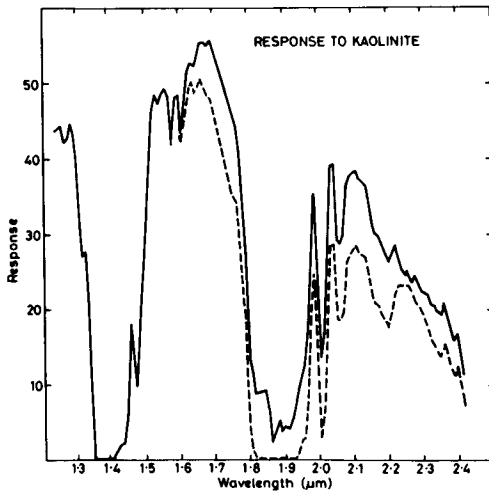
Figure 10. Computed AIS response to kaolinite, presented in format above.

ATMOSPHERIC-WATER ABSORPTION FEATURES NEAR 2.2 MICROMETERS AND THEIR IMPORTANCE IN HIGH SPECTRAL RESOLUTION REMOTE SENSING

FRED A. KRUSE and ROGER N. CLARK, Geologic Division, U.S. Geological Survey, Box 25046, DFC, MS 964, Lakewood, Colorado 80225, USA

ABSTRACT

Selective absorption of electromagnetic radiation by atmospheric gases and water vapor is an accepted fact in terrestrial remote sensing. Until recently, only a general knowledge of atmospheric effects was required for analysis of remote sensing data; however, with the advent of high spectral resolution imaging devices, detailed knowledge of atmospheric absorption bands has become increasingly important for accurate analysis.

Detailed study of high spectral resolution aircraft data at the U.S. Geological Survey has disclosed narrow absorption features centered at aproximately 2.17 and 2.20 micrometers not caused by surface mineralogy. Published atmospheric transmission spectra and atmospheric spectra derived using the LOWTRAN-5 computer model indicate that these absorption features are probably caused by water vapor. Spectral modeling indicates that the effects of atmospheric absorption in this region are most pronounced in spectrally flat materials with only weak absorption bands. For example, convolution of a weak montmorillonite spectrum with a LOWTRAN atmospheric transmission spectrum at Airborne Imaging Spectrometer (AIS) wavelengths and resolution results in a composite spectrum that somewhat resembles that of kaolinite. This example demonstrates that a correction accounting for the atmospheric effects near 2.2 micrometers must be applied to the data prior to analysis. Without this correction and detailed knowledge of the atmospheric effects, accurate mapping of surface mineralogy (particularly at low mineral concentrations) is not possible.

INTRODUCTION

New high spectral resolution remote sensing systems collect data in many narrow bands, producing a continuous reflectance spectrum for each image pixel. Analysis of data from these systems has concentrated on using various techniques to attempt to remove atmospheric and solar flux effects so that the available spectral information can be extracted (Vane and Goetz, 1985). These techniques have been only partially successful, but in several cases individual clay minerals have been uniquely identified on the basis of absorption features near 2.2 micrometers (Marsh and McKeon, 1983; Goetz and others, 1985; Kruse and others, 1985). This report identifies atmospheric absorption features near 2.2 micrometers that may adversely affect mineral identification. The importance of correcting for these features prior to data analysis is discussed below.

IDENTIFICATION OF THE PROBLEM

High spectral resolution spectroradiometer data of an area in Nevada were processed to reflectance without an atmospheric correction to compare corrected and uncorrected spectra for the same area. Analysis of these data revealed kaolinite-like absorption features at approximately 2.17 and 2.20 micrometers throughout the field area in the uncorrected data (Fig. 1). Samples collected from this area were analyzed using laboratory reflectance measurements and did not contain kaolinite.

A literature search disclosed that many of the published atmospheric transmission curves in common use today have been generalized and indicate that atmospheric transmittance is essentially uniform in the 2.2 micrometer region (Sabins, 1978; Lillesand and Kiefer, 1979; Siegal and Gillespie, 1980; Suits, 1983; (Figs. 2a, 2b, 2c). However, other published curves (Wolfe, 1965; Kneizys and others, 1980) show detailed atmospheric transmission spectra measured over varying path lengths that indicate that narrow atmospheric absorption features caused by atmospheric water exist in this region of the spectrum (Fig. 2d, 2e, 2f).

METHODS AND DISCUSSION OF RESULTS

The effect of the atmospheric water absorption bands near 2.2 micrometers on the appearance of mineral absorption features was modeled using laboratory measurements of selected clay minerals and the LOWTRAN-5 computer model (Kneizys and others, 1980; Blake, 1983). The LOWTRAN-5 model produced a high resolution spectrum with absorption minima at 2.156, 2.183 and 2.198 micrometers caused by atmospheric water (Fig. 3) and is in good agreement with the published atmospheric transmission curves shown in figure 2. The atmospheric transmission spectrum was then calculated for an actual AIS path length using midlatitude atmospheric characteristics (Kneizys and others, 1980), and the
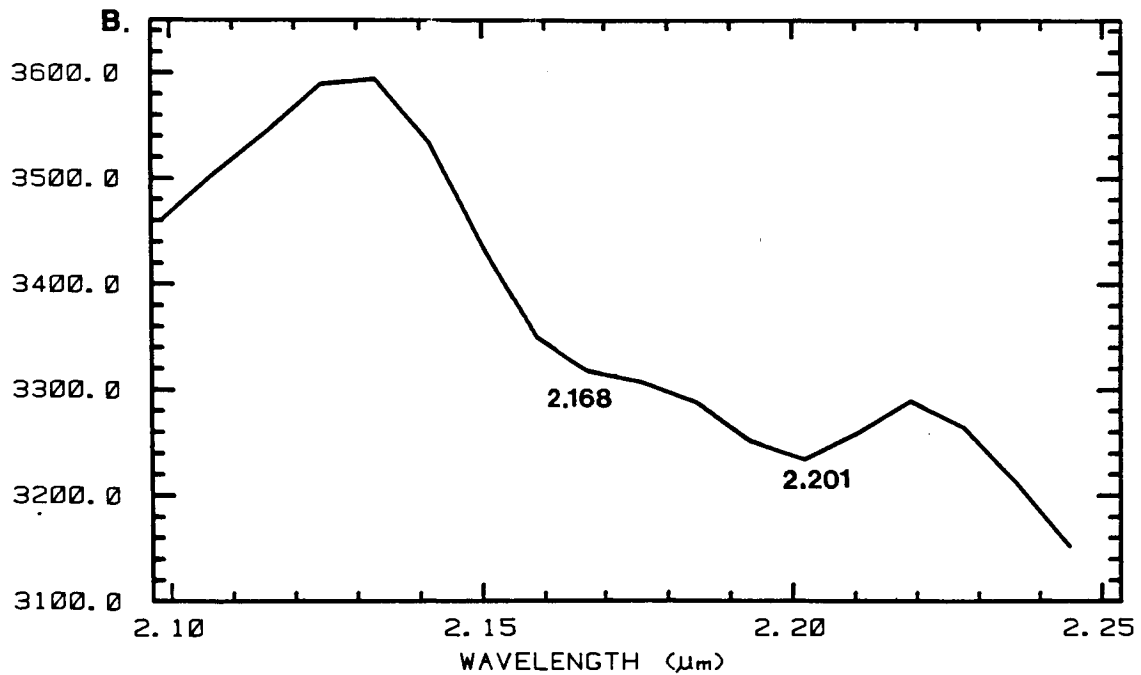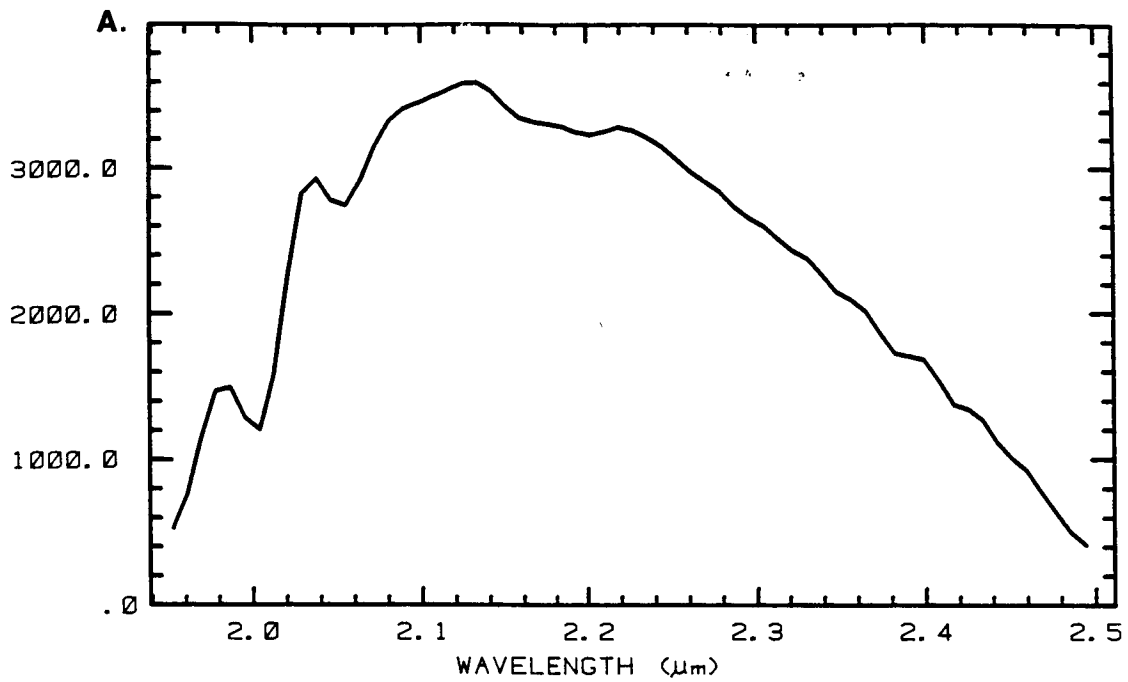
Figure 1. Geophysical Environmental Research Inc. high spectral
resolution aircraft spectroradiometer spectrum for an area
showing no strong mineral absorption features. Spectrum "A"
covers the full range of the instrument (1.96 to 2.5
micrometers). Spectrum "B" shows the absorption features near
2.2 micrometers at an expanded scale. The resolution of this
instrument is similar to that of the AIS (Collins and others,
1981; Goetz and others, 1985). The solar irradiance curve and
the atmospheric transmission function have not been removed;
however, the data have been normalized to 1.0 at 2.13
micrometers.

65
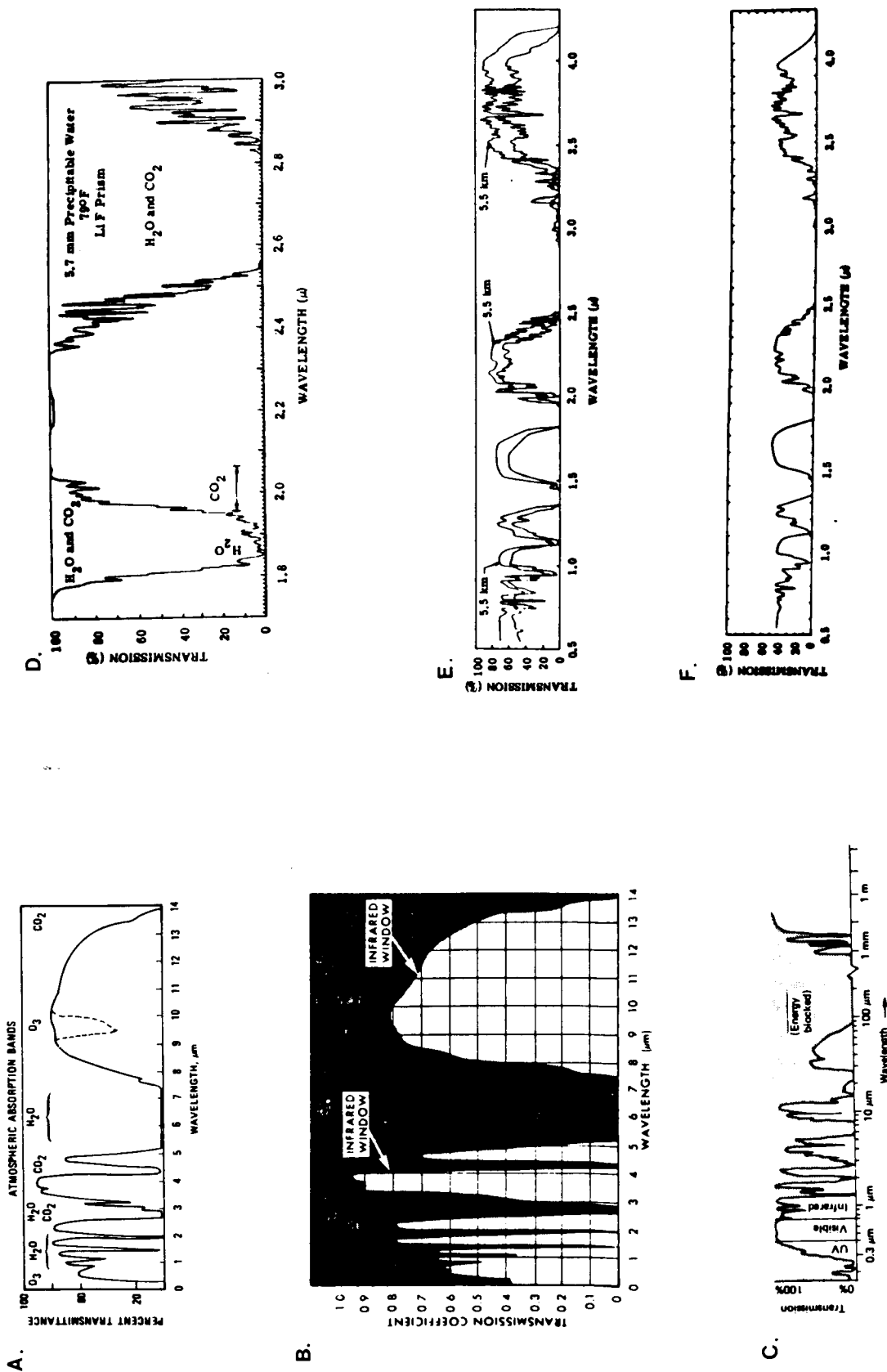
Figure 2. Figures 2A, 2B, and 2C show examples of generalized atmospheric transmission curves from the published geologic remote sensing literature. Note that no absorption features are shown at 2.2 micrometers. Figures 2D, 2E, and 2F are examples of measured transmission curves over varied atmospheric path lengths. Figure 2D is for a 0.3 km horizontal path, figure 2E shows transmission for 5.5 and 16.25 km paths, and figure 2F shows atmospheric transmission for a 27.7 km path. All transmission curves were measured at sealevel. Note that both the structure and the depth of the bands near 2.2 micrometers varies with increasing path length. (Figure 2A from Santa Barbara Reseach Center, 1975, in Sabins, 1978); (Figure 2B from Siegal and Gillespie, 1980); (Figure 2C from Lillesand and Kiefer, 1979) (Figures 2D, 2E, and 2F from Yates and Taylor, 1960, in Wolfe, 1965).

66
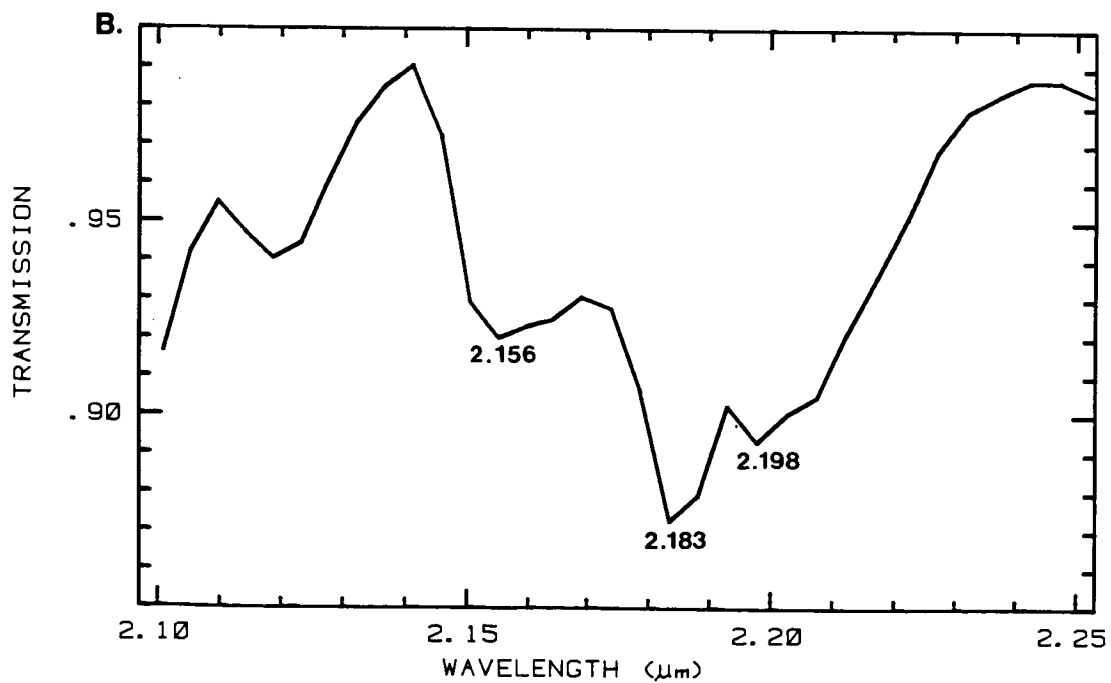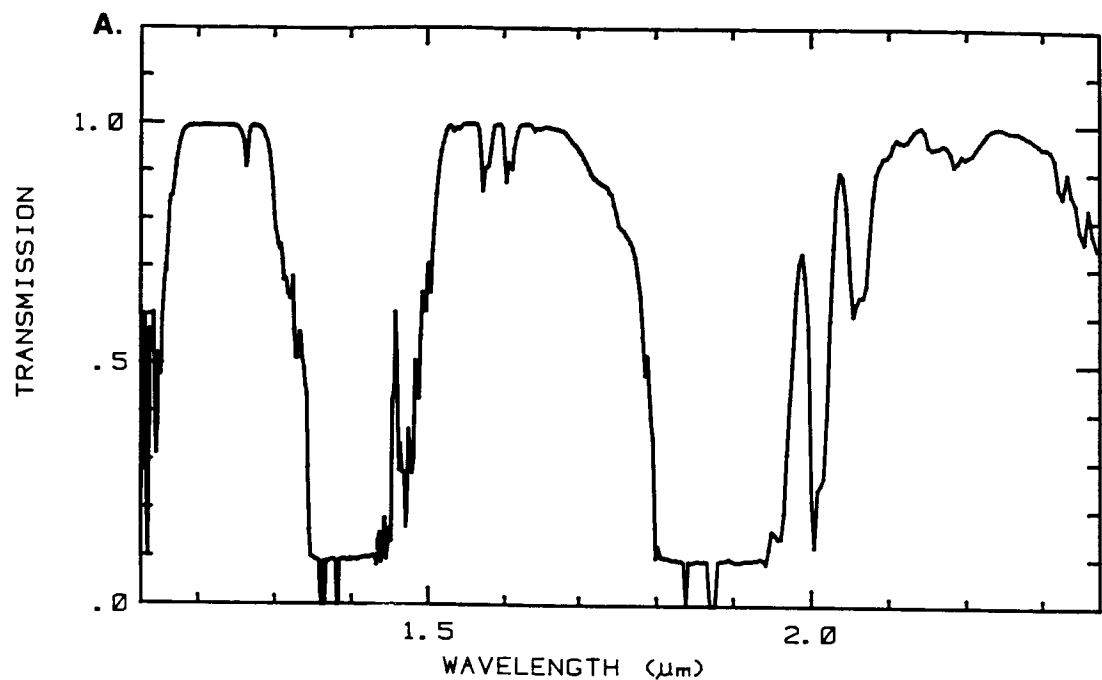
Figure 3. Figure 3A shows the LOWTRAN-5 calculated transmission
spectrum for the 1.15 to 2.5 micrometer region. Figure 3B shows the
same curve on an expanded scale. This spectrum was calculated for
midlatitude atmospheric parameters (Kneizys and others, 1980) for a
typical AIS acquisition pathlength.

resulting spectrum was convolved to AIS wavelengths and resolution (Fig. 4). Laboratory spectra of selected reference clay minerals were measured and digitally recorded on a Beckman 5270 laboratory spectrometer (Clark, 1986, unpublished data).

Spectral processing software (Clark, 1980) was used to model the effect of the atmosphere on the spectra of several different minerals; one example is shown here. When the atmospheric transmission spectrum was applied to a montmorillonite spectrum with a strong absorption feature at 2.206 micrometers (Fig. 5a, spectrum 2), the position of the main absorption feature remained unchanged although an additional small absorption band appeared near 2.16 micrometers (Fig. 5a, spectrum 3). However, when the atmospheric transmission spectrum was applied to a montmorillonite spectrum with a weak absorption feature near 2.2 micrometers (Fig. 5b, spectrum 2), the composite spectrum was grossly similar in appearance to kaolinite even when no kaolinite was present (Fig. 5b, spectrum 3, spectrum 4). Comparison of Fig. 5b with Fig. 1 shows that the kaolinite-like absorption features occurring in the aircraft spectra could be explained by the combination of atmospheric effects and weak mineral absorptions near 2.2 micrometers. Other combinations of weak mineral absorptions and varying atmospheric water vapor concentrations might result in an even closer approximation to the kaolinite spectrum.

CONCLUSIONS

The importance of narrow atmospheric absorption bands near 2.2 micrometers to the analysis of high spectral resolution remote sensing data is immediately apparent. The assumption that the atmospheric transmission is relatively constant in the 2.2 micrometer region is not valid, and it is apparent that a correction accounting for the atmospheric effects near 2.2 micrometers must be applied to high spectral resolution remote sensing data prior to analysis. If atmospheric conditions are not fully known, or if the model does not account for atmospheric absorption features near 2.2 micrometers, then the interpreter must be aware of possible atmospheric effects in this wavelength region and should take care, particularly where absorption features are weak, to insure that interpretation of absorption features does not erroneously include atmospheric effects. It is important to remember that varying atmospheric conditions and particularly mineral mixtures could add to the complexity of the problem. Additional atmospheric modeling and on site measurement of atmospheric parameters are required before complete resolution of atmospheric absorption problems will be possible.
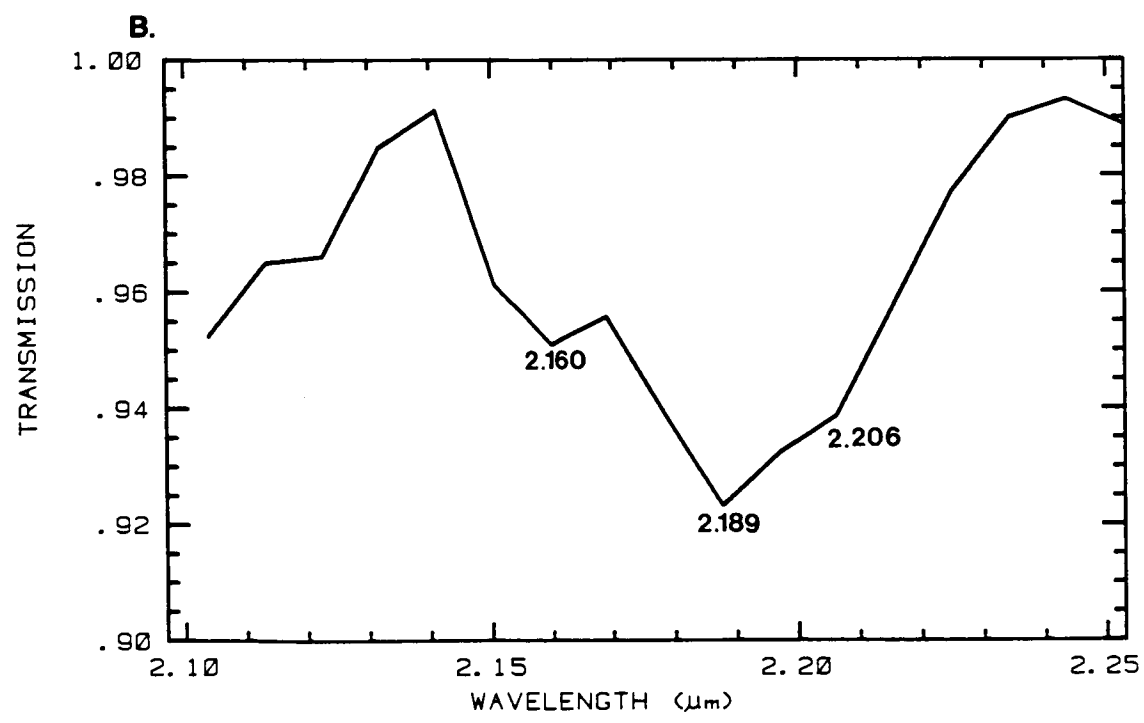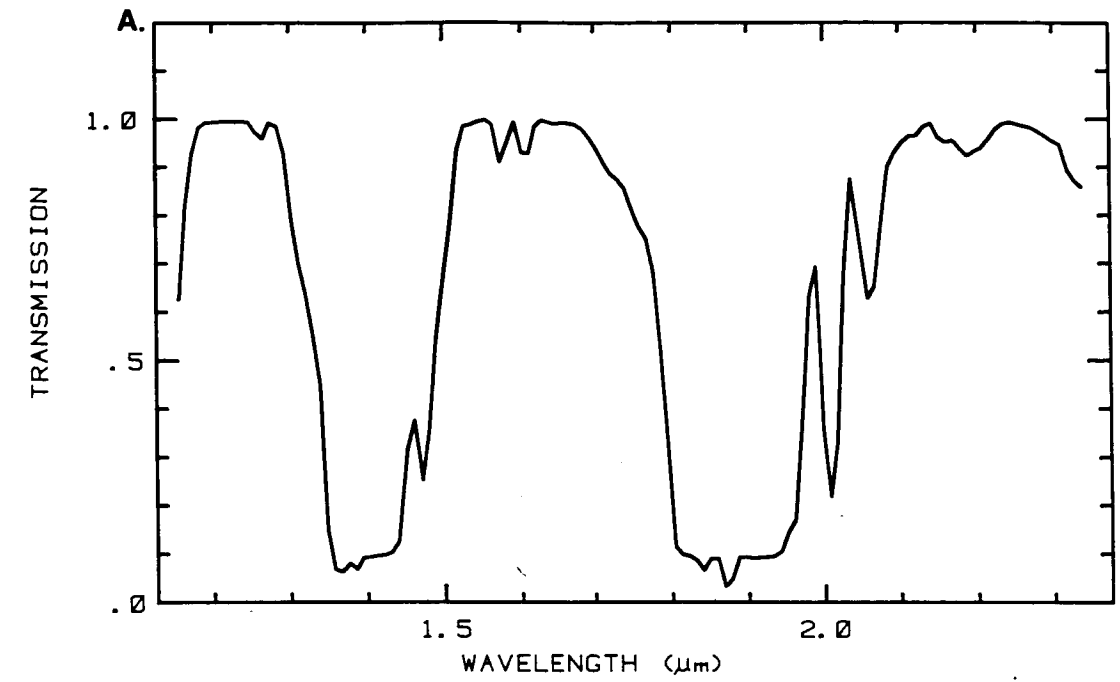
Figure 4. Figure 4A shows the LOWTRAN-5 calculated atmospheric transmission from figure 3A convolved to AIS wavelengths and resolution. Figure 4B shows the same curve on an expanded scale.

69
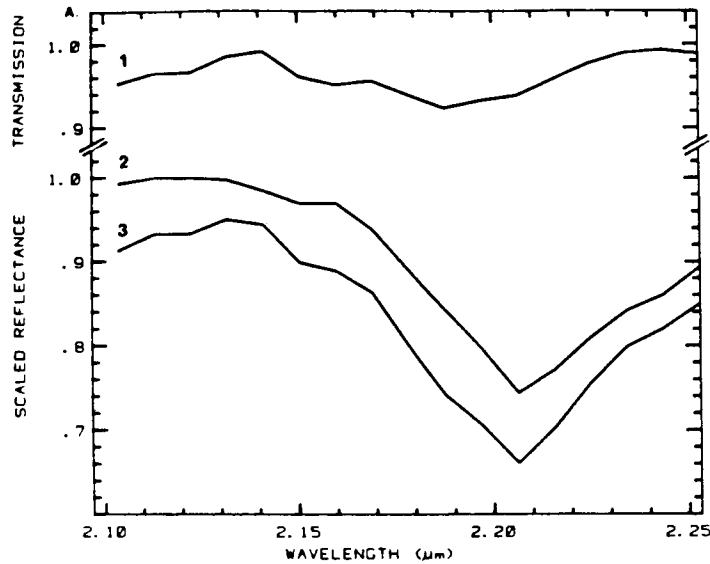
Figure 5A.   Spectrum 1 is the LOWTRAN-5 atmospheric spectrum convolved
to AIS wavelengths and resolution.   Spectrum 2 is a laboratory spectrum
for montmorillonite convolved to AIS wavelengths and resolution.
Spectrum 3 results when the atmospheric function shown in spectrum 1 is
applied to spectrum 2.   All spectra have been scaled to approximately
1.0 at their highest points and spectra 2 and 3 have been vertically
offset for clarity.
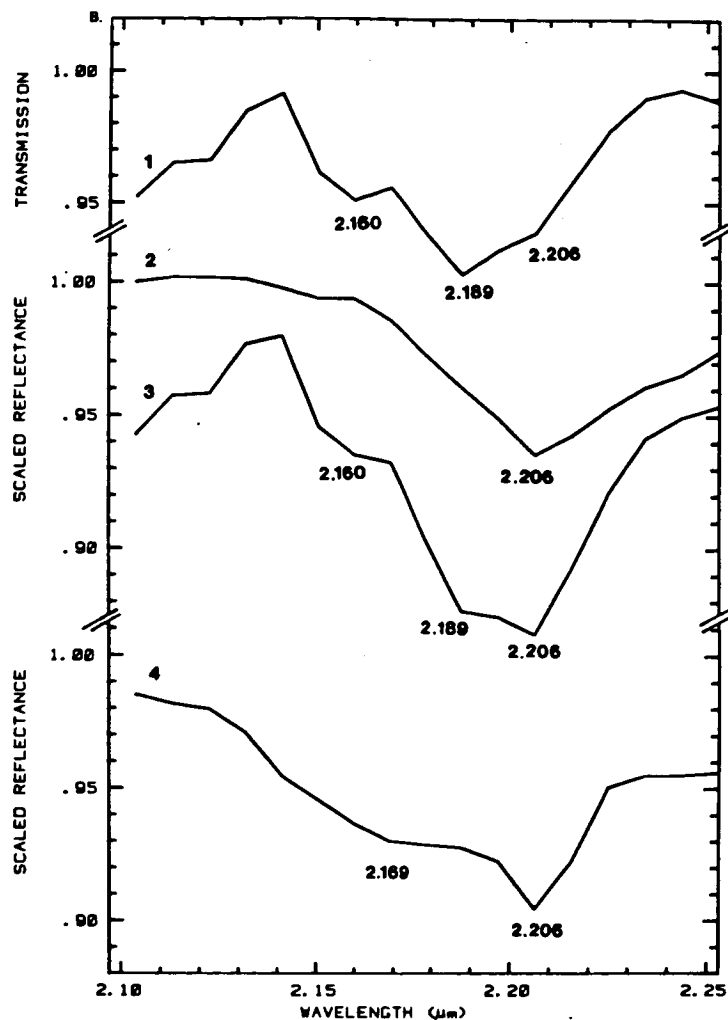
Figure 5B. Spectrum 1 is the LOWTRAN-5 atmospheric spectrum convolved to AIS wavelengths and resolution. Spectrum 2 shows a typical "weak" montmorillonite absorption. This absorption is similar to a montmorillonite absorption feature when the montmorillonite is mixed with other minerals that do not have absorption features in this region. Spectrum 3 results when the atmospheric function from spectrum 1 is applied to spectrum 2. Spectrum 4 shows a typical "weak" (poorly crystalline) kaolinite spectrum similar to that which might be seen in mineral mixtures. Note the gross similarities between spectra 3 and 4. All spectra have been scaled to approximately 1.0 at their highest points.

71

REFERENCES

Blake, P. L., 1983, Analytical removal of atmospheric absorptions from remotely sensed near-infrared data of geologic targets: M.S. thesis (unpublished), University of Hawaii, 96 p.

Clark, R. N., 1980, A large-scale interactive one-dimensional array processing system: Publications of the Astronomical Society of the Pacific, v. 92, p. 221-224.

Collins, W., Chang, S. H., and Kuo, J. T., 1981, Infrared airborne spectroradiometer survey results in the western Nevada area: Columbia Univ., Aldridge Lab. Appl. Geophysics, Final Rept. to NASA, Contract JPL 955832, 61 p.

Goetz, A. F. H., Vane, Gregg, Solomon, J. E., and Rock, B. N., 1985, Imaging spectrometry for earth remote sensing: Science, v. 228, p. 1147-1153.

Kneizys, F. X., Shettle, E. P., Gallery, W. O., Chetwynd, J. H. Jr., Abreu, L. W., Selby, J. E. A., Fenn, R. W., and McClatchey, R. A., 1980, Atmospheric transmittance/radiance: Computer code LOWTRAN 5: AFCRL Environmental Research Paper, No. 697, AFCRL-80-0067, 233 p.

Kruse, F. A., Raines, G. L., and Watson, Kenneth, 1985, Analytical techniques for extracting geological information from multichannel airborne spectroradiometer and imaging spectrometer data: in Proceedings, International Symposium on Remote Sensing of Environment, Thematic Conference on Remote Sensing for Exploration Geology, 4th, San Francisco, California, 1-4 April, 1985, University of Michigan, Ann Arbor, p. 309-324.

Lillesand, T. M., and Kiefer, R. W., 1979, Remote sensing and image interpretation: John Wiley & Sons, New York, 612 p.

Marsh, S. E., and McKeon, J. B., 1983, Integrated analysis of high-resolution field and airborne spectroradiometer data for alteration mapping: Economic Geology, v. 78, no. 4, p. 618-632.

Sabins, F. F. Jr., 1978, Remote sensing principles and interpretation: W. H. Freeman and Company, San Francisco, p. 6.

Santa Barbara Research Center, 1975, The SBRC Brochure; Goleta, California.

Siegal B.S. and Gillespie, A. R., (eds.), 1980, Remote Sensing in Geology: John Wiley & Sons, New York, 702 p.

Suits, G. H., 1983, The nature of electromagnetic radiation, in Colwell, R. N. (ed), Manual of Remote Sensing: American Society of Photogrammetry, Falls Church, Virginia, p. 40.

Vane, Gregg, and Goetz, A. F. H., (eds), 1985, Proceedings of the
Airborne Imaging Spectrometer Data Analysis Workshop, JPL
publication 85-41, Jet Propulsion Laboratory, Pasadena, California,
173 p.

Wolfe, W. L., (ed.), 1965, Handbook of military infrared technology:
Office of Naval Research, Department of the Navy, Washington, D.
C., p. 252, 255, 256.

Yates, H.W., and Taylor, J. H., 1960, Infrared transmission of the
atmosphere, NRL report 5453, U. S. Naval Research Laboratory,
Washington, D. C., ASTIA AD 256952.

DESTRIPING AIS DATA USING FOURIER FILTERING TECHNIQUES

CHRIS HLAVKA, NASA/Ames Research Center, Moffett Field,CA,USA.

ABSTRACT

Airborne Imaging Spectrometer (AIS) data collected in 1984 and 1985 showed pronounced striping in the vertical and horizontal directions. This striping reduced the signal to noise ratio so that features of the spectra of forest canopies were obscured or altered by noise. This noise was removed by application of a notch filter to the Fourier transform of the imagery in each waveband.

BACKGROUND

Remote sensing data are being studied as a potential source of information about nutrient cycling in forests(Peterson et al., 1985). A process model is being developed to describe the cycling of carbon, nitrogen, and phosphorus in forest ecosystems (Running et al., 1985). High resolution infrared imagery will be used to estimate concentrations of nitrogen and carbon compounds in leaf canopies for input to the model. The leaf concentrations of some of these compounds, in particular lignin and nitrogen, have been correlated with reflectances at several IR wavelengths measured in the laboratory (D. Card et al.,1986). AIS spectra will be analyzed for similar correlations. Also, subtle differences in the structure of spectra will be analyzed by correlating measures of shape, such as first and second derivatives, with chemical concentrations, as has been done with lab spectra (Williams et al.,1983).

The presence of noise, such as striping, in AIS spectra can be expected to decrease correlations with chemistry (Brownlee, 1965). If R' is a large sample correlation between reflectance in a single AIS channel, or a linear combination of reflectances in several channels, and the concentration of a chemical, and R is the correlation that would be observed if the data were noise-free, then

$$R' = R/SQRT(1 + 1/SNR).$$

Therefore, it is clearly an advantage to improve the signal to noise ratio (SNR) of the AIS data. This can be achieved with processing techniques which reduce noise content more than information content.
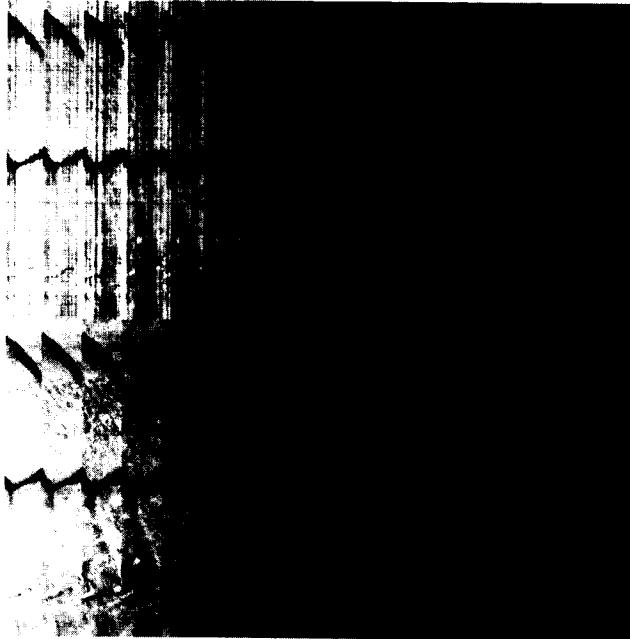
a)
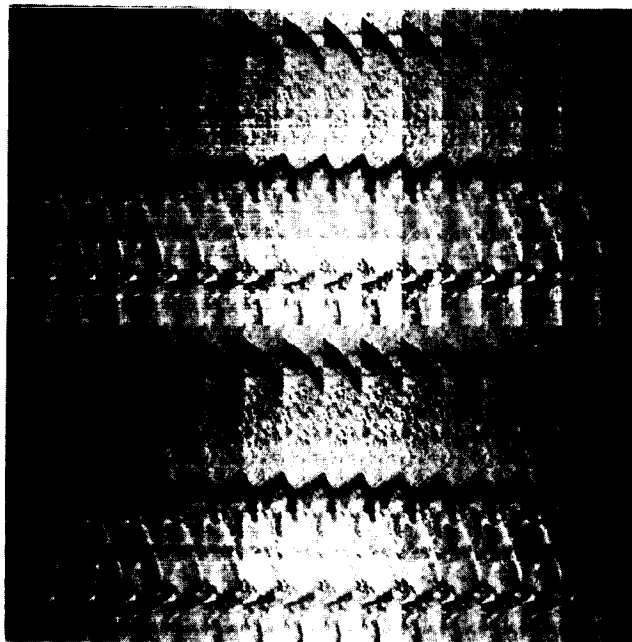
b)

Figure 1. Blackhawk Island AIS data before (top) and after (bottom) filtering. a) Channels 1-16 of grating position 0. b) Channels 1-16 of grating position 1.

Figure 2. The |FT| of band 1 of grating position 0, enhanced by the logarithm transformation to show detail.

```
VHF    - frequencies    DC    + frequencies    VHF
                        |
VHFF                                            VHFF
```
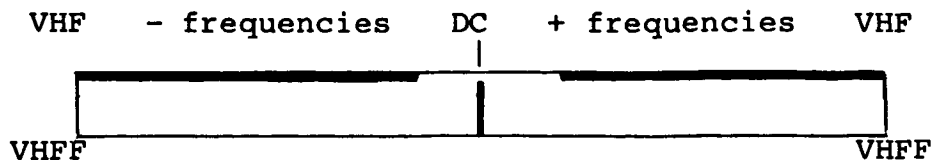
Figure 3. A schematic drawing of the notch filter. Note that the horizontal axis is for vertical frequencies and the vertical axis is for horizontal frequencies.
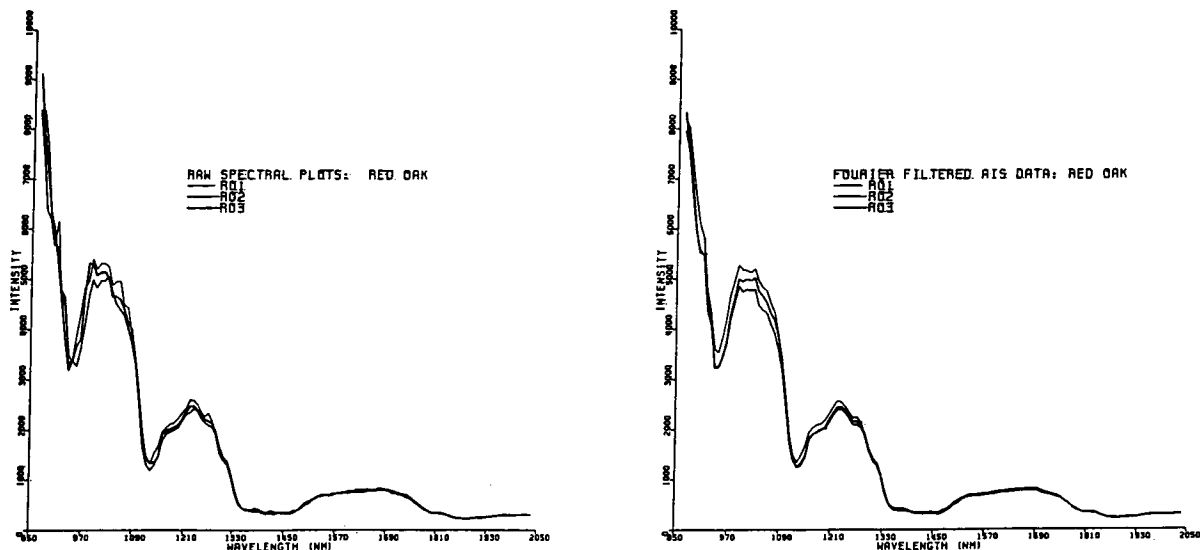
Figure 4. Plots of AIS spectra for sites within Blackhawk Island. Left: Before filtering. Right: After filtering.

DESTRIPING TECHNIQUES

Visual examination of AIS imagery revealed striping both in the along track (vertical) and across-track (horizontal) directions in imagery collected in 1984 and 1985, as can be seen in a portion of a flightline shown in Figure 1. Vertical striping, caused by small differences in calibration among the 32 sensors for each waveband, was particularly prominant. In addition to the striping, the imagery contained drop-out lines in some channels. These lines contained spurious grey levels of 4096, usually in every pixel in a row, in every band in a grating position.

A straightforward technique for removing striping in both directions was desired to satisfy the following requirements: 1) reduction of noise (striping in both

76

directions) with retention of information content, and 2) minimal software development for implementation.

Histogram normalization techniques were considered. This type of technique involves collection of histogram statistics, such as the mean and standard deviation (Barker,1983) or bin frequencies (Dykstra and Segal, 1985) for each row and/or column in the image. A transformation for each row and/or column is applied to equalize the statistics. Dykstra and Segal applied histogram normalization to AIS data to remove vertical striping. They noted that the success of the technique depended upon the condition that "over the course of a complete flight line, each of the 32 detectors has covered, on the average, very similar surface materials". Such an assumption was plausable for many of our flight lines, but a similar condition clearly could not be assumed for rows only 32 pixels wide. "Flat field" radiometric corrections (Conel,1985) have been used to destripe data, while also removing effects due to the solar spectrum and atmospheric absorption and radiance. This technique requires an area of spectrally flat and homogenous material across the flight line, a condition not met in all of our flight lines. Fourier filtering was considered as a means for destriping because the technique does not require the special conditions required by the techniques described above.

Improvement in SNR with Fourier filtering was expected because the striping patterns were in two very specific directions, the vertical and horizontal, therefore the energy associated with these patterns would be confined to small portions of the two-dimensional Fourier transform, namely the axes associated with zero frequency in the horizontal and vertical directions. These portions can be removed by notch filtering, .i.e. zeroing out the Fourier transform over selected areas and then taking the inverse transform. The striping pattern is thus removed with little reduction in information content.

FOURIER FILTERING AIS DATA

Fourier filtering techniques were applied on two flightlines of AIS imagery. One flightline, acquired in 9/84, contained the portion of Blackhawk Island, Wisconsin shown in Figure 1. This is a forested island preserve, with stands of pines near its shores, and mixed deciduous hardwoods in the interior. The island is surrounded by farmland. The other flightline was acquired over areas of spruce forests, birch forests, and marshes in Alaska in 8/85.

As a first step, drop-out lines were located in the image by visual inspection. Each drop-out line was then "repaired" by replacement with the average of the average values in the two lines directly above and below it. The magnitude of the Fourier transform (|FT|) of the 256 line portion of the Blackhawk Island flightline was created, and several individual bands, such as the |FT| of band 1 of

grating position 1 shown in Figure 2, were visually examined
to determine a design for the notch filter. As expected,
the grey levels in the axes associated with zero frequencies
in the horizontal or vertical axes were high compared with
grey levels in most other areas. High magnitudes were
spread out along the axes, rather than concentrated in a few
spatial frequencies. The other pixels on the |FT| image
with high grey levels were clustered around diagonal lines,
and were associated with the patterns made by the river
around the island, or were clustered around the DC point
(the origin), and were associated with the pattern of
forests and fields, which were primarily low frequency
patterns as are most patterns on remotely sensed imagery
(Moik,1980). A few (two or three) notch filters that were
low pass filters in the horizontal and vertical directions
were tested on the image of Blackhawk Island. The filtered
images were examined on an interactive display. The "best"
filter was then applied to a portion of the Alaska
flightline.

Fourier filtering implementation - AIS images were
filtered using programs in a commercial image processing
package, IDIMS, on a VAX11/780. The technique can be
implemented with VICAR software developed at JPL as well,
and probably with other image processing packages.
Figure 3 shows the notch filter that was most
successful in destriping the Blackhawk Island image. A
binary image was created with ones in the white areas, and
zeroes in the black areas by creating a 17 row by 256 column
image of ones and inserting three small images of zeroes.
All non-zero frequencies in the vertical axis (rows 2-17)
were zeroes, and all frequencies above .43 cycles/pixel
(columns 1-110 and 147-256). An image containing the
complex two dimensional FT of each of the 128 channels of
AIS was created and each FT was multiplied by the binary
notch filter. The inverse FT was then applied to each
channel in the product image to obtain the destriped AIS
imagery.

Results - The results of filtering the Blackhawk Island
image are shown in Figure 1, for selected channels.
Vertical striping was completely removed. This indicates
that the striping was due to differences in bias among the
32 detectors associated with each band, because zeroing out
all non-zero frequencies along the central vertical axis of
the FT is mathematically equivalent to adding a constant to
AIS grey levels to make the average grey level of each
column equal to the average grey level for the channel.
Most of the horizontal striping was also removed. Some
sudden apparent changes in detector response level were
noted on AIS data, for example after row 190, shown in
Figure 1b). The filtered image showed a dark band around
this row, an artifact of the filter. An image containing
1024 rows of the Alaska flightline was processed using the
same filter(the same in terms of frequency, the notch filter

dimensions were 17 rows by 1024 columns overall, with zeroes in columns 1-440 and 585-1024). A visual examination of the filtered image indicated successful removal of striping in both directions.

Plots of spectra of 2x2 pixel areas on the filtered images were much smoother after filtering, and features such as the position of the NIR plateau were more consistant from site to site, as can be seen in plots of sites with red oak canopy shown in Figure 4.

CONCLUSIONS AND FUTURE WORK

The Fourier filtering procedure that has been developed appears to remove most of the vertical and horizontal striping in AIS imagery, and it does so with minimal decrease in information content. The removal of vertical striping is an indication that miscalibrations among the 32 sensors in each band have been corrected in the imagery. Occasionally, the filter distorts the imagery when there is a sudden change in the apparent response level in the AIS instrument. Some modifications in the filter will be tested in an attempt to correct this problem.

When a final filter has been selected, all 1984 and 1985 AIS imagery cover study sites to be used for research at Ames Research Center will be destriped as a first step in processing. Other radiometric corrections for solar spectra and atmospheric corrections can then be applied uniformly to output from all sensors within a band, because relative miscalibration has been corrected.

REFERENCES

Barker, J.L. 1983. Relative Radiometric Calibration of Landsat-4 Thematic Mapper Reflective Bands. In: Landsat-4 Science Characterization-Early Results. NASA Conference Publication 2355, III:1-220.

Brownlee, K.A. 1965. The Effects of Errors of Measurement. In: Statistical Theory and Methodology-Second Edition. (John Wiley and Sons, Inc., New York), pp.414-418.

Card, D., D. Peterson, N. Swanberg, and W. Westman. 1985. Personal communication.

Conel, J.E. 1985. Calibration of AIS Data Using Ground-Based Spectral Reflectance Measures. In: Proceedings of the Airborne Imaging Spectrometer Data Analysis Workshop, JPL 85-41 (Pasadena, California: The Jet Propulsion Laboratory), pp.84-85.

Dykstra, J.D. and D.B. Segal. 1985. Analysis of AIS Data of the Recluse Oil Field, Recluse Wyoming. Proceedings of the Airborne Imaging Spectrometer Data Analysis Workshop, JPL 85-41(Pasadena, California: The Jet Propulsion Laboratory), pp.86-91.

Moik, J.G. 1980. Unitary Transforms. In: Digital Processing of Remotely Sensed Images. NASA SP-431. pp. 15-33.

Peterson, D.L., P.A. Matson, J.G. Lawless, J.D. Aber,

P.M. Vitousek, S.W. Running. 1985. Biogeochemical Cycling in Terrestial Ecosystems: Modeling, Measurement, and Remote Sensing. Presented at The 36th International Astronautical Federation Congress, Stockholm, Sweden, October 9-12, 1985.

Running, S.W., J.D. Aber, D.L. Peterson, P.A. Matson, and P.M. Vitousek. 1985. A Simulation Model Integrating Carbon, Water, and Nitrogen Cycles in Forests. In: Proc. Symp. IUFRO Whole Plant Physiology, Oak Ridge, TN.

Spanner, M.A., D.L. Peterson, W. Acevedo, and P. Matson. 1985. High Resolution Spectrometry of Leaf and Canopy Chemistry for Biogeochemical Cycling. In: Proceedings of the Airborne Imaging Spectrometer Data Analysis Workshop, JPL 85-41(Pasadena, California: The Jet Propulsion Laboratory), pp. 92-99.

Williams, P.C., K.H. Norris, C.W. Gehrke, and K. Berstein. 1983. Comparison of Near-Infrared Methods for Measuring Protein and Moisture in Wheat. In: Cereal Foods World, Vol. 28, No. 2, pp. 149-152.

ABUNDANCE AND DISTRIBUTION OF MINERAL COMPONENTS ASSOCIATED WITH MOSES ROCK (KIMBERLITE) DIATREME

MUSTARD, JOHN F. and PIETERS, CARLE M., Brown University, Department of Geological Sciences, Box 1846, Providence, Rhode Island 02912

ABSTRACT

The surface mineralogy in and around Moses Rock diatreme, a kimberlite-bearing dike in SW Utah, was examined using internally calibrated AIS data. Distinctive near-infrared absorption characteristics of clays, gypsum, and serpentine (a key marker for kimberlite concentration) allowed the surface units containing these components to be identified spatially and the relative abundance of each component measured. Within the dike itself, channels and dispersed components of kimberlite and blocks of country rocks were accurately determined.

GEOLOGY OF MOSES ROCK.

Moses Rock kimberlite-bearing diatreme is one of several tertiary age diatremes on the Colorado plateau. At the present level of exposure, the diatreme is in contact with three members of the Permian Cutler formation: The Halgito tongue composed of reddish brown siltstone and sandstone with minor limestone, the Cedar Mesa sandstone consisting of buff sandstone, siltstone, grey limestone and gypsum, and the Organ Rock tongue, a sequence of reddish brown siltstone, variegated siltstone and sandstone. A simplified geological map of the region is shown in Figure 1. The geology and geochemistry of the dike have been described in detail by McGetchin (McGetchin, 1968; McGetchin and Silver 1970, 1972). The contact between the dike and sediments is sharp and the vent walls are steep. The dike itself is composed largely of blocks up to 100 meters across derived from the units exposed in the vent walls. The interstices between these blocks contain fragments of the larger blocks as well as limestone, crystalline rock fragments and mafic and ultramafic constituents. Kimberlite in the dike is characterized as a highly serpentinized ultramafic microbreccia and spatially comprises about 1% of the dike. Additional kimberlitic material (about 12%) is found dispersed throughout the dike.

DATA ACQUISITION AND CALIBRATION.

Airborne Imaging Spectrometer (AIS) data were acquired over Moses Rock dike and surrounding area in July of 1984 and 1985. Field work was conducted in the summer of 1985 to become familiar with the surface geology as well as 1) to collect samples for bidirectional laboratory reflectance measurements 2) to assess the nature of surface material and extent of vegetation coverage and 3) to measure reflectance spectra in the field with a portable field spectrometer (IRIS). The summary presented here is discussed in more detail in Mustard and Pieters (1986a).

AIS data were processed using VICAR and SPAM on a Vax 750. The data were calibrated by first dividing the raw data by a carefully selected internal standard. The standard area chosen is a region of low topography consisting of windblown sand. Field spectra were obtained of this area and surface samples were collected. High precision bi-directional reflectance spectra of these samples measured in the laboratory are in excellent agreement with the field measurements (see below). A homogeneous region within the standard consisting of about 60 lines of AIS data was averaged along track maintaining the independence of individual lines. Each line of the AIS scene was divided by the average radiance of the standard. The resulting AIS relative reflectance spectra were then multiplied by the laboratory spectrum of the standard collected from the field area and measured at the same phase angle as the AIS data.

This calibration procedure not only removes the effects of the solar irradiance spectrum, but also corrects for overall system response and, since no across track averaging was done, helps to correct for across track system or detector variations. To first order these calibrated

AIS data are true reflectances. The AIS data in the atmospheric water bands, however, still contain very low signal to noise ratio; these lower quality data in the wavelength regions 1.31-1.51 μm and 1.78 to 2.03 μm were thus not used in the analyses for mineral detection and abundance measurements.

MINERAL IDENTIFICATION.

From the calibrated true reflectance AIS data, three prominent spectral units were identified and interpreted mineralogically. These are a serpentine-bearing unit, a gypsiferous unit and a clay bearing unit. Additional surface compositions (such as desert varnish, carbonate) are discussed in the more detailed Mustard and Pieters (1986a) manuscript. Diagnostic spectral features of these three types of materials are shown in Figures 2-4. There is very good agreement between the spectral character of calibrated AIS spectra, field (IRIS) spectra, and laboratory (RELAB) bi-directional spectra.

AIS spectra of the serpentinized kimberlite are shown in Figure 2 along with field spectra measured with the IRIS field spectrometer and a laboratory spectrum of a surface sample collected from this unit. The strong 2.33 μm absorption band is evident in all these spectra as well a 2.2 μm reflectance peak and overall increase in reflectance from the visible towards longer wavelengths. X-ray diffraction of the field samples confirmed that serpentine is the dominant mineral in these samples.

In Figure 3 are shown AIS, IRIS and laboratory spectra from the standard area. The overall spectrum is generally flat in the wavelength region covered by AIS with a small (5%) absorption at 2.2 μm. This absorption feature is due to a minor clay component in the sand, interpreted to be illite.

Spectra of a unit containing gypsum are shown in Figure 4. Shown in this figure are laboratory spectra of a pure gypsum sample (sub-surface), a gypsum bearing soil collected at Moses Rock, and AIS spectra from a gypsiferous unit. The features to note are the overall decrease in reflectance toward longer wavelength, a 1.68 μm reflectance peak and a 2.21 absorption band centered between asymmetric reflectance peaks, the higher one at 2.08 μm and a lower one near 2.3 μm.

The laboratory spectrum of the gypsiferous soil shown in Figure 4, clearly shows there are multiple mineral species contributing to the observed reflectance spectrum of this soil. The strong Fe^{+3} absorptions throughout the visible wavelengths indicates the presence of ferric oxide bearing sand or siltstone; the presence of gypsum is equally well indicated by the diagnostic gypsum features near 1.4, 1.68, 1.9 and 2.2 μm.

APPROACH TO MINERAL MIXTURES.

Important geologic information relating to the proportions or abundances of minerals is contained within the reflectance spectra of mineral mixtures. One of the objectives in examining Moses Rock dike with mapping spectrometer data is to identify and determine the distribution of the mantle derived mafic kimberlite component in the dike. Spatial concentrations of kimberlite indicate that the eruption of this primary mantle material was confined to channels during emplacement. On the other hand, homogeneous kimberlite distribution throughout the dike would imply an entirely different style of eruption. To obtain this mineral abundance information from reflectance spectra of multicomponent surface soils requires the development of analytical tools to deconvolve complex spectra into contributions from individual components, or endmembers. Reflectance spectra of intimate or microscopic mixtures, however, cannot be modeled using a simple linear relationship between the end-member spectra.

The complex interactions of reflected light with particulate media have been modeled by Hapke (1981) with a rigorous application of radiative transfer models. In this model for bidirectional reflectance it is predicted that mixing systematics are linear if reflectance is expressed as single scattering albedo, SSA, a fundamental optical property of a material. Reflectance is a function of SSA, as well as viewing geometry, particle size, porosity, etc. However, to derive complete solutions to Hapke's (1981) equations for bidirectional reflectance, multiple viewing geometries are required. Mustard and Pieters (1986b) have simplified Hapke's equation to be applicable to a fixed viewing geometry and tested this

82

approach with laboratory measurements of well characterized mixtures of igneous rock forming minerals and mixtures of naturally occuring soils.

In this analytical approach the reflectance spectrum of a mixture is converted to single scattering albedo and the proportion of each endmember contributing to the mixture is calculated by a least squares fit of endmember SSA spectra to the measured mixture spectrum. The abundance coefficient calculated for each component is called the relative geometric cross section, or F parameter, and is directly proportional to mass fraction and inversely proportional to particle diameter of the specific mineral component. The results of this laboratory test of the analytical model (see Mustard and Pieters, 1986b) indicate that this technique accurately predicts the abundance of endmember components from the reflectance spectrum of a mixture, provided strongly opaque components (reflectance < 10%) are not present.

MINERAL ABUNDANCE DERIVED FROM AIS DATA.

This approach to derive mineral abundance information for naturally occurring surface intimate mixtures (Mustard and Pieters, 1986b) was implemented on the JPL SPAM software package. The routine MIXTURE was modified to convert the calibrated AIS reflectance data to single scattering albedo prior to a least squares regression of the endmember SSA spectra to the AIS SSA spectra. The modified routine produces the desired relative geometric cross-section, or F-parameter, for individual components (endmembers) in the mixture.

An important consideration prior to deconvolving the AIS image spectra is the determination of appropriate endmembers to be used in the analyses. Initial choices of endmembers for abundance determination in the Moses Rock region include standard soil (sand dunes), illite, a sample from the Cedar Mesa sandstone, gypsum and kimberlite (serpentine). Spectra for these endmembers are shown in Figure 5. All these carefully selected components except illite were collected from the field area.

The results of deconvolving spectra from an AIS flight line (indicated in Figure 1) into the abundances of the endmember components is shown in Figure 6 (BROWN U. Slide 1). The first two endmembers (standard soil and illite) dominate the abundance calculations. This result is consistent with the geology these endmembers represent; the reddish brown fine grained derivative of sandstones and siltstones are a pervasive component of all soils. Since they are fine grained, the F-parameter values, which are inversely proportional to particle diameter, are high. The other mineral abundance maps correspond well with known geology. The Cedar Mesa unit occurs at moderate values (0.35-.4) throughout the area of the Cedar Mesa sandstone covered by the flight line. The gypsum unit can be seen to have two primary occurences midway down the strip. The F-parameter values are low because the typical gypsum grain size is large compared to the fine grained oxide and clay bearing component found intimately mixed with the gypsum. These F-parameter values of close to 0.3 thus correspond to actual gypsum abundances of up to 70%.

From analyzed field samples, it is known that serpentine is a direct indicator of kimberlite occurence and concentration. It occurs in local concentrations within the dike as is shown in Figure 6. With the current spectral coverage of AIS an ambiguity sometimes arises between serpentine and carbonate (which contains an absorption centered near 2.33 μm). Therefore the occurrences of "serpentine" in the sedimentary units actually correspond to known limestone beds. The greater spectral range of AVIRIS should allow these two components to be distinguished. Nevertheless, in the body of Moses Rock diatreme the distribution of serpentine corresponds directly with the results of detailed mapping of kimberlite by McGetchin (1968).

The distribution and abundance for serpentine was analyzed in more detail and is shown in Figure 7 (BROWN U. Slide 2). The F-parameter values in the oval shaped region of high concentration range from 0.4 to 0.7 and the peak values occur for the region mapped by McGetchin as pure kimberlite. On the opposite side of the dike is another patch containing a significant concentration of serpentine. These areas are clearly primary channels for the kimberlite. It is apparent from figures 6 and 7 that this approach also maps the diluted

83

kimberlite of the dike quite efficiently. The vacant (non-serpentine) regions in the dike correspond to large breccia blocks of the Cutler formation.

It is clear even from this initial AIS study that a wealth of geological and geochemical information is contained in mapping spectrometer data. We look forward to the coming era of advanced airborne and spacebased sensors which will certainly open valuable opportunities for geological applications of remotely acquired data.

REFERENCES

Hapke, B. 1981. Bidirectional reflectance spectroscopy 1. Theory, *J. Geophys. Res.*, 86, 3039-3054.

McGetchin, T.R. 1968. The Moses Rock dike: Geology, petrology, and mode of emplacement of kimberlite-bearing breccia dike, San Juan County, Utah, Ph.D. thesis, 405 pp., Calif. Inst. of Technol., Pasadena.

McGetchin, T.R. and Silver, L.T. 1970. Compositional relations in minerals from kimberlite and related rocks in the Moses Rock Dike, San Juan County, Utah. *The American Mineralogist, Vol. 55*, 1737-1771.

McGetchin, T.R. and Silver, L.T. 1972. A crustal-upper mantle model for the Colorado Plateau based on observations of crystalline rock fragments in the Moses Rock Dike. *J. Geophys. Res., 77,* 7022-7037.

Mustard, J.F. and Pieters, C.M. 1986a. Characterization of eruption channels in Moses Rock kimberlite diatreme with mapping spectroscopy, to be submitted, *J. Geophys. Res.*

Mustard, J.F. and Pieters, C.M. 1986b. Quantitative abundance estimates from bidirectional reflectance measurements. *Proc. Lunar Planet. Sci. Conf. 17th, J. Geophy. Res.,* submitted.
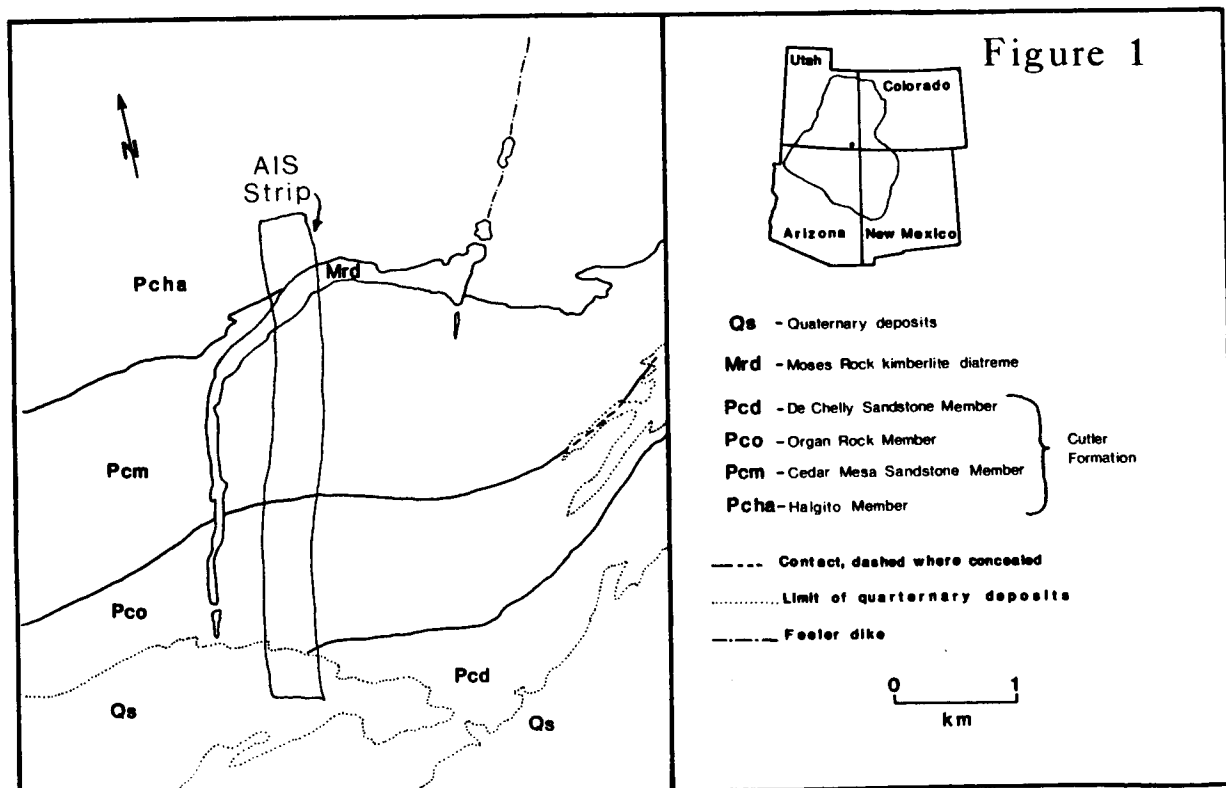
Figure 1

C·2
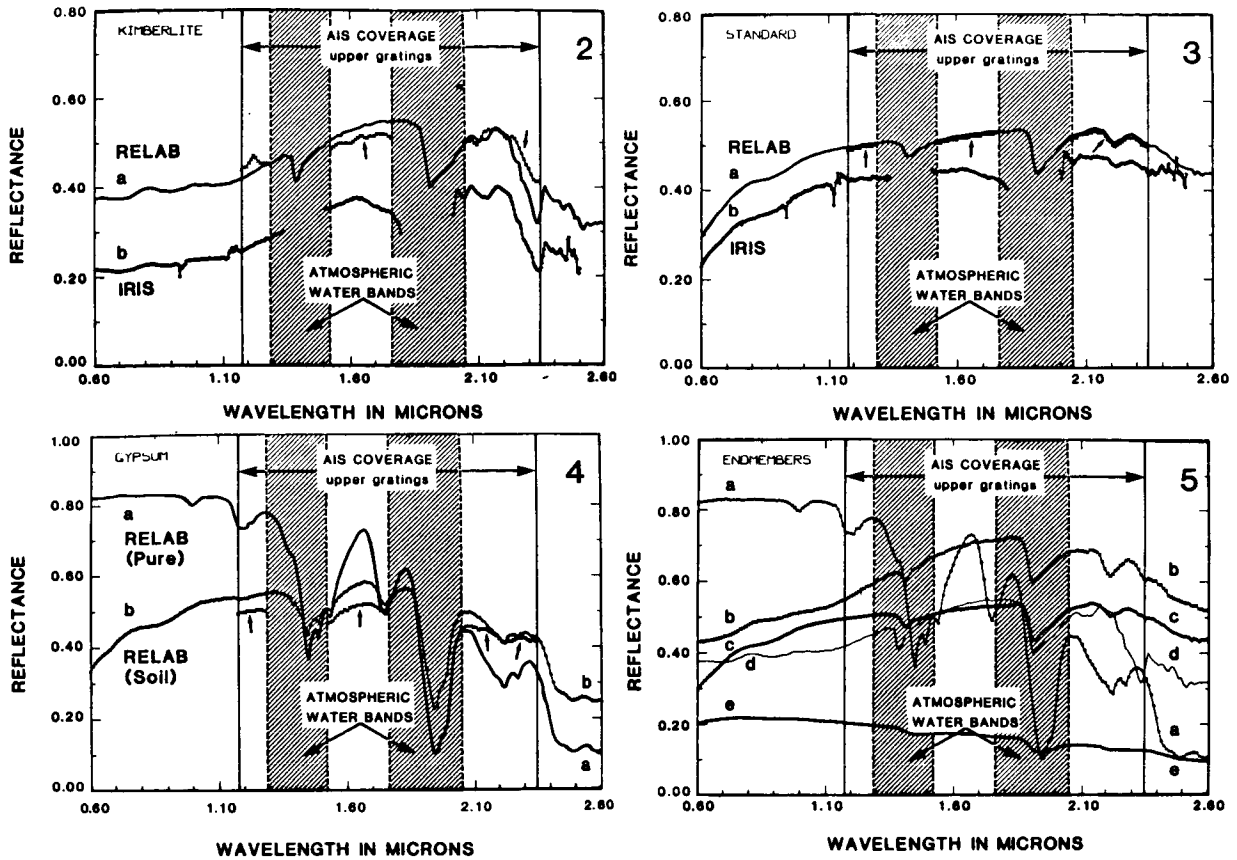
Figure 2, 3, 4 Laboratory (RELAB), field (IRIS), and AIS spectra (small arrows) of Moses Rock materials. **Figure 5.** Laboratory (RELAB) bidirectional reflectance spectra of samples used as endmember for deconvolution of AIS spectra: **a** (gypsum), **b** (illite), **c** (standard soil), **d** (kimberlite soil), and **e** (Cedar Mesa samples).
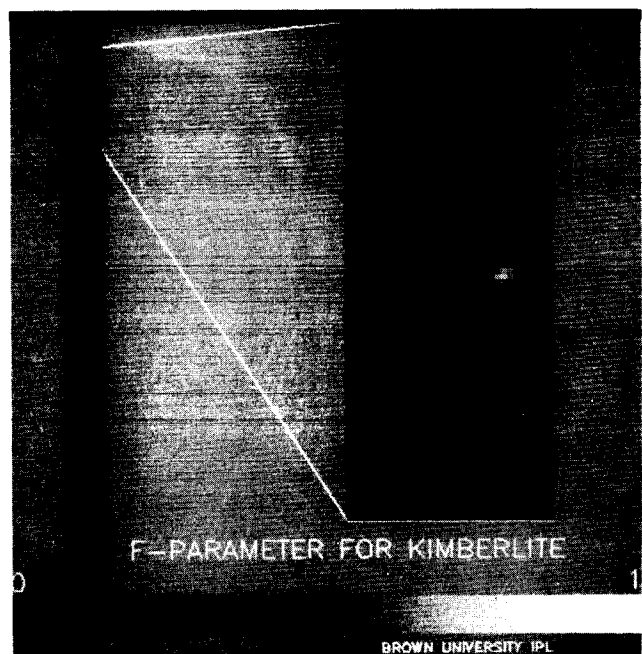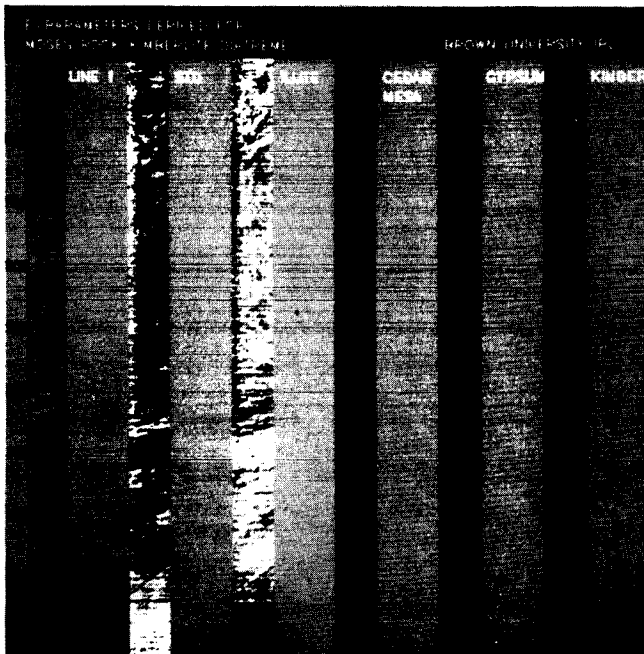
Figures 6 and 7 Deconvolution of AIS spectra into mineral abundance images (F-parameter for endmembers). (See color slides numbers 3 and 4 in the back cover pocket of this publication.)

COMPARISON OF THE 1984 & 1985 AIS DATA OVER THE SINGATSE RANGE (YERINGTON) NEVADA.

R.J.P.LYON, Applied Earth Sciences Department,Stanford University,USA

ABSTRACT

The Singatse Range is composed of a series of 53 types of volcanic, plutonic, metamorphic and sedimentary rocks. In addition the Jurassic plutonic rocks are also of economic interest for their copper mineralization which is contained in a porphyry dike swarm. This paper contrasts and compares the 1984 and the 1985 flight results from the AIS instrument flown in the NASA/JPL C-130 aircraft. Due to the long thin nature of the economically-interesting target (hydrothermal alteration) the flights were flown as parallel lines, with only one flight crossing at right angles. The 1984 data are less noisy than the 1985, in which many sets of vertical stripings from bad detectors can be seen. Significantly however, enough of the hydrothermal alteration patterns can be seen in each line at the mutual crossing points that one can say that the specific targets were detected in both year's flights. The spectra of both years are corrupted by the "second-order" effect from the grating, but O-H bond absorptions at essentially-correct wavelengths for sericite and/or kaolinite can be seen. Internal adjustments for wavelength calibrations were made using initially the H-O-H water vapor absorptions at 1.386 and 1.868 um, and with refinement by using the CO_2 bands at 2.006 and 2.053 um respectively. AIS-II flights in 1987, and especially AVIRIS in 1987/88 would help to extend this detailed, site-specific mapping to much broader, regional mapping experiments along the whole length of the Singatse Range.

INTRODUCTION

The porphyry complexes of the Singatse Range at Yerington and Ann Mason, NV have been the target of extensive studies by our laboratory at Stanford for the past fifteen years. Because both geological and remote sensing studies have taken place (4 Ph.D. theses in geology; 4 Ph.D. and 3 MS theses in remote sensing) this geological site has a breadth of ground information unlike many in the US. In 1985/86 six remote sensing papers alone will have

been published which deal with the aspects of the geological-remote sensing connections of this site.

Geology of the Site.

Geologically the Singatse Range area (12 Km N-S by 6 E-W) contains over 53 rock types-- 15 sedimentary, 20 volcanic ,17 igneous plutonic, and 4 metamorphic-- of which all have formation names, indicating their differentiation (and significance) in conventional ground-based mapping.

Table 1. Rock types in the Singatse Range (Yerington) site
(from Proffett & Dilles, 1984)

PLUTONIC (17)		VOLCANIC (20)	SEDIMENTARY (15)	METAMORPHIC (4)
	Ja	Tba	Qal	Skarns-
	Jr	Tha	Qls	(Ludwig)
Shamrock	Jqp	Thai	Ta	(Mason V)
"	Jsa	Tb	Tws	(Bluestone)
"	Jqms	Td	Tcg	Hornfels
"	Jgdp	Tbs	Jq	
Yerington	Jqmp	Tbm	Jgu	
"	Jpq	Ts	Jl	
"	Jpqm	Tsl	JT_rcl	
"	Jgd	Trt	JT_rcv	
"	Jqm	Twh	JT_rlb	
"	Jbqm	Tru	T_rl	
"	Jdb	Tgm	T_rvl	
Strosnider	Mzqp	Tei	T_rla	
Ranch	Mzap	Teb	T_rll	
"	Mzqm	Jaf		
"	Mzdi	T_rad		
		T_rr		
		T_ra		
		T_rv		

Ages range from earliest Triassic for the sedimentary rocks through Upper Jurassic for the plutonic rocks. Cover-rocks range from Eocene to Middle·Miocene for the ash-fall tuffs ("ignimbrites") up to Quaternary alluvium. Over 50 rocks have been age-dated from this range. Those which are published were often the average of a series of datings, all performed for the Anaconda Co. (Proffett & Proffett,1976). Estimates of the geological efforts of the Anaconda Company's geological staff indicate that about 100 man-years of professional mapping has been done on this range alone. Because of the personal experience with this mapping effort of several of our Faculty and students (especially M.T.Einaudi,J.Dilles, etc.), the Remote Sensing Laboratory is in an excellent position to assess the geological-remote sensing relationships.

Drilling by Anaconda in the range totals over 250,000 feet and thus provides excellent vertical control on the cross-sections which appear in the recently published maps at a 1:24,000 scale (Dilles & Proffett, 1984)

Structurally this range is of great geological significance as one of the first, well-documented examples in which listric (curved,concave-upward) faulting forms a dominant feature of the blocks which were rotated around sub-horizontal axes increasing with time (from 28 M.Y. to the present) (Proffett, 1977). Originally deposited as flat-lying ash-fall and -flow tuffs, the oldest (27.5 M.Y.) tuffs of the Guild Mine member now have 70^{0} W dips, with the middlemost (T_{10}) rhyolitic tuff of 26 M.Y. age having a 50^{0} W dip. The youngest in this sequence, the 17-19 M.Y. old Lincoln Flat hornblende andesite has only about 15^{0} W dip.

As both the Triassic /Jurassic rocks and the Miocene tuffs have rotated together to the west, the oldest Triassic beds dip almost vertically with a well developed fold axis which has a 70^{0} W plunge. The Jurassic rocks(of economic interest) plunge 20^{0} East towards their batholithic base,having being rotated 70^{0} W from vertical.
Thus one can walk across outcrop, from an original -2Km depth downwards to -8Km depth merely by walking towards the SE.

Local Description Pertinent to AIS

Detailed descriptions of the terrain overflown by the AIS appear in last year's report (Lyon & Lanz, 1985). Other parallel studies will be reported elsewhere in 1986 (IGARSS,Zurich & ERIM,Reno,1986). In addition the range site will be the first major stop on the field trip for the ERIM, Reno Conference, October 3, 1986.

RATIONALE FOR AIS SITE SELECTION

The following summarizes the rationale for selection of this site for the AIS flights;

1. The site is well mapped geologically and mineralogically at 1:4800 scale (Dilles, 1983) and this is also published at a scale of 1:24,000 (Dilles & Proffett,1984).

2. An extensive set of remote sensing studies performed by our laboratory exist, with coverages by Landsat MSS,TM,TMS and now AIS ('84 & '85), together with SKYLAB (S-191), HCMM, etc.

3. Large areas of man-made homogeneous materials exist for calibration targets, as mine dumps, tailings ponds, etc. as well as large, natural, alluvial fans which have been shown to be spectrally-flat (for "flat-field" corrections to AIS).(Roberts, et.al.,1985).

4. Over 300 high-resolution VIRIS spectra (Collins Visible Infrared field spectrometer) have been collected to date (5/86) and more will be taken in the up-coming field season this Summer.

SPECIFIC AIS TARGETS-1984/85 FLIGHTS

Detailed studies of the hydrothermal rock alteration (Dilles,1983) together with our field mapping indicated that while the Singatse Range trended N-S, the quartz monzonite dike swarms with their attendant rock alterations (both the "Early-hypogene" and the "Late-stage" geothermally-induced) followed a SE-NW direction, starting at the N-S Bluestone Fault, for over 5 Km (roughly 4 Km NE of the small town of Mason on the Walker River). Patterns repeated by extensive, roughly N-S block-faulting interrupt this continuity, but the trend can be followed 2-4 Km across the Mason Pass road to the Blue Hills, and on over to the Buckskin Ranges 5-6 Km to the NE. This total distance of 22 Km represents (vertically) about 8-9 Km of the original cogenetic dike-extrusive volcanic pile, fed by the dikes from the deeper-seated batholithic rock, now to the SE, almost 100% extension due to faulting, (Proffett,1977).

The outcrop of the alteration of interest ("Late-stage", or geothermal) is quite narrow starting at the crest of the Singatse Range where it covers about 400m. As one progresses NW ("upwards" in the section). the northernmost edge becomes hidden under the ignimbrites lying over the (now) flat-lying Singatse Fault. At the Mason Pass road (5 Km to the NW) the altered zone broadens out (tree-like) to cover about 1-2 Km. In the Blue Hills the zone is 2-3 Km wide and in the uppermost zone (in the cogenetic lavas) at the Buckskin Range the zone widens to about 6 Km in the N-S direction.
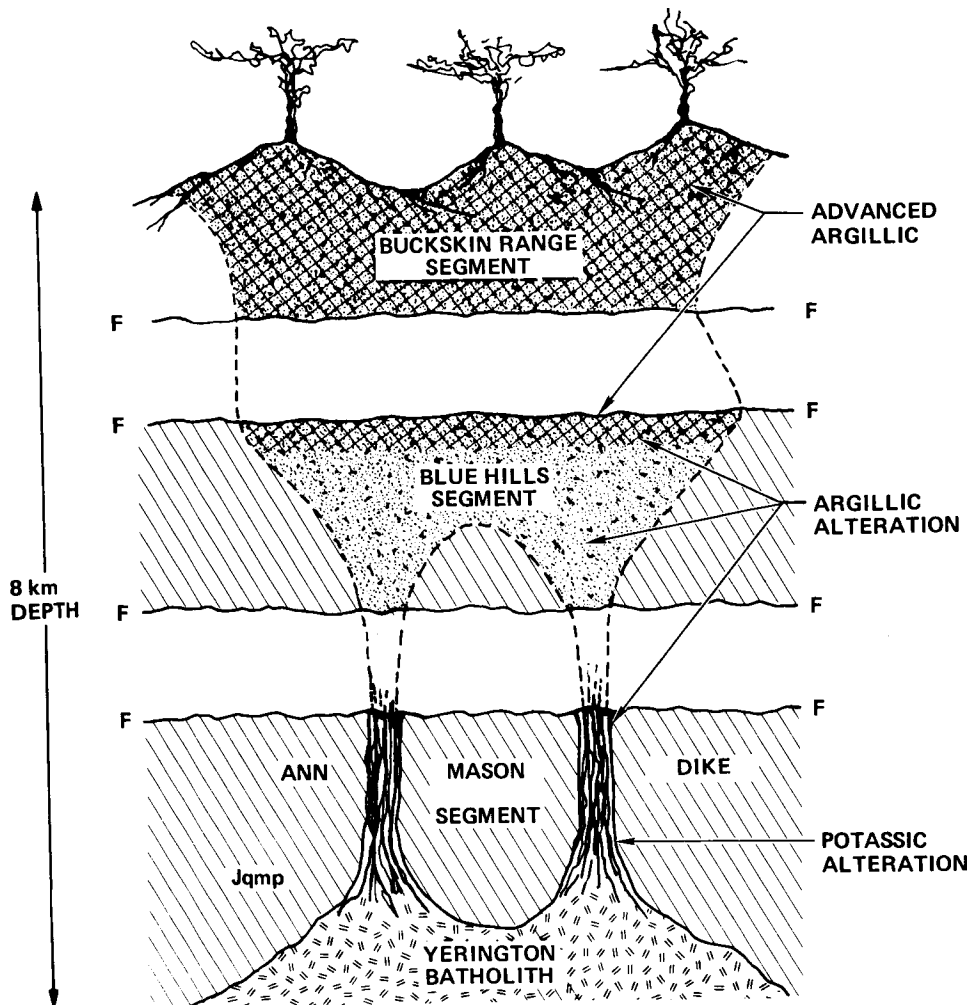
Figure 1. Cartoon-style vertical cross-section of the original plutonic-volcanic pile, showing the relative position of the Ann Mason dikes, the Blue Hills alteration and the Buckskin Range volcanics (heavily altered "advanced argillic" zone). F-F ; breaks due to faulting.

The outcrop of the alteration of interest ("late-stage",geothermal) is quite narrow, starting at the central spine of the Singatse Range covering about 400-600 m, with its northern edge hidden under the ignimbrite cover which lies over the (now) flat-lying Singatse Fault. At the Mason Pass road (5 Km to the NE) it rapidly broadens, tree -like up to a 1-2 Km width. In the flat lying Blue Hills the altered zone is 4 Km wide, and at the upper-most level in the Buckskin Range the width reaches 6 Km.

AIS flight lines were directed mostly in a SE-NW direction so as to maximize the coverage along this thin alteration zone, and to look for specific mineral changes (originally vertical) in the volcanic-geothermal hydrothermal plumbing system. Operationally this meant vectoring the C-130 in to hit a target only 400 m wide but over 6 Km in length. Three parallel flights (# 407,409,508) up the structure, with one flight crossing at

90

about 60^0 (# 410) from the SW-NE direction completed the strategy. Ten Km to the north another " faulted-off slice" of the structure (MacArthur) was traversed by two parallel lines (# 408,509) also flown in the basic SE-NW direction.

AIS INSTRUMENT--WAVELENGTH CALIBRATIONS

1984 Flight Calibrations (10 July, 1984)

In the 1984 data it was clear from inspection of the relatively broad H_2O vapor absorptions, that the wavelength calibration originally provided by JPL was somehow in error, and that the O-H absorptions also were displaced. By carefully studying the deepest absorptions near 1.386 um in the raw data set we were able to shift the channel-lambda relationship a offset of several channels to a better fit. When the corrected Channel-lambda values were later supplied our empirically-derived values were found to be quite close. The O-H absorptions in the AIS data over sites of known O-H-bearing mineralogy were found to agree. (Roberts, et.al, in press).

As with the 1985 data we retroactively applied the further correction based upon the 2.006 and 2.053 um CO_2 absorptions, although the latter appeared to be in the middle of a grating change.(See companion paper by Roberts, et.al., in this 1986 issue).

1985 Flight Calibrations.

Again we obtained our flight data set without calibration data. It was soon apparent that quite different grating settings had been used (relative to those of 1984), and that about a seven channel shift to shorter wavelengths was involved (see Table I). This analysis again was based upon the water vapor lines (in the raw-data mode). In addition, at the suggestion of Dr.A.A.Green (4/21/86) we looked for the presence of (and used) the 2.006 and the 2.053 um CO_2 peaks in both the raw- and processed-data sets, even though in "log-residual" data these should have been removed.

Most of the pixels we examined in the log-residual data carried very small peaks with the correct separation of 47 nm. These were used to " correct" the lambda-channel relationships in our table (Table 1). What did worry us however, was that these peaks oscillated about 1-2 channels down the flight line, and produced a wavering line in the imagery--no explanation for this was available, but it appears to be a grating wobble".

91

* 25 JUL 84 GRATING SETTINGS		** 23 SEP 85 GRATING SETTINGS		25 JUL 84 GRATING SETTINGS		23 SEP 85 GRATING SETTINGS		25 JUL 84 GRATING SETTINGS		23 SEP 85 GRATING SETTINGS	
1	1.155	1	1.229	49	1.601	49	1.683	97	2.048	97	2.134
2	1.164	2	1.238	50	1.610	50	1.692	98	2.057	98	2.143
3	1.174	3	1.247	51	1.620	51	1.702	99	2.067 CHANGE	99	2.152
4	1.183	4	1.257	52	1.629	52	1.711	100	2.076 GYPSUM	100	2.162 KAOLINITE
5	1.192	5	1.266	53	1.638	53	1.720	101	2.085	101	2.171 PYROPHYLLITE
6	1.201	6	1.275	54	1.647	54	1.729	102	2.095	102	2.180
7	1.210	7	1.284	55	1.657	55	1.738	103	2.104	103	2.189
8	1.220	8	1.293	56	1.666	56	1.748	104	2.113	104	2.198
9	1.229	9	1.303	57	1.675	57	1.757	105	2.123	105	2.208 KAOL,SER,MONT,ALUN.
10	1.238	10	1.312	58	1.684	58	1.766	106	2.132	106	2.217
11	1.247	11	1.321	59	1.694	59	1.775	107	2.141	107	2.226
12	1.257	12	1.330	60	1.703	60	1.784	108	2.150	108	2.235
13	1.266	13	1.339 H2O	61	1.712	61	1.794	109	2.160	109	2.244
14	1.275	14	1.349 H2O	62	1.721	62	1.803	110	2.169	110	2.254
15	1.284	15	1.358 H2O	63	1.731	63	1.812	111	2.178	111	2.263
16	1.293	16	1.367 H2O	64	1.740	64	1.821 H2O	112	2.188	112	2.272
17	1.303	17	1.376 MAX-H2	65	1.748	65	1.835 CHANGE	113	2.197	113	2.281
18	1.312	18	1.386 MAX-H2	66	1.757	66	1.844 H2O	114	2.206	114	2.290
19	1.321	19	1.395 H2O	67	1.767	67	1.853 H2O	115	2.216	115	2.300
20	1.330	20	1.404 H2O	68	1.776	68	1.863 H2O	116	2.225	116	2.309
21	1.339 H2O	21	1.413 H2O	69	1.785	69	1.872 H2O	117	2.234	117	2.318
22	1.349 H2O	22	1.422 H2O	70	1.794	70	1.881 MAX-H2	118	2.244	118	2.327
23	1.358 H2O	23	1.432 H2O	71	1.804	71	1.890 MAX-H2	119	2.253	119	2.336 CALCITE
24	1.367 H2O	24	1.441 H2O	72	1.813 H2O	72	1.899 H2O	120	2.262	120	2.346 SERICITE
25	1.376 MAX-H	25	1.453 H2O	73	1.822 H2O	73	1.909 H2O	121	2.272	121	2.354
26	1.386 MAX-H	26	1.462 H2O	74	1.832 H2O	74	1.918 H2O	122	2.281	122	2.364
27	1.395 H2O	27	1.471	75	1.841 H2O	75	1.927 H2O	123	2.290	123	2.373
28	1.404 H2O	28	1.481	76	1.850 H2O	76	1.936 H2O	124	2.300	124	2.382
29	1.413 H2O	29	1.490	77	1.859 H2O	77	1.945 H2O	125	2.309	125	2.391
30	1.422 H2O	30	1.499	78	1.869 MAX-H2	78	1.955 H2O	126	2.318	126	2.400
31	1.432 H2O	31	1.508	79	1.878 MAX-H2	79	1.964 H2O	127	2.327	127	2.410
32	1.441 H2O	32	1.518 CHANGE	80	1.887 H2O	80	1.973	128	2.337	128	2.419
33	1.453 H2O	33	1.536	81	1.897 H2O	81	1.982				
34	1.462 H2O	34	1.545	82	1.906 H2O	82	1.991				
35	1.471	35	1.554	83	1.915 H2O	83	2.001				
36	1.481	36	1.564	84	1.925 H2O	84	2.010				
37	1.490	37	1.573	85	1.934 H2O	85	2.019 CO2 2006				
38	1.499	38	1.582	86	1.943 H2O	86	2.028				
39	1.508	39	1.591	87	1.952 H2O	87	2.037				
40	1.518	40	1.600	88	1.962	88	2.047				
41	1.527	41	1.610	89	1.971	89	2.056				
42	1.536	42	1.619	90	1.980	90	2.065 CO2 2053				
43	1.545	43	1.628	91	1.990	91	2.074 GYPSUM,MONT				
44	1.555	44	1.637	92	1.999	92	2.083				
45	1.564	45	1.646	93	2.008	93	2.093				
46	1.573	46	1.656	94	2.017	94	2.102				
47	1.583	47	1.665	95	2.027	95	2.111				
48	1.592	48	1.674	96	2.036	96	2.120				

* D.TUCKER LTR 6/26/84
** D.TUCKER PHONE CALL 5/2/86

Table 2 Comparison of Lambda-Channel relationships, 1984/85.

JOINT CROSSINGS OF AIS FLIGHTS.

One method of testing the repeatability of the AIS flight data is to cross the same area several times. Because it is difficult to hit the same flight path twice due to the normal uncertainties of aircraft navigation, we chose to fly parallel, N-S offset flight lines. As our target at Ann Mason was long and thin this seemed to be a better plan.

In July 25,1984 we placed one of our lines (# 410) at about 60^0 to the others, and produced two (2) crossings (A and B) with lines 407 and 409 over the most-altered area. In September 23,1985 we only were able to have two lines due to a tight flight-time schedule, and elected one (# 508) to be parallel with the main trend again, crossing the older #410 at crossing C.
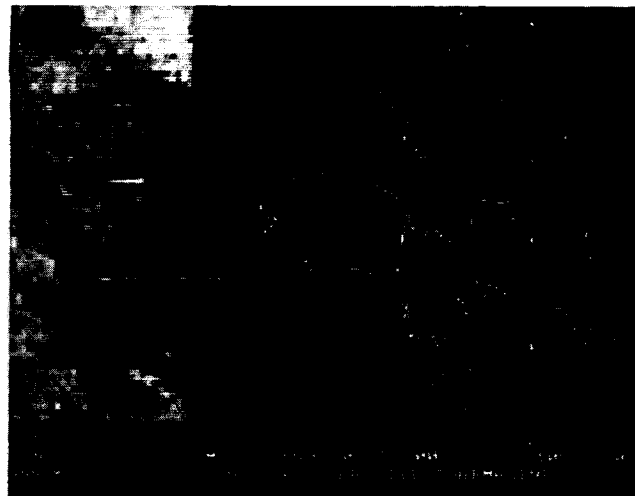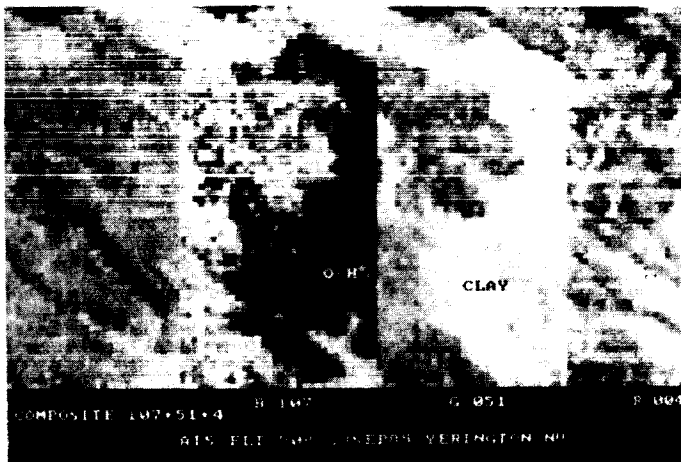
Fig 2. (Left) B/W copy of a color composite of three
      channels (107,51,3) showing the strong O-H absorption
      of sericite (black).

Fig 3. (Right) Graphical form of the same data, showing the
      spectra with pronounced O-H absorptiona at 2.206 um
      (vertical line).

1984 Crossings A & B

Crossing A, with # 409 & 410 is 1.0 Km to the SE of the 4 x 4 Km altered zone of interest, missing it entirely. Accordingly neither line in Crossing A show marked O-H absorption areas, although some patchy areas can be discerned.

Crossing B, of # 407 & 410, is of much more interest, as the two lines intersect over an ESE extension of the main altered zone in the quartz monzonite and quartz monzonite porphyry system. Here it is possible to define geographically-similar areas of O-H absorption common to both lines.

1985/84 Crossing C

As with many well-planned things in experimental studies, this crossing of the 1984 line with the new 1985 line took place exactly over a small valley filled with alluvium and wind-blown sand of very recent origin. Portions of the 32-pixel swath do intersect parent rock, and the presence of the O-H absorptions can be used to define the altered ground. Examples of the patches of O-H absorbing clay can be well seen in Figures 2 & 3 taken from Run 508 at line 800.

CONCLUSIONS.

A. Despite the variability of the wavelength settings, it is possible to establish the " correct " positions using the atmospheric bands at 1.386, 1.868 2.006 and 2.53 um.

B. Comparable spectral evidence exists from repeated flights over the same terrain, that the spectral patterns can be repeated in the 1984 and the 1985 data.In addition continuing ground spectral measurements, using the Collin's VIRIS spectrometer confirm the types of O-H bearing minerals seen in the flight data.

C. Flights in 1986/87 with the AIS-II instrument would be extremely significant, given the degree of ground spectral work being performed in the Singatse Range.

D. AVIRIS flights (with the markedly wider swath width), flown N-S along the crest of the Singatse Range in the 1987/88 time period, and extending both to the south and to the north, would allow the REGIONAL MAPPING of these same rock types, presently intensively studied in detail only in this smaller (Ann Mason)site.

REFERENCES

Dilles, J.H., 1983, The petrology and geochemistry of the Yerington batholith and the Ann-Mason porphyry copper deposit, western Nevada, Unpublished Ph.D. thesis, AES Department, Stanford University.

Einaudi, M.T.,1977,Petrogenesis of the copper-bearing skarn at the Mason Valley mine,Yerington district, Nevada: Econ.Geol. 72,769-795

Green,A.A., Craig,M.D., 1985,Analysis of aircraft spectrometer data with logarithmic residuals: Proc. AIS Data Analysis Workshop,April 8-10,1985,G.Vane & A.F.H. Goetz, eds. Jet Propulsion Lab,Cal.Tech.,Pasadena, CA, 111-119

Lyon,R.J.P. and Lanz, K, 1985, Field utilization of AIS 128-Channel imagery using microcomputers: Application to Yerington,NV,field: Proc. AIS Data Analysis Workshop,April 8-10,1985,G.Vane & A.F.H. Goetz, eds. Jet Propulsion Lab,Cal.Tech.,Pasadena, CA, 35-40

Proffett,J,M, 1977, Cenozoic geology of the Yerington district, Navada, and implications for the nature and origin of basin and range faulting: Geol.Soc. Amer., Bull 88:247-266

Proffett,J.M.Jr., and Dilles,J.H., 1984, Geological Map of the Yerington, District, Map 77, published by the Nevada Bureau of mines & Geology,University of Nevada,Reno,NV. One page map in folder.

Proffett,J.M.Jr. and Proffett,B.H.,1976, Stratigraphy of the Tertiary ash-flow tuffs in the Yerington, district, Nevada: Nevada Bureau of mines and Geology, Report 27, 28p.

Roberts,D.A.,Yamaguchi,Y. and Lyon,R.J.P., 1985, Calibration of airborne imaging spectrometer data to percent reflectance using field spectral measurements: Proc. Nineteenth Int.Symp. Rem.Sens.Environ.,Ann Arbor ,MI, Oct 21-25,1985 (in press)

Roberts,D.A.,Yamaguchi,Y. and R.J.P.Lyon,1986, Calibration of various techniques for calibration of AIS Data: Proc. Second AIS Data Analysis Workshop, May 6-8, 1986, G.Vane & A.F.H.Goetz, eds. Jet Propulsion Lab,Cal.Tech.,Pasadena, (in this issue).

IDENTIFICATION OF HYDROTHERMAL ALTERATION ASSEMBLAGES USING AIRBORNE IMAGING SPECTROMETER DATA

SANDRA C. FELDMAN and JAMES V. TARANIK, Mackay School of Mines,
University of Nevada-Reno, Reno, NV 89557, USA

ABSTRACT

Airborne Imaging Spectrometer (AIS) data, field and laboratory
spectra and samples for x-ray diffraction analysis were collected in
argillically altered Tertiary volcanic rocks in the Hot Creek Range,
Nevada. From laboratory and field spectral measurements in the 2.0 to
2.4 um range and using a spectroradiometer with a 4 nm (0.004 um)
sampling interval, the absorption band centers for kaolinite were
located at 2.172 and 2.215 um, for montmorillonite at 2.214 um and for
illite at 2.205 um. Based on these values and the criteria for
resolution and separation of spectral features, a spectral sampling
interval of less than 4 nm (0.004 um) is necessary to separate the
clays. With an AIS spectral sampling interval of 9.3 nm (0.0093 um),
a spectral matching algorithm is more effective for separating kaoli-
nite, montmorillonite and illite in the Hot Creek Range than using the
location of absorption minima alone.

INTRODUCTION

Airborne Imaging Spectrometer (AIS) data were collected in an
area of hydrothermally altered and unaltered carbonate rocks and
rhyolitic ash-flow tuffs in the southern Hot Creek Range, Nevada.
Atmospherically corrected AIS data were used to separate argillically
altered Tertiary ash-flow tuffs from unaltered tuffs. The separation
was possible because of spectral absorption features near 2.2 um
caused by molecular vibrations related to the hydroxyl ion and struc-
tural water (Feldman and Taranik, 1985). Although this work demon-
strated that altered rock could be differentiated from unaltered rock,
it did not determine whether kaolinite, montmorillonite and illite,
found in the altered ash-flow tuffs, could be spectrally and spatially
separated from each other using AIS data. This paper addresses the
identification of clays by resolution of narrow absorption features in
their reflectance spectra and by spectral curve-matching procedures.
Clay identification was accomplished by comparing AIS spectral signa-
tures with those acquired in the field and laboratory with a Geo-
physical Environmental Research (GER) IRIS spectroradiometer and also
by computer processing AIS imagery using the Spectral Analysis Manager
(SPAM) software developed by the Jet Propulsion Laboratory (JPL).
Detailed field mapping and x-ray diffraction analysis supplement the
spectral methods.

COLLECTION OF FIELD AND LABORATORY SPECTRA

Alteration mineral spectra are most distinctive in the portion of the spectrum between 2.0 and 2.4 um where overtone and combination features related to anion vibrations occur (Hunt and Ashley, 1979; Goetz and Rowan, 1981). The following discussion will be limited to this portion of the spectrum.

The spectra of Hot Creek rocks were measured in the field and laboratory with a GER IRIS spectroradiometer. The instrument measures the radiance of the sample and the Fiberfrax standard simultaneously using a dual beam system. The radiance measurements can then be converted to percent reflectance of the target relative to the standard. In the 2.0 to 2.4 um region, the instrument spectral bandwidth is 4 nm.

Kaolinite, montmorillonite and illite spectra recorded with the spectroradiometer, possess absorption features which are similar in form and very close in wavelength (Figures 1 and 2). The kaolinite spectrum shows a characteristic doublet (the first absorption feature will be referred to as kaolinite A and the second absorption feature as kaolinite B). The illite spectrum has a minimum at a shorter wavelength than the dominant kaolinite minimum. The absorption minimum for montmorillonite has a wavelength close to the second kaolinite minimum and is similar in form to illite. The montmorillonite absorption feature, however, is broader, more asymmetrical and the depth of the feature is not as great as in illite even in pure samples.

Sensor spectral sampling interval greatly influences the detection of absorption features. Using kaolinite as an example, at a spectral sampling interval of 20 nm, the first kaolinite absorption feature begins to lose definition and becomes a shoulder in the spectral curve (bottom curve, Figure 3). Resolution of these spectral absorption features is dependent on both the width and depth of the feature and the separation between two absorptions. In order to resolve an absorption feature, a spectral sampling interval equal to no more than one half the width of the feature is necessary (Nyquist criterion). For kaolinite, the separation between the two absorptions is about 40 nm (less if the points of inflection on the curves rather than minima are considered). The kaolinite absorption features should be resolved at a 20 nm or smaller spectral sampling interval. Since the GER bandwidth is 4 nm and AIS spectral sampling interval is 9.3 nm, the kaolinite doublet should be resolved with both the field and airborne instruments. For AIS1 the sampling interval is the same as the instrument resolution because the system is diffraction limited. In the resolution of two absorption features in the same mineral or, two or more minima from different clays in mixtures, the feature being resolved is actually the peak or portion of the spectrum between the minima.

Using the digital data acquired with the IRIS spectroradiometer, the average absorption minimum and difference between minima were calculated for kaolinite, montmorillonite and illite samples (Tables 1 and 2). Only samples which showed just one clay group in the x-ray diffraction pattern were used in the calculation of the clay statistics.

Figure 1. GER spectroradiometer curves for kaolinite and illite.

TUFF OF TWIN PEAKS, LAB SPECTRA
FILES: LTC-5111 LTC-5112 LTC-5121 LTC-5131
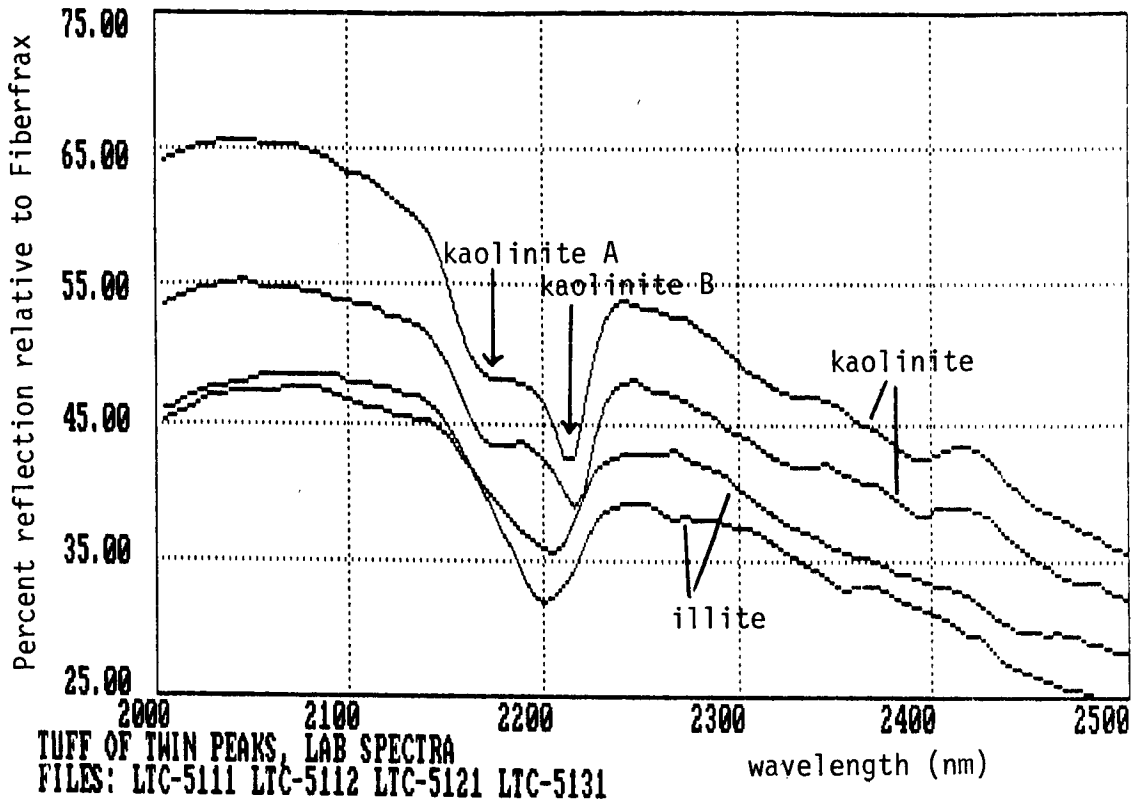
Figure 2. GER spectroradiometer curves for three samples of montmorillonite.

SHINGLE PASS TUFF, LAB SPECTRA
FILES: RC-71211 RC-31221 RC-31231
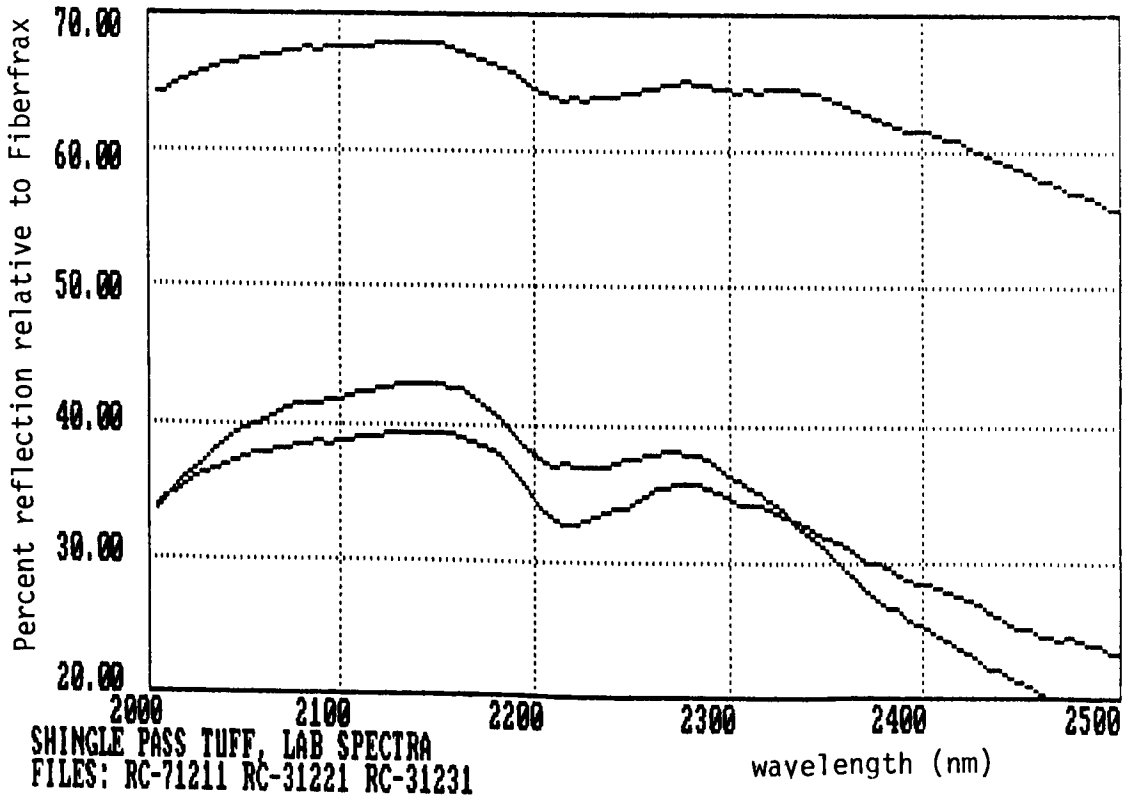
Figure 3. Kaolinite spectra at 4 to 20 nm spectral
        sampling intervals (JPL, 1983).

EFFECT OF SAMPLING INTERVAL ON KAOLINITE REFLECTANCE SPECTRUM
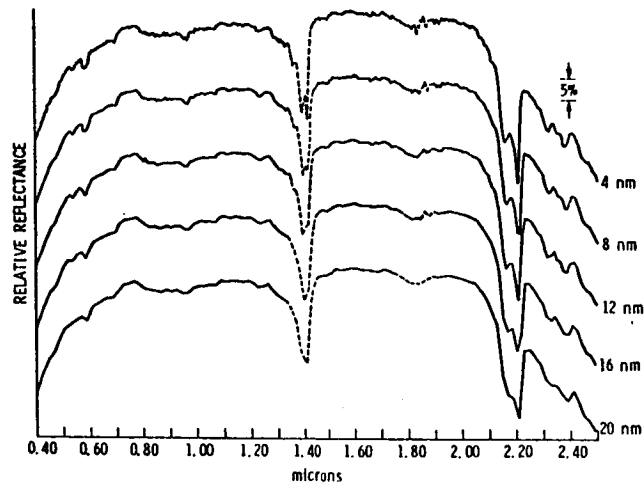
Table 1. Band center of clay absorption features recorded with
          GER spectroradiometer; Hot Creek Range, Nevada samples

	Wavelength (um)	
Kaolinite	2.172	2.215
Montmorillonite		2.214
Illite		2.205

Table 2. Difference between clay spectral absorption features
          from spectrometer measurements; Hot Creek Range,
          Nevada samples

	Difference (nm)
Kaolinite A - Kaolinite B	43
Kaolinite B - Montmorillonite	42
Kaolinite A - Montmorillonite	1
Kaolinite A - Illite	33
Kaolinite B - Illite	10
Montmorillonite - Illite	9

PROCESSING OF AIS DATA

Using the 32 spectral bands between 2.0 and 2.4 um to which a
flat field correction has been applied, a spectral signature-matching
algorithm from the SPAM software was employed to find picture elements
in the AIS imagery with spectral signatures similar to kaolinite,
montmorillonite and illite library spectra.   The algorithm does not
rely on resolution of spectral minima but on the comparison of binary
encoded spectral curves (Goetz, Vane, Solomon, and Rock, 1985).
Pixels in a scene which have signatures similar to each of the clays
are located and colored on the 32-pixel wide image.
Two areas on the Hot Creek AIS flight lines were examined using
this curve-matching algorithm, Red Rock Canyon and the Fairbanks
Canyon area.   In Red Rock Canyon, the montmorillonite-altered Shingle
Pass Tuff and the kaolinitically altered Tuff of Orange Lichen Creek
were correctly identified using the SPAM algorithm.   In Fairbanks
Canyon, one tuff hydrothermally altered to kaolinite and another
altered to illite were correctly identified.   A shale was also identi-
fied as illite.   Areas with another tuff were matched with a mont-
morillonite spectrum.   X-ray diffraction analysis of rocks from areas
of matched signatures confirmed the presence of the clay minerals with
the exception of the area of montmorillonite in Fairbanks Canyon, yet
to be sampled.

SUMMARY

Based on the Nyquist criterion, the spectral sampling interval
must be no more than one half the difference in wavelength between the
two absorption minima (or strictly speaking, the inflection points on
the curve) for resolution or separation of features.   Based on the
distance between clay spectral absorption features, the following
absorption features can be classified as "separable" or "inseparable"
in AIS data, based on location of minima alone:

Separable on Basis of Wavelength of Minima on AIS

        Kaolinite A - Kaolinite B
        Kaolinite A - Montmorillonite
        Kaolinite A - Illite

Inseparable on Basis of Wavelength of Minima on AIS

        Kaolinite B - Montmorillonite
        Kaolinite B - Illite
        Montmorillonite - Illite

To effectively separate kaolinite, montmorillonite and illite
absorption features near 2.2 um, a sensor spectral sampling interval
of less than 4 nm would be necessary.   With the current AIS sensor
(Vane, Goetz and Wellman, 1985) and family of instruments, without
increasing spectral resolution, the most productive approach to the

100

identification of clay minerals is to use signature matching algo-
rithms. In the Hot Creek Range, spectral matching procedures have
identified the location of kaolinite, montmorillonite and illite.

ACKNOWLEDGEMENTS

REFERENCES

Feldman, S. C., and Taranik, J. V., 1985. A first look at Airborne
    Imaging Spectrometer (AIS) data in an area of altered volcanic
    rocks and carbonate formations, Hot Creek Range, south central
    Nevada. In Proceedings of the Airborne Imaging Spectrometer Data
    Analysis Workshop, 1985. Jet Propulsion Laboratory Publ. 85-41,
    p. 56-61.
Goetz, A. F. H., and Rowan, L. C., 1981. Geologic remote sensing.
    Science, V. 211, p. 781-791.
Goetz, A. F. H., Vane, G., Solomon, J. E., and Rock, B. N., 1985.
    Imaging spectrometry for earth remote sensing. Science, v. 228,
    p. 1147-1153.
Hunt, G. R., and Ashley, R. P., 1979. Spectra of altered rocks in the
    visible and near infrared. Economic Geology, v. 74, p. 1613-1629.
Jet Propulsion Laboratory, 1983. Shuttle Imaging Spectrometer
    Experiment (SISEX), A proposal to the National Aeronautics and
    Space Administration for a Shuttle Experiment, July 18, 1983
    (Pasadena, California: California Institute of Technology).
Vane, G., Goetz, A. F. H., and Wellman, J. B., 1983. Airborne Imaging
    Spectrometer: A new tool for remote sensing. In Proceedings IEEE
    1983 Int'l Geoscience and Remote Sensing Symp., IEEE Cat. No.
    83CH1837-4, 5p.p

DETECTION OF HYDROTHERMAL ALTERATION AT VIRGINIA CITY, NEVADA, USING AIRBORNE IMAGING SPECTROMETRY (AIS)

AMY HUTSINPILLER and JAMES V. TARANIK, Mackay School of Mines, University of Nevada-Reno, Reno, Nevada 89557

ABSTRACT

Airborne imaging spectrometer (AIS) data were collected over Virginia City, Nevada; an area of gold and silver mineralization with extensive surface exposures of altered volcanic rocks. The data were corrected for atmospheric effects by a flat-field method, and compared to library spectra of various alteration minerals using SPAM. We were able to identify areas of strong clay alteration on the AIS images that were mapped as kaolinitic, illitic, and sericitic alteration zones. Kaolinitic alteration is distinguishable in the 2.1 to 2.4 and 1.2 to 1.5 micrometer wavelength regions. Montmorillonite, illite, and sericite have absorption features similar to each other at 2.2 micrometers wavelength. Montmorillonite and illite also may be present in varying proportions within one GIFOV. Therefore, it is difficult to distinguish montmorillonite, illite, and sericite from each other on the AIS images. In propylitically altered areas, the spectral contribution of vegetation leads to ambiguous identification of chlorite, calcite, and epidote in the 2.1 to 2.4 micrometer region. In general, AIS data is useful in identifying alteration zones that are associated with or lie above precious metal mineralization at Virginia City.

INTRODUCTION

Virginia City is located 30 kilometers southeast of Reno in the Virginia Range. From the 1850's to the present, over 260 million grams (9 million ounces) of gold and 6 billion grams (200 million ounces) of silver have been produced from the Comstock Lode district. Extensive surface exposures of bleached and altered rocks are associated with the precious metal mineralization. Zones of hydrothermal alteration are identifiable on Landsat Thematic Mapper (TM) and Thermal Infrared Multispectral Scanner (TIMS) images due to the presence of iron-oxide and silicate alteration minerals.

The purpose of acquiring AIS data at Virginia City is to use the finer spatial and spectral resolution to try and identify specific alteration mineral assemblages and their distributions, and to differentiate the volcanic host rocks and their derivative soils. Also, the contribution of vegetation spectral response to the discrimination of rock and alteration types will be assessed.

This paper presents our initial results on the identification of specific alteration minerals and the spectral contribution of vegetation along portions of three AIS flight lines.

GEOLOGY AND ALTERATION

The oldest rocks exposed in the district are Mesozoic metasediments and metavolcanics that have been intruded by Cretaceous granodiorite and granite. Unconformably overlying the Mesozoic rocks are a series of silicic ash-flow tuffs. These are overlain by thick andesite flows and breccias of the Miocene Alta Formation, the main host of orebodies in the district. Dikes and stocks of Davidson Diorite intrude the Mesozoic rocks and the Alta Formation. Overlying the Alta Formation are andesitic to dacitic flows and associated dikes and stocks of the Kate Peak Formation. During emplacement of the lower member of the Kate Peak Formation, normal faulting, mineralization, and alteration occurred. The Late Miocene or Pliocene Knickerbocker Andesite unconformably overlies the Kate Peak Formation.

Mineralization and hydrothermal alteration in the Comstock Lode district are mostly confined to the northerly-trending Comstock, Silver City, and Occidental fault zones, although some ore was mined in hanging-wall faults. The faults dip moderately to the east but are nearly vertical at the surface. Post-mineral faulting has displaced the hanging-wall ore bodies as well as portions of ore bodies within the fault zones. Hudson (1984,1986) has recently studied hydrothermal mineral assemblages at Virginia City. He defines seven major alteration types based on field mapping, petrography, and x-ray diffraction:

1. PROPYLITIC - albite + chlorite ± epidote ± calcite ± white mica ± quartz ± pyrite.
2. ILLITIC (+ MONTMORILLONITE) - illite + quartz + pyrite ± mixed-layered illite-montmorillonite.
3. KAOLINITIC - kaolinite + quartz + pyrite.
4. ALSIC - pyrophyllite + quartz ± diaspore ± kaolinite ± pyrite.
5. ALUNITIC - quartz + alunite + pyrite.
6. SERICITIC - sericite + quartz + pyrite.
7. SILICIFICATION and STOCKWORK VEINING - quartz ± adularia ± calcite.

Alteration assemblages vary with depth from the paleosurface and horizontal distance from major faults. Stockwork veining and sericitic alteration associated with the deeper-level ore horizon are exposed at the surface in the footwall of the Comstock Lode because of post-mineral faulting. At the surface in the hanging wall, alunitic and alsic ledges grade laterally into kaolinitic alteration. The kaolinitic zones in turn grade into illitic and finally into propylitic

alteration. The alunitic, alsic, kaolinitic, and illitic mineral assemblages represent near-surface and intermediate levels of deeper alteration types that are associated with ore. The deeper alteration assemblages include the minerals sericite, quartz, calcite, adularia, anhydrite, illite, and kaolinite (Hudson, 1986).

Propylitic alteration is by far the most widely exposed in the district. Illitic and kaolinitic assemblages occur in smaller zones from several meters to over 500 meters in width. Narrow alunitic and alsic ledges occur within the illitic and kaolinitic zones. Patches of sericitic alteration up to 800 meters wide occur west of Virginia City.

DATA COLLECTION AND ANALYSIS

Three flight lines of AIS data were collected in 128 continuous spectral bands between 1.2 and 2.4 micrometers (9.3 nm bandwidth) over the Virginia City area on 2 July 1985 at 11:00 am local time. The altitude of the sensor varied from 5.0 to 5.3 kilometers above mean terrain. The ground instantaneous field of view (GIFOV) averaged 10.4 meters and the swath width averaged 330 meters.

Two types of atmospheric corrections were applied to the data. First, the effects of the solar spectral irradiance curve were removed from the data using an algorithm developed at the Jet Propulsion Laboratory (JPL). Secondly, a flat-field method was used to correct for solar spectral irradiance, atmospheric absorption, and detector calibration errors. Spectrally flat areas (400 to 500 meters by 330 meters in size) were found at the end of each flight line away from alteration at Virginia City. The spectrally flat areas were used to normalize the remainder of the flight lines. Figure 1 compares spectral curves for raw data (RAW) to data that has been corrected using a solar irradiance method (SOLAR) and a flat-field method (FF). The upper and lower plots show spectra derived from 5x5 pixel areas of unaltered and altered volcanic rocks, respectively. The flat-field method appears to better resolve spectral features, and was applied all the AIS data collected at Virginia City.

A spectral analysis program (SPAM) developed at the JPL was used to analyze the data. Most spectral comparisons were made with only the last 32 bands (grating position 4) of the AIS data. This was done because 1.) absorption features of many important alteration minerals occur in this wavelength region, 2.) there were less spectral noise and line drops in grating position 4 than in other grating positions, and 3.) the spectral data had slight discontinuities where two grating positions met (bands 32/33, 64/65, 96/97), making it difficult to compare these spectral regions with library spectra. AIS spectra and library spectra were compared using FIND (a SPAM function). The comparisons were made with spectral amplitude and not slope. When spectral slope
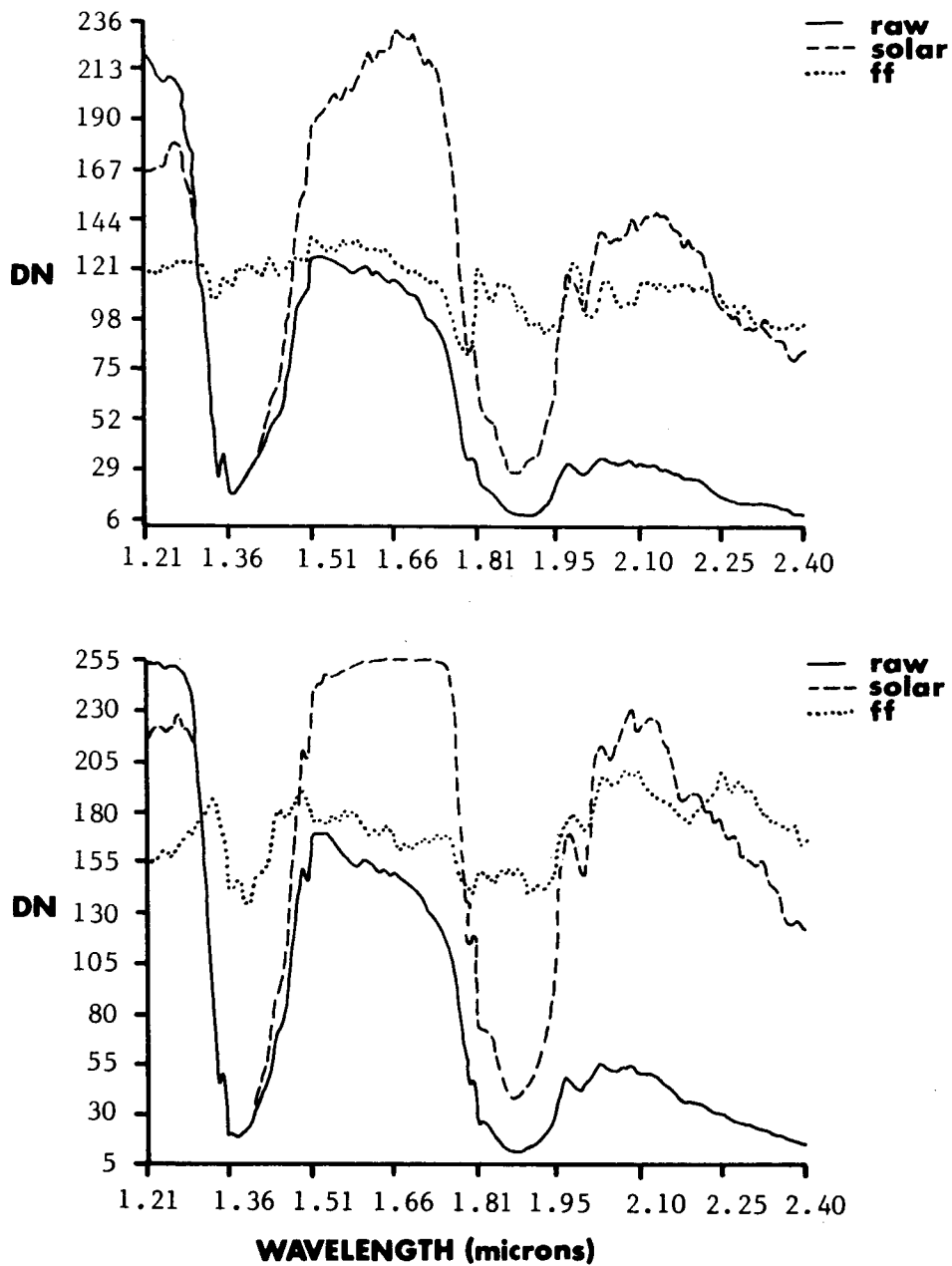
Figure 1. Spectral curves for raw data (raw), and data that
has been corrected using a solar irradiance method
(solar) and a flat-field method (ff). Upper plot
is for unaltered volcanic rocks and lower plot is
for altered volcanic rocks.

similarities were compared, irregularities in the spectra of the AIS data resulted in erroneous mineral matches.

RESULTS

Segments of the three flight lines that cover known areas of alteration in andesitic volcanic rocks were chosen for initial analysis. Propylitic, kaolinitic, illitic, and sericitic alteration assemblages are present, as well as disturbed ground, mine dumps, alluvium, roads, and buildings.

Identification of Alteration Minerals

To identify alteration minerals on the AIS images, SPAM library spectra were compared to spectra from individual pixels in the 2.1 to 2.4 micrometer wavelength region. Clay minerals which exhibit strong reflectance minima near 2.2 micrometers, including kaolinite, montmorillonite, muscovite, and illite, were identified on the images. The locations of these pixels correlate with kaolinitic, illitic, and sericitic alteration zones, and portions of mine dumps and disturbed areas. Scattered pixels with strong 2.2 micrometer absorption features also occur in propylitic alteration zones.

Pixels with kaolinite-like spectra are distinguishable from other pixels whose spectra show a single absorption feature near 2.2 micrometers. Concentrations of kaolinitic-pixels correlate with mapped kaolinitic alteration and portions of mine dumps. The spectra of kaolinite-like pixels can also be identified in the 1.2 to 1.5 micrometer wavelength region, based on the characteristic absorption doublet at 1.4 micrometers (see figure 2).

In the 2.1 to 2.4 micrometer wavelength region, pixels identified as montmorillonite, illite, or muscovite show considerable overlap. That is, the same pixel may be classed as montmorillonite, illite, and/or muscovite, depending on which library spectrum is called upon for the comparison. This is because montmorillonite, illite, and muscovite have similar absorption features near 2.2 micrometers, and because of mixed-pixel problems. Both illite and montmorillonite may be present in the illitic alteration zone, and there is a gradation between illitic and other types of alteration. The result is that illite, montmorillonite, sericite, and/or kaolinite may be present within a single GIFOV.

Vegetation Contribution

An attempt was made to find pixels with spectra similar to calcite, chlorite, and epidote, which are common in the propylitically altered volcanics. These minerals exhibit absorption features near 2.3 micrometers. The lower-wave-
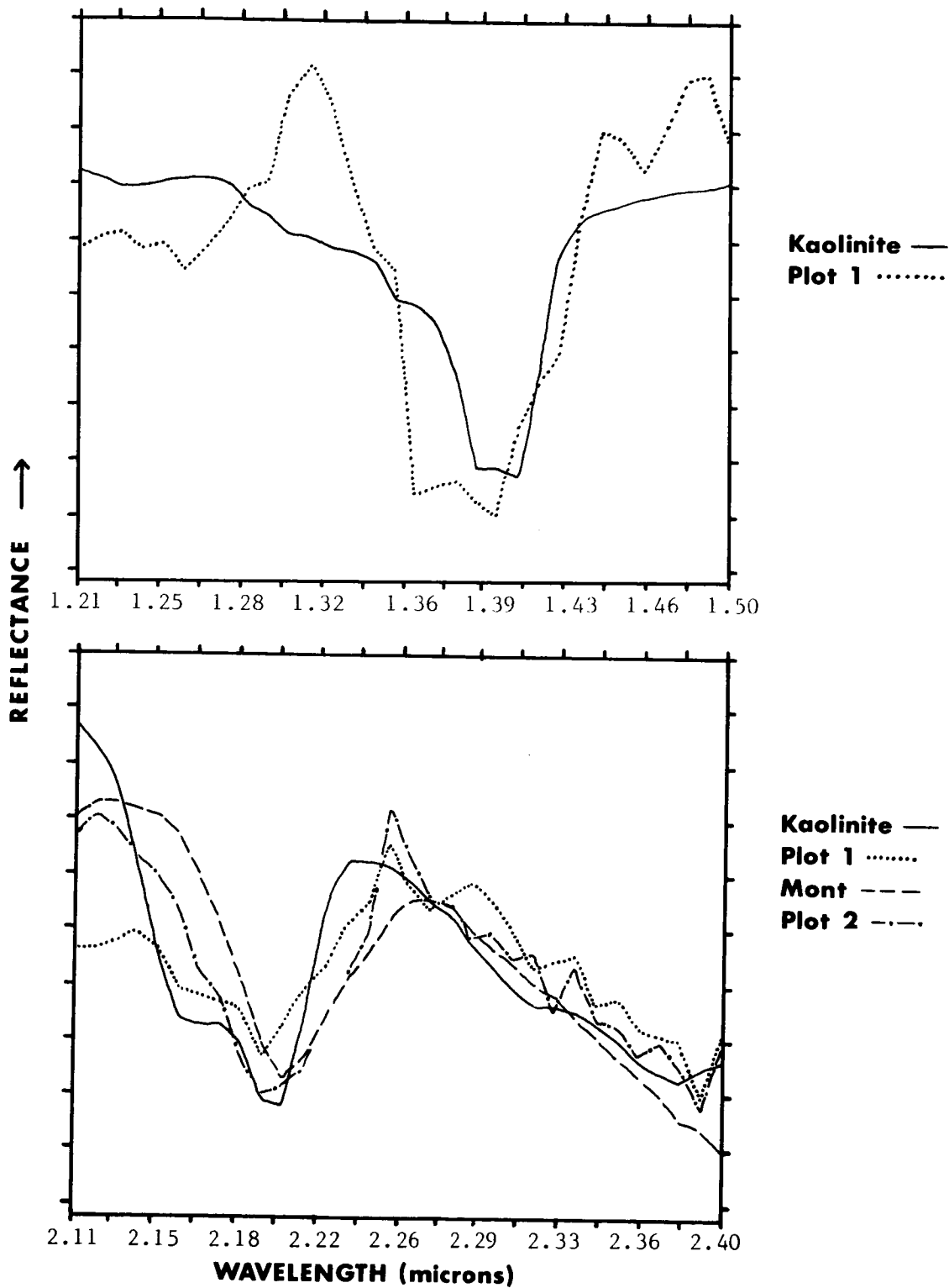
Figure 2. Area-normalized spectral curves for library minerals and flat-field corrected AIS data. Upper plot is library spectrum of kaolinite and spectrum from 3x3 pixel area of kaolinitic alteration (PLOT 1) in 1.2-1.5 micrometer wavelength region. Lower plot shows library spectra of kaolinite and montmorillonite (MONT), kaolinitic alteration (PLOT 1), and spectrum from 3x3 pixel area of mine dump with clay-altered volcanics (PLOT 2) in 2.1 - 2.4 micrometer wavelength region.

107

length side of the absorption feature coincides with the shoulder of a broad reflectance maxima for vegetation that occurs at about 2.2 micrometers.

Most undisturbed ground at Virginia City is sparsely to moderately vegetated with grasses, sage, juniper, and pinyon. Propylitically altered rocks were not extensively prospected and are relatively undisturbed and therefore vegetated. The result is mixed-pixels of vegetation and propylitically altered andesites.

The mixed-pixel problem combined with similarities between the spectral features of vegetation and propylitic alteration minerals, makes identification of calcite, chlorite, and epidote ambiguous. Pixels that had chlorite-like spectra proved in the field to be propylitized andesite with epidote-coated fractures and grassy areas (one was a baseball field). Some of the calcite-like spectra, however, were indeed small areas of abundant calcite within propylitic alteration zones.

CONCLUSIONS

The AIS spectra of kaolinitic, illitic, and sericitic alteration in volcanic rocks are distinguishable from unaltered or weakly propylitized rocks in the 2.1 to 2.4 micrometer spectral region. Strong 2.2 micrometer absorption features in the AIS spectra may be attributable to montmorillonite, illite, and/or sericite. Pixels with kaolinite-like spectra can be identified and correlate with mapped kaolinitic alteration zones. Vegetation influences spectral identification of the minerals calcite, chlorite, and epidote associated with propylitically altered volcanic rocks.

At Virginia City, AIS data is useful in identifying alteration zones that are associated with or lie above precious metal mineralization. The ability to discriminate individual alteration minerals depends on the amount of mineral mixing within a pixel and the amount of vegetation. We hope to quantify these factors in future work with the AIS data.

REFERENCES

Hudson,D.M., 1986, The Comstock District, Storey County, Nevada: Geologic Society of Nevada Field Trip Guidebook #4, 13 p.

Hudson,D.M., 1984, Geology of the Comstock District, Storey County, Nevada: report prepared for United Mining Company of Nevada, Virginia City, Nevada, 29 p.

Whitebread,D.H., 1976, Alteration and Geochemistry of Tertiary Volcanic Rocks in Parts of the Virginia City Quadrangle, Nevada: U.S.Geol.Sur. Prof.Paper 936, 43p.

PRELIMINARY GEOLOGICAL INVESTIGATION OF AIS DATA AT MARY KATHLEEN, QUEENSLAND, AUSTRALIA

JON F. HUNTINGTON, ANDY A. GREEN, MAURICE D. CRAIG, AND TERRY D.COCKS, CSIRO DIVISION OF MINERAL PHYSICS AND MINERALOGY, NORTH RYDE, NSW, AUSTRALIA

ABSTRACT

The Airborne Imaging Spectrometer (AIS) was flown over granitic,volcanic and calc-silicate terrain around the Mary Kathleen Uranium Mine in Queensland, in a test of its mineralogical mapping capabilities. Previous airborne spectrometer surveys over this terrain identified amphibole, carbonate, marble, epidote, kaolinite, smectite, and garnet minerals and provided new lithological subdivisions. An analysis strategy and new restoration and enhancement techniques have been developed to process the 128 band AIS data.

A preliminary analysis of one of three AIS flight lines has shown that the data contains considerable spectral variation but that it is also contaminated by second-order leakage of radiation from the near-infrared region. This makes the recognition of expected spectral absorption shapes very difficult. The effect appears worst in terrains containing considerable vegetation. Techniques that try to predict this supplementary radiation coupled with the log residual analytical technique show that expected mineral absorption spectra of some of the above minerals can be derived. The techniques suggest that with additional refinement correction procedures for the Australian AIS data may be devised.

Application of the log residual analysis method has proved very successful on the Cuprite, Nevada data set, for highlighting the alunite,kaolinite and SiOH mineralogy.

INTRODUCTION

As part of the US/Australia Joint Scanner Project (a NASA/CSIRO/BMR multi-agency and company remote sensing mission), some 54 separate Australian test sites were surveyed with the AIS aboard NASA's AMES C130 aircraft in October, 1985. Approximately 1597 kms of AIS data were acquired. This paper along with Cocks and Green (this volume) represents the first detailed analysis of the Australian AIS data.

Four AIS flight lines (one north-south and three east-west) were flown over the Mary Kathleen site in Queensland (Fig. 1) on October 19th. Sky conditions were generally clear, though a few small clouds in the vicinity implied a moist and varying atmospheric environment. NS001 and TIMS scanner data were acquired concurrently with three of the

four AIS lines, along with 9 x 9 inch colour infrared (CIR) photography and 35 mm black and white tracking photography.

The NS001 and CIR data are invaluable for location and for determination of vegetation conditions as well as for the usual photogeological interpretation. The AIS 35 mm photography is important for exact ground track recovery, particularly when the aircraft was yawing, but is of generally very poor quality.

Flight details of the survey are given in Table 1. This test site was chosen for the initial Australian evaluation because of two previous, highly successful airborne profiling spectrometer surveys that showed the considerable potential for imaging spectrometry.

GEOLOGICAL SETTING

The Mary Kathleen test site is centred around the now mined-out Mary Kathleen Uranium-Rare Earth mine situated at latitude 20 45' S, longitude 140 00'30" E, some 55 kilometres east of the city of Mt Isa (Fig.1).

The major rock groups and structures of the area are depicted on Figure 2. The most complete presentation of the regional geology is given by Derrick et al. (1971 & 1977), whilst Scott and Scott (1985) provide the most recent account of the detailed geology of the Mary Kathleen syncline and the uranium mineralisation.

Two major rock units occur in the area: a Lower Proterozoic to Carpentarian central,crystalline, basement block which is flanked by the Carpentarian metasedimentary eastern succession. The western end of the AIS flight-line covers basement granite, and acid volcanics of the basement,Tewinga Group (Fig.2) represented by the Argylla Formation.

Resting unconformably on the basement complex is the arenaceous and carbonate-rich Mary Kathleen Group. Local depressions in the carbonate shelf contain areas of sulphide-bearing black shales. In the Rosebud and Mary Kathleen Synclines (Fig.2), the Group is represented by the lower arenaceous Ballara Quartzite and the upper,calcareous and skarn-rich Corella Formation. East-west compression formed folds and major north-south trending high-angle reverse faults, and major northeasterly and northwesterly trending conjugate faults in the basement and cover. Metasedimentary bedding is steep to near-vertical. Granite intrusion and low pressure greenschist and amphibolite facies metamorphism accompanied the deformation. Numerous dolerite dyke swarms intrude both the basement and the metamorphic cover.

A more detailed view of the geology and the individual

litholgies and minerals in the vicinity of the AIS flight-line is given in Fig.3. The Mary Kathleen Uranium deposit occurs half-way along the flight-line and is associated with an Allanite,Garnet,Diopside Skarn (Pkc2g on Fig.3). Apart from the clay and muscovite bearing granites and clay weathering acid volcanics it can be seen that the major minerals present are those that have primarily 2.3 to 2.4 micrometre absorption features.

PREVIOUS SPECTROMETER SURVEYS

Two previous spectrometer surveys have been conducted by the authors over the same terrain as flown with the AIS at Mary Kathleen. In 1982 two parallel, across strike, flight lines were flown with the Geophysical Environmental Research (GER) Mark II airborne spectrometer system (Huntington, 1984). This instrument collected 512-channel, visible and near infrared (VNIR) spectra and 64-channel, shortwave infrared (SWIR) spectra. The SWIR spectra covered the range 1.9 to 2.45 micrometres with 9 nanometre sampling. In 1984 the area was re-flown with an airborne, circular variable filter (CVF) spectrometer developed by the CSIRO. This instrument has 128 spectral channels of approximately 1% wavelength resolution covering the range 1.4 to 2.45 micrometres. Both surveys were flown with a ground pixel of approximately 20 metres. The ground tracks crossed the same geological sequences but were, on average, separated by about 500 metres.

These two data sets provide an excellent background against which to evaluate the AIS. In both cases the spectral data were processed to logarithmic residuals (Green and Craig, 1985) to enhance the subtle mineral absorption features that were not evident in the raw radiance data. Both surveys demonstrated excellent mineralogical discrimination, producing interpreted geology that matched the published 1:50,000 and 1:10,000 mapping and provided improved lithological subdivision of some formations. In particular, identification was achieved of the minerals, amphibole,epidote,kaolinite,calcite, marble,andradite garnet and smectite. Results from the two instruments matched extremely well, particularly for the calc-silicate lithologies.

Comparisons of typical log residual spectra from the two instruments for various lithologies are shown in Figs. 4 and 5. The spectra are averages of blocks of terrain varying from 4 to 50 samples. Apart from the epidote/amphibole spectra (Fig. 4) these surveys also picked up unusual absorptions at 2.24 micrometres associated with a calcium rich smectite in the Mary Kathleen open pit(Fig.5A). Also, unusual 2.28 to 2.25 micrometre absorptions were located, assocated with andradite garnet/diopside quartzites and garnetites east of the mine (Figs.5A & 5C). Substantial spectral measurement of field samples (backed-up by XRD

analyses) confirmed the mineralogy and demonstrated the
close correspondence between the bi-directional reflectance
characteristics of field spectra and log residual
reflectance characteristics of airborne samples.

AIS PROCESSING AND DATA RESTORATION

Figure 6 illustrates schematically the processing steps
developed to analyse the AIS data. They allow parallel
analysis of the data in several different formats. These
include three band composited images, "fanned" terrain
images spread out laterally with respect to wavelength
(Fig.7), "fanned" spectral images spread out according to
the 32 pixel columns, or graphical analysis of individual or
averaged spectral curves (Fig.12). Results can be converted
between the various display formats and data base types by
programs AIX and FAN (Fig. 6).

Three steps of data restoration were implemented for
this paper. The first was a replacement of "bad" data
records. The second was a correction of the vertical
detector striping by forcing all image columns to have the
same mean as the central column (Program SHAD1). A
normalization to the mean of all columns would be better to
avoid particularly noisy detectors. Subsequent data analysis
revealed that residual, vertical detector striping still
exists and varies in intensity along the flight line. This
finding suggests some time-dependent variation in the
instrument's aircraft operating environment that is not
fully corrected for by the ground-based calibration. A test
of these restoration techniques on the 1983 Cuprite data set
(Goetz and Srivastava,1985) worked particularly well and did
not show variations along the flight line, though it was a
much shorter line than any at Mary Kathleen.

The third correction was to remove the horizontal
striping, particularly strong in some wavelength bands, and
believed to be due to grating wobble causing variable
starting wavelengths of each spectral scan (Cocks and Green,
this volume). This correction (Program DMEAN) forces all
lines to have a mean defined by the smoothed response of a
moving window of lines. Atypical lines and pixels can be
skipped in this process to avoid "outliers" affecting the
window statistics. The two correction processes, for
vertical and horizontal striping, were run independently and
sequentially on each of the 128 spectral bands. A comparison
of log residuals run on both the raw and corrected data
produced the same results, confirming that the correction
procedures do not appear to introduce artifacts into the
data.

MARY KATHLEEN AIS DATA ANALYSIS AND RESULTS

Given our previous experience with airborne SWIR
spectrometer data in Australia,that little or no

mineralogical information is visible in the raw radiance data (Fig. 7), the log residual technique (Green and Craig, 1985) was applied to the AIS data to enhance potential mineral absorption features.

Initially a new set of 128 log residual bands were computed using all 128 input bands, including those covering the 1.4 and 1.9 micrometre atmospheric water absorption bands. Fig. 8 illustrates the results, which proved to be unsatisfactory. This figure shows the dominating influence of the water bands. They are inversely correlated with the atmospheric windows in which there is no mineralogical discrimination , particularly between 2.1 and 2.4 micrometres where it was expected. It should also be noticed that the last eight or so spectral bands, between 2.35 and 2.4 micrometres, behave like the water absorption bands and are positvely correlated with them. These channels are indeed approaching the edge of the next water absorption band at 2.7 micrometres and their low response may imply a marked drop-off in the sensitivity of the AIS detectors at these wavelengths.

The log residuals were computed again utilizing only bands in the three atmospheric windows, 1.23 - 1.35, 1.49 - 1.77 and 1.96 - 2.40 micrometres. Residuals were computed for each of these windows quite separately. The resulting "fanned" wavelength images are displayed in Fig. 9 which now shows considerable absorption variation (the zones of light and dark across the image). Residual effects from the 1.4 micrometre water absorption band are seen in the pattern of residuals on each side suggesting that a greater number of bands should be omitted from the calculation in this region.

Though considerable spectral variation is visible in various parts of the flight line in the central 1.5 - 1.8 micrometre window, we have yet to interpret the significance of this information. We have long held this to be a significant information window that deserves greater attention. In this paper most attention has been directed to the 2.0 - 2.4 micrometre region.

Figure 10 shows a detailed, annotated image of log residuals in the 1.96 - 2.45 window, equivalent to the long wavelength end of Fig. 9.

Detailed analysis of Figs. 8, 9 and 10 illustrates several unexpected characteristics of the data that bear on a) the instrument performance and b) the geological interpretation. These characteristics are:

1. Signs, and variations along the flight line,of the two CO_2 absorption bands centred near 2.00 and 2.06 micrometres (Fig. 10).

2. General, broad absorptions at unusual wavelengths

centred near 2.28 micrometres (Fig.10).

3. A sharp spectral boundary at 2.35 micrometres whether residuals alternate between positive and negative.

4. A lack of clear and expected absorptions due to the calc-silicate minerals, particularly near 2.34 micrometres. This result is no doubt related to point 3 above.

The CO_2 bands, being present in the ubiquitous atmospheric spectrum, should be completely removed by the log residual process. Their continued presence implies an unpredictable and varying spectral response along the flight line that we suggest is due to additive components described by Cocks and Green,(1986, this volume). These components appear to be an unexplained offset and supplementary,terrain dependent radiation from shorter wavelengths, resulting from an order overlap problem in the instrument.

The order overlap effect means that observed radiances, at 2.0 micrometres, for example, are supplemented by terrain dependent radiation from 1.0 micrometres. The addition of this shorter wavelength energy to the region of the CO_2 bands means that they cannot be adequately corrected by the log residual process, which assumes a multiplicative model of the data. We believe that the unusual absorptions, seen particularly near 2.28 micrometres (dark zones on Fig.10),can be explained by this same order overlap problem.

Modelling of the addition of first and second-order radiances by Cocks and Green, (1986,this volume) for the vegetation case (Fig.11) shows a very pronounced, broad absorption in the spectrum centered on 2.28 micrometres. This is similiar to the observed 2.28 micrometre absorption seen in the data in Fig. 10. It is a relatively unusual, though not unheard of, absorption wavelength and is not expected in the locations indicated. We believe this feature to result from the addition of energy from the 1.13 to 1.15 micrometre region, which straddles a water absorption band. The high reflectance of vegetation at these wavelengths (the infrared plateau) causes this 1.14 micrometre water absorption to have a particularly strong relative effect at 2.28 micrometres, where vegetation is otherwise quite dark.

At Mary Kathleen and many arid Australian test sites there is enough desert grass present to generate this "pseudo" absorption at 2.28 micrometres. It is then due not to any mineralogy but to the mixing of vegetation that has a major spectral absorption contrast at one-half this wavelength.

Previous spectrometer surveys, without the order overlap problem, do not show this 2.28 feature. They have

also shown that the calc-silicate mineralogy can be detected even in the case of up to 40% grass cover.

Because the amount of Australian AIS data is so large, a serious attempt must be made to correct for this supplementary radiation. A complete removal of the effect is probably impossible as it would require a knowledge of the ground cover in every pixel and its spectral characteristics: i.e. just the information that we are trying to elucidate. However, we believe a partial correction is feasible.

A number of correction procedures may be imagined that might use the uncontaminated AIS region between 1.2 and 1.6 micrometres or the NS001 data to correct the longer wavelength AIS bands.

One initially promising technique has been tested. Using bands 1-14 and 29 - 60, some of which are free from order overlap and some of which are affected, we used a multiple linear regression method to predict bands 80 - 128. We argue that these predicted bands contain the common, supplementary energy resulting from the order overlap and that component of the true longer wavelength radiation which can be predicted from the shorter wavelengths. Subtraction of these predicted bands from the raw data yields a new set of residual bands (not log residuals !) that we believe are freer of the short wavelength contamination. These new, corrected, residual AIS bands for the 1.96 - 2.40 are still correlated with each so were used as input to the log residual process to yield, equivalent reflectance-like spectra.

This process essentially removes the ambiguous 2.28 micrometre feature and generates spectra (Figs. 12 and 13), that though still very noisy, approximate the shapes and absorption wavelength positions predicted from the known mineralogy and the previous surveys. Comparisons of Figs. 4 A & 4B with Fig 12C for carbonate/epidote targets and of Fig. 5A with Figs. 13A & 13B, for the mine smectite, illustrate that the AIS data do, after correction, have the expected characteristics.

However, some spectra are still unusual in their absorption wavelengths, hence further work is clearly required. The AIS garnetite spectra have more of a dry grass (cellusose-type) spectrum (Fig.13D) than the previously located, garnetite characteristics (Figs.5B & 5E). In addition, the noisy nature of the AIS spectra, even after averaging within similar spectral blocks and after all the processing that has been necessary, attests to a need to apply more thorough noise removal techniques at the outset. This pre-processing we intend to do in future analyses.

Colour composites of the three AIS bands indicated in

Table II, made prior to the removal of the order overlap effect by the least-squares prediction, gave colours that were totally the reverse to those expected. For example, known clay-rich alluvium appeared blue rather than red. The same composites made after the correction process yield the predicted colours of clays in orange-red, and of carbonates and calc-silicates in blue.

CONCLUSIONS

From the preliminary analysis of the Mary Kathleen AIS data carried out so far, we can draw the following conclusions.

1. As expected from previous surveys, no mineralogical differences were detectable in the raw radiance data.This finding is due to diminution of the mineralogical signatures by weathering and mixing with grass cover.

2. Mineralogical absorption features appear only after removal of backgound and atmospheric effects by computation of log residual spectra. Log residuals should be computed separately for each atmospheric window and should exclude the atmospheric water absorption regions.

3. Greatest attention has been given to the 2.0 – 2.4 micrometre window,but significant spectral variation evident in the 1.5 – 1.8 micrometre window is deserving of further attention.

4. General spectral pattern boundaries defined by the pattern of log residuals match some of the known geological boundaries.

5. Raw log residual spectra do not, however, match the spectral absorption shapes expected from laboratory studies and earlier spectrometer surveys.

6. The raw AIS data appear to be degraded by addition of first and second-order radiation that generates "pseudo" absorption features at incorrect wavelengths. This effect is worst in the case of pixels containing appreciable amounts of vegetation. The effect also masks true mineralogical absorption features.

7. Unexpected variations in the intensity of the CO_2 bands along the flight line atest to a problem related to item 6 above.

8. A multiple linear regression technique has been applied prior to the calculation of log

residuals that appears to correct, to some extent, the second order radiation leakage for the 1.96 - 2.4 micrometre region.

9. After correction, spectra can be extracted that exhibit the expected spectral characteristics of clays, epidote, amphibole and carbonates.

10. The region 2.35-2.40 micrometres exhibits very low sensitivity and often responds poorly to the log residual method. In this environment this fact is significant because of the dominance of mineral absorptions near 2.35 micrometres.

11. A software strategy for AIS data restoration and analysis has been devised using relatively conventional image processing methods blended with some novel techniques. It has been shown to work well on the 1983 Cuprite data set in which no order overlap effect existed.

12. Additional strategies need to be explored for correction of the order overlap problem, and greater attention given to noise removal techniques.

ACKNOWLEDGEMENTS

REFERENCES

Cocks,T.C. and Green,A.A. (1986). Airborne Spectroradiometry: The Application of AIS Data to the Detection of Subtle Mineral Absorption Features. Proceedings of the Second Airborne Imaging Spectrometer Data Analysis Workshop, May 6-8, 1986 (this volume).

Derrick,G.M.,et.al.(1971). Geology of the Marraba 1:100,000 sheet area, Queensland,BMR Record 1971/56 (unpublished).

Derrick,G.M.,et.al.(1977).Geology of the Mary Kathleen 1:100,000 sheet area, northwest Queensland,,BMR

Bulletin 193, 114 pages.

Goetz,A.F.H. and Srivastava,V., (1985). Mineralogical Mapping in the Cuprite Mining District,Nevada. Proceedings of the Airborne Imaging Spectrometer Data Analysis Workshop,April 8-10,1985, JPL Publication 85-41,pp. 22-31.

Green,A.A. and Craig,M.D. (1985). Analysis of Aircraft Spectrometer Data with Logarithmic Residuals. Proceedings of the Airborne Imaging Spectrometer Data Analysis Workshop, April 8-10, 1985, JPL Publication 85-41, pp. 111-119.

Huntington,J.F., (1984). Interpretation of visible,near and short wavelength infrared,field and airborne spectra from Mary Kathleen, Queensland,Australia,Proceedings of the Int. Symp. on Remote Sensing of Environment,Third Thematic Conference: Remote Sensing for Exploration Geology, April 16-19, Colorado Springs,USA, Abstract, p.227.

Scott,A.K. and Scott,A.G., (1985). Geology and genesis of uranium-rare earth deposits at Mary Kathleen, Northwest Queensland, Bull. Proc. Austral.Inst.Min. and Metal., Vol.290, No.1, pp.79-89.

TABLE I

AIS AND C130 FLIGHT DETAILS
MARY KATHLEEN TEST SITE, QUEENSLAND, AUSTRALIA
SITE # S723, RUN 2, LINE 1, ACQUIRED 19 OCT 1985

AIS MODE:	Rockscan 1.4 to 2.4 micrometres
PIXEL SIZE:	8.3 metres (approx)
DETECTOR No:	AIS1
MEAN ALTITUDE ABOVE TERRAIN:	14,300 feet (4358 metres)
AIRSPEED:	167 knots
FLIGHT DIRECTION:	East to west (flipped west to east for analysis)
TOPOGRAPHIC VARIATION:	180 metres
No. OF SAMPLES (lines):	2560
LINE LENGTH:	18 kilometres (approx)
LINE WIDTH:	266 metres (approx)

TABLE II

COLOUR COMPOSITE CHARACTERISTICS

SPECTRAL BAND (micrometres)	ASSIGNED COLOUR	MAJOR ABSORBING MATERIALS	IMAGE COLOURS
2.22	Blue	Clays Granitic Terrain	Red
2.27	Green	Epidote Garnet	–
2.34	Red	Carbonates Garnetite – Epidote – Calc-silicates	Blue
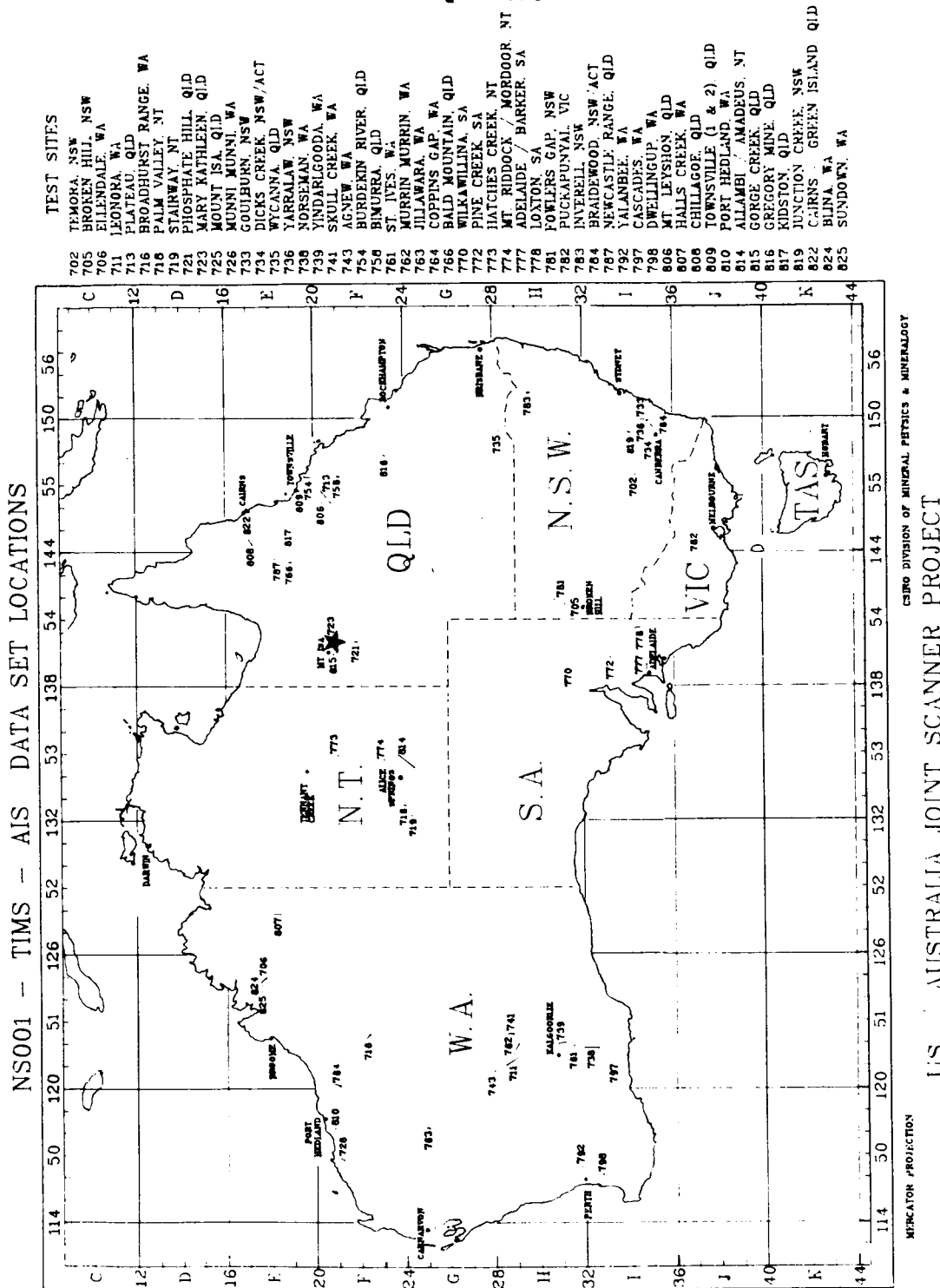
Fig. 1. Location of Mary Kathleen Site No. 723 (star) and other Australian Test Sites.
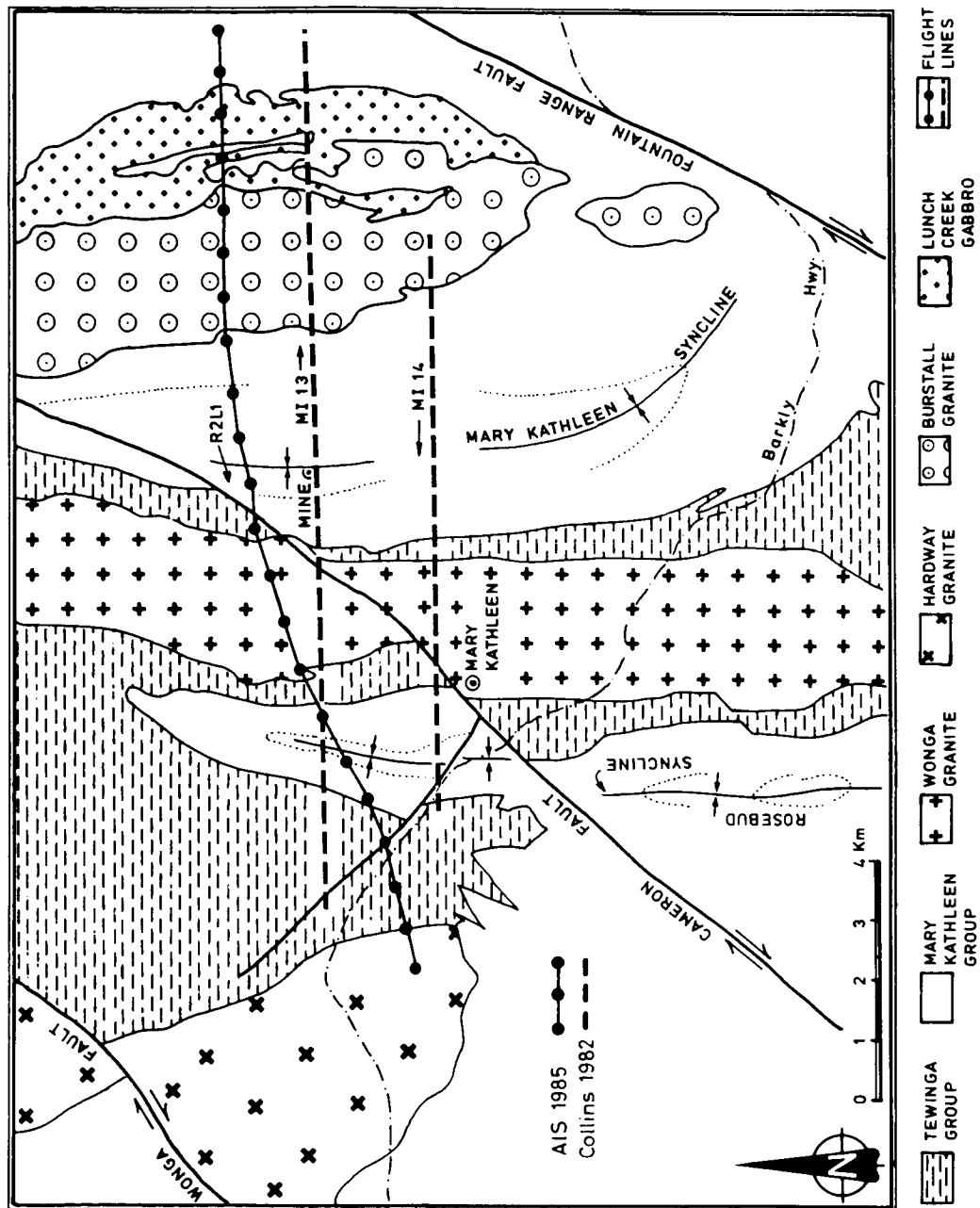
Fig. 2. Major geological groups and structure of the Mary Kathleen Region showing AIS and previous spectrometer flight lines.

LEGEND

Argylla Formation

Pea — Quartz feldspar porphyry, rhyolitic to dacitic crystal tuff (?), quartzite, schist, minor limestone.

Pem — Metabasalt, amphibolite, basalt-quartzite breccia, agglomerate.

Corella Formation

Pkb — Quartzite minor conglomerate.

Pkb_2 — Quartzite, micaceous quartzite, minor limestone and granofels, cordierite and andalusite schist.

Pkc — Calcareous scapolite granofels, limestone, scapolite, cordierite and andalusite schist, quartzite.

Pkc_1 — Fine feldspathic quartzite, metasiltstone, limestone, calcareous granofels.

Pkc_2 — Calcareous sandstone, slate, schist, marl, calc-silicate rocks.

Pkc_{2c} — Cordierite - biotite schist, mica schist.

Pkc_{2g} — Garnetite, garnet-diopside skarn.

Pkc_{2l} — Limestone, calcareous granofels with diopside, vesuvianite, wollastonite and garnet.

Pkc_{2n} — metaconglomerate

Pkc_{2q} — Quartzite

Pkc_r — Calcareous breccia, limestone, hematite pods.

Wonga Granite

Pgw — Coarse foliated granite, megaporphyritic granite, medium leucogranite, aplite, minor orthogneiss

Burstall Granite

Pgb — Medium to coarse granite, microgranite, aplite.

Lunch Creek Gabbro

Pbk — Olivine - pyroxene gabbro, biotite, diorite, hybrid diorite and tonalite.

Other Rocks

Do — Dolerite, metadolerite.

Cz — Cainozoic alluvium.
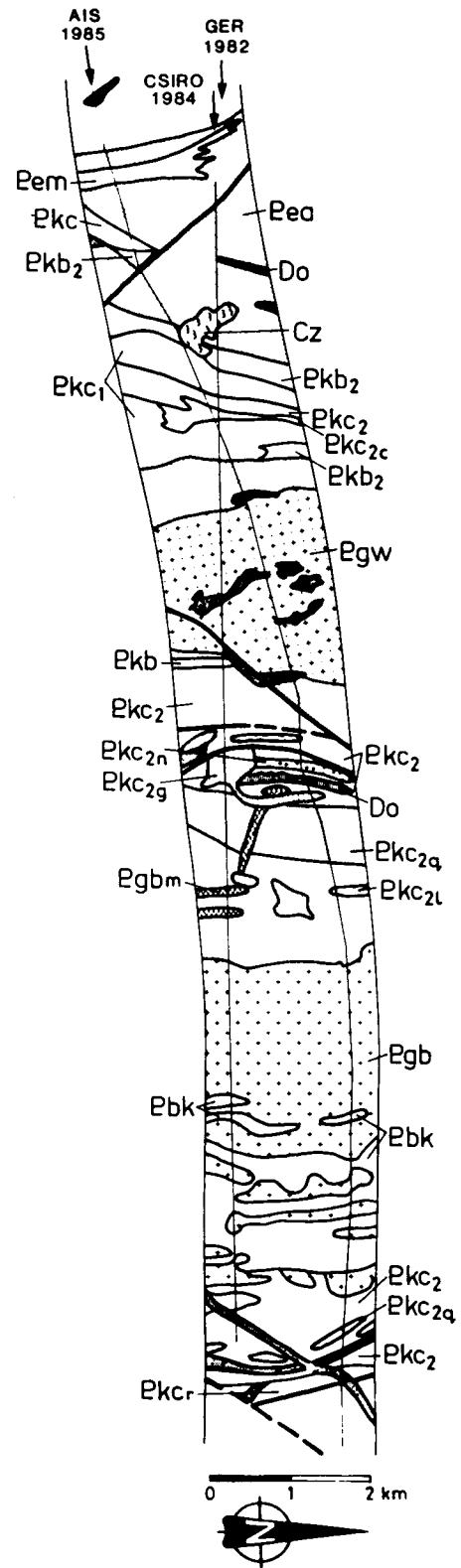
Fig. 3. Geology and legend for the AIS flight line.
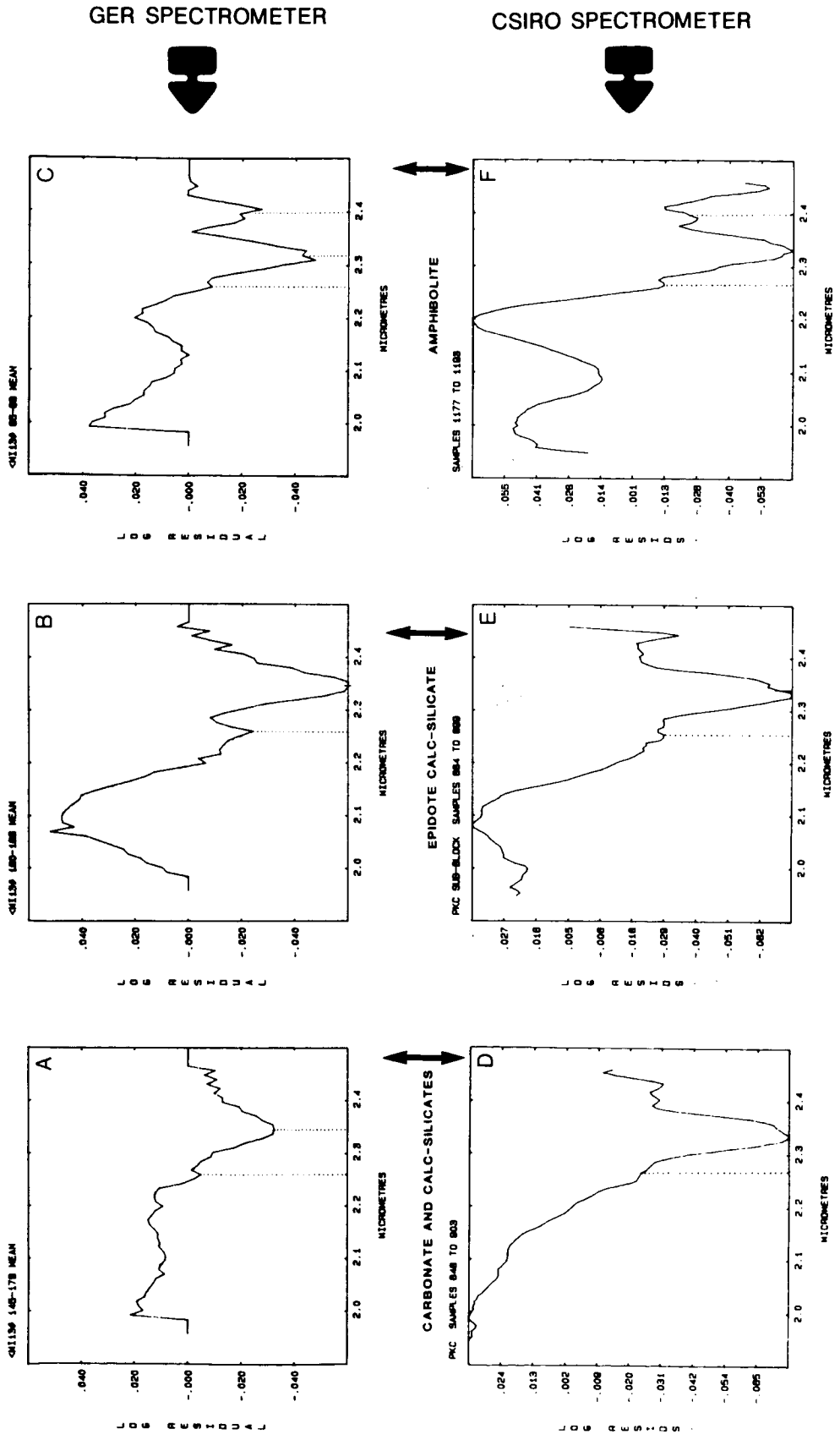
Fig. 4. Comparison of carbonate, calc-silicate and amphibole spectra from previous GER and CSIRO spectrometer surveys adjacent to the AIS track.

123

GER SPECTROMETER

CSIRO SPECTROMETER
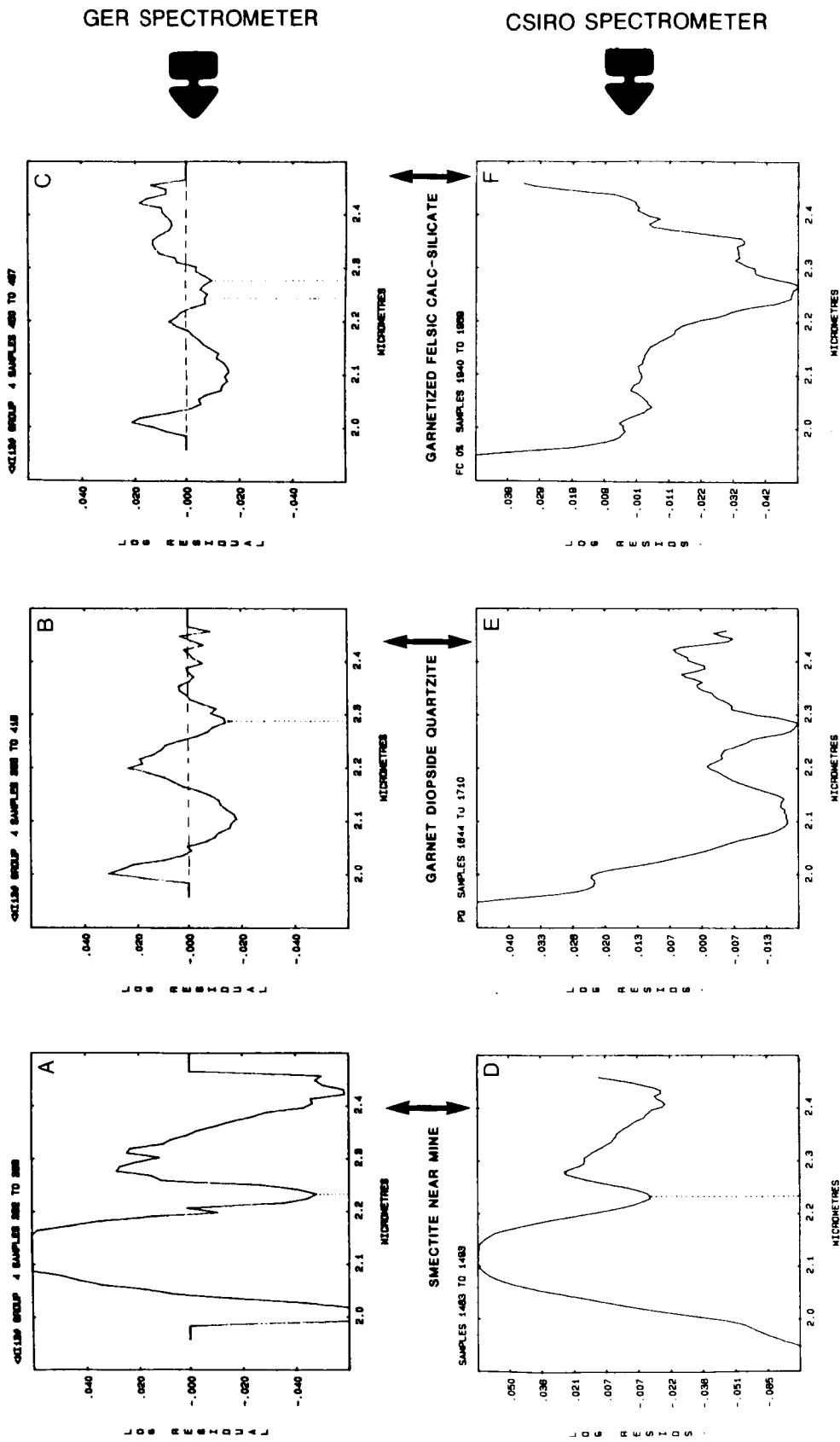
Fig. 5. Comparison of smectite, garnet/diopside quartzite and garnetized calc-silicate spectra from previous GER and CSIRO spectrometer surveys adjacent to the AIS track.
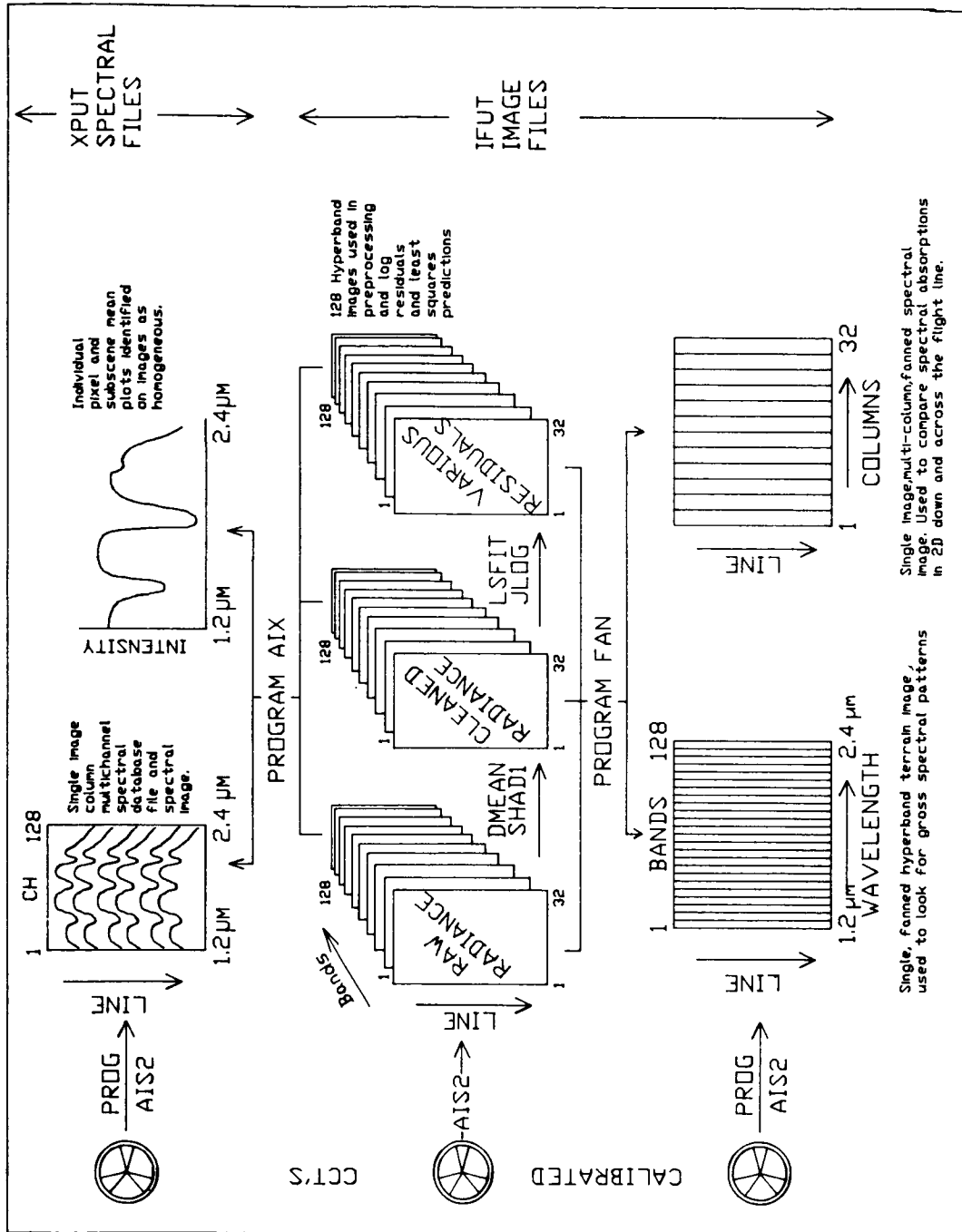
Fig. 6. Schematic of processing and analysis strategy developed for AIS data.
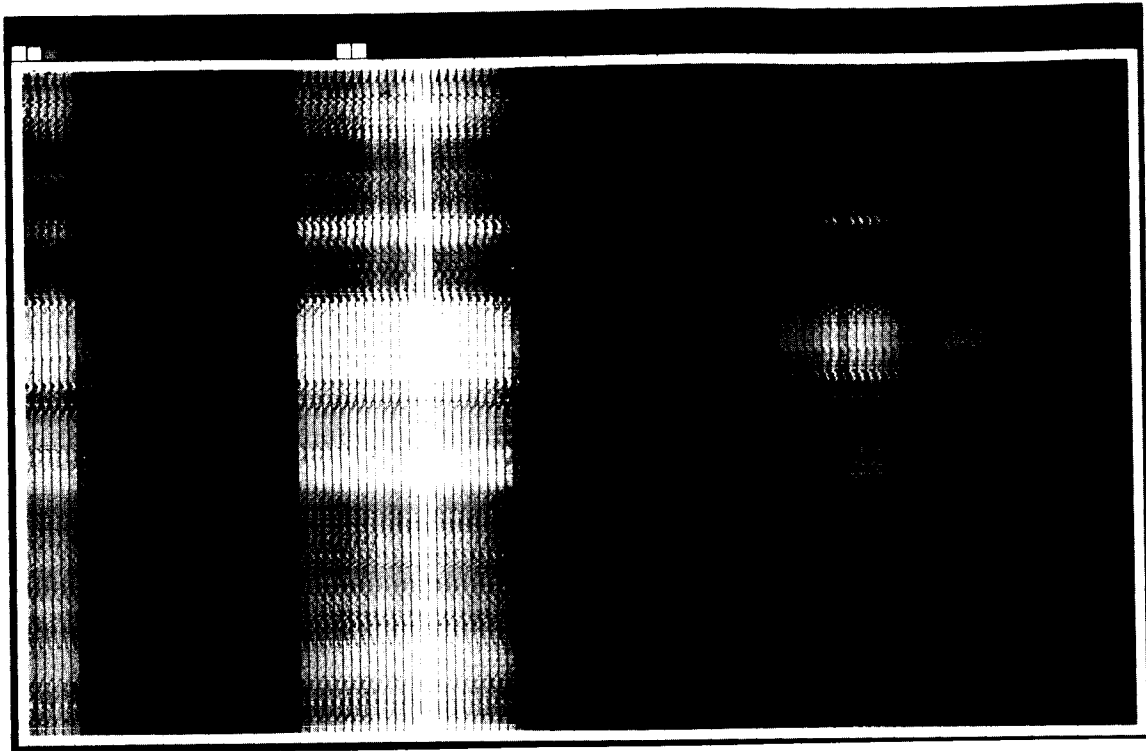
Fig. 7. 128 "fanned" radiance images for the Mary Kathleen flight line. Wavelengths are 1.2 on the left edge to 2.4 micrometres on the right edge. The two dark bands are the atmospheric water absorption bands. Note: a) The variation in some individual band calibration levels and b) The absence of any apparent absorption features at any specific wavelengths. All grey level variations are due to albedo and water absorption.
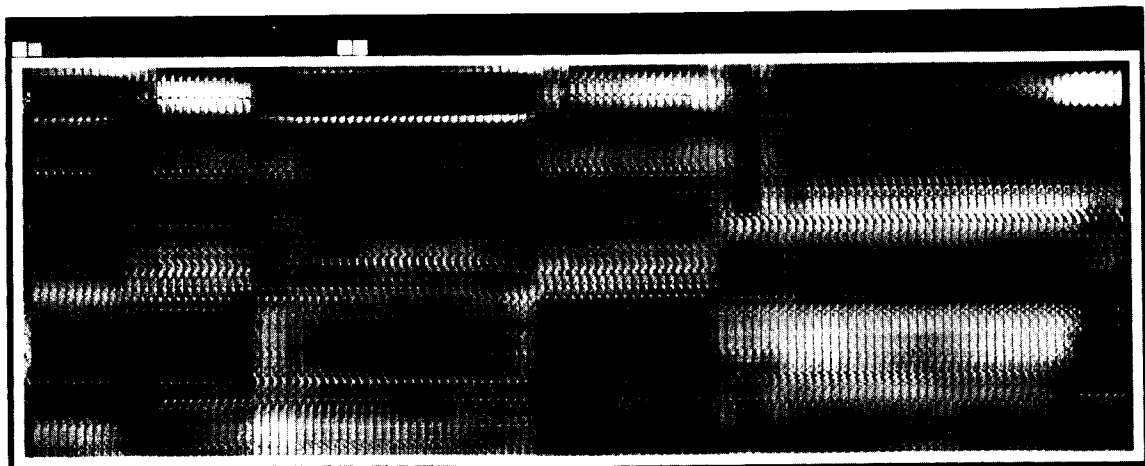
Fig. 8. 128 "fanned" log residual images computed with incorporation of the 1.4 and 1.9 water absorption bands. Dark equates to negative and white equates to positive residuals relative to the flight line mean.
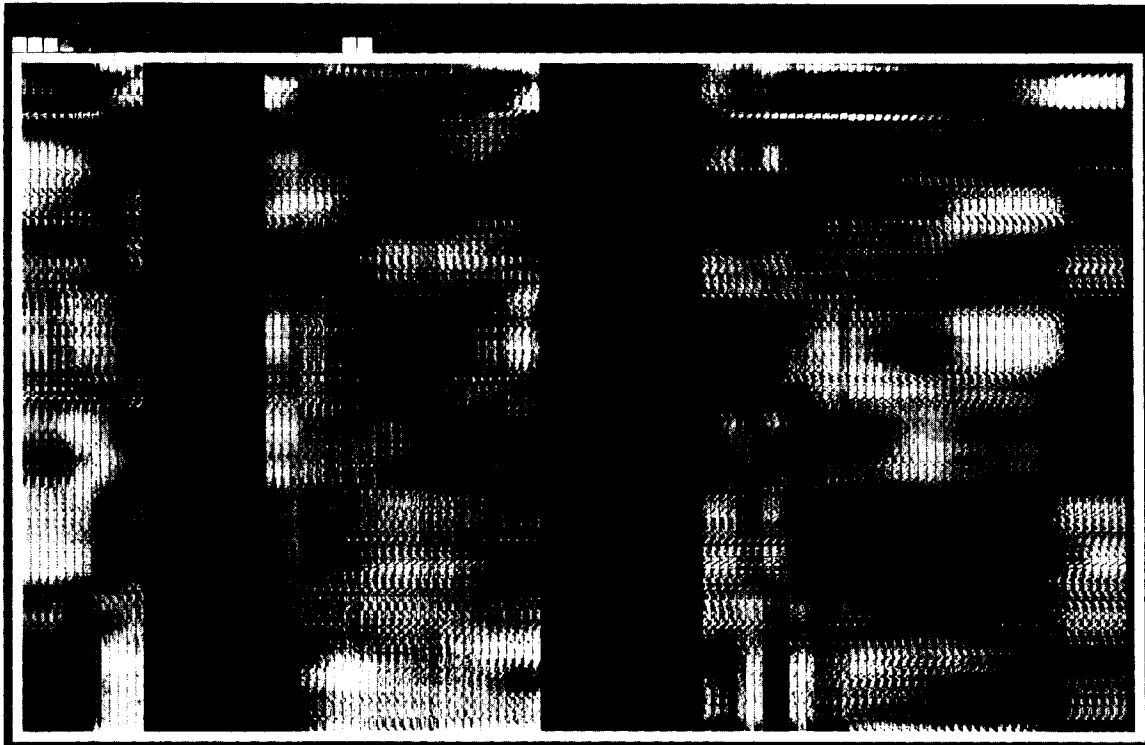
Fig. 9. "Fanned" log residual images computed on the three atmospheric windows separately. Wavelengths extremes as in Figure 6. The two black columns are the zeroed atmospheric water absorption bands. Note the considerable high frequency pattern of light and dark residuals that represent absorption features now evident down the flight line. The vertical dimension represents flight line direction.
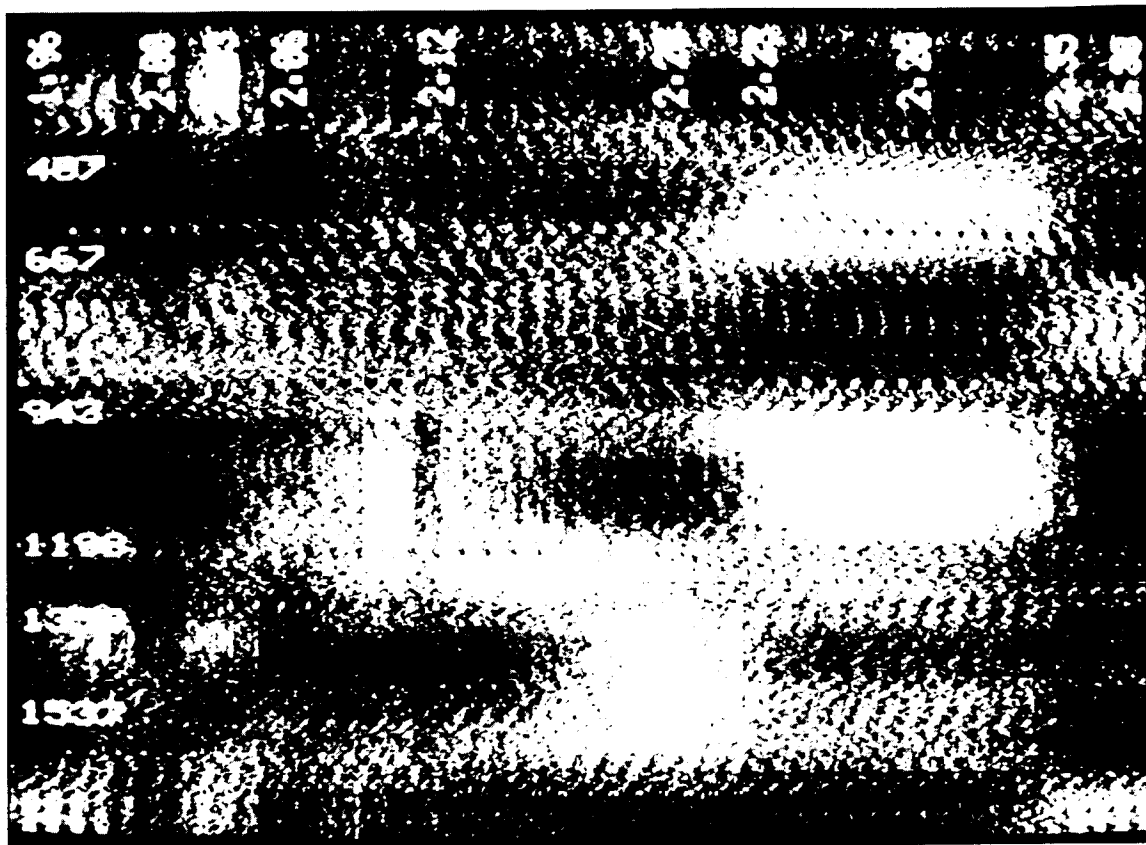
Fig. 10. Detail of "fanned" log residuals for the 1.96 -2.4 micrometre window illustrating the CO_2 bands at 2.00 and 2.06 micrometres, and broad, intense absorption features at 2.28 micrometres (for example, between lines 667 and 943). (See color slide number 5 in the back cover pocket of this publication.)

128

CSIRO-MINERAL PHYSICS

AIS SPECTRORADIOMETRIC MODEL

RESPONSE TO VEGETATION

(COMBINED)

(1ST ORDER)

WAVELENGTH UM
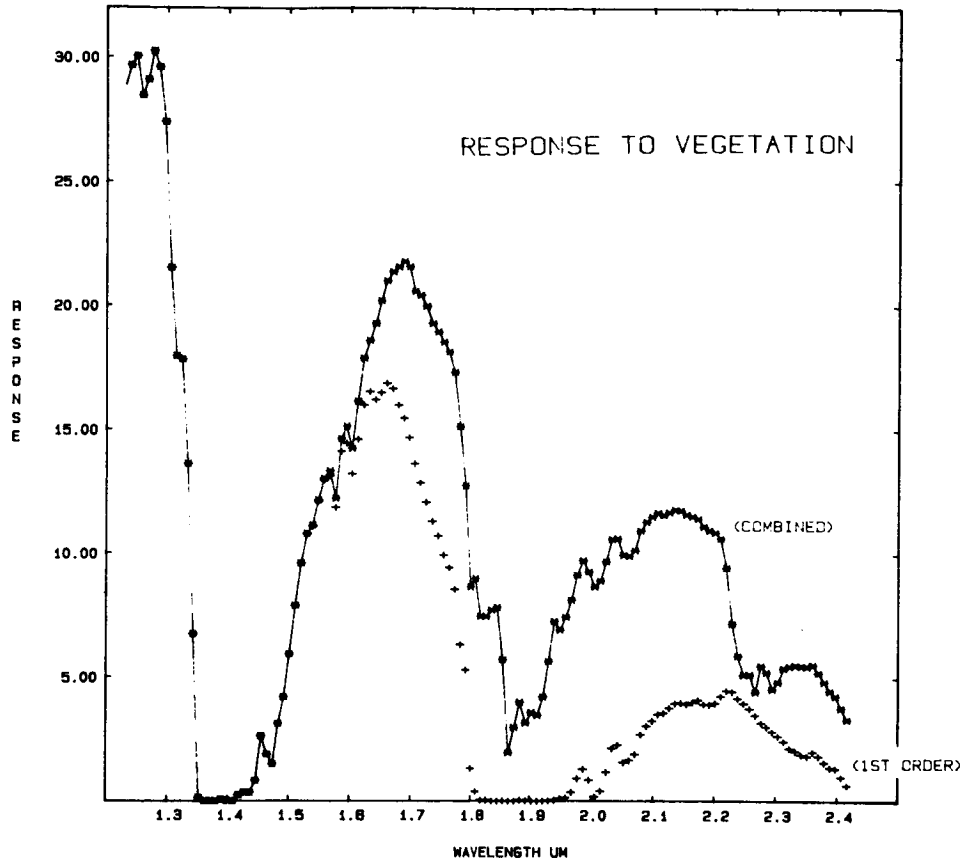
Fig. 11.   Comparison of the predicted, first-order, AIS radiance for
   a vegetated target (lower curve) with the modelled addition of first
   and second-order energies (upper curve).   Note the strong absorption
   centred on 2.28 micrometres in the combined spectrum.
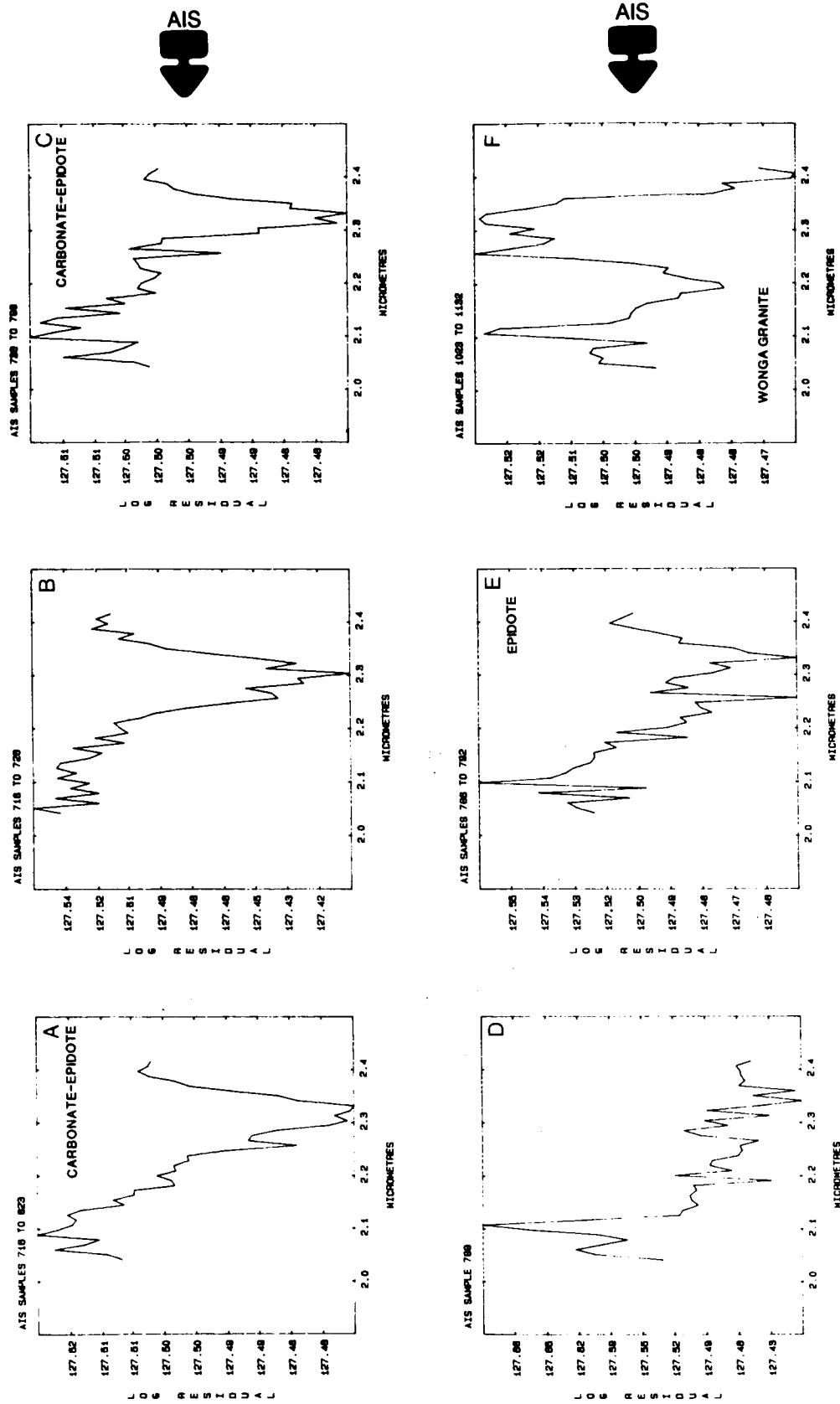
Fig. 12. Block mean log residual AIS spectra of carbonate/cal-silicate terrain after correction for second-order overlap.
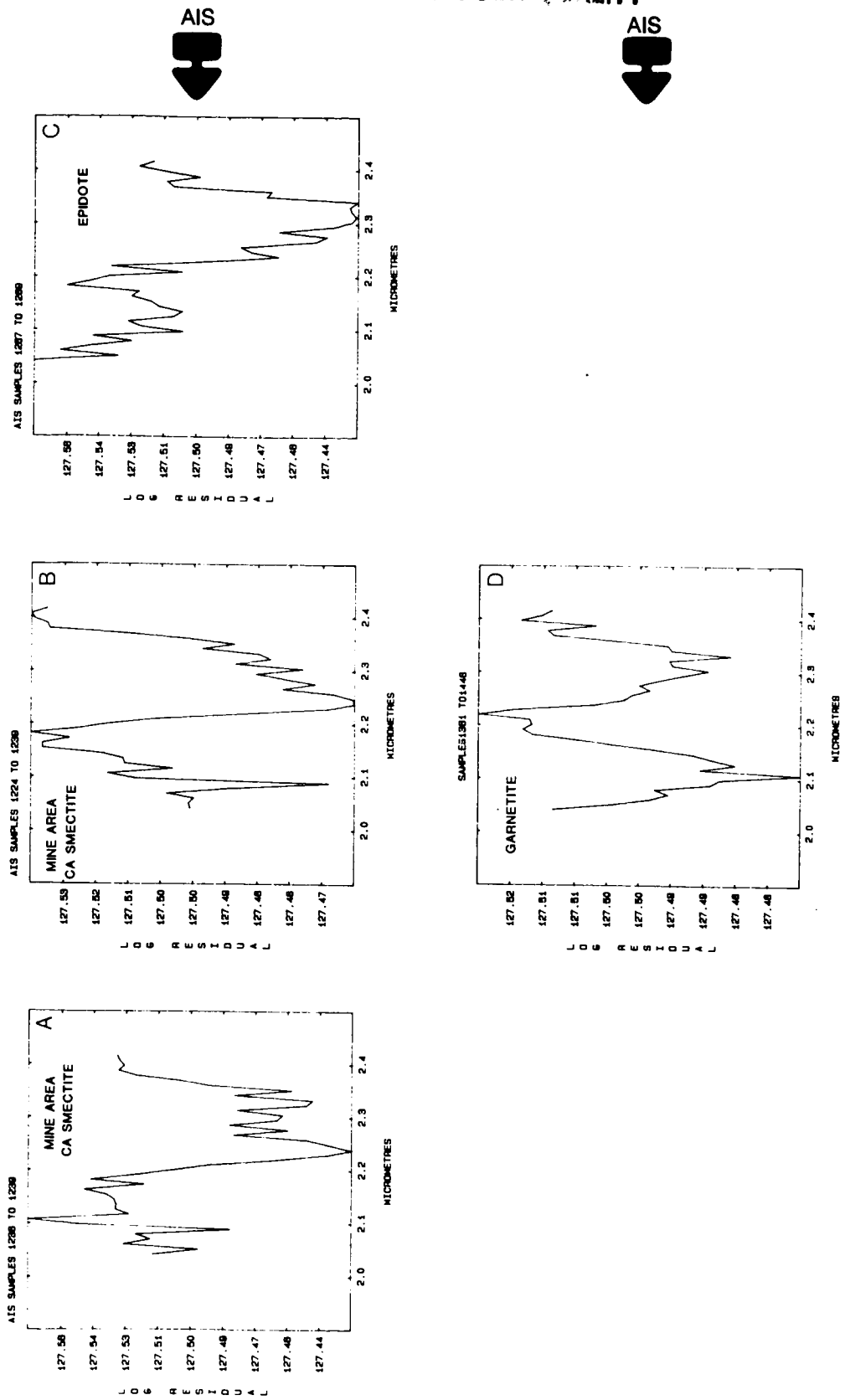
Fig. 13. Block mean log residual AIS spectra of smectite, epidote and garnetite rich terrain after correction for second-order overlap.

USE OF DIGITAL MUNSELL COLOR SPACE TO ASSIST INTERPRETATION OF IMAGING
SPECTROMETER DATA -- GEOLOGIC EXAMPLES FROM THE NORTHERN GRAPEVINE
MOUNTAINS, CALIFORNIA AND NEVADA

FRED A. KRUSE, DANIEL H. KNEPPER JR., and ROGER N. CLARK, Geologic
Division, U.S. Geological Survey, Denver Federal Center, Mail Stop 964,
Box 25046, Denver, Colorado 80225, USA

ABSTRACT

Techniques using Munsell color transformations have been developed
for reducing 128 channels (or less) of Airborne Imaging Spectrometer[1]
(AIS) data to a single color-composite-image suitable for both visual
interpretation and digital analysis. Using AIS data acquired in 1984
and 1985, limestone and dolomite roof pendants and sericite-illite and
other clay minerals related to alteration have been mapped in a quartz
monzonite stock in the northern Grapevine Mountains of California and
Nevada. Field studies and laboratory spectral measurements verify the
mineralogical distributions mapped from the AIS data.

SUMMARY

Four flightlines of Airborne Imaging Spectrometer (AIS) data over a
hydrothermally altered stock in the northern Grapevine Mountains,
California and Nevada, were analyzed primarily to detect and map
carbonate rocks possibly containing skarn deposits and clay minerals
associated with hydrothermal alteration of the stock. Initially, the
AIS data were processed to relative reflectance using procedures
described by Kruse and others (1985a; 1985b); data processed in this
fashion can be used to generate near-laboratory-quality reflectance
spectra. Additional algorithms were then developed to automatically
detect and characterize the most prominent absorption feature in each
spectrum according to band position, width, and depth and to display
this spectral information in a single color-composite-image suitable for
visual interpretation. The color-composite-image may also be analyzed
digitally and used to prepare thematic maps of selected absorption
features (minerals) by classifying the Munsell color characteristics of
the image data.

[1]Use of trade and company names is for descriptive uses only and does
not imply endorsement by the U.S. Geological Survey.

A key element to this analysis procedure is to reduce the dimensionality and complexity of the AIS data to manageable proportions. This task was accomplished by limiting the extracted spectral information to the three absorption feature parameters—band position, band depth, and band width—for only the dominant absorption feature in each spectrum (Fig. 1); to avoid water absorption bands, only the wavelength interval 2.0-2.4 micrometers (~36 channels) was considered. Band position is defined as the lowest point of the absorption feature after a continuum is removed. Band depth is defined as one minus the ratio of the reflectance at the band position to the reflectance of the continuum (Clark and Roush, 1984). Band width is defined as the absolute difference of the wavelengths at one-half the band depth. These three parameters were then mapped into digital Munsell color space (Raines, 1977; Kruse and Raines, 1984) such that hue represents the band position, value (intensity) represents the band depth, and saturation represents the band width (Fig. 2). Digital analysis of Munsell parameters was used to classify the hue, saturation and value images (band position, depth, and width) and produce thematic mineralogical maps (Kruse, 1984; Raines and Knepper, 1983) based on the known spectral characteristics of the carbonate and clay minerals (Fig. 3). In addition, the Munsell classified data can be inverted to tristimulus color space (red, green, blue) and used to prepare a color composite image that allows the direct visual interpretation of mineral distribution based on the observed colors.
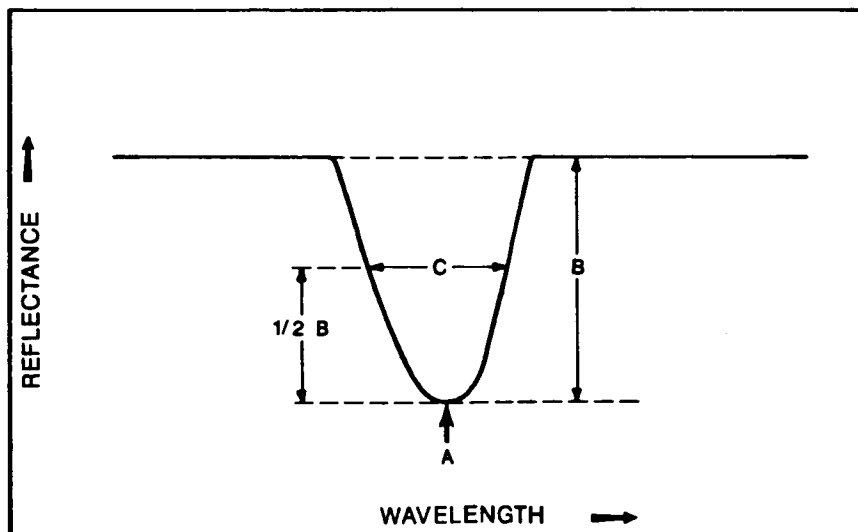
Figure 1. Illustration of the three absorption band parameters from a reflectance spectrum after continuum removal.: - A, band position (wavelength); B, band depth; and C, band width.

A. BAND POSITION (HUE)

Munsel Hue → Blue → Green → Yellow → Red

Wavelength → 2.100 → 2.215 → 2.280 → 2.350

B. BAND DEPTH (VALUE)

Value) Bright → Dark

Depth) Strong → Weak
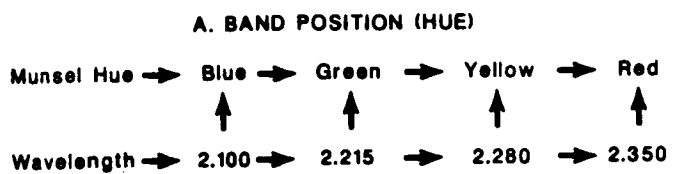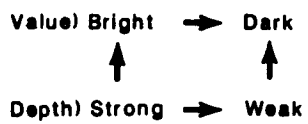
C. BAND WIDTH (SATURATION)

Saturation) Saturated → Less Saturated

Width) Wide → Narrow
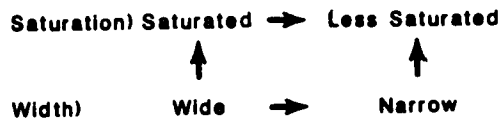
Figure 2. Mapping scheme used to put absorption band parameters into digital Munsell coordinates.
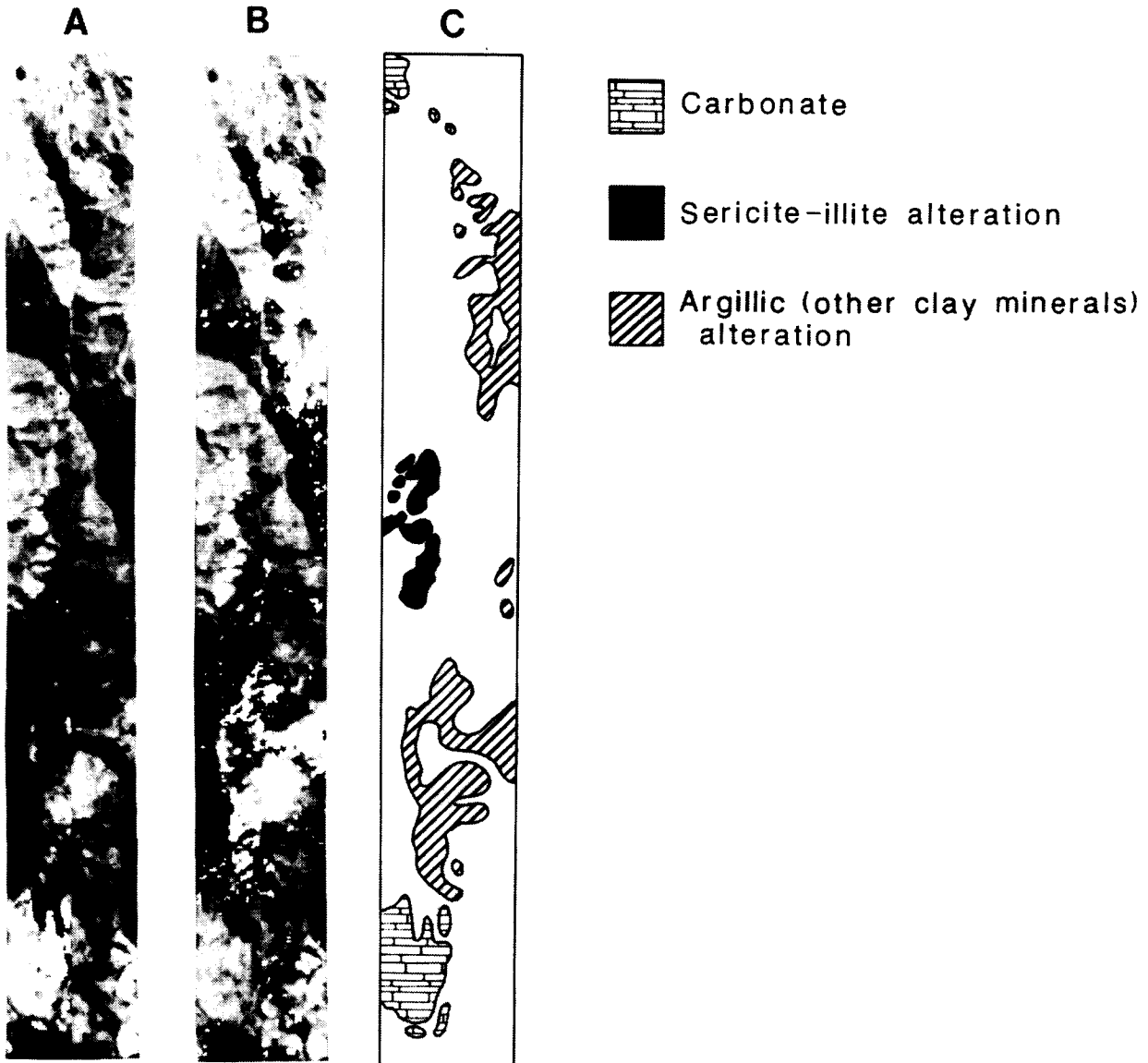
Figure 3. Thematic mineralogical images (note that these images consist
of two 32-pixel flightlines concatenated to form a single 64-
pixel-wide image) and thematic map interpreted from the image
and individual spectra. A, Overlay of pixels identified as
carbonates (white) on a single band image; B, overlay of
pixels identified as clay (white) on a single band image; C,
Map interpreted from images A and B and individual spectra.
(See color slide number 6 in the back cover pocket of this
publication.)

Thematic mineral maps of carbonate rocks and clay alteration of the quartz monzonite stock were produced from the AIS data (Fig. 3). Further subdivision of the broadly mapped mineral groups was accomplished by examining individual spectra (Fig. 4). The identification and mapping of mineral distribution from the AIS data was verified by field and laboratory reflectance measurements and field alteration mapping. The mapping of the primary absorption band position, depth, and width on the AIS images accurately reflects the predominant mineralogy of the surficial materials. Additional techniques are being developed that will allow secondary absorption features to be examined and mapped and mineralogical mixture problems to be addressed.

A.

B.
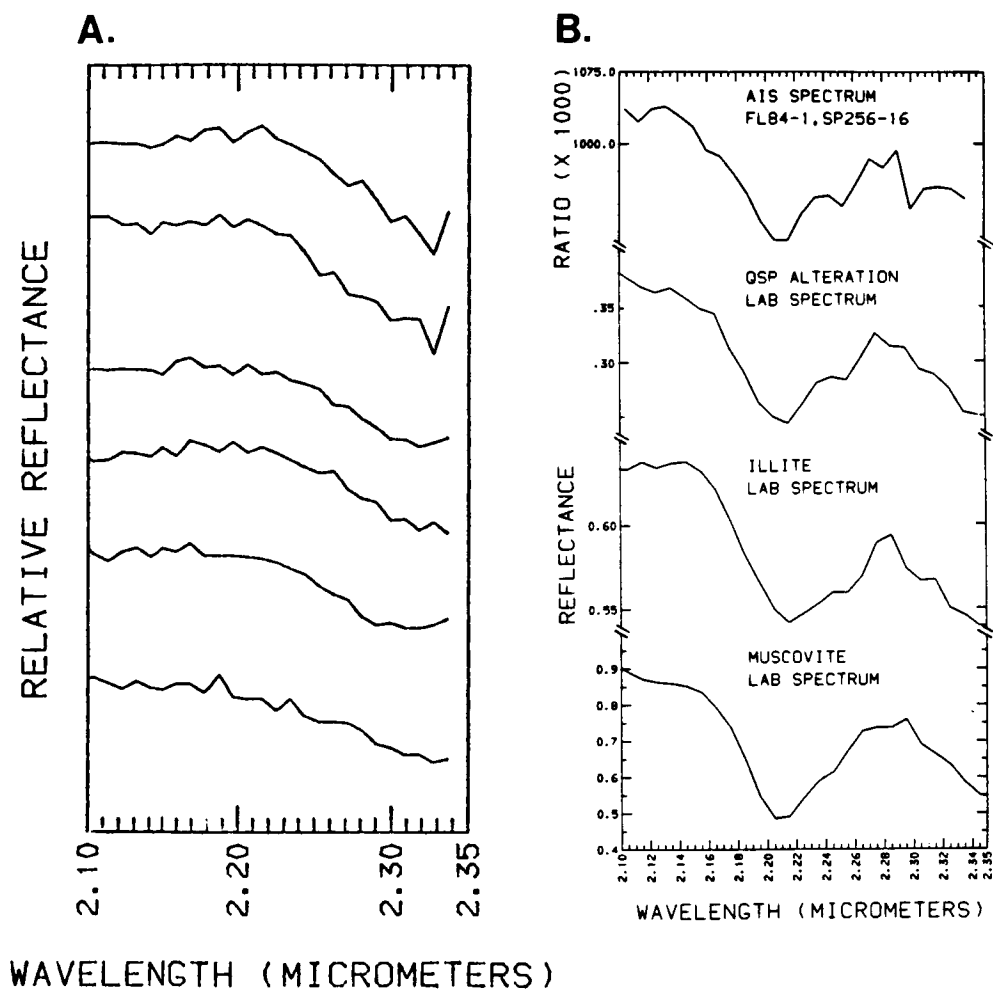
Figure 4. Individual spectra from the AIS images. A, carbonate spectra; B, comparison of an AIS clay spectrum with laboratory spectra. The QSP (quartz-sericite-pyrite) spectrum is from a sample collected in the area of sericite-illite alteration in Figure 3.

REFERENCES

Clark, R. N., and Roush, T. L., 1984, Reflectance spectroscopy: Quantitative analysis tehniques for remote sensing applications, J. Geophys. Res., v 89., p. 6329-6340.

Kruse, F. A., 1984, Munsell color analysis of Landsat color-ratio-composite images of limonitic areas in southwest New Mexico: in Proceedings, International Symposium on Remote sensing of Environment, Third Thematic Conference, "Remote Sensing for Exploration Geology", Colorado Springs, Colorado, 16-19 April 1984, University of Michigan, Ann Arbor p. 761-773.

Kruse, F. A., and Raines, G. L., 1984, A technique for enhancing digital color images by contrast stretching in Munsell color space: in Proceedings, International Symposium on Remote Sensing of Environment, Third Thematic Conference, "Remote Sensing for Exploration Geology", Colorado Springs, Colorado, 16-19 April 1984, University of Michigan, Ann Arbor, p. 755-760.

Kruse, F. A., Raines, G. L., and Watson, Kenneth, 1985a, Analytical techniques for extracting mineralogical information from multichannel airborne imaging spectrometer data (Abs.): in Proceedings, AIS workshop, 8-10 April, 1985, Pasedena, California, JPL Publication 85-41, Jet Propulsion Laboratory, Pasadena, California, p. 105.

Kruse, F. A., Raines, G. L., and Watson, Kenneth, 1985b, Analytical techniques for extracting geologic information from multichannel airborne spectroradiometer and airborne imaging spectrometer data: in Proceedings, International Syposium on Remote Sensing of Environment, Fourth Thematic Conference, "Remote Sensing for Exploration Geology", San Francisco, California, 1-4 April, 1985, University of Michigan, Ann Arbor, p. 309-324.

Raines, G. R., 1977, Digital color analysis of color ratio composite Landsat scenes: in Proceedings, Eleventh International Symposium on Remote Sensing of Environment, University of Michigan, Ann Arbor, p. 1463-1472.

Raines, G. R., and Knepper, D. H., Jr., 1983, A hue-saturation-intensity transform to improve hydrothermal alteration mapping: in International Geoscience and Remote Sensing Symposium Digest, 1983: Institute of Electrical and Electronic Engineers, v. 2, se. FP-6, p. 1.1-1.3.

NEAR-INFRARED DETECTION OF AMMONIUM MINERALS AT IVANHOE HOT SPRINGS, NEVADA

M. DENNIS KROHN, U.S. Geological Survey, Reston, VA 22092

ABSTRACT

Airborne Imaging Spectrometer (AIS) data were collected over the fossil hot spring deposit at Ivanhoe, Nev. in order to determine the surface distribution of NH_4-bearing minerals. Laboratory studies show that NH_4-bearing minerals have characteristic absorption features in the near-infrared (NIR). Ammonium-bearing feldspars and alunites were observed at the surface of Ivanhoe using a hand-held radiometer. However, first look analysis of the AIS images showed that the line was about 500m east of its intended mark, and the vegetation cover was sufficiently dense to inhibit preliminary attempts at making relative reflectance images for detection of ammonium minerals.

INTRODUCTION

Minerals having NH_4 bound in their crystal structure are reported from several economically important geologic environments. Ammonium minerals are observed in Hg-bearing hot springs, undersea "black smoker" hydrothermal vents, disseminated Au-deposits, exhalative Pb-Zn-Ag deposits, in coal- and oil-shale-bearing formations and in several other crystalline and sedimentary lithologies. Yet little is known about the detailed distribution and role of ammonium in geologic system, primarily due to difficulty of analyzing for NH_4-bearing minerals in the laboratory. NH_4 minerals typically resemble their K-bearing analogs can usually only be defined by small differences in X-ray diffraction patterns or by mid-infrared analysis.

Recently, NH_4-bearing mineral were shown to have diagnostic spectral absorption bands in the near-infrared (0.7 - 2.5 um) (Krohn and Bethke, 1984; Krohn, 1986) and were observed remotely using the Airborne Imaging Spectrometer (Goetz and Srivastava, 1985). The near-infrared appears to be the analysis technique of choice for detecting ammonium in minerals and its discovery at Cuprite, Nev. is one of the earliest achievements of high-resolution airborne spectrometry.

SPECTRAL FEATURES

Ammonium has three diagnostic absorption bands in the near-infrared located at 1.56 um, 2.02 um, and 2.12 um (Figure 1). These bands are overtones and combination tone of N-H stretching and bending vibrational modes that occur in the mid-infrared near 3 um and 7 um. The two bands near 2 um are broad spectral features and are the primary means for discriminating NH_4 in minerals. In spectrally flat minerals, such as feldspars, the NH_4 spectral features are the only absorption features seen. In phyllosilicates and other OH-bearing minerals, the NH_4 spectral features are observed as shoulders to the primary Al-OH absorption band near 2.2 um or as a doublet band of equal intensity.

Although the band centers of the NH_4 spectral features shift with different mineralogies, the ammonium bands are readily distinguished from OH bands in the laboratory samples examined to date.
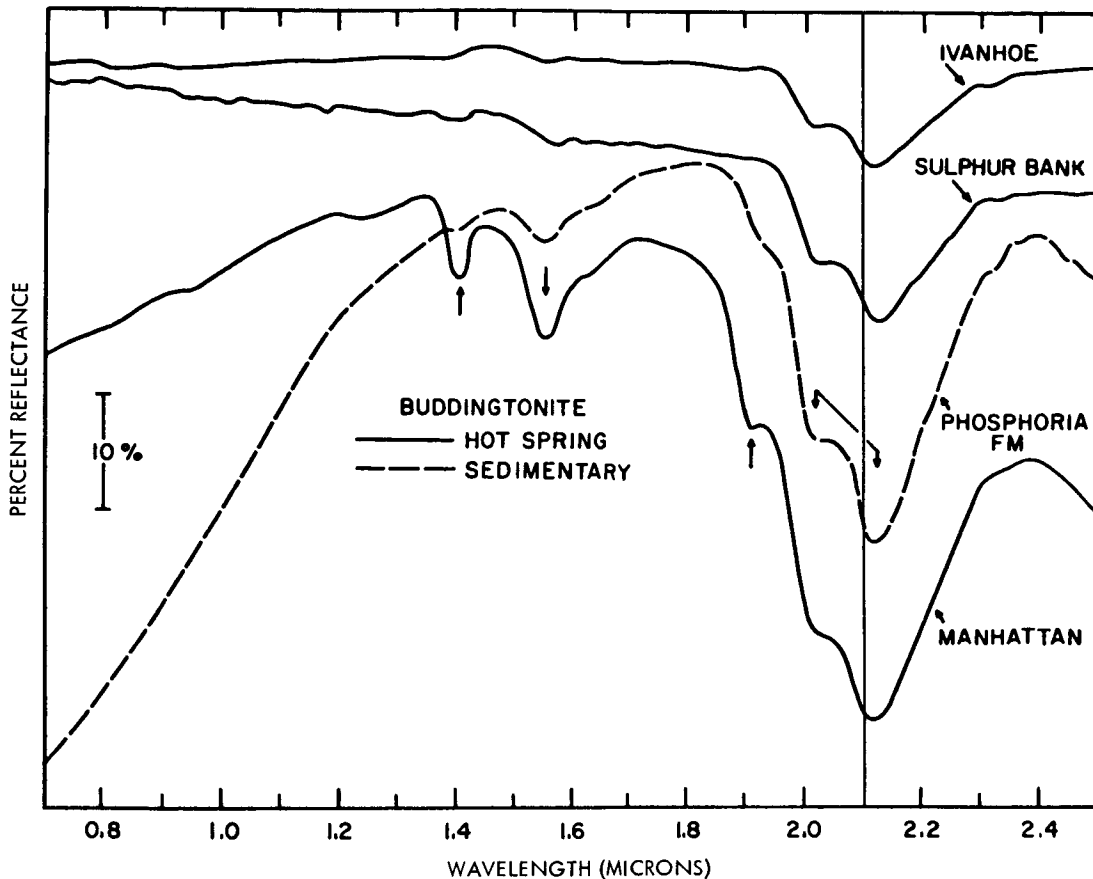
Figure 1. Laboratory near-infrared reflectance spectra of buddingtonite from several hot spring and sedimentary localities in the western U.S.

SPECTRAL CONTRAST

Since the NH_4 absorption features are relatively broad bands, the depth of the spectral band or the spectral contrast becomes a key parameter for distinguishing ammonium minerals remotely. Mid-infrared (2.5 to 25 um) intensities in transmittance are directly proportional to the concentration of NH_4 in the mineral and band depth of the 7 um band maybe used to estimate the amount of ammonium in mineral samples. However in near-infrared reflectance, spectral contrast is a function of several factors including NH_4 concentration, particle size, and absorption coefficients of other sample constituents, all of which have a large role in determining the NIR detectability of NH_4.

Figure 1 shows laboratory reflectance spectra of buddingtonite from several localities. The spectral contrast varies greatly both within

and between localities. Smaller amounts of NH_4 are observed as small shoulders in spectra of micas (Krohn, 1986). Experience with AIS and AVIRIS systems will be needed to determine the minimum spectral contrast of NH_4-minerals needed to be observed by airborne systems.

AMMONIUM AT IVANHOE

Buddingtonite was initially identified at Ivanhoe, Nev. in drill core by x-ray diffraction (Bloomstein, 1984). Fieldwork has shown that NH_4 is stable or metastable in the oxidizing environment at the surface at Ivanhoe and can readily be identified using a hand-held ratioing radiometer. Both buddingtonite and NH_4-bearing alunite are observed. Most of the NH_4-bearing minerals at Ivanhoe are found in a zone of intensely hydrothermally-altered basalt. This lithology sits below a leach cap of porous silica and chalcedony, a zone of argillic alteration consisting primarily of kaolinite, and hydrothermally-altered rhyolitic tuffs that overlie and surround the basalt outcrops. NH_4-bearing minerals are observed around the periphery of the deposit rather than in the central silicified area. On the ground, the distribution of NH_4 minerals is shown to be highly variable rather than forming broad continuous halos. NH_4- bearing minerals appear localized along fault and fracture surfaces, suggesting NH_4 is transported and deposited by hydrothermal fluids of the hot spring system.

AIS OVERFLIGHT

On July 24, 1985, the C-130 flew both the Carlin and Ivanhoe sites on its first leg of a major two month deployment. Flight lines were chosen in a N-S and E-W transect intersecting at the hot spring. The N-S line covered Antelope Creek, some of the Tertiary basalt, and Big Butte, a flowdome that is a major landmark of the area. The E-W line covered a barite mine, that is part of a trend of mineralization near the Carlin mine. Several large brush fires had occurred in the previous month and can be seen as large blackened areas on the ground. In-situ spectral measurements were gathered the previous day on the hydrothermally-altered rocks and on one of the burned areas. Partial cloud cover hindered the gathering of in-situ spectral data.

The aircraft was flown at maximum altitude of 19,000 ft (5800 m) to cover as much ground area as possible. AIS instruments appeared to be working nominally during the mission. However, the NS001 scanner experienced intermittent data interrupts which worsened as the flight progressed.

FIELD RESULTS

Initial field examination of the AIS line showed it to be located 500 m east of the proposed line. The line covers a portion of hydrothermally altered and bleached rhyolitic tuff and a siliceous opaline leach cap of the hot spring system. However, neither of these lithologies are believed to be favorable for hosting NH_4-bearing minerals because of the lack of K-feldspar suitable for substitution. Laboratory NIR spectra of rock samples showed that both kaolinite and alunite are present, although no NH_4 was observed in the alunite samples. Identification of alunite and kaolinite minerals at Cuprite by

the AIS led to the detection of buddingtonite, so that analogous
processing at Ivanhoe should also reveal other localites of NH_4-minerals
if present. The flightline did cover the inactive Butte #1 Hg-mine.
The mine site consists of a trench and tailings. The mine site plus the
burn areas should make a good light and dark targets for calibration.
Fieldwork also showed that large mining cuts and bulldozer swaths about
8 m wide were visible, but smaller mining roads and jeep trails were not
distinguishable. Presumably the jeep trails constitute a small enough
fraction of the pixel and are spectrally similar to surrounding terrain
not to effect the DN values of the AIS.

PRELIMINARY DATA CHARACTERISTICS

AIS data were wavelength calibrated using a LOWTRAN atmospheric
model (Fig. 2). Strong CO_2 features were observed in the wavelength
range between 2.0 and 2.4 um. Analysis showed that the data needed to
be offset approximately 70 nm to shorter wavelength from the 1984
calibration specifications. Calibration performed on the last 32
channels seemed to hold for the rest of 96 channels, indicating that the
inter-grating calibration performed well.
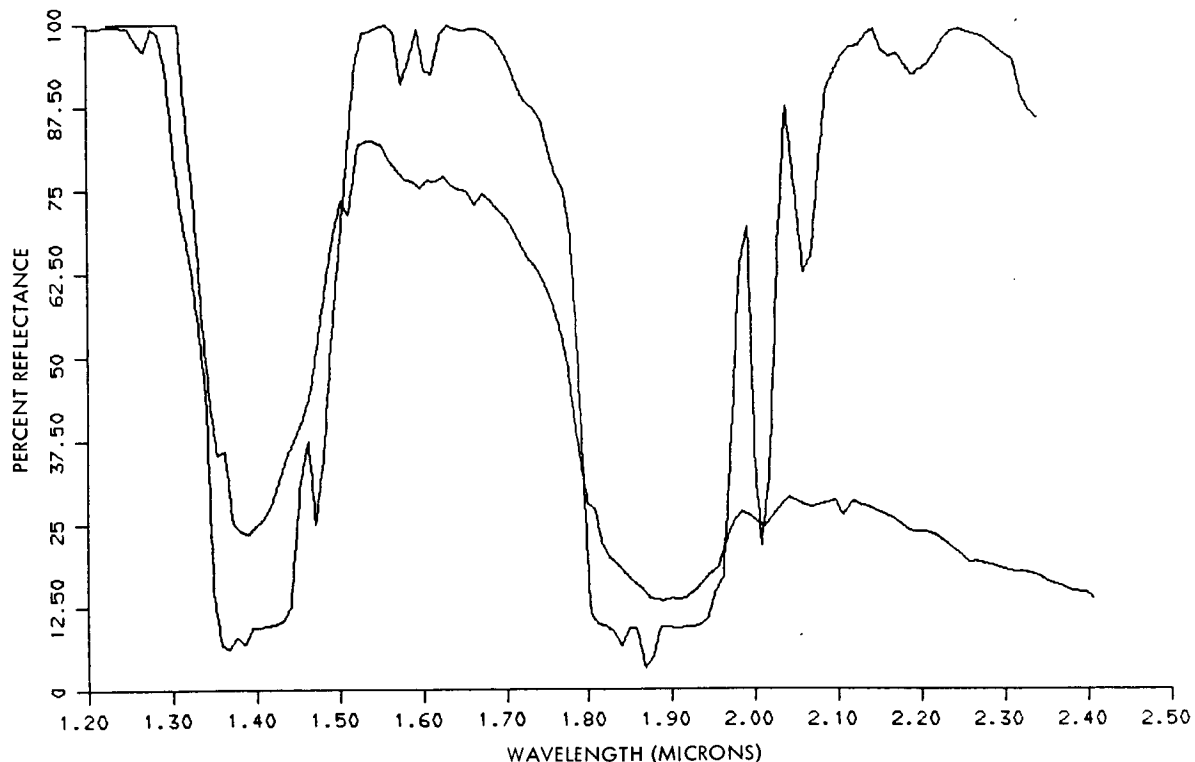
Figure 2. Average AIS spectrum for flightline compared with LOWTRAN
atmospheric model to show alignment of carbon dioxide bands
near 2 um. Upper spectrum - LOWTRAN model; lower spectrum
AIS average reflectance from pixel column 16.

A relative reflectance spectrum was created along a single pixel column to test spectral properties of the data set. Such techniques have worked well at defining alteration minerals at the Grapevine Mt, Nev. (Kruse, this volume). Spectra of data points located at Butte and Ivanhoe mine sites (Fig. 3) showed different patterns, but were sufficiently noisy to be unrecognizable spectrally. This type of fluctuating spectral pattern appears to be characteristic of sites with moderate vegetation cover. The variability appears to be a combination of mixed pixel and second-order effects (resonance spectral energy from shorter wavelength due to absence of a blocking filter on the AIS) (Terry Cook, this volume). Refined processing techniques need to be developed to compensate for this spectral variability.
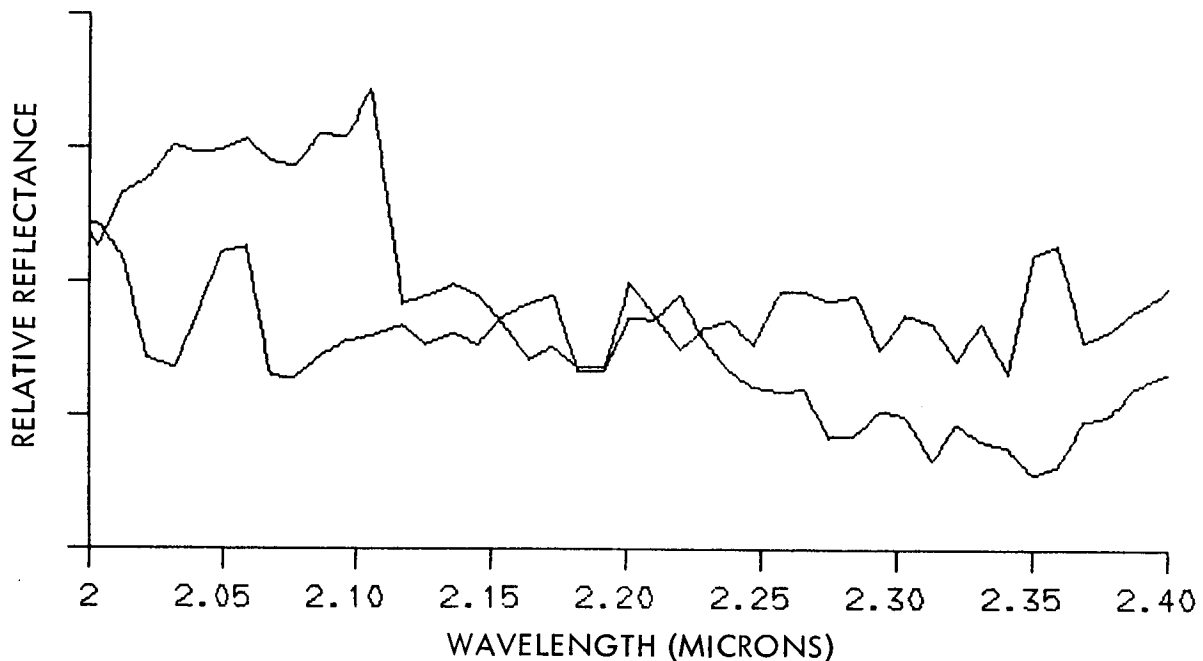
Figure 3. Relative reflectance AIS spectra for the Ivanhoe and Butte no. 1 mine site localities at Ivanhoe, Nevada. Variability is due to defining average using areas with a vegetation cover.

CONCLUSIONS

Near-infrared detection of ammonium minerals is feasible using hand-held and airborne instruments. Detection of ammonium minerals depends upon finding a suitable host rock with K^+ or other cation site for substition, in addition to the presence of ammonium and a proper geochemical environment. Unlike O-H-bearing minerals, NH_4 is not essential to the structure of its constituents minerals and can vary in concentration, giving rise to additional variability in band depth not present in O-H bearing minerals. Initial field work has shown the AIS line passed to the east of known NH_4-minerals, but did encounter spectrally-diagnostic minerals kaolinite and alunite. Vegetation density and second-order effects have hindered initial spectral processing of AIS data at Ivanhoe, Nev. and processing techniques need to be developed for spectral variability.

REFERENCES

Bloomstein, E.I., 1984, Ammonia alteration as a geochemical link in gold
    deposits of the Carlin-Midas belt (abs.): Symposium of the Assoc.
    of Exp. Geochem., Exploration for ore deposits of the North
    American Cordillera, March 1984, Reno, p. 27.

Goetz, A.F.H., and Srivasta, V., 1985, Mineralogical mapping in the
    Cuprite mining district, Nevada: in Vane, G. and Goetz, A.F.H,
    Proceedings of the Airborne Imaging Spectrometer Data Analysis
    Workshop, Jet Propulsion Laboratory Publication 85-41, pp. 22-31.

Krohn, M.D., and Bethke, P.M., 1984, Near-infrared spectral features of
    ammonium minerals: applications for remote sensing of hot spring
    deposits (abs.): Geol. Soc. Am. Abstracts with Programs, v. 16, p.
    566.

Krohn, M.D., 1986, Spectral properties (0.4 to 25 microns) of selected
    rocks associated with disseminated gold and silver deposits in
    Nevada and Idaho: J. Geophys. Res., v. 91, B. 1, pp. 767-783.

ANALYSIS OF AIS DATA OF THE BONANZA CREEK EXPERIMENTAL FOREST, ALASKA

MICHAEL A. SPANNER, TGS Technology, Inc., NASA Ames Research Center, Moffett Field, CA, USA 94035; DAVID L. PETERSON, NASA Ames Research Center, Moffett Field, CA, USA 94035.

ABSTRACT

Airborne Imaging Spectrometer (AIS) data were acquired in 1985 over the Bonanza Creek Experimental Forest, Alaska for the analysis of canopy characteristics including biochemistry. Concurrent with the AIS overflights, foliage from fifteen coniferous and deciduous forest stands were analyzed for a variety of biochemical constituents including nitrogen, lignin, protein and chlorophyll. Preliminary analysis of AIS spectra indicates that the wavelength region between 1450-1800 nanometers (nm) displays distinct differences in spectral response for some of the forest stands. A flat field subtraction (forest stand spectra - flat field spectra) of the AIS spectra assisted in the interpretation of features of the spectra that are related to biology.

INTRODUCTION

The taiga forests of interior Alaska are composed of a variety of vegetation types including pure and mixed stands of white and black spruce, paper birch, aspen, balsam poplar, alder and willow. At the Bonanza Creek Experimental Forest near Fairbanks, Alaska, a good understanding of the productivity and nutrient cycling of taiga forest ecosystems has been developed (Van Cleve et al., 1983; Viereck et al., 1983; Yarie and Van Cleve, 1983; Van Cleve et al., 1981). Environmental factors including large seasonal variations in day length and temperature, and the occurrence of permafrost result in generally lower rates of primary production and nutrient cycling compared to temperate forest ecosystems.

At NASA Ames Research Center, we are investigating the use of remote sensing data to study the biogeochemical cycling of forest ecosystems (Peterson et al., 1985). Various organic compounds present in foliage absorb visible and infrared radiation. The absorption features correspond to fundamental stretching frequencies of organic bonds. These organic compounds are of importance to nutrient cycling because they are composed of key nutrients (carbon, nitrogen, phosphorous, etc.) that are required for plant

growth.   Quantification of the concentration of the various organic compounds in the canopy may be possible using high spectral resolution remote sensing data obtained from instruments like the Airborne Imaging Spectrometer. Because of the understanding of the biogeochemical cycling of the taiga forests developed in Alaska, we initiated a study at the Bonanza Creek Experimental Forest to determine the sensitivity of high spectral resolution remote sensing data to leaf and canopy biochemistry.

BACKGROUND

Last year we reported laboratory and AIS analysis of leaf and canopy chemistry from Blackhawk Island, Wisconsin (Fownes and Aber, 1985; Spanner et al., 1985). A fertility gradient trends east-west across the mixed deciduous forests of Blackhawk Island. Total canopy nitrogen prior to senescence does not vary substantially across the gradient, but the lignin content of the canopy does vary with increased lignin in the less fertile west and less lignin in the more fertile east. The green state lignin to nitrogen ratio is strongly related to the underlying mineralization rate. Laboratory analyses of ground, dried leaves from this gradient using spectro-photometers demonstrated that the reflectance spectra is related to variations in nitrogen and lignin content with high predictability (Card, personal communication 1986; Wessman, personal communication 1986).

Analysis of the 1984 AIS data indicated the presence of considerable spatial noise in the data (Figure 1b). During the past year, a Fourier filtering algorithm was developed to reduce spatially correlated noise (Hlavka, 1986) (Figure 1a). The influence of solar irradiance and atmospheric water absorption on these spectra are still dominant. However, absorption features of these spectra now occur at the same wavelength and the spectra are much smoother. Analysis of total canopy biochemical contents of six stands on Blackhawk Island indicated that there is a strong inverse relationship between wet foliage biomass and AIS data for most wavelengths outside the atmospheric water absorption bands (Figure 1c). Lignin content is also inversely related to the AIS data at wavelengths near 1330 nm and from 1500 to 1700 nm (Figure 1d).

STUDY AREA AND METHODS

Forest stands at the Bonanza Creek Experimental Forest, Alaska vary from relatively highly productive aspen, paper birch and white spruce on south facing well-drained slopes, to black spruce forests of low production on north facing slopes underlain by permafrost. In the Tanana River floodplain, forest stands of balsam poplar and white spruce are productive where permafrost is absent; conversely, less
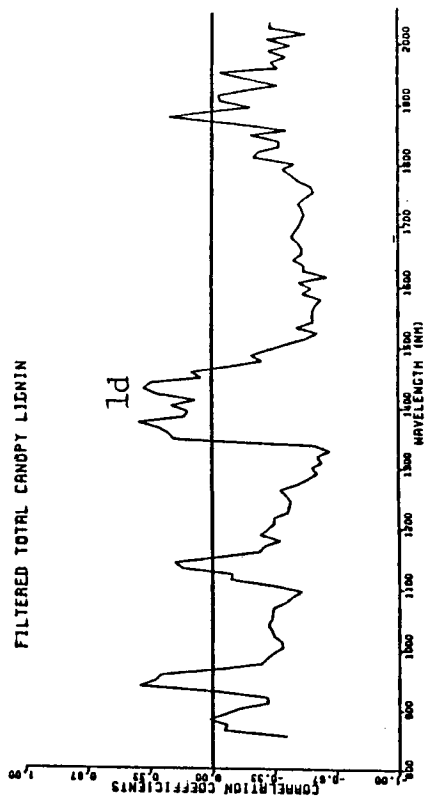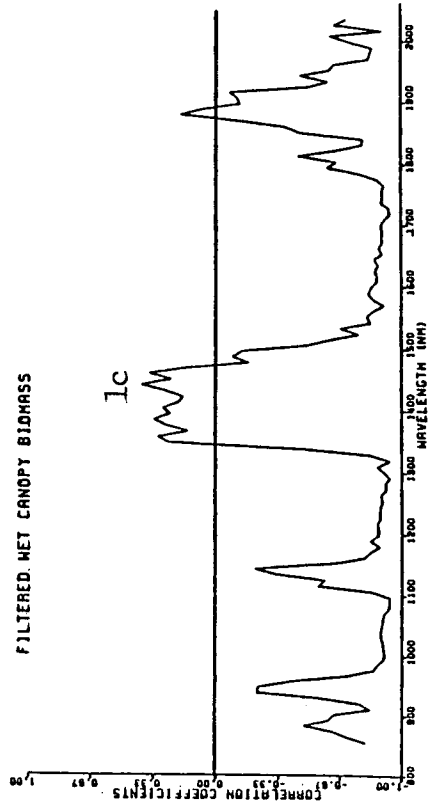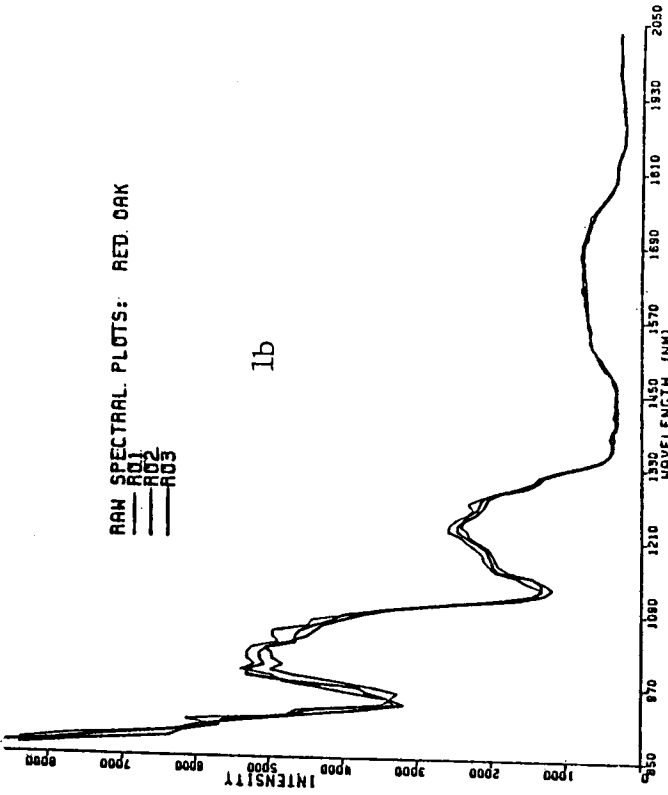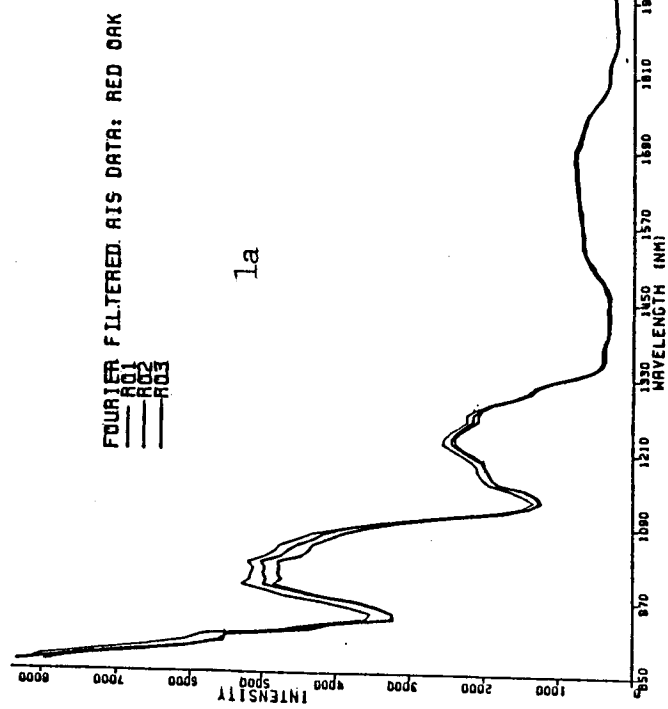
Figures 1a-1d.   Results from analysis of 1984 AIS data of Blackhawk Island, Wisconsin

productive black spruce stands are located on river terraces underlain by permafrost. Twenty-one forest stands have been established by researchers in the Bonanza Creek Experimental Forest. Detailed measurements of tree and foliage biomass, production and nutrient cycling were made at a number of these stands.

During August 1985 we collected foliage at fifteen of the stands for biochemical analysis. At each stand foliage was obtained from three trees of each species. Using a shotgun, foliage was sampled from four canopy layers (dominant, upper codominant, lower codominant and suppressed). Samples were also obtained from understory vegetation consisting mostly of mosses and lichen. A subsample of the foliage was freeze dried and analyzed for nitrogen, chlorophyll A, chlorophyll B, total chlorophyll, protein, amino acids, lignin, cellulose, starch, sugar and phosphorus. The freeze-dried samples were scanned on a Perkin-Elmer spectro-photometer that measured reflectance from 400-2450 nm, with 2 nm resolution at 5 nm intervals. Stepwise multiple regression analysis will be performed on these data to determine relationships between biochemical content and spectral response.

The Airborne Imaging Spectrometer onboard a C-130 aircraft obtained data from nine flightlines over the Bonanza Creek Experimental Forest on August 28, 1985. The AIS data were acquired in rock scan mode covering wavelengths from approximately 1220 to 2400 nm. The spatial resolution of the AIS data was approximately 8 meters. High diffuse clouds at the time of overpass resulted in variable illumination conditions. Twelve of the fifteen forest stands sampled were imaged. A calibration flightline was flown perpendicular to a runway, road and highway to allow for flat field corrections.

ANALYSIS AND DISCUSSION

Raw spectral plots of the forest stands were generated from the AIS data and analyzed. Presented in Figure 2 are spectral plots of four forest stands extracted from flightline 1. The spectra are mean AIS intensities for forest stands of at least 3 by 3 pixels. Of particular interest is the region between 1450 and 1800 nm. Intensity increases for all four stands from 1400 nm to beyond 1700 nm, and then declines. The pattern of increase and decline varies between the four stands. These curves exhibit large differences in reflectance between deciduous and coniferous stands. Noise in the form of intensity variations between grating positions is evident on these plots.

Compare the difference between the biologically derived spectra in Figure 2 with the spectra from a runway, highway and road in Figure 3. The spectra in Figure 3 were

Figure 3. Targets used for flat field correction

Figure 2. Raw stand spectra from flightline 1

148

Figure 5. Flat field correction for deciduous stands

Figure 4. Flat field correction for flightline 1

149

extracted from the calibration flightline. Each target (runway, highway and road) extended across the full width of the flightline (32 pixels)' and varied from 2-4 lines in length. These are termed flat field spectra because they are essentially spectrally flat without major absorption or increased reflectance features. Note that between 1500 nm and 1700 nm the spectral is fairly flat, compared to the biological spectra. The dip at approximately 1660 nm is a sensor artifact.

The biological spectra were subtracted by a flat field spectrum under the assumption that atmospheric water vapor and solar irradiance effects of these spectra are similar. Thus, the "relative difference" signal should represent a residual biological signal without first order atmospheric and solar effects. An example of subtraction of the stand spectra from flightline 1 by the runway spectrum is presented in Figure 4. The magnitude of the reflectance is not of interest, instead we are interested in the slope (positive or negative) of each curve. A decrease indicates absorption relative to a flat field spectrum. An increase represents increased reflectance with respect to the flat field.

In Figure 4 dramatic differences between the paper birch stands and the spruce stands are evident that are not as noticeable on Figure 2. For the birch stands, reflectance increases relative to the runway from 1400 nm to approximately 1680 nm and then drops off. For the spruce stands, there is an absorption relative to the runway from 1400 nm to about 1500 nm. The spectra level off until about 1580 nm and then increase until approximately 1800 nm. Structural and morphological differences between coniferous and deciduous stands probably account for the coarse differences in intensity seen in Figure 2. The differences observed in Figure 4, however, are due to characteristics of the canopy that we need to understand.

Figure 5 displays a flat field subtraction for a variety of forest stands. It is clear from this figure that the trend in reflectance relative to the runway flat field spectrum are different for each vegetation type. These variations occur near and within the region of Thematic Mapper band 5 (1.53um - 1.73um), indicating that there is fine spectral information within this broad region. A relative difference minima occurrs at 1400 nm for the birch stand corresponding to atmospheric water absorption. For the aspen, alder and willow stands, however, the relative difference minima is closer to 1500 nm. The alder stand composed mostly of nitrogen fixing alder has a strong absorption centered at 1520 nm. The relatively flat signal from the willow site is probably dominated by the exposed soil because the vegetation cover is sparse and of low stature. It is premature to attribute these features to specific vegetation characteristics such as biochemical

absorption, but we are continuing to examine this aspect using stand estimates of biochemical content from foliage samples that are currently being analyzed. Additional analysis is required to account for second order optical errors in the AIS instrument (Conel, this volume), for solar spectral irradiance variations, and for atmospheric absorption and scattering to permit direct comparisons of biological spectra.

Our data indicate that conifer and deciduous stands have spectral variations that are not solely related to intensity differences. There is evidence of absorption that can be seen in the "relative difference" plots for many of the forest stands. Once our field data is extrapolated to the canopy level, we should have an improved understanding of the sensitivity of AIS data to the biochemistry of taiga forest canopies. Advanced high spectral resolution remote sensing instruments like the Airborne Visible and Infrared Imaging Spectrometer (AVIRIS) should provide improved data for the analysis of canopy biochemistry.

ACKNOWLEDGEMENTS

REFERENCES

Hlavka, C., 1986, Destriping AIS data using fourier filtering techniques, Proceedings of the 1986 Airborne Imaging Spectrometer Data Analysis Workshop, this volume.

Pastor, J., J.D. Aber, C.A. McClaugherty and J.M. Melillo, 1984, Aboveground production and N and P cycling along a nitrogen mineralization gradient on Blackhawk Island, Wisconsin, Ecology, 65:256-268.

Peterson, D.L., J.G. Lawless, P.A. Matson, J.D. Aber, P.M. Vitousek and S.W. Running, 1985, Biogeochemical Cycling in Terrestrial Ecosystems, 36th International Astronautical Federation Congress, Stockholm, Sweden.

Spanner, M.A., D.L. Peterson, W. Acevedo and P. Matson, 1985, High resolution spectrometry of leaf and canopy chemistry for biogeochemical cycling, Proceedings of the 1985 Airborne Imaging Spectrometer Data Analysis Workshop,

pp.   92-99.

Van Cleve, K., l. Oliver, R. Schlentner, L.A. Viereck and C.T.   Dyrness, 1983, Productivity and nutrient cycling in taiga forest ecosystems, Canadian Journal of Forest Research 13:747-766.

Van Cleve, K., R. Barney and R. Schlentner, 1981, Evidence of temperature control of production and nutrient cycling in two interior Alaska black spruce ecosystems, Canadian Journal of Forest Research, 11:258-273.

Viereck, L.A., C.T. Dyrness, K. Van Cleve and M.J. Foote, 1983, Vegetation, soils and forest productivity in selected forest types in interior Alaska, Canadian Journal of Forest Research, 13:703-720.

Yarie, J. and K. Van Cleve, 1983, Biomass and productivity of white spruce stands in interior Alaska, Canadian Journal of Forest Research, 13:767-772.

SOIL TYPES AND FOREST CANOPY STRUCTURES IN SOUTHERN MISSOURI:
A FIRST LOOK WITH AIS DATA

GLEN M. GREEN and RAYMOND E. ARVIDSON, McDonnell Center for the Space
Sciences, Washington University, St. Louis, Missouri 63130

ABSTRACT

Spectral reflectance properties of deciduous oak-hickory
forests covering the eastern half of the Rolla Quadrangle
were examined using Thematic Mapper data acquired in
August and December, 1982 and AIS data acquired in August,
1985. For the TM data distinctly high relative
reflectance values (>0.3) in the near infrared (Band 4,
0.73-0.94 micrometers) correspond to regions characterized
by xeric (dry) forests that overlie soils with low water
retention capacities. These soils are derived primarily
from rhyolites. More mesic forests characterized by lower
TM band 4 relative reflectances are associated with soils
of higher water retention capacities derived predominately
from non-cherty carbonates. The major factors affecting
canopy reflectance appear to be the leaf area index (LAI)
and leaf optical properties. The Suits canopy reflectance
model predicts the relative reflectance values for the
xeric canopies. The mesic canopy reflectance is less well
matched and incorporation of canopy shadowing caused by
the irregular nature of the mesic canopy may be necessary.
Preliminary examination of high spectral resolution AIS
data acquired in August of 1985 reveals no more
information than found in the broad band TM data.

INTRODUCTION

The relationship between forest canopies in the Missouri Ozarks
(Figure 1) and underlying soil types are explored in this paper. In
particular we develop explanations for the variation in canopy
characteristics sensed by Thematic Mapper and the Airborne Imaging
Spectrometer as a function of soil water retention capacities. The
intent is to eventually utilize reflectance data from aircraft or from
space to determine canopy characteristics and to then infer soil
characteristics. We stress TM observations over a number of control
sites in the Ozarks, use of the Suits canopy reflectance model, and
whether there is additional information to be gained from AIS data.

A Thematic Mapper image (band 4) acquired in August, 1982 for the
eastern half of the Rolla Quadrangle is shown in Figure 2A. A color
slide using bands 4 (red component), 5 (green) and 7 (blue) processed to
radiance values is inserted in the plastic holder at the end of these
proceedings. Agricultural fields appear as white, while other regions
which are covered by oak-hickory forests show a variety of colors. Most
of the color variety is driven by variations in band 4 radiance values.
A winter TM band 4 scene of the same area is shown in Figure 2B. While
fields are light, the bland brightness patterns demonstrate that most
forested lands are spectrally homogeneous in band 4 in the winter season.
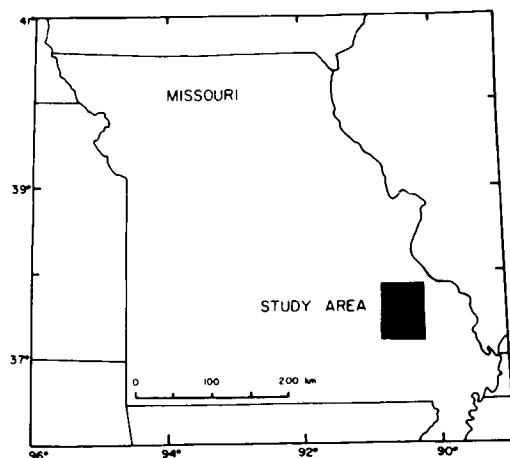
Fig. 1. Study location: the eastern half of the Rolla Quadrangle.
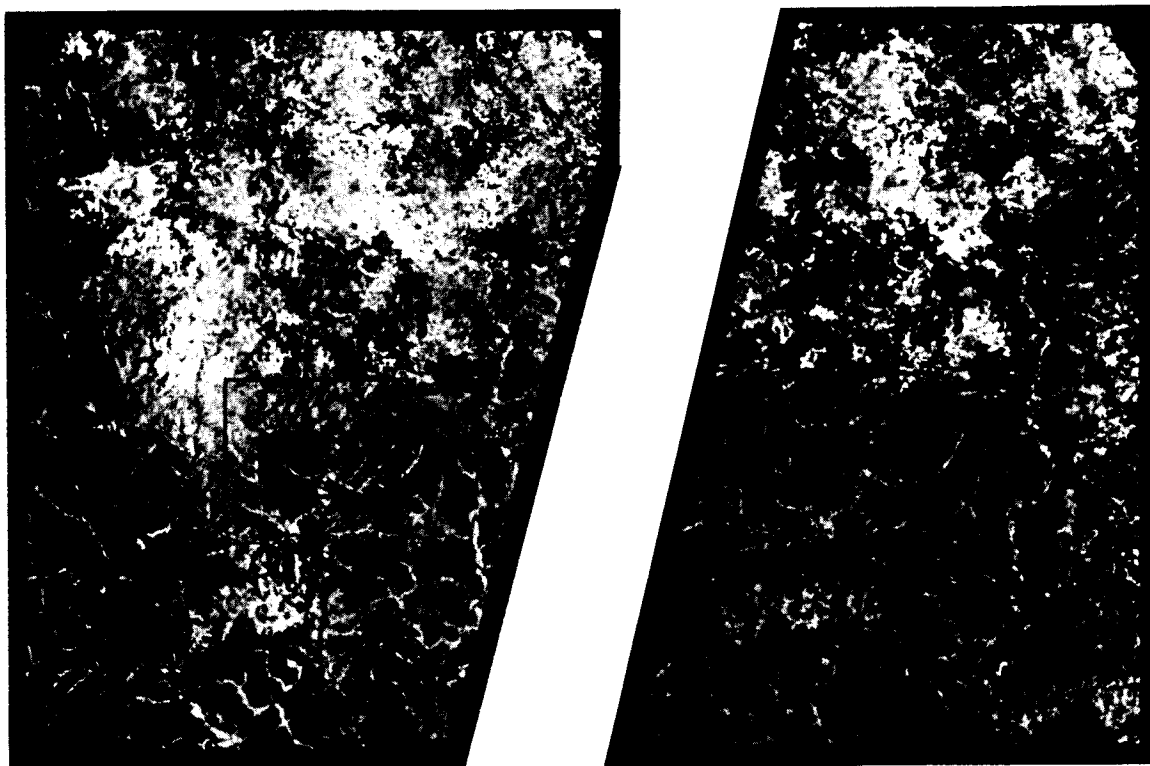
Fig. 2A, 2B. August (2A) and December (2B), 1982, TM band 4 images of the eastern half of the Rolla Quadrangle. (Figure 2A is color slide number 7 in the back cover pocket of this publication.)

Color composites of the winter scene corroborate this conclusion. Spectral variations in the August scene are thus controlled by structures and/or optical properties of the foliated oak-hickory canopy.

GEOLOGIC CONTROL

In general, soils in the study area are derived as weathering products from the underlying bedrock and as a consequence they preserve signatures of the underlying geology. Geologically the central region of the eastern half of the Rolla quadrangle is underlain by Precambrian granites and rhyolites of the St. Francois uplift. These rocks are surrounded by flat-lying Paleozoic carbonate sedimentary rocks. The box in Figure 2A includes outcrops of both rhyolites and carbonates. This area is shown enlarged in Figure 3, and Figure 4 shows a simplified geologic map for the region. A color slide of this area, processed in the same way as the slide described previously, is inserted in the plastic holder at the end of these proceedings.

The rhyolites and granites typically develop thin rocky soils, while most carbonates weather to produce a thick clay-rich residuum. This contrasting soil texture can produce a significant impact on perennial vegetation through a process linked to the local climate (Green et al., 1985). Specifically, spring rainfall is high and all soils are brought to water holding capacity; however summers are hot and dry so the soil water retention capacity of the soil controls the survival of perennial plants. The thin, rocky soils on rhyolites have low water retention capacities that produce local seasonally xeric (dry) environments. Xeric forests and glades (naturally treeless areas) tend to develop in these area. On the other hand, the higher clay content of carbonate derived soils causes water to be retained through the summer and thus supports more mesic (moist) forests. Some carbonates have a high chert content that forms a soil with an impermeable residual layer (fragipan) that restricts water infiltration. These fragipan soils also create a seasonally xeric environment. The rhyolites of Figure 4 are usually associated with a high August TM band 4 reflectance shown as lighter tones in Figure 3 and as an orange color in the accompanying slides. The carbonates are generally associated with lower August TM band 4 reflectance for the detailed study area except for a region near the western margin of Figure 3. Ground observations in this region reveal an abundance of chert pebbles within stream beds and as float on the ground surface.

To explore the vegetative control on the August TM reflectances within the study area (Figure 3), fifteen study sites were chosen for detailed study. These sites are also along an AIS flightline where data were acquired in August, 1985. At each of these sites 3 permanent chart quadrats were laid out along transects in which all tree species were identified and measured. These sites were chosen to encompass the majority of the August TM spectral variations.

Three broad Oak-Hickory forest types were identified in the study sites: mesic, xeric, and very xeric. These three endmembers differ markedly in species composition and canopy structure (see Figure 5). The mesic forests, predominantly overlying carbonate rocks, exhibit trees of the largest diameter, tallest height, and lowest density. These forests are dominated by the moist favoring white oak (<u>Quercus</u> <u>alba</u>) and scarlet
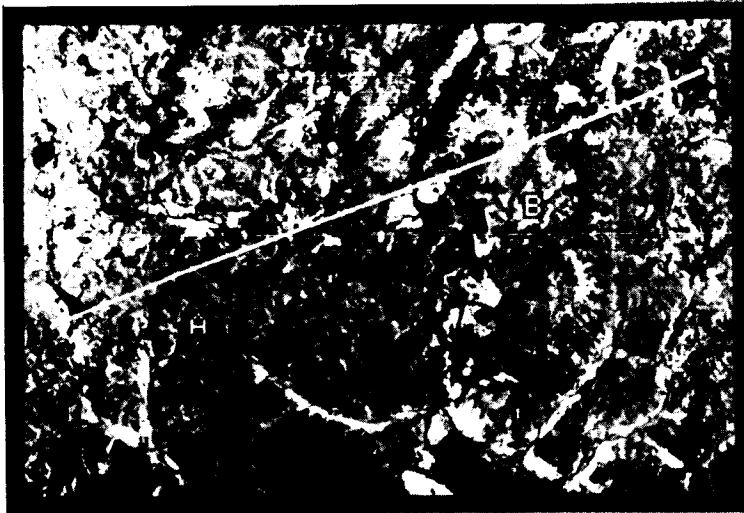
Fig. 3. August, 1985 band 4 image of the de-detailed study area. (~25km wide) The white line marks the AIS flightline. (See color slide number 8 in the back cover pocket of this publication.)
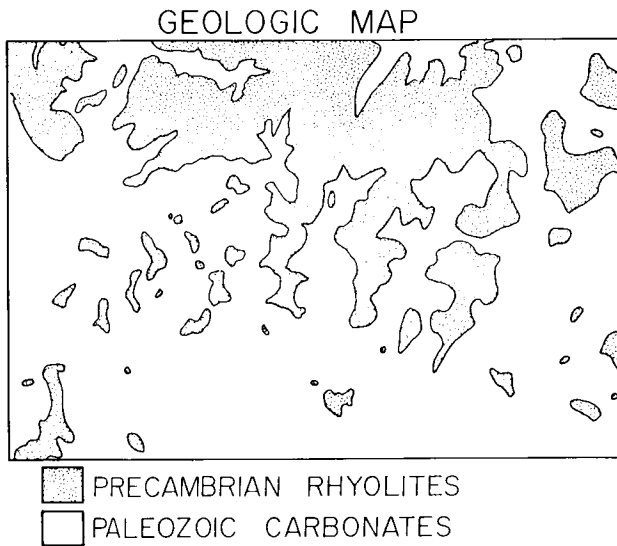
Fig. 4. Simplified geologic map of study area.

GEOLOGIC MAP

☐ PRECAMBRIAN RHYOLITES
☐ PALEOZOIC CARBONATES

Fig. 5. Measured cross-sections of three oak-hickory forest types.

MEASURED CANOPY X-SECTIONS

MESIC FOREST

XERIC FOREST

VERY XERIC FOREST

156
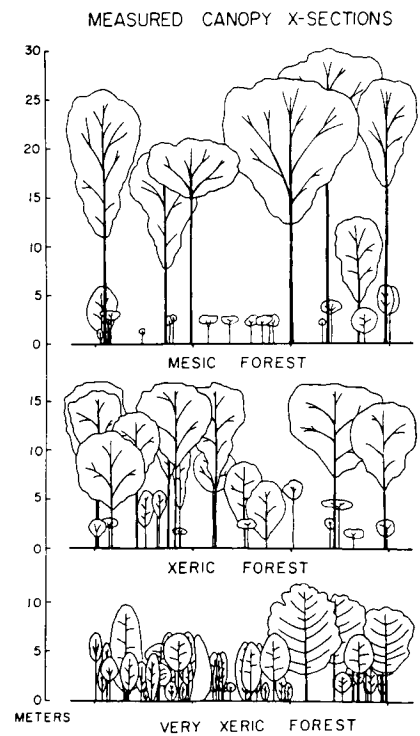
oak (Quercus coccinea). Aerial photographs acquired along the AIS flightline reveal that these forests usually develop an irregularly topped canopy. In contrast, xeric forests underlain mainly by rhyolites generally develop flat topped canopies. These forests support smaller diameters and lower height trees of the dry favoring species black oak (Quercus velutina) and mochernut hickory (Carya tomentosa). Very xeric forests develop a very short, sparse canopy of small diameter post oak (Quercus stellata) and blackjack oak (Quercus marilandica) and hickory species which favor very dry environments. These forests are associated with glades, where perennial plant growth is absent. Glades offer the most extreme xeric environments, since perennial plant growth cannot survive the dry August season. These glades are generally covered by herbaceous growth and lichen-covered rock. The very xeric forests and glades are associated with high TM band 5 and 7 reflectances (1.5-1.8 and 1.9-2.4 micrometers respectively) that produce light blue colors in the August TM color slides.

The spectral characteristics of these forest types as measured by TM were examined at locations A (two sites) and B (one site) along the study line. These three sites are shown enlarged in Figure 6. The corresponding TM reflectances for these study sites extracted from 3x3 pixel areas are plotted in Figure 7, using standard procedures to reduce TM data to Lambertian reflectance. Figure 7 reveals that the xeric forest stand exhibits the highest reflectance (>0.30) in band 4, though these forests generally have lower biomass (as revealed in basal area measurements) than mesic forests. In the visible (TM band 3, 0.56-0.74 micrometers) both xeric and mesic forests exhibit low reflectances. These observations call into question the use of simple vegetation indices such as the ratio of TM 4 over 3 or the normalized difference vegetation index. These indices may give erroneously high biomass estimates to the xeric forests.

SUITS CANOPY REFLECTANCE MODEL

To quantitatively understand the radiative transfer characteristics of xeric and mesic forests that give rise to the distinctive TM signatures, the Suits (1972) canopy reflectance model was used with data obtained for the study sites at A and B. The Suits canopy reflectance model is based on Duntley's (1942) diffuse-scattering radiative transfer theory. The model predicts the bidirectional reflectance properties of the canopy that are traceable to specific geometric and optical characteristics, using a number of infinitely extended horizontal layers. Leaves and branches are idealized as a combination of vertical and horizontal flat panels. The Suits model also takes into account the lighting and viewing geometry, factors that can have great effects on canopy reflectances.

While many of the parameters used by botanists and foresters were recorded in this study, such as tree height and diameter, these measurements may not directly indicate the causative factors controlling the spectral properties of these forest types. Thus, we also collected data that directly measure more relevant structural and optical parameters, data that can be incorporated into the Suits model. Hemispherical reflectance measurements of the leaves of all dominant species as well as those of branches and trunks were acquired. Sunlit leaves were collected from the top of the canopy by means of an
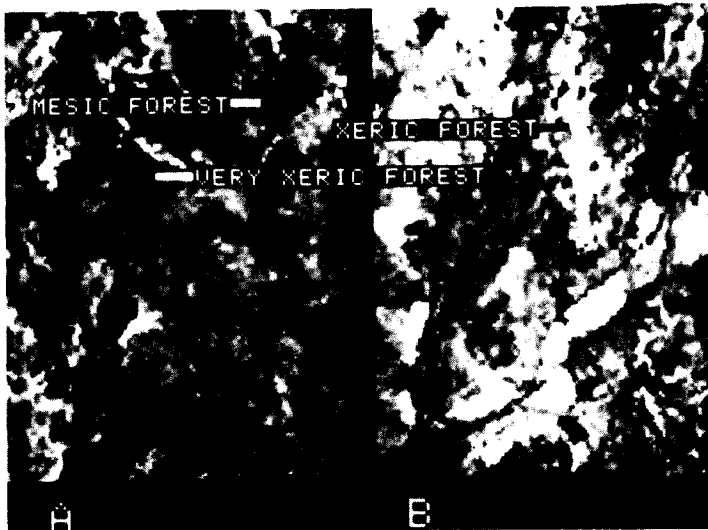
Fig. 6. Forest study
sites along AIS
flightline at
locations A and
B. (see figure
3.)

**FOREST CANOPY REFLECTANCE
AUGUST TM**

- MESIC
- XERIC
- VERY XERIC

REFLECTANCE

WAVELENGTH (μm)

**FOREST CANOPY REFLECTANCE
SUITS MODEL**

- MESIC
- XERIC
- VERY XERIC

REFLECTANCE

WAVELENGTH (μm)
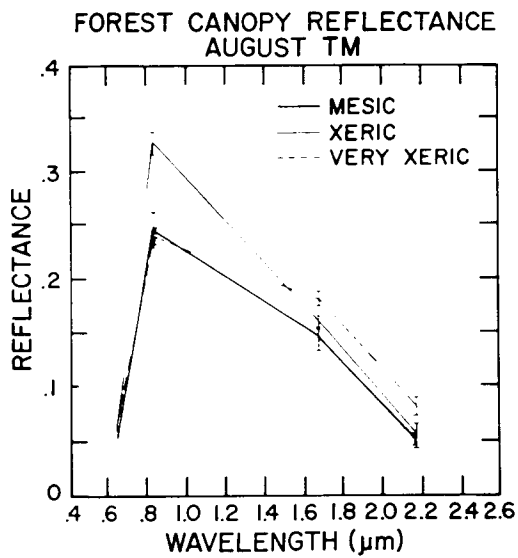
Fig. 7. Canopy bidirectional
reflectances of forest
study sites from
August, 1982 TM image.
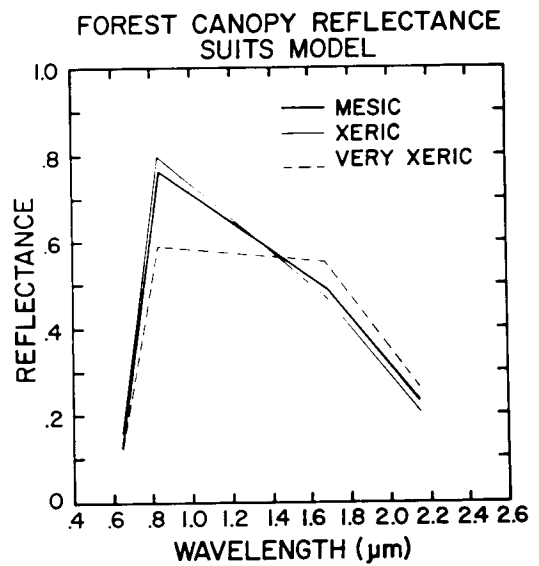
Fig. 8. Predicted canopy
bidirectional reflec-
tance of forest study
sites using the
Suits (1972) model.

158

expandable pole. The horizontal and vertical leaf area indices of both leaves and branches were measured by means of point counting 35 mm slides taken up through the canopy at various angles (Suits, 1976).

The results of the first of these canopy model reflectance plots are shown in Figure 8, for the three sites referred to earlier. Although the magnitudes are different from TM data, the Suits model successfully predicts the relative canopy bidirectional reflectance for both xeric and very xeric forests. It appears that the reflectance of the very xeric forest is controlled in large part by its low leaf area index (less than 1) which exposes ground material that is typically bright at TM band 5 and 7 wavelengths. Both the LAIs of the xeric and mesic forests are high enough to minimze the contribution from ground materials.

The slight difference in modeled canopy reflectance between the xeric and more mesic canopies (Figure 8) is traceable to higher near IR leaf hemispherical reflectance in the xeric species. At longer wavelengths hemispherical reflectance measurements of all leaves are similar. This difference in near IR leaf reflectance is probably explained by a thicker wax coating and the double layer of palisade cells typical of xeromorphic leaves (Kramer and Kozlowski, 1960). These differences contribute to more internal reflections and greater leaf reflectances. The differences in near IR leaf hemispherical reflectances, however, do not appear to be enough to account for the low August TM reflectance in band 4 (Figure 7) for the mesic forests. Mesic forests commonly have a more irregular canopy surface than do xeric forests and, thus, more canopy shadowing. This shadowing is not taken into account in the Suits model, which uses plane parallel layers. Incorporation of shadowing would probably lower the canopy reflectance of mesic forests, bringing the modeled results closer to actual data.

AIS DATA

To examine the added information higher spectral resolution AIS data may provide, AIS radiance values from 5x5 pixel averages of the 3 study sites are plotted in Figure 9. The AIS data were acquired on August 2, 1985 in the tree mode (0.80 to 2.20 micrometers). The plot of a predominantly gladed area is also included. Unfortunately, that portion of the spectrum that contains most of the TM variation (band 4) and that can be used to distinguish mesic and xeric forests is not included in the wavelength interval acquired with the AIS.

Figure 9 reveals considerable differences in radiances between forest types and glades, although the shapes of all curves appear similar. To enhance the spectral differences the curves were normalized to equal areas using the JPL SPAM software. The results are shown in Figure 10. Both Figures 9 and 10 show that the AIS observations are in general accord with those from TM data. At wavelengths greater than 1.4 micrometers, glades exhibit significantly higher relative radiances than the forest types. At shorter wavelength glades exhibit low relative radiances. Very xeric forest show these same trends to a lesser extent. As discussed, the small LAI in the gladed and very xeric forests apparently exposes materials, dead vegetation, and bare rock (rhyolite), which are spectrally similar and much brighter than leaves at wavelengths greater than 1.4 micrometers. Xeric and mesic forests have similar AIS spectra, although xeric forests do show somewhat higher values at shorter

AIS DATA

MESIC ———
XERIC ——
VERY XERIC - - - -
GLADE ·······
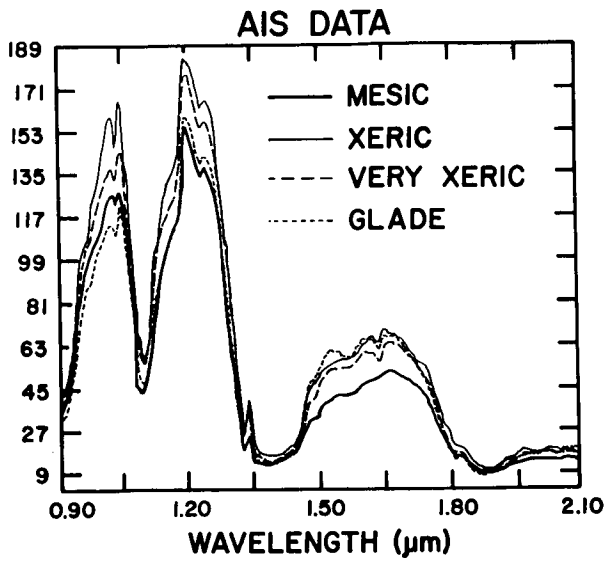
WAVELENGTH (μm)

Fig. 9. Raw AIS data for the forest sites plus glade using 5 x 5 pixel areas.

AIS DATA

EQUAL AREA
NORMALIZATION

MESIC ———
XERIC ——
VERY XERIC - - - -
GLADE ·······
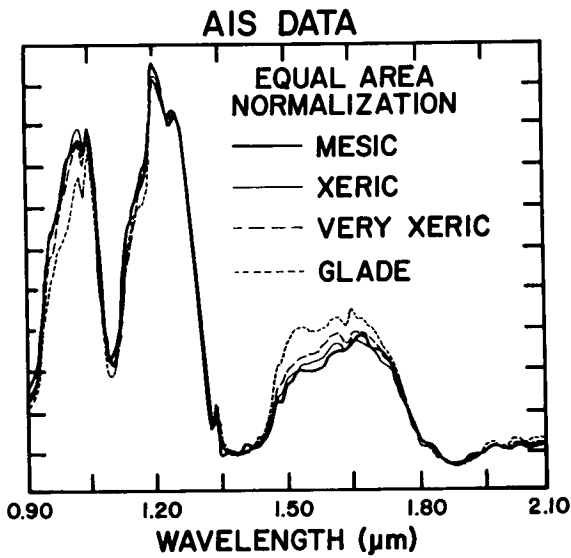
WAVELENGTH (μm)

Fig. 10. AIS data normalized to equal area under the curves.

160

wavelengths, consistent with TM observations.

Since no destriping was applied to the AIS data and in the light of the second order overlap, interpretation of the more subtle features, especially those greater than 1.6 micrometers, may not be warranted. At this early stage in our analysis the AIS data do not seem to contain more information than TM images. This may be caused by the inherent diffusing nature of leaves and of forest canopies and by the complex mixtures of vegetative components present, which would tend to dampen specific spectral features.

CONCLUSIONS

Spectral variations in TM and AIS data are caused by differing forest types. Three oak hickory forest types were identified based on field observations: mesic, xeric and very xeric stands. Glades form the most extreme xeric environment. Forest type distribution is controlled primarily by variation in the soil water retention capabilities of the soils, which in turn are controlled by bedrock, primarily the presence of rhyolite or carbonate. Canopy bidirectional reflectances in xeric and very xeric areas can be predicted by a reflectance model developed by Suits. In mesic forests, canopy texture and shadowing may have to be incorporated into this model, since the first order trends are not predicted. AIS data reveal essentially the same trends as observed in TM images.

BIBLIOGRAPHY

Duntley, S.Q., 1942, The optical properties of diffusing materials, Opt. Soc. Am., v.32, pp.61-70.
Green, G., R. Arvidson, M. Sultan, and E. Guinness, 1985, Geobotanical information contained in Landsat Thematic Mapper images covering southern Missouri. In Proceedings of the Fourth Thematic Conference: "Remote Sensing for Exploration Geology", San Francisco, CA, April 1-4, 1986, ERIM, pp.371-380.
Kramer, P.J. and Kozlowski, T.T. (1960), Physiology of Trees, McGraw-Hill, New York.
Suits, G., 1972, The calculation of the directional reflectance of a vegetative canopy, Remote Sensing of Environment, v.2, pp.117-125.
Suits, G., 1976, Instructions for making vegetation canopy measurements suitable for reflectance modeling. In Suits monograph available through ERIM.

GEOBOTANICAL STUDIES AT PILOT MOUNTAIN, NORTH CAROLINA, USING THE AIRBORNE
IMAGING SPECTROMETER

N.M. MILTON, P.A. WALSH, and T.L. PURDY, U.S. Geological Survey, Reston,
Virginia 22092.

ABSTRACT

Airborne Imaging Spectrometer (AIS) data were acquired of several vegetation
types within the humid temperate eastern United States. The spectral region
covered, 0.9 μm to 2.1 μm, has been little used in vegetation studies. A
preliminary analysis of spectral curves suggests that variations between
vegetation spectra may be useful for discriminating plant communities.
Calibration and normalization procedures must be refined to compensate for
cloud cover, detector and other system noise, and possible second-order
effects.

INTRODUCTION

The distributions of plant communities composed of deciduous and coniferous
trees in the Piedmont of the eastern United States are associated with
lithologic variations. Remotely sensed data from the Landsat MSS and TM
satellites have been used to determine some of these distributions (Krohn and
others, 1981; Milton and Krohn, 1982), but little attention has been given to
the high resolution spectral characteristics of tree species in the 0.9-2.1 μm
region. Data from the Airborne Imaging Spectrometer (AIS) were evaluated to
determine the significance of this spectral region for discrimination of
different plant communities.

STUDY AREA

The AIS data were acquired over Pilot Mountain, a hydrothermally altered
monadnock in the Piedmont physiographic province of North Carolina.
Enrichments of Cu, Mo, Sn, and Au are associated with the alteration. The
vegetation around the crest of the monadnock, where concentrations of metals
are highest, is composed primarily of chestnut-oak (Quercus prinus) forest.
Mixed oaks and pines (Pinus) comprise the forested slopes; the area to the
west within and outside the alteration zone is pine plantation. The geology,
vegetation, and results of an analysis of data from an earlier high-resolution
airborne radiometer experiment have been discussed in Milton and others
(1983). Fields, pasture, and lowland forests surround the monadnock and were
also imaged during the AIS surveys.

NEAR-INFRARED REFLECTANCE OF PLANTS

Spectral reflectance of plants in the 0.9 to 2.1 μm region is controlled by
scattering from cell walls and absorption by water (Knipling, 1970). This
portion of the electromagnetic (EM) spectrum has been less intensively studied
for plants than the visible portion of the spectrum. Spectral features which
appear to be species specific must still be considered tentative. Wickland
(1985) reported variations in an absorption feature at 1.19 μm in deciduous
versus pine forests. In broadband spectral data, spectral changes due to
plant water content have been used to separate plant communities or to mask
vegetation for rock discrimination in images.

AIS DATA

AIS and NS001 data were acquired over the study area on August 11, 1985. Two flightlines were requested, one oriented SE to NW and the other SW to NE, crossing over Pilot Mountain. The latter line was flown as requested, but the former, which would also have passed over two additional monadnocks, was flown approximately 1 mile to the southwest, thus missing all monadnocks. The NASA C-130 aircraft flew at a maximum of 4500 m, resulting in a ground swath width of approximately 300 m. Scattered cloud cover was present throughout the flights.

Preliminary processing of the AIS data was done using software developed by F. Kruse, U.S. Geological Survey, Denver and modified by D. Krohn, U.S. Geological Survey, Reston. The spectrometer seemed to be functioning well, as data from both flightlines are clean with relatively little noise, line-drops, etc. Whereas the spectrometer was operating in "tree mode" (0.9-2.1 μm), the processing parameters were still set for "rock mode" (1.2-2.4 μm). To compensate, calibration was done using a LOWTRAN atmospheric model, matching H_2O and CO_2 absorption features. The offset was determined to be approximately 210 nm from "rock mode" (90 nm from "tree mode"), and beginning and ending wavelengths were computed to be 0.99 μm and 2.19 μm. Calibration appeared to be correct for all grating intervals.

An enlarged gray-level raster plot of the AIS data was made for each flightline. The plots proved useful in plotting the precise location of each flightline and in delineating specific field or forest areas from which to derive spectra (figure 1). Average spectral curves were derived for both flightlines, and relative reflectance images were produced. These initial images were noisy because the average spectrum was computed from the entire flightline, including clouds and cloud shadow, so that artifacts were introduced and noise obscured any useful information. Possible interference from second order effects will also need to be identified and corrected before the data can be used reliably (Terry Cook, this volume). Average (3 x 3 pixel) spectral curves were derived for several vegetation types and then compared to the average spectrum for the flight line.

AIS SPECTRA

Derived spectra from deciduous and coniferous forests, cropland, pasture, and water are shown in figures 2-6. The spectral variations reported by Wickland at 1.19 μm are not observed in the raw spectral data (figures 2 and 3).

Differences in the shape of the curves between the two water bands at 1.4 μm and 1.9 μm appear to provide a more promising region for discrimination of vegetation types. Deciduous forests are more reflective than coniferous forests and less reflective than cropland. Pasture is the least reflective of the vegetation types. The pasture curve is closest to the average curve, though, as mentioned earlier, the average was derived from clouds and shadow as well as plant cover. The slope of the curve in this region also varies, but more analysis of the data will be needed to discern patterns.

CONCLUSIONS

1. Airborne Imaging Spectrometer data provide a high-resolution look in the spectral region 0.9 μm to 2.1 μm, a part of the electromagnetic spectrum not previously well studied for plants.

2. Processing of the AIS data requires calibration and normalization, as well as compensation for the effects of second-order reflections.

3. Spectral variations at 1.19 μm which were previously reported were not observed, but variations between 1.4 μm and 1.9 μm may allow discrimination of major vegetation types.

REFERENCES

Knipling, E.B., 1970. Physical and physiological basis for the reflectance of visible and near-infrared radiation from vegetation: Remote Sensing of Environment, v. 1, p. 155-159.

Krohn, M.D., Milton, N.M., Segal, D.B., and England, A.W., 1981. Discrimination of a chestnut-oak forest unit for geologic mapping by means of a principal component enhancement of Landsat multi-spectral scanner data: Geophysical Research Letters, v. 8, p. 151-154.

Milton, N.M., Collins, W., Chang, S.H., and Schmidt, R.G., 1983. Remote detection of metal anomalies on Pilot Mountain, Randolph County, North Carolina: Economic Geology, v. 78, no. 4, p. 605-617.

Milton, N.M., and Krohn, M.D., 1982. Chestnut-oak (Quercus prinus L.) distribution in the Virginia Piedmont as an aid to geologic mapping (abs.): Virginia Journal of Science, v. 33, no. 3, p. 128.

Wickland, D.E., 1985. AIS spectra for stressed and unstressed plant communities in the Carolina slate belt: in Vane and Goetz, eds., Proceedings of the Airborne Imaging Spectrometer Data Analysis Workshop, JPL Publication 85-41, p. 46-50.
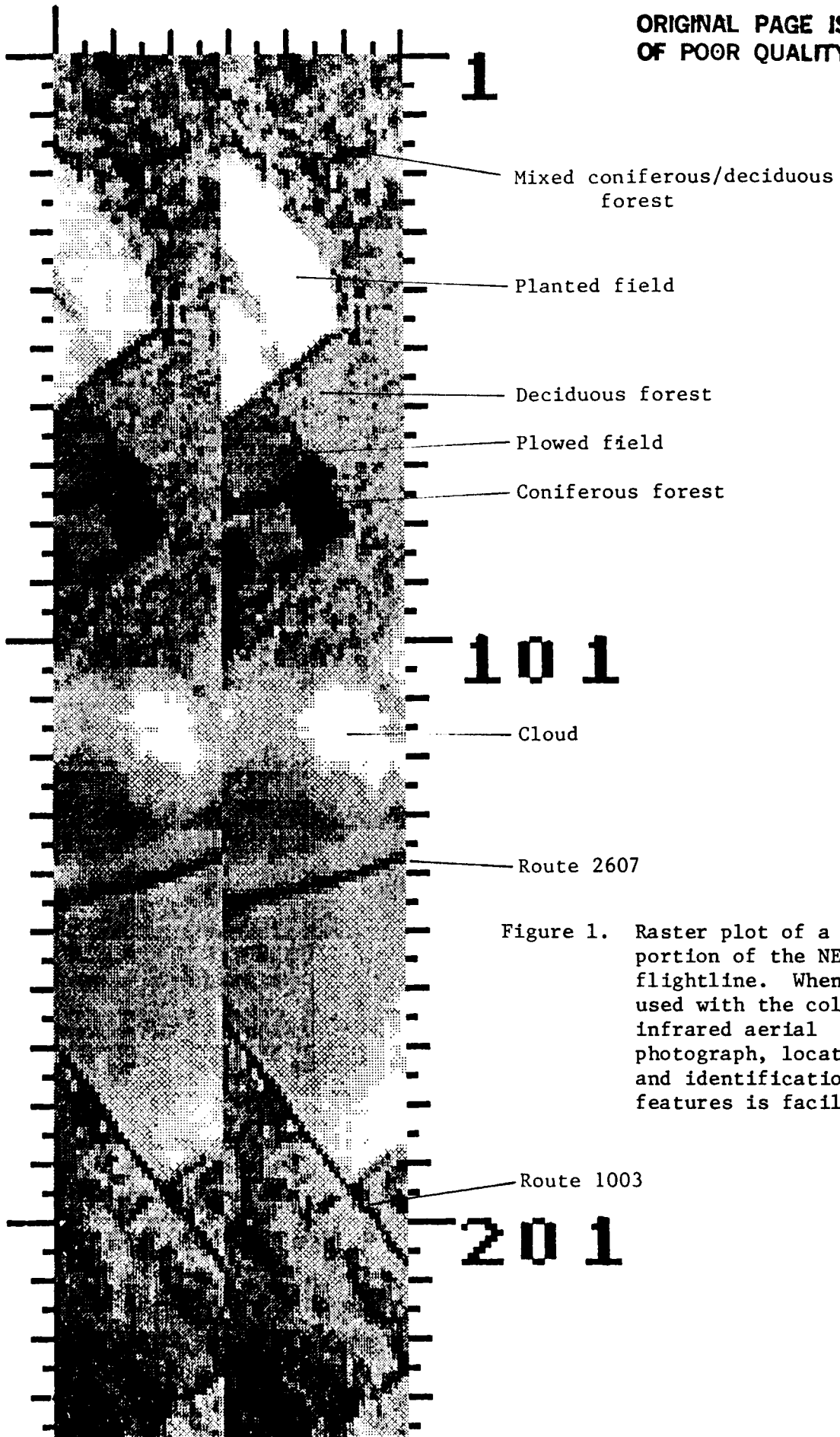
Figure 1. Raster plot of a portion of the NE-SW flightline. When used with the color-infrared aerial photograph, location and identification of features is facilitated.

165
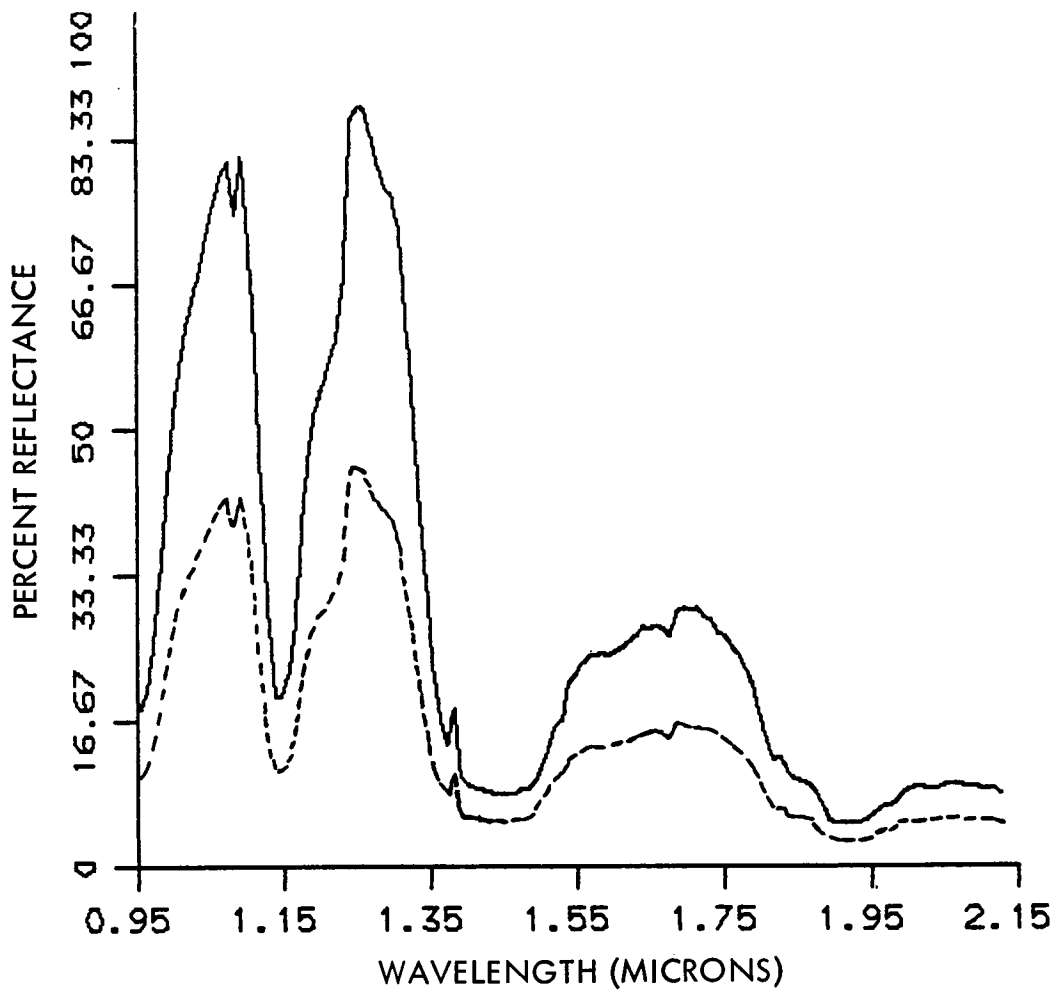
Figure 2. Average spectral curve (3 x 3 pixels) of deciduous forest (solid
line) and average of all spectra along the flightline (dashed line).
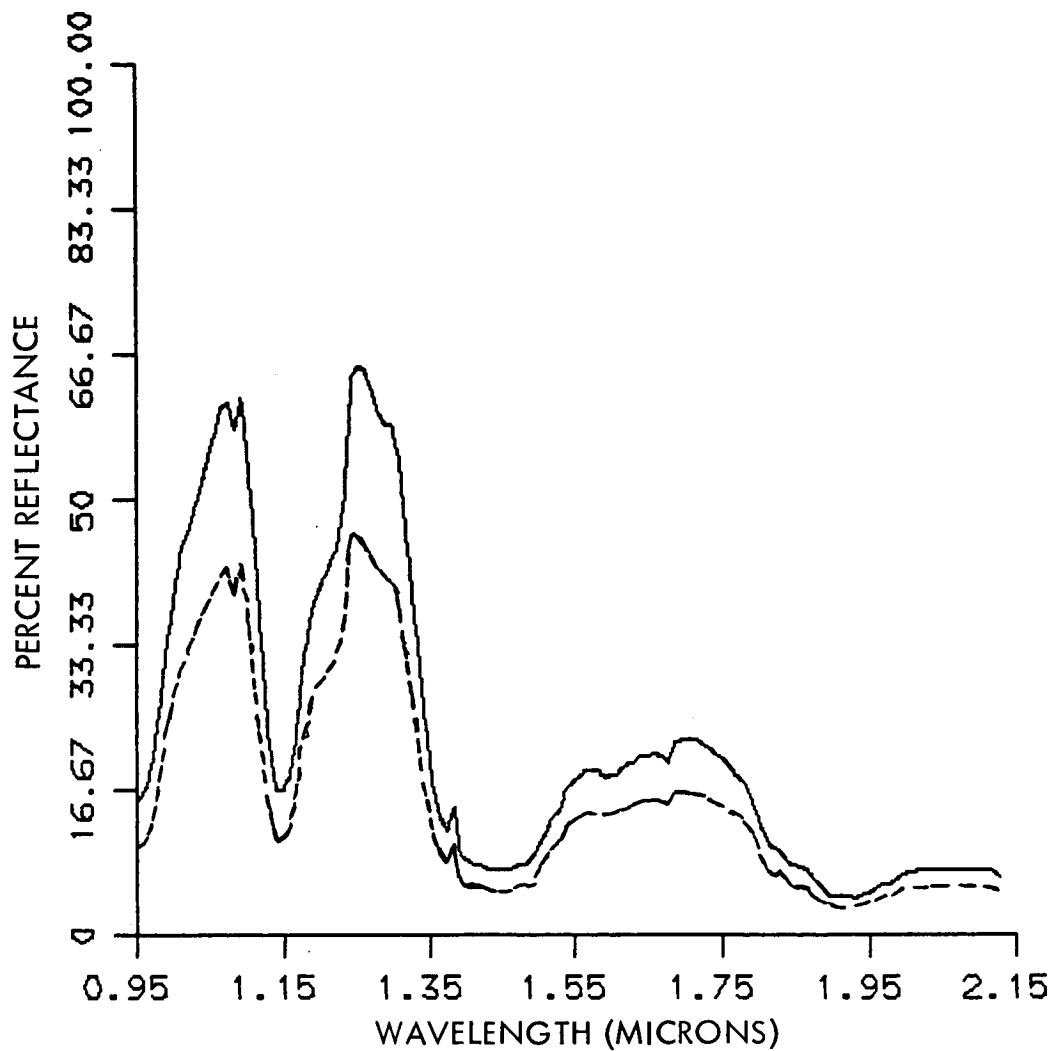
Figure 3. Average spectral curve (3 x 3 pixels) of coniferous forest (solid line) and average of all spectra along the flightline (dashed line).
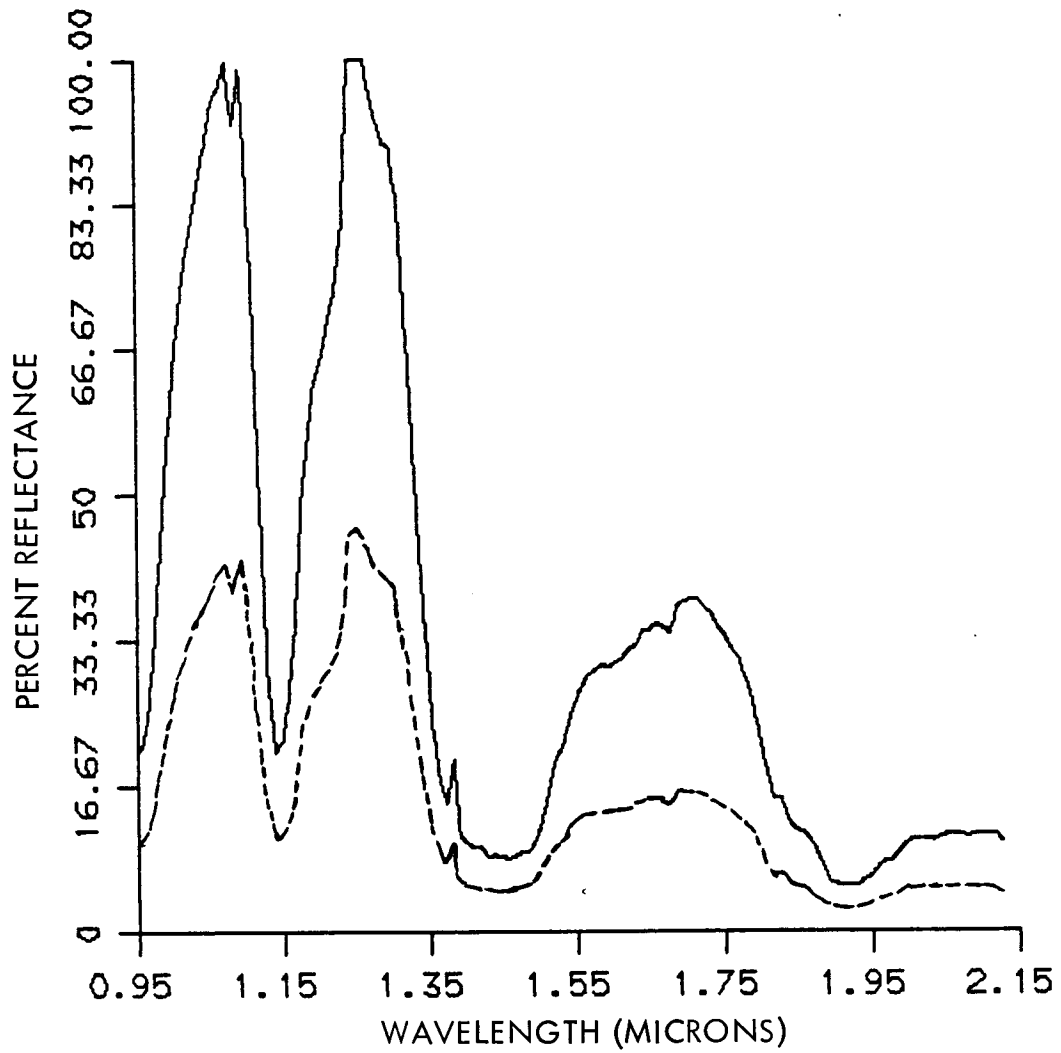
Figure 4. Average spectral curve (3 x 3 pixels) of cropland (solid line) and
average of all spectra along the flightline (dashed line).
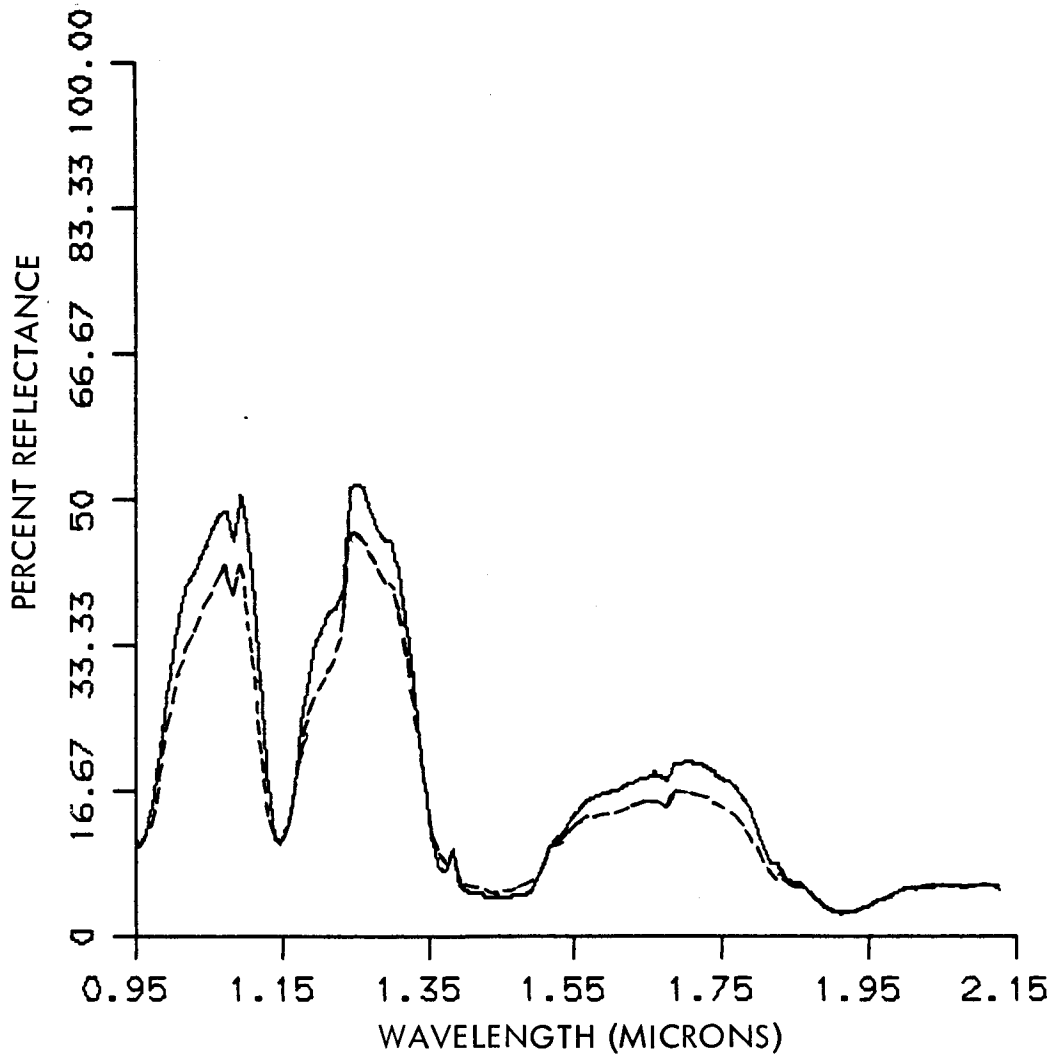
Figure 5. Average spectral curve (3 x 3 pixels) of pasture (solid line) and
average of all spectra along the flightline (dashed line).
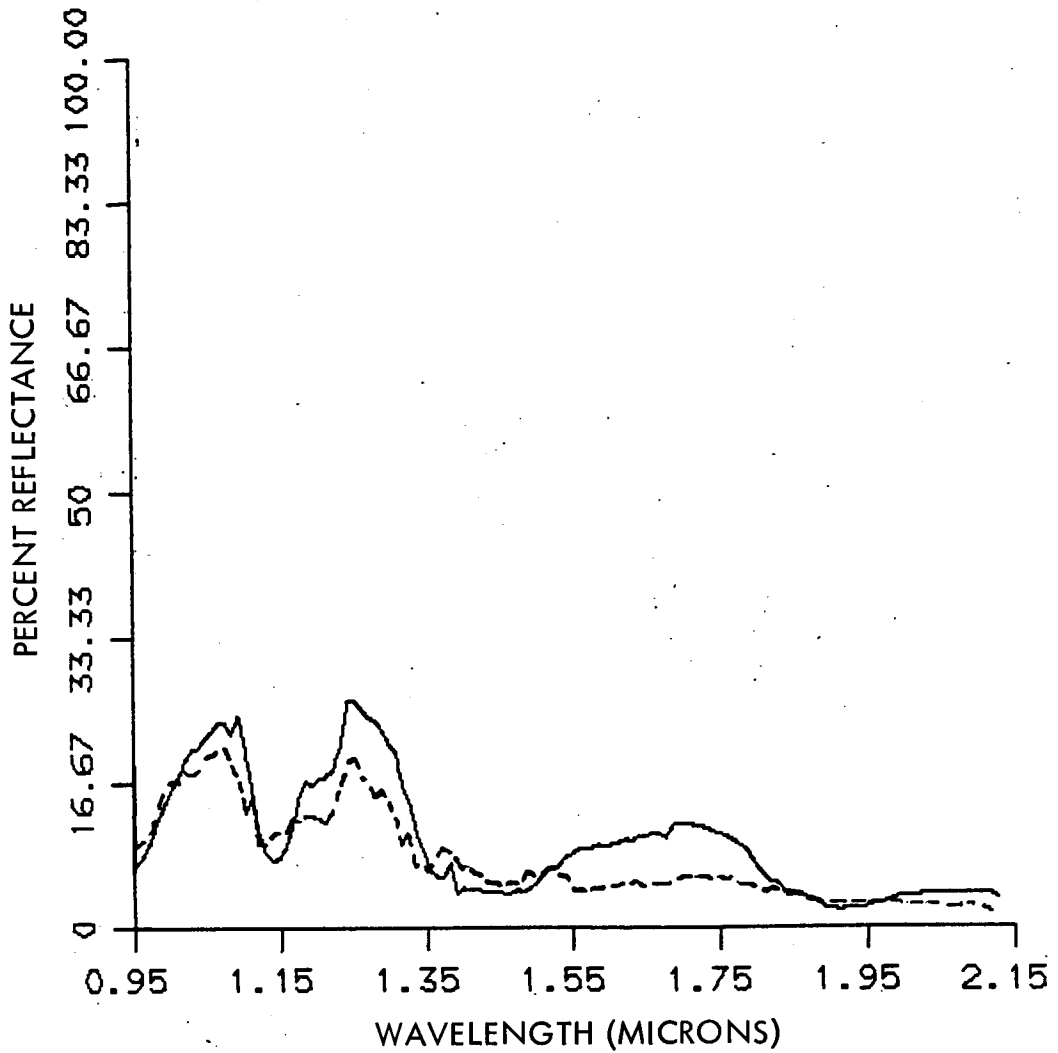
Figure 6. Average spectral curves (3 linear pixels) for water (pond [solid line] and creek [dashed line]).

TRACE ELEMENT-INDUCED STRESS IN FRESHWATER WETLAND VEGETATION: PRELIMINARY RESULTS

BYRON L. WOOD, TGS Technology, Inc., NASA/Ames Research Center, Moffett Field, CA, USA; LOUISA H. BECK, Remote Sensing Research Program, University of California, Berkeley, CA, USA.

ABSTRACT

Airborne Imaging Spectrometer (AIS) data were acquired over an area of freshwater wetlands in Central California on September 23, 1985. Plant samples were subsequently collected along the flight line with the goal of relating plant tissue chemistry to spectral reflectance in the near-infrared region. It was determined that a consistent relationship existed between spectral response and plant tissue chemistry. This was especially evident in the 1500 to 1700 nm region.

INTRODUCTION

For a number of years the authors have been conducting research on the use of remote sensing data to identify and map freshwater wetlands in California. The results of this research have shown that some types of remote sensing data can be used to characterize wetlands in terms of species composition, as well as plant morphology and phenology. These differences can, in turn, be related to environmental factors such as soil and water quality. The wetlands previously studied were found on similar basin soils and maintained by good quality irrigation water. As such, they are considered to be representative of healthy freshwater wetland ecosystems. Many wetlands in California are, however, maintained by agricultural drainage water which often contains a variety of potentially toxic pollutants.

Studies by the United States Bureau of Reclamation and Fish and Wildlife Service have shown that unusually high trace element levels are found in food chain organisms at Kesterson National Wildlife Refuge (Blum, 1984). For nearly a decade, Kesterson, a freshwater wetland in California's Central Valley, has served as a disposal site for agricultural drainage water. This water contains abnormally high concentrations of such trace elements as boron, molybdenum, selenium, and lead, which are known to cause plant stress. Therefore, the Kesterson wetlands provided the authors with an opportunity to extend their previous research to the characterization of stressed and non-stressed wetlands. Based on a review of management practices at wetlands surrounding Kesterson, the nearby Volta Wildlife Refuge was

C-3

selected for control purposes. A key consideration in the selection process was that, unlike Kesterson, the wetlands at Volta have been maintained using good quality irrigation water.

Although trace elements are essential to healthy plant growth, deficiencies or excesses of these same elements can result in plant stress (Kabata-Pendias and Pendias, 1984). A frequent non-specific stress response is chlorosis, or yellowing of leaves due to decreasing chlorophyll concentration in a plant's mesophyll cells. The relationship between chlorophyll concentration and leaf spectral reflectance has been demonstrated by several researchers, including Thomas and Gausman (1977), Myers (1975), and Horler et al. (1983a,b). Although many factors affect leaf chlorophyll content, including senescence (Tucker, 1977), nutrient stress (Kabata-Pendias and Pendias, 1984), soil salinity (Ward, 1969), and disease (Colwell, 1956; Suits and Safir, 1972; Wildman, 1979; Murtha, 1982), it is possible to track changes in leaf chlorophyll content by examining reflectance measures (Benedict and Swidler, 1961; Thomas and Gausman, 1977).

OBJECTIVES

The objectives of this research are to determine if field and laboratory spectral data can be used to characterize stressed and non-stressed wetland vegetation. Specific goals are to (a) determine which wetland plant species bioaccumulate high levels of trace elements; (b) determine if these high concentrations affect moisture and/or chlorophyll content, and therefore, spectral response; and (c) test the feasibility of using airborne- or satellite-based remote sensing data for the identification, monitoring, and mapping of these effects.

APPROACH

Achieving the stated objectives required a multi-layered procedure. Figure 1 illustrates the general flow of the approach, which involves the initial analysis of laboratory data, and the extension of these results to a regional-scale remote sensing system. Remote sensing data used in this research were acquired with the following systems: (a) 1000-channel Barringer field spectrometer; (b) 1000-channel Perkin-Elmer laboratory spectrophotometer; (c) 12-channel Daedalus Thematic Mapper Simulator (TMS); and (d) 128-channel Airborne Imaging Spectrometer (AIS).

```
Laboratory Biochemical/High Resolution        |    High Resolution/Broad Band
          Spectral Relationships              |      Spectral Relationships
------------------------------------------------|------------------------------------------
                                              |
Field                                         |    Thematic
HR* Spectra┐                                  |    Mapper
(green veg) │                                  |    Data
           │    ┌→ Statistical ──────────┐    | .    │
           │    │   Analyses             │    |      │
           │    │              Chemical/Spectral    ↓
Biochem'l ─┤    │                 Analyses  |──────────────────→ Map Products
Analyses ──┤    │   Statistical ───────────↑  | .    ↑
           │    └→ Analyses              |    |      ┊
           │                             |    |      ┊
Laboratory │                             |    |    Airborne
HR*        │                             |    |    Imaging
Spectra ───┘                             |    |    Spectro.
(dry veg)                                |    |    Data
                                         |    |
------------------------------------------------|------------------------------------------
                                         |
          IDENTIFICATION                 |         MONITORING AND MAPPING
                                         |

* High Resolution
```

Figure 1.   General flow of the research approach.

The data analysis procedure is as follows:

(1)   Identify the relationships between trace element content and high resolution visible and infrared spectrometer data

    a)   collect and prepare plant tissue samples from both a 'stressed' and a non-stressed area

    b)   obtain high resolution spectrometer data

        i)   from fresh plant samples (using the Barringer spectrometer)

        ii)   from dried plant samples (using the Perkin-Elmer spectrophotometer)

    c)   perform biochemical analysis on plant samples to measure trace element and chlorophyll content

    d)   correlate biochemical and spectrometer data using statistical analyses

173

(2) Extend correlations to a broad-band remote sensing system

    a) isolate wavelengths in high resolution data critical for diagnosing plant stress, and analyze the equivalent channels in Thematic Mapper Simulator (TMS) 12-channel data

    b) extend site-specific correlations to a regional scale

    c) perform an accuracy assessment.

In addition to the laboratory spectrometer data and the TMS data, we are also using digital data from the Airborne Imaging Spectrometer (AIS). Since this instrument records in the 900 to 2100 nm region (tree mode), it cannot be used for analyzing shifts in the chlorophyll absorption edge, the "red edge"*, located at approximately 700 nm. Research by Tucker (1980) has shown that changes in the geochemical environment can affect a plant's water availability. Therefore, a chemically-stressed plant may also exhibit water stress symptoms which would show up in the near-infrared region between 1600 and 2200 nm, where reflectance levels represent an accurate indication of leaf water content. Work by Wood and Wrigley (1985) in the near-infrared region using AIS spectra from agricultural crops, determined that the shape and amplitude of the reflectance curves in the 1550 to 1700 nm region were related to crop condition rather than crop type. Their findings suggest that the curve slope in the 1550 to 1700 nm region might be related to crop senescence or moisture stress. Perkin-Elmer laboratory spectra for stressed and non-stressed _Typha_ spp. and _Scirpus_ spp. samples indicated that, within the range of the AIS data, spectral differences were primarily ones of curve amplitude rather than shape. It was, however, noted that the stressed samples generally had less well-defined absorption features than the non-stressed samples. The shape of the curves in the near-infrared region suggests that AIS spectra can be utilized for characterizing stressed and non-stressed plants.

DATA ACQUISITION

Remote sensing data were collected over the study area throughout the summer of 1985. These included six Daedalus TMS acquisitions between June and October, three dates of

---

* Geobotanists and mineral exploration groups often use shifts in the red edge as an indicator of metal- or mineral-induced plant stress. For a discussion of this topic, see Goetz et al. , 1983.

color-infrared high altitude photography, and a single date of AIS data. The AIS data were acquired from the NASA C-130 aircraft on September 23, 1985. Additional data acquired during this flight included 8-channel NS-001 digital data, 35mm black-and-white photography, and VHS video imagery.

Immediately following the AIS flight, the video imagery was viewed in order to locate the flight line on the ground; this was done for purposes of directing field data collection. Plant sample collection at Kesterson and Volta was undertaken on September 27-28. A total of 98 samples, representing ten species, were collected for chemical and laboratory spectral analyses. For purposes of comparison, the same plant species were sampled at both Kesterson and Volta. The sample sites at Kesterson were selected from a set previously used by the U.S. Bureau of Reclamation for analyzing soil and water chemistry; samples at Volta were randomly selected.

DATA ANALYSES

Prior to oven drying, all fresh plant samples were scanned with the Barringer spectrometer, which records in the 450 to 2450 nm range at 2 nm resolution. Both hardcopy and digital output products were generated for each sample.

Individual samples were weighed before and after oven drying to determine percent plant water content. All dried samples were taken to the Laboratory of Biomedical and Environmental Biology at the University of California, Los Angeles, for chemical analysis. Samples were separated into leaf, stem, and flower parts, which were then individually ground to a uniform size using a Wiley mill with a 40-mesh screen. A total of 138 samples was prepared for analysis. All samples were analyzed for twenty-eight elements using optical emission spectrometry and X-ray fluorescence techniques.

Generation of the AIS spectral reflectance curves was performed on a VAX 11/780 using IDIMS image processing software and additional programs developed specifically for the analysis of AIS data. No pre-processing (i.e., atmospheric correction) was attempted prior to the generation of spectral curves. The dominant plant species found within the AIS flight line was _Typha_ spp. Approximately seventy-five two-by-two pixel blocks of pure _Typha_ spp. stands growing in standing water were selected for curve generation so as to represent a range of water quality and plant tissue chemistry conditions throughout the study area.

DISCUSSION

As stated previously, our objectives are to (a) determine which wetland plant species bio-accumulate high levels of trace elements; (b) determine how these concentrations affect spectral response; and (c) examine the feasibility of using airborne- or satellite-based remote sensing data for identifying, monitoring, and mapping these effects. To date, our research efforts have focused on the first two objectives.

The plant chemistry analyses have shown that plants from Kesterson had significantly higher concentrations of most of the trace elements (notably boron and selenium) than the same species collected at Volta. This difference was found for all species.

The results of the plant chemistry analyses also showed that levels of trace elements differed by species. Typha spp. had the highest concentration of selenium among the species sampled. The highest boron levels were found in Typha spp., Scirpus spp., and Atriplex spp. Molybdenum levels were highest for Typha spp. and Distichlis spp. It should be noted that Typha spp. and Scirpus spp. are the dominant species in the permanently-flooded portions of Kesterson and Volta. Atriplex spp. and Distichlis spp. are found only in the seasonally-flooded areas of these wetlands. In addition, plant chemistry data varied by plant part, with leaf tissue generally having the highest concentrations.

Analysis of the spectral data taken from fresh plant samples (Barringer spectrometer data) may be inconclusive because of problems relating to instrument calibration. These data, however, suggest that as plant moisture content decreases, reflectance in the 600 to 700 nm region increases. Laboratory reflectance data (Perkin-Elmer spectrophotometer) from Typha spp. samples with different leaf moisture and trace element levels appear to be similar to the Barringer data in this same 600 to 700 nm region. Further analysis of the Barringer and Perkin-Elmer reflectance data in relation to plant chemistry is currently underway.

The seventy-five AIS reflectance curves were generated in order to represent a range of plant chemistry and/or water quality conditions found throughout the Kesterson and Volta wetlands. Based on a preliminary comparison between these curves and plant chemistry data, it appears that there is a significant spectral difference between areas with high and low concentrations of trace elements. These differences are primarily in terms of curve amplitude rather than shape. Figure 2 illustrates this difference. The lower curves are representative of Volta where Typha spp. had low levels of
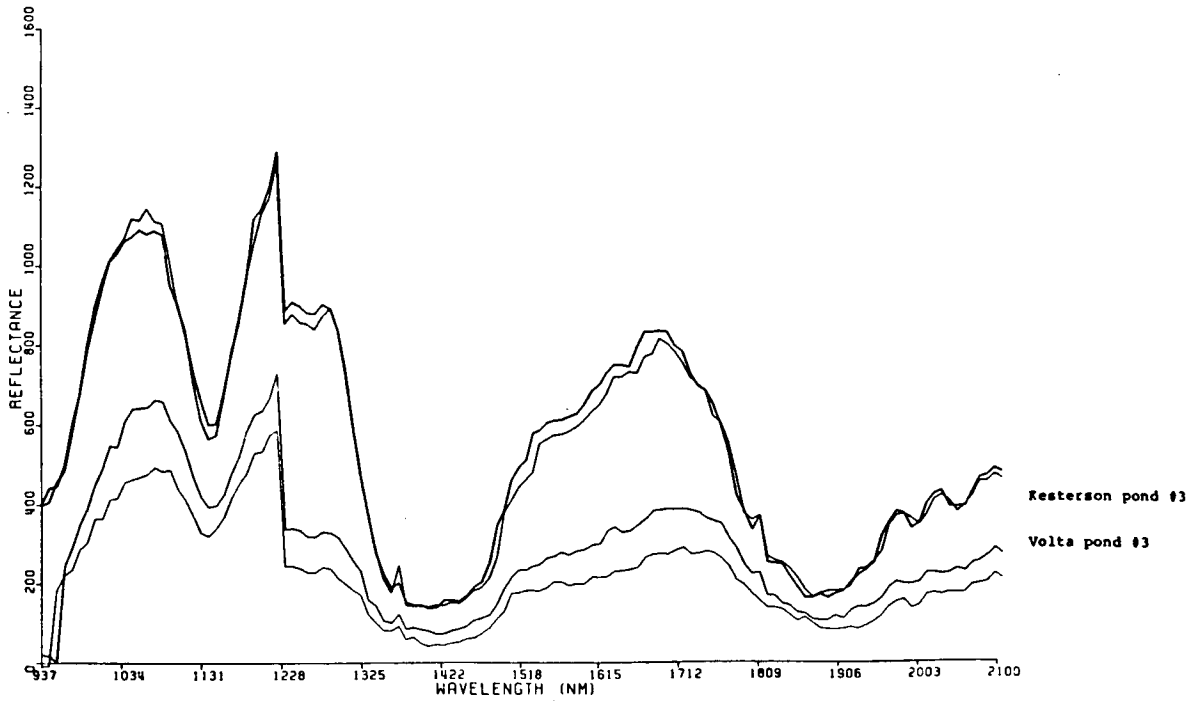
Figure 2. AIS spectral reflectance curves for _Typha_ spp. from Kesterson and Volta. The lower two curves represent samples containing low concentrations of selected trace elements; the upper two contain high concentrations.
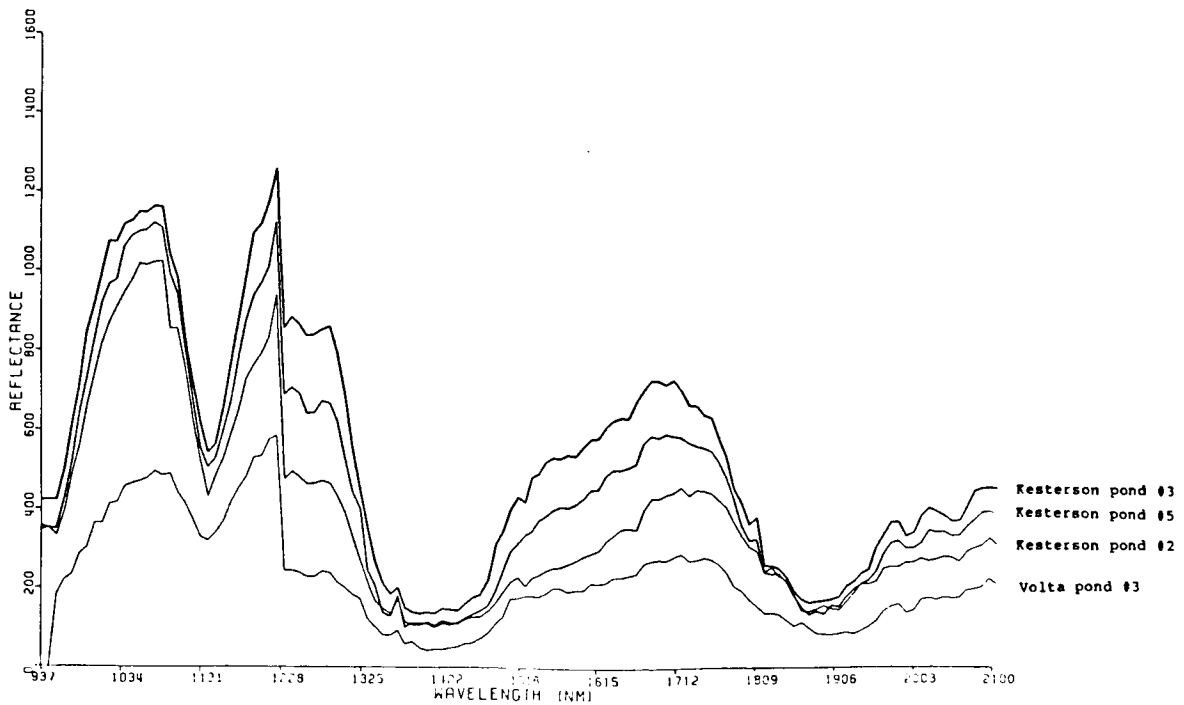
Figure 3. AIS spectral reflectance curves for _Typha_ spp. from Kesterson and Volta. This series of curves represent increasing levels of trace element concentration in plant tissue from Volta (low) to Kesterson (high).

177

boron, selenium, and lead; the upper curves represent the same species from Kesterson, where these elements were present in abnormally high concentrations. In addition, it was found that the slope of the reflectance curve in the 1500 to 1700 nm region was significantly steeper for the spectra from Kesterson. This phenomenon is also illustrated in Figure 3 which shows a series of curves representing a range of plant chemistry conditions. These show the amplitude shift from low to high trace element concentrations, as well as the increasing change in slope angle in the same spectral region. Although the biological cause of the reflectance shifts shown in Figures 2 and 3 is not entirely understood, it appears to be consistent for all AIS plots generated; the shifts may be related to changes in plant tissue chemistry. At the present time we are completing an analysis of plant tissue chlorophyll content in hopes of further understanding the phenomenon illustrated by the AIS curves.

CONCLUSIONS

Results of this research suggest that there exists a consistent relationship between plant tissue chemistry and spectral reflectance in the near-infrared. Preliminary analysis of the data shows that an increase in trace element concentration often corresponds to an increase in spectral reflectance in the 1500 to 1700 nm region. Ongoing research into the spectral-chemical-biological relationships suggested by these results is being conducted by the authors.

REFERENCES

Benedict, H.M. and R. Swidler. 1961. Nondestructive method for estimating chlorophyll content of leaves. Science , vol. 133:2015-2016.

Blum, J.R. 1984. Testimony of J.R. Blum (U.S. Fish and Wildlife Service) before the State Water Resources Control Board. Sacramento, California.

Colwell, R.N. 1956. Determining the prevalence of certain cereal crop diseases by means of aerial photography. Hilgardia , vol. 26(5):223-86.

Goetz, A.F.H., B.N. Rock, and L.C. Rowan. 1983. Remote sensing for exploration: an overview. Econ. Geol. , vol. 78(4):573-590.

Horler, D.N.H., J. Barber, J.P. Darch, D.C. Ferns, and A.R. Barringer. 1983a. Approaches to detection of geochemical stress in vegetation. Adv. Space Res. , vol. 3(2):175-179.

Horler, D.N.H., M. Dockray, and J. Barber. 1983b. The red
    edge of plant leaf reflectance. Intl J. Rem. Sens.
    , vol. 4(2):273-288.

Horler, D.N.H., M. Dockray, J. Barber, and A.R. Barringer.
    1983c. Red edge measurements for remotely sensing
    plant chlorophyll content. Adv. Space Res. , vol.
    3(2):273-277.

Kabata-Pendias, A. and H. Pendias. 1984. Trace elements in
    soils and plants. CRC Press, Boca Raton, Fla.

Murtha, P.A. 1982. Detection and analysis of vegetation.
    In : Remote Sensing for Resource Management, Chapter
    13. C.J. Johannsen and J.L. Sanders, ed. Soil
    Conservation Society of America, Ankeny, Iowa.

Myers, V.I. 1975. Crops and soils. In : Manual of Remote
    Sensing. L.W. Bowden, ed. American Soc. Photogram.,
    Falls Church, VA, pp.1715-1813.

Suits, G.H. and G.R. Safir. 1972. Verification of a
    reflectance model for mature corn with applications to
    corn blight detection. Rem. Sens. Environ. , vol.
    2:183-192.

Thomas, J.R. and H.W. Gausman. 1977. Leaf reflectance
    versus leaf chlorophyll and carotenoid concentrations
    for eight crops. Agron. J. , vol. 69:799-802.

Tucker, C.J. 1980. Remote sensing of leaf water content in
    the near-infrared. Rem. Sens. Environ. , vol.
    10:23-32.

Tucker, C.J. 1977. Spectral estimation of grass canopy
    variables. Rem. Sens. Environ. , vol. 6(1):11-26.

Ward, J.M. 1969. The significance of changes in infrared
    reflectance in sugar maple (Acer saccarum Marsh),
    induced by soil conditions of drought and salinity.
    In : Proc. of the 6th Intl Symp. on Rem. Sens. of
    Environ., ERIM, Ann Arbor, Michigan, pp.1205-1226.

Wildman, W.E. 1979. Color infrared: a valuable tool in
    vineyard management. In : Proc. of the 7th Biennial
    Workshop on Color Aerial Photography in the Plant
    Sciences and Related Fields. Amer. Soc. of
    Photogram., Falls Church, VA.

Wood, B.L. and R.C. Wrigley. 1985. AIS investigation of
    agricultural monocultures. In : Proc. of the
    Airborne Imaging Spectrometer Data Analysis Workshop,
    April 8-10, 1985. Jet Propulsion Laboratory,
    California Institute of Technology, Pasadena,
    California.

PATTERNS OF VEGETATION IN THE OWENS VALLEY, CALIFORNIA

SUSAN L. USTIN, Remote Sensing Research Program, Space Sciences
Laboratory, University of California, Berkeley, CA 94720, USA, and
Department of Botany, University of California, Davis, CA 95616 USA;
BARRETT N. ROCK, Jet Propulsion Laboratory, Pasadena, CA 91109, USA; and
ROY A. WOODWARD, Remote Sensing Research Program, Space Sciences
Laboratory, University of California, Berkeley, CA 94720, USA, and
Department of Botany, University of California, Davis, CA 95616 USA

ABSTRACT

Spectral characteristics of semi-arid shrub
communities were examined using AIS data collected in
the "tree" mode on 23 May 1985. Mesic sites with
relatively high vegetation density and distinct zonation
patterns exhibited greater spectral signature variations
than sites with more xeric shrub communities. Spectral
signature patterns were not directly related to
vegetation density or physiognomy, although spatial
patterns were consistent with ecological changes, and
maps derived from an 8-channel maximum likelihood
classification were supported by photo-interpreted
surface features. In AIS data, the principal detected
effect of shrub vegetation on the alluvial fans is to
lower reflectance across the spectrum. These results
are similar to those reported during a period of minimal
physiological activity in autumn, indicating that
shadows cast by vegetation canopies are an important
element of soil-vegetation interaction under conditions
of relatively low canopy cover.

INTRODUCTION

The primary objective of our study has been to evaluate the
contribution of vegetation to pixel spectra under semi-arid conditions,
where total canopy leaf area and surface cover are low. Owens Valley was
chosen as a test site because of its diverse semi-arid shrub communities
and substrate types (Ustin and Rock, 1985; Ustin et al., 1986).
Last year, preliminary results of late autumn AIS data showed that
vegetation had little apparent effect on the spectral signatures of pixels
from several different rock/soil types having shrub canopy covers varying
between 10 and 65% of the ground surface (Ustin and Rock, 1985).
Regardless of substrate type (sand, granitic alluvium, or basalt) or
vegetation type (Great Basin sagebrush or saltbush communities), the only
detectable response to the presence of vegetation was a change in surface
albedo consistent with increasing shadows cast by the plant canopies as
density increased (Ustin et al., 1985; Ustin and Rock, 1985). Because
these data were obtained when most of the species in the shrub communities
were dormant, or nearly dormant, we suggested that more spectral
differences attributable to vegetation would be apparent during periods

of greater physiological activity. Here we report spectral responses
that exemplify the range of patterns observed on a spring date coinciding
with peak growth and physiological activity at these localities.

AIS DATA ACQUISITION AND CALIBRATION PROCEDURES

Although several flights have been conducted over our sites
(Science Investigators Guide to AIS Data, Suppliment, 1986), only two
dates appear to have reasonably high quality data. No AIS data were
obtained on 2 April 1985 because of equipment malfunction; data on 10 July
1984 are of questionable value because of atmospheric haze and smoke, and
on 22 May 1985, because of clouds and atmospheric moisture. However, data
acquired on 30 October 1984 are cloud-free and 23 May 1985 data are cloud-
free on most flight lines.
Data reported here are from flightlines 507 and 509 on 23 May
1985. The flight occurred between 11.30 and 12.00 hours PST and flight
altitude was about 5.0 km above the terrain. The data were analysed at
the Space Sciences Laboratory, University of California, Berkeley using
the SPAM (Spectral Analysis Manager) developed by the Jet Propulsion
Laboratory. The data were rectified for radiometric differences and
corrected for solar-irradiance by the JPL prior to our analyses. Spectra
of pixels selected from Diaz lake show peak reflectance dn values of 55 to
80 at 1.10 and 1.30 um, indicating a significant non-zero offset. A
vertical stripe is pronounced between the 22nd and 32nd pixels.
Eight channels of the AIS data were selected for further analysis
using an unsupervised clustering algorithm (derived from ISOCLAS)
followed by a maximum likelihood classification of the scene using the
ELAS program. These channels (7, 19, 32, 40, 64, 72, 88, 117) were
selected from near infrared and shortwave infrared bands which exhibited
significant spectral brightness variation when examined with SPAM.
Vertical striping was pronounced and was removed prior to clustering
analysis by calculating the means of each pixel column and the mean of the
512 by 32 pixel line segment. The difference between each column mean and
the scene mean was determined and this difference was added or subtracted
to each pixel in the column.

RESULTS AND DISCUSSION

On most of the flight lines examined, there were few apparent
differences in spectral signatures from shrub communities differing in
species composition or plant density. These results are similar to those
reported for these communities during autumn when physiological activity
was minimal (Ustin and Rock, 1985). In contrast, sites with available
soil water, where plant cover and green biomass tend to be relatively
high, have more diverse spectral responses (Figure 1). Vegetated
surfaces have distinct spectral signature patterns with different slopes
in the 1.4 to 1.8 um spectral region and brightness differences between
the near infrared and shortwave infrared spectral regions. These
spectral responses resemble those reported from agricultural and marsh
habitats (Gross and Klemas, 1985; Wood and Wrigley, 1985; Vanderbilt,
1985). However, it is not clear how surface interactions are affecting
the spectral responses, since slope differences and brightness changes
are not clearly related to vegetation density or to specific plant
physiogonomic types, such as grasses or shrubs. Soils are fine-grained

alkaline quartz sands and do not account for the spectral variation; such patterns are not evident in field-collected soil spectral data. Although second order energy overlap is affecting reflectance at wavelengths longer than 1.6 um, the spectral patterns we observed are evident also at shorter wavelengths, and thus are not explained by this source of contamination.
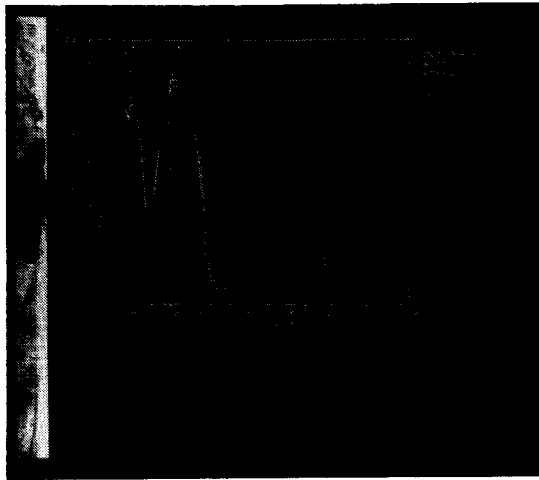
Figure 1. Reflected radiance curves for vegetation types near Diaz Lake. Upper curve is from an irrigated grassland on a golf course, the next lower curve a saltbush community, a dry meadow community, and a wet meadow community, respectively.
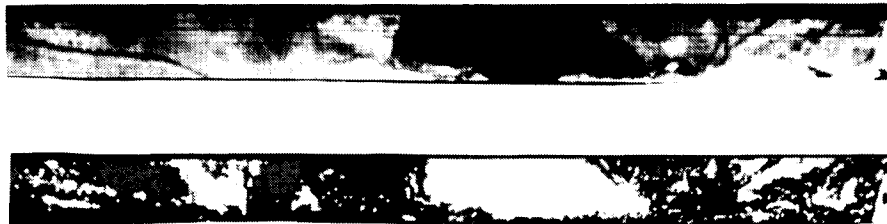
Figure 2. Above, a 3-color composite of the scene in Figure 1, after removal of most vertical striping. Below, the 8-band maximum likelihood classification map. (See color slide number 9 in the back cover pocket of this publication.)

182

Despite the uncertainties in interpreting the physical basis for the spectral patterns they appear to be clearly related to ecological differences between plant communities. Figure 2 shows the spatial distribution in spectral classes near Diaz Lake in the southern Owens Valley. The upper image (refer to appendix for color slide) is a three color composite (channels 19, 32, 64) and the 8-band classification map (below). These classes represent an irrigated and clipped grass golf course (red) in the triangular unit on the left margin, an unirrigated saltgrass (Distichlis) meadow (turquoise), a denser meadow with cottonwoods (Populus) (red, cream), lake (pink), a sand pit (green), a saltbush scrub (Atriplex) community (blue) and other disturbed areas having low (less than 5% canopy cover) saltbush vegetation (yellow). The speckled area near the right of the line is a trailer court. The wavy line nearby is U.S. Route 395. Spectral patterns clearly differentiate ecologically distinct spatial units on the ground, with most spectral differences apparently due to changes in the vegetation type or to variation in canopy density related to soil moisture patterns rather than soil morphology.

Figure 3 shows representative spectra from 3 x 5 pixels from a line segment crossing the Sierra Nevada bajada west of the town of Independence. The left third of this line segment crosses an older alluvial fan surface, which is overlain by a younger fan surface covering the remainder of the flight line. A sagebrush-blackbrush (Artemisia-Coleogyne) community of comparable canopy cover is found on both soil types. In addition to the soil changes, the line crosses two old wildfire sites where the vegetation canopy has not yet recovered to the level ovserved on the adjacent unburned surfaces. Pixels were selected from each of these surface types. It can be seen that all vegetation and soil surfaces have a similar spectral signature pattern. Only the burned surface having the least canopy cover (near the right margin of the line), having the least canopy cover, has a sufficiently higher albedo to distinguish it consistently from the other surfaces. Plant cover at this site is only half that on the surrounding surfaces (17% versus 33%). These signature patterns are like those previously obtained during autumn (Ustin and Rock, 1985), again suggesting that the principal effect of semi-arid shrub vegetation on the AIS pixel spectra is to lower brightness nearly equally in all bands, probably as a consequence of the relatively sparse, spreading canopies shading the ground.

Last summer (1985), a new wildfire removed nearly 100% of the surface vegetation in a 5000 ha area, leaving intact only a few isolated stands of the unburned shrub community and the formerly youngest burn site. New AIS data were obtained for this area 16 May 1986. To gain greater insight into the influence of vegetation on these pixel data, we plan to examine in detail the spectral response characteristics on the three dates, comparing the physiologically dormant and active periods with the substrate surface lacking vegetation. Because of the wider path width of AIS-2, at least a portion of each of the flight lines can be coregistered.
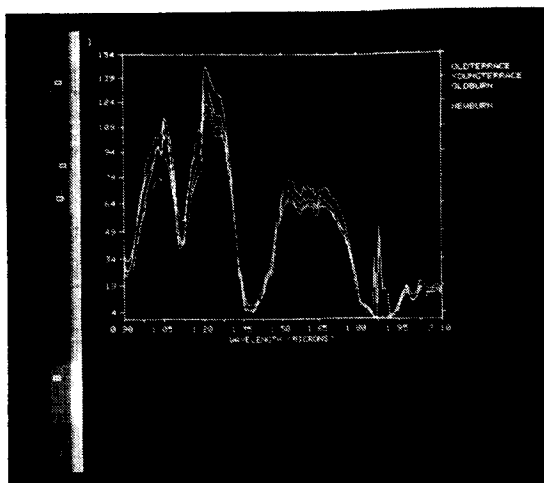
Figure 3. Selected spectra of alluvial fan sites differing in soil or vegetation characteristics. Upper curve is from the younger burn site on the younger soil surface, next lower curve from the older burned site also on the younger soil surface, lowest two curves from the unburned sagebrush community on the younger and older soil surfaces, respectively.
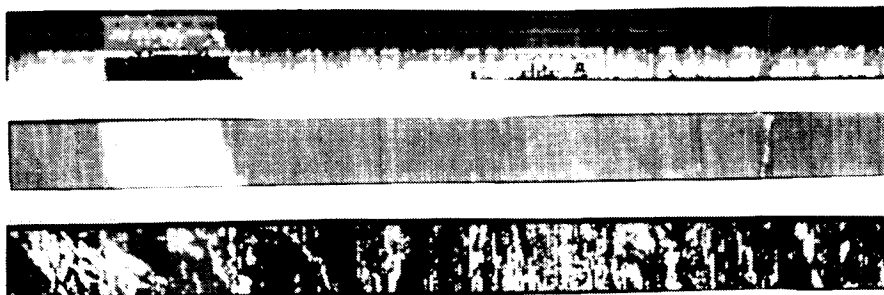
Figure 4. Alluvial fan region depicting an unsupervised 8-band maximum likelihood classification map before destriping (top), a 3-band color composite (middle) after removal of vertical striping, and the maximum likelihood classification of the region before destriping (middle) and after destriping (bottom). (See color slide number 10 in the back cover pocket of this publication.)

The Thematic Mapper had been previously used to classify ecological units at this site (Ustin et al., 1986). In the TM classification, the differently aged alluvial surfaces were found to be spectrally distinct in the infrared region. Figure 4 shows the results of a maximum likelihood classification of the bajada AIS sequence. Clearly, prior to removing the vertical banding, most of the mapping relates to noise. However, destriping produces a significant improvement and bajada features are seen in considerable detail. Although neither of the two soil surfaces are clearly delineated in the AIS classification map, the numerous stream channels and riparian communities stand out as west-east trending features; colors appear to relate to the size and amount of riparian vegetation present (red=shallow washes; blue=deeper washes with riparian vegetation). The open fan surface is generally green (33% shrub cover), although the two burns are distinguished by belonging to the turquoise (28% cover) and yellow (17% cover) classes. Dirt roads are visible as the cream-colored class. Despite the similarity of spectral features, the small albedo differences, and the presence of instrument noise even after destriping, the AIS data appear to be valuable in mapping surface features at considerable spatial detail.

Despite the usefulness of data enhancement techniques, such as log-residual transformations, and spectral signature comparisons of specific absorption features for geologic applications, these techniques appear to have limited success for vegetation analyses. Further vegetation studies should concentrate on understanding the physical basis for signature differences in AIS data and on developing new analytical techniques better suited to the relative spectral changes observed among differing vegetation types. Developing techniques for modeling spectral mixtures, such as described by Smith and Adams (1985), may be useful.

REFERENCES CITED

Gross M.F., and V. Klemas. 1985. Discrimination of coastal vegetation and biomass using AIS data. in Proceedings of the Airborne Imaging Spectrometer Data Analysis Workshop, April 8-10, 1985. Gregg Vane and Alexander F.H. Goetz, eds. JPL Publ. No. 85-41, p. 129-133.

Smith, M.O. and J.B. Adams. 1985. Interpretation of AIS images of Cuperite, Nevada using constraints of spectral mixtures. in Proceedings of the Airborne Imaging Spectrometer Data Analysis Workshop, April 8-10, 1985. Gregg Vane and Alexander F.H. Goetz, eds. JPL Publ. No. 85-41, p. 62-67.

Ustin, S.L., and B.N. Rock. 1985. Preliminary analysis of AIS spectral data acquired from semi-arid shrub communities in the Owens Valley, California. in Proceedings of the Airborne Imaging

Spectrometer Data Analysis Workshop, April 8-10, 1985. Gregg Vane and Alexander F.H. Goetz, eds. JPL Publ. No. 85-41, p. 41-45.

Ustin, S.L., B.N. Rock, and R.A. Woodward. 1985. Analysis of substrate and plant spectral features of semi-arid shrub communities in the Owens Valley, California. Proceedings of the International Symposium on Remote Sensing of Environment. Fourth Thematic Conference: Remote Sensing for Exploration Geology, San Francisco, CA, April 1-4, 1985, p.347-360.

Ustin, S.L., J. B. Adams, C.D. Elvidge, M. Rejmanek, B.N. Rock, M. O. Smith, R.W. Thomas, and R.A. Woodward. 1986. Thematic mapper studies of semiarid communities. BioScience. (in press)

Vanderbilt, V.C. 1985. Urban, forest, and agricultural AIS data: Fine spectral structure. in Proceedings of the Airborne Imaging Spectrometer Data Analysis Workshop, April 8-10, 1985. Gregg Vane and Alexander F.H. Goetz, eds. JPL Publ. No. 85-41, p. 158-165.

Wood, B.L., and R.C. Wrigley. 1985. AIS investigation of agricultural monocultures. in Proceedings of the Airborne Imaging Spectrometer Data Analysis Workshop, April 8-10, 1985. Gregg Vane and Alexander F.H. Goetz, eds. JPL Publ. No. 85-41, p. 134-140.

AIS SPECTRA OF DESERT SHRUB CANOPIES

RJAY MURRAY, Milne Computer Center, DENNIS L. ISAACSON, BARRY J. SCHRUMPF, WILLIAM J. RIPPLE, ANTHONY J. LEWIS, Environmental Remote Sensing Laboratory, Oregon State University, Corvallis, OR, USA

ABSTRACT

Airborne Imaging Spectrometer (AIS) data were collected 30 August 1985 from a desert shrub community in central Oregon. Spectra from artificial targets placed on the test site and from bare soil, big sagebrush (Artemesia tridentata wyomingensis), silver sagebrush (Artemesia cana bolanderi) and exposed volcanic rocks were studied.

Spectral data from grating position 3 (tree mode) were selected from 25 ground positions for analysis by Principal Factor Analysis (PFA). In this grating postion, as many as six factors were identified as significant in contributing to spectral structure. Channels 74 through 84 (tree mode) best characterized between-class differences. Other channels were identified as non-discriminating and as associated with such errors as excessive atmospheric absorption and grating position changes.

The test site studied was relatively simple with the two species (A. tridentata and A. cana) representing nearly 95 percent of biomass and with only two mineral backgrounds, a montmorillonitic soil and volcanic rocks. If, as in this study, six factors of spectral structure can be extracted from a single grating postion from data acquired over a simple vegetation community, then AIS data must be considered rich in information-gathering potential.

INTRODUCTION

Eight transects of AIS data were collected 30 August 1985 from flights crossing Papoose Lake, a dry lakebed in central Oregon. A typical data line traversed an A. tridentata-dominated desert shrub community on the approach to the lake, a sparse A. cana-dominated shrub canopy on the lakebed of bright soil (a montmorillonitic, frigid, aquic palexeralf) and A. tridentata again on the overrun. Exposed outcoppings of basalt ring the lakebed in the A. tridentata-dominated community (Fig. 1).

Ancillary data were collected coincidentally with AIS coverage. NS001 spectra, black and white 35mm photographs (Fig. 1), and 9x9 inch CIR photographs were collected aboard the NASA C-130, and large scale natural 70mm natural color photographs were collected on 8 September 1985. A. cana biomass data were collected 27-28 August 1985 and canopy-held water estimates were derived.

For preliminary investigations, AIS data from selected areas were processed. Artificial targets on the test site were used in local registration of features, and representative data sets were chosen. Spectral traces, selected graymaps and files of raw radiance values were generated for first-order inspection of the data.

Principal factor analysis has been used to characterize spectral data (Murray 1983) and was the basis for the extraction and comparison of information from AIS data. PFA is useful for isolating causal
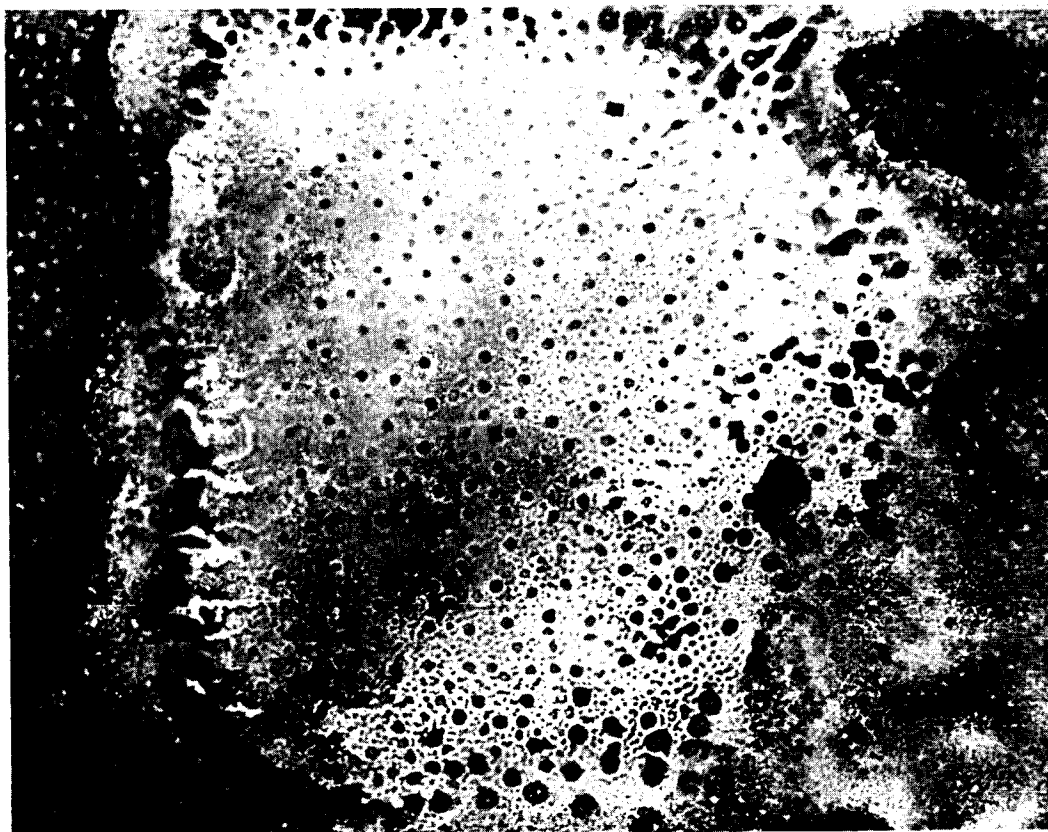
Figure 1. Enlarged 35mm photograph of Papoose Lake acquired during NASA C-130 overpass. Scale is about 1" = 500', and each square target is the area-equivalent of two pixels.

("real") factors, marking unique sites, and indicating important spectral variables; morever, most results can be presented graphically.

SITE AND SPECTRAL DATA DESCRIPTIONS
AIS data from 25 ground sites were selected: six big sage and four outcrop sites had low radiance values, seven silver sage sites had intermediate radiance values, and seven bare soil sites were highly reflective. These four classes span the reflectivity range for surface features in the Papoose Lake area. The spectra of 4 to 22 pixels were averaged and the mean site radiance was used in subsequent analyses. Big sage sites are more elevated and have dense canopies. Silver sage sites are lower and are surrounded by bare soil. The soil areas have standing water during spring run-off and dry to a highly reflective surface. The 6-to-8 feet high rock outcrops have scree and scattered vegetation at the foot. Letter designations for figures and color designations for the accompanying slides are: O = Outcrop(black), B = Big sage(blue), C = Silver sage(red), and SL = Bare soil(green).

188

Outcrop spectra were selected from one flight line and from a small area. The other sites were selected from any of three flight lines, and because the overpasses were made under high cloud cover, incoming solar radiation and ground shadows are sources of variation in the recorded radiance. Moreover, no corrections were made for the usual errors in AIS data, e.g., vertical and horizontial striping. For visual comparison (Fig. 2) the spectra were equal-area normalized (AIS 1985); however, for PFA the original, unaltered data were used (Fig. 3). Only 32 channels in the 1.5-1.8 micrometer (tree mode) region are used in the following PFA. Thus, the data matrix is a 25-row (sites) by 32-column (spectral variables) matrix.

PRINCIPAL FACTOR MODEL

In PFA, observed responses in a data matrix are modeled as an optimized linear combination of n cofactors. For AIS data:

$$d(i,j) = \sum_{k=1}^{n} r(i,k) \times c(k,j); \quad i=1,2, \ldots ,rows; \quad j=1,2, \ldots ,columns.$$

where $d(i,j)$ is the response of the ith site in the jth channel. A matrix row contains the spectra from one of r sites and a column contains the spectral response in one of c channels over all sites. Because of the variance optimizing design of PFA only n independent factors will be needed to approximate the data matrix. In matrix notation:

$$[D''] = R(1)*C(1) + R(2)*C(2) + \ldots +R(n)*C(n) = [R'']*[C''] \qquad (1)$$

where " denotes the n-factor approximation and * defines an outer product. The cofactor $R(i)$ is generated by projecting each row in the original data matrix, [D], onto the eigenvector associated with the ith eigenvalue (ordered largest to smallest) computed from the covariance matrix $Z (=[D]^T[D])$. The cofactor $C(i)$ is the ith column eigenvector transposed. Thus,

$$[R''] = [D][Q'']; \quad [C''] = [Q'']^T; \quad \text{and} \quad [D''] = [R''][C'']$$

where columns of $[Q'']$ contain eigenvectors corresponding to the n largest eigenvalues of $[Z]$. The designations R and C are used to emphasize that the R cofactors are associated with the <u>row</u> (site) variance, and the C cofactors are associated with the <u>column</u> (spectral channel) variance. No centering or standardization was applied prior to forming the covariance matrix. Consequently, the R and C cofactors are based on a "covariance about the origin" (a CO matrix) which also is called a scatter matrix.

Measures for estimating n proposed by Malinowski (1977a; 1977b) have been used previously for site-spectra matrices (Murray 1983). The approximation [D''] is the matrix sum of R(i)*C(i) cofactors [Equation (1)]. When n matrices have been summed, the remaining (c-n) matrices (assuming r > c) will only add random error. Determining n exactly requires a distribution of random measurement error rarely, if ever, found in real data. Nevertheless, the estimates are useful and easily computed.

RESULTS

In Figure 4, Malinowski's Indicator function is shown for the 25-site by 32-channel AIS data and, for comparison, the responses for two matrices with known characteristics (Malinowski 1977b; data sets A and C). For a well-behaved error distribution the Indicator function
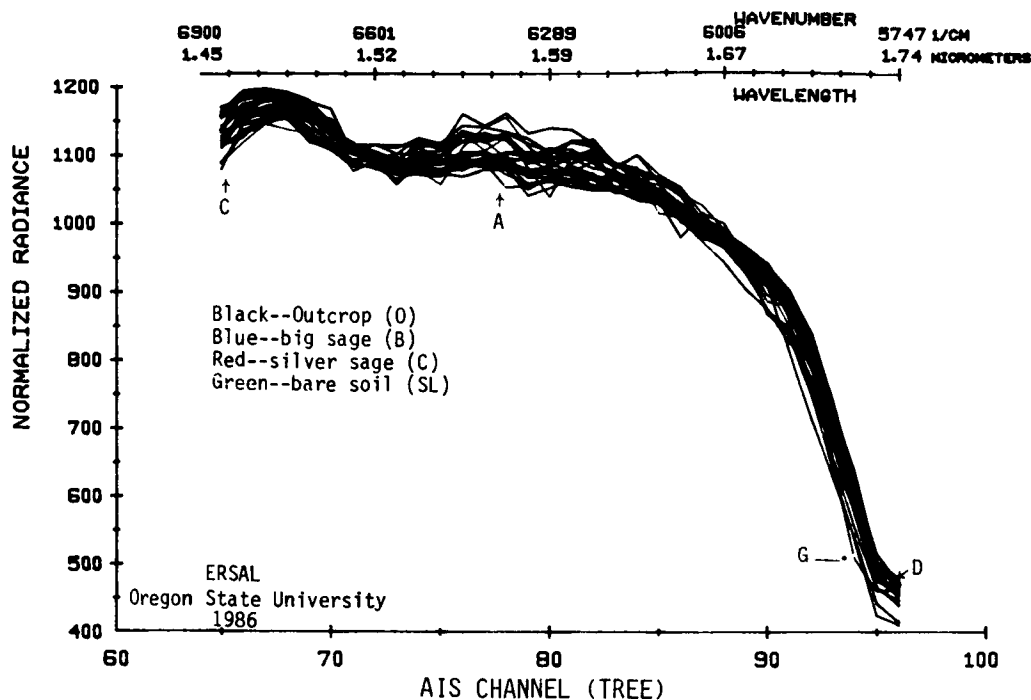
Figure 2. Equal-area normalized spectra for Papoose Lake sites. Wavelength and wavenumber scales are approximate. (See color slide number 11 in the back cover pocket of this publication.)
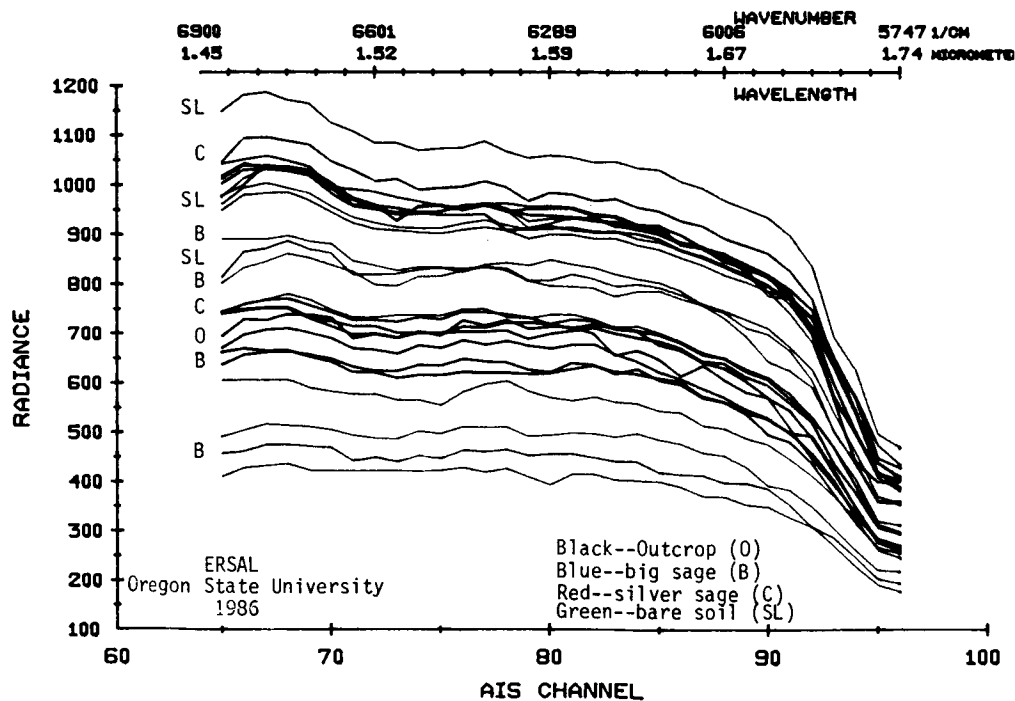

Figure 3. Original spectra for Papoose Lake sites. Letters indicate general position of ground classes. Wavelength and wavenumber scales are approximate. (See color slide number 12 in the back cover pocket of this publication.)

190

has a minimum at the correct n value. In the matrix of random numbers only locally equal amounts of random variation are added with each factor, and the error minimum occurs with the first factor. For AIS data, the broad minimum implies unique factors for a single site or a single channel, or large, isolated measurement errors, or all three. For smaller eigenvalues, real factors are mixed with a singular factor, and always with some error.

The combined R1*C1 and R2*C2 approximations account for the major differences in site radiance and in canopy characteristics. In Figure 5, the R1 and R2 cofactors indicate separation between classes is good. Re-examination of photographs indicates class overlap results as much from inexact site location and description as from spectral confusion. Based on the R3 plot, site 12 has a spectral response differing significantly from the other silver sage sites. Also, cofactor R8 has a strong pattern of variance associated with individual sites rather than with classes.

Figure 6 is a plot of cofactors C1 and C2 with two additional C3 values for channels 93 and 94. Because the square of an eigenvalue component comprising a C cofactor is directly proportional to the spectral variance spanned by the vector, Figure 6 depicts spectral discrimination by channel where channels near the origin contain little discriminating power. Of the three clusters located away from the origin, cluster 1 (channels 74 to 84) best discriminates the real differences between classes. Clusters 2 and 3 are associated with erroneous values caused by grating position changes (channels 65,66,95,96) and atmospheric absorption peaks (88-94). For these latter channels, error is the superimposition of inexact radiance values and possibly wavelength ranges on a sharply dropping wing of a water absorption peak. In particular, the occurrence of dead cell nearest-neighbor interpolation in channels 93 and 94 generates severe bias in the averaged site spectral curve. As an example, 40 percent of the variance spanned by C3 is associated with channels 93 and 94, indicating the R3*C3 product (cf. Fig. 4) is accounting primarily for the errors caused by the dead cells in site 12 data. In Figure 2 the curve for site 12 is the left-most trace in region G, but the other traces for silver sage sites are to the extreme right.

In Figure 7 a similar result is shown for channel 65 which accounts for 39 percent of C5 variance. For channels 65 and 66 not only do dead cells bias the spectral curves, but also there apparently is a skidding effect of grating change: the response often is flat for the first two or three channels. The C5 cofactor heavily weights the channel 65 site responses in order to differentiate the flat curves and the otherwise increasing radiance response (Fig. 2).

Additional analysis of real and error interactions in the first nine principal factors indicates that in factors three through six, a pattern of real factor and error mixing occurs, and factors numbered greater than six are the result of noise in the AIS data. For example, the R8*C8 matrix adds mostly small random adjustments to the individual sites (Figs. 5 and 7). Six factors produce a better representation of real site-spectra responses and are acceptable if the influence of errors are recognized. The first two factors will separate the four major cover classes. Additional between-class and within-class differences are associated with the real parts of factors three through six.
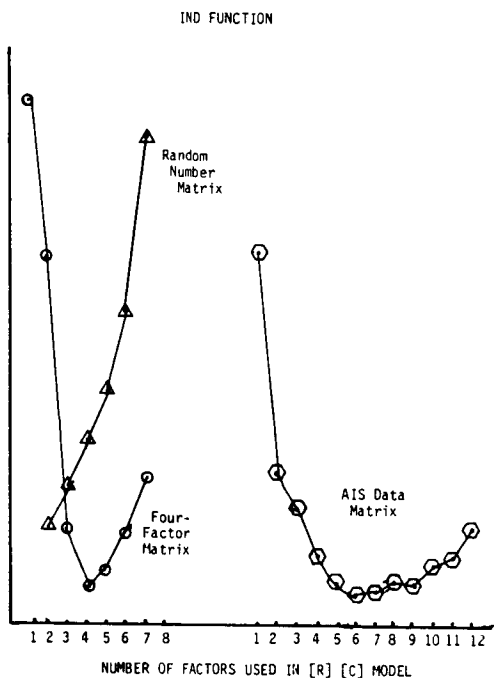
Figure 4. Indicator function responses. Indicator values are proportionally correct but with different scales. Four factor and random matrices are from Malinowski (1977b).
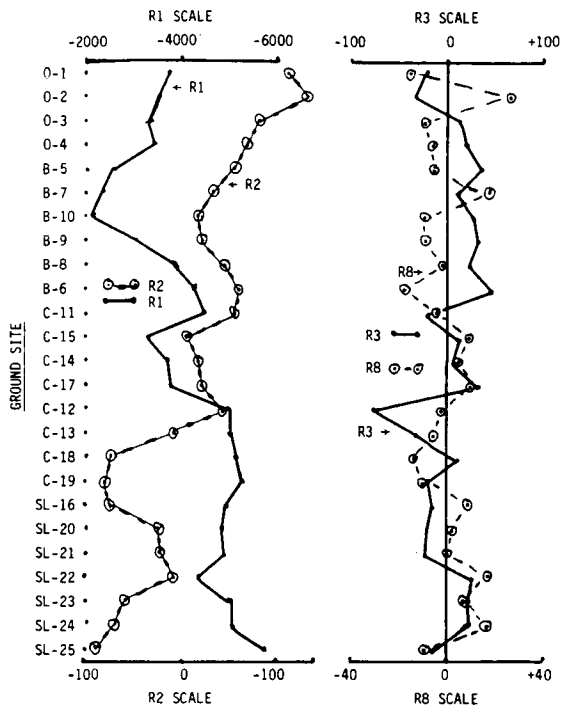
Figure 5. Variation of selected R cofactors by site. The arbitrarily scaled ordinate designates the class (0=rock outcrop; B=big sage; C=silver sage; SL=soil) and site number. Note scale changes for R's.
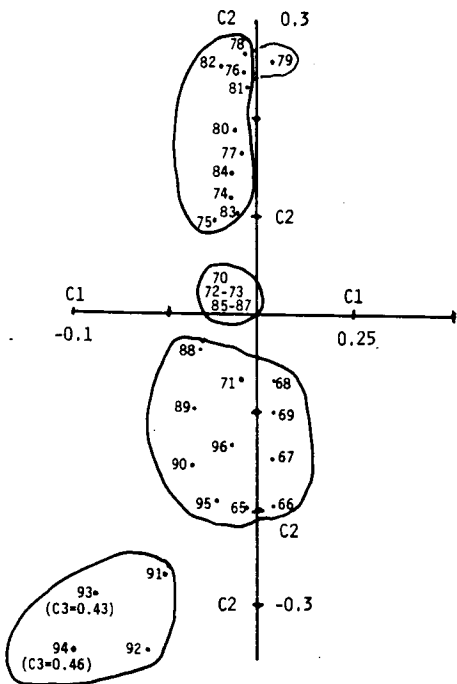
Figure 6. Distribution of spectral channel weights from column factors C1, C2, and C3. The channel number denotes the position in the C1, C2, or C3 plane. Shown in parentheses are the C3 values for channels 93 and 94.
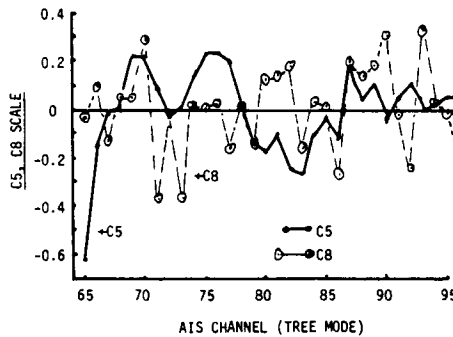
Figure 7. Responses of cofactors C5 and C8 for 32-site data.

CONCLUSIONS

This preliminary study used a limited data set; nevertheless, the results appear valid for other sites and other AIS spectral regions. Therefore the following results are expected:

1. In spite of variable scene radiance, valuable information can be extracted from the raw values (DNs). Note that this information is lost in equal-area normalization (Figs. 2 and 3).

2. Spectral selectivity is concentrated in a small number of wavelength bands (Fig. 2, region A). Identification of appropriate channels will reduce computational requirements and facilitate interpretation, including the assignment of spectral characteristics to basic physical properties and chemical structure.

3. AIS channels at starting and stopping grating positions contain excessive noise and should not be included in most analyses (Fig. 2, regions E and D).

4. Measurements on the shoulders of strong absorbance peaks should be examined with healthy skepticism. In particular, dead cell interpolation can severely bias responses for a specific channel if pixel spectra are averaged (Fig. 2, region G).

5. Because of real factor and error mixing, fine spectral details (e.g., peak wavelength shifts, changes in slope) will require extensive corrections, assumptions, and ancillary data. In the end, the results still may be suspect.

6. Imaging spectrometer data contains more information than that of broad-band sensors. Using only the first-order spectral responses of AIS data will provide more spectral selectivity and subsequent site discrimination of vegetated surface features than previous systems.

REFERENCES

AIS 1985. Airborne Imaging Spectrometer: Science Investigator Guide, Jet Propulsion Laboratory, Pasadena, CA, Appendix III, p. 2-4.

Malinowski, E.R. 1977a. Theory of error in factor analysis, Analytical Chemistry, Vol. 49, 606-612.

Malinowski, E.R. 1977b. Determination of the number of factors and experiential error in a data matrix, Analytical Chemistry, Vol. 49, 612-617.

Murray, R. 1983. Abstract Factor Analysis of multispectral data, Proc. Internat. Conf. Renewable Resource Inventories for Monitoring Change and Trends, 15-19 August 1983, Corvallis, Oregon, 348-252. (College of Forestry, Oregon State University, Corvallis, OR)

APPENDIX 1

ATTENDEES OF THE
SECOND AIS DATA ANALYSIS WORKSHOP

MAY 6–8, 1986

	Name	Representing
1	Abbott, Elsa	JPL
2	Abrams, Michael	JPL
3	Adams, Steven	JPL
4	Albee, Arden	California Institute of Technology
5	Anderson, Jim	NASA/NSTL
6	Arvidson, Ray	Washington University
7	Balick, Lee	EG & G Energy Measurements Inc.
8	Banninger, Cliff	Research Center Joanneum, Austria
9	Barge, Lisa	JPL
10	Bolef, Larry	University of Colorado
11	Cimino, JoBea	JPL
12	Cocks, Terry	CSIRO, North Ryde, Australia
13	Conel, Jim	JPL
14	Cox, Bill	Autometric
15	Curlander, John	JPL
16	Curtiss, Brian	California Institute of Technology
17	Eliason, Patricia	University of Colorado
18	Elvidge, Chris	JPL
19	Evans, Carla S.	University of Maryland
20	Evans, Diane	JPL
21	Feldman, Sandra C.	University of Nevada, Reno
22	Gerstl, Sigfried	Los Alamos National Lab
23	Goetz, Alexander	University of Colorado
24	Green, Glen	Washington University
25	Green, Robert O.	Unocal, International Division
26	Hayashi, Joan	University of Hawaii
27	Herring, Mark	JPL
28	Heyada, Jan	JPL
29	Hlavka, Chris	Ames Reseach Center
30	Hoffer, Roger M.	Purdue University
31	Hollinger, Allan	Moniteq Ltd., Canada
32	Hoover, Gordon	JPL
33	Hunt, Gavin A.	Open University, United Kingdom
34	Huntington, Jon	CSIRO, North Ryde, Australia
35	Hutsinpiller, Amy	University of Nevada, Reno
36	Kahle, Anne	JPL
37	Klemas, Vic	University of Delaware
38	Koch, Barbara	University of Munich
39	Kohno, Itoshi	ERSDAC, Japan

	Name	Representing
40	Kowalick, William S.	Chevron Oil Field Reseach Co.
41	Krohn, Dennis	USGS, Reston
42	Kruse, Fred	USGS, Denver
43	Lang, Harold	JPL
44	Lawrence, Geoff	BP Petroleum Development Ltd, England
45	Lee, James	BHP Central Research Lab, Australia
46	Lee, Meemong	JPL
47	LeVine, Catherine	JPL
48	Lozano, Fabian	Purdue University
49	Lyon, Ron J. P.	Stanford University
50	Mahoney, Colin	JPL
51	Martin, Miki	JPL
52	Matson, Dennis	JPL
53	Maughan, Paul M.	Space Development Systems
54	Miller, Edward A.	JPL
55	Milne, Tony	University of New South Wales, Australia
56	Milton, Nancy	USGS, Reston
57	Molinari, Lou F.	JPL
58	Mouat, David	University of Nevada, Reno
59	Mouginis-Mark, Pete	NASA Code EEL
60	Munday, Tim J.	University of Durham, England
61	Murray, RJay	Oregon State University
62	Mustard, John	Brown University
63	Norris, Dave	JPL
64	Ocampo, Adriana C.	JPL
65	Paley, Helen	JPL
66	Palluconi, Frank D.	JPL
67	Paylor, Earnest D.	JPL
68	Pieters, Carle M.	Brown University
69	Prelat, Alfredo	Unocal, Reseach Division
70	Press, Harry	JPL
71	Rand, Robert	USAETL
72	Reimer, John	JPL
73	Ridd, Merrill	University of Utah
74	Riggs, George A.	University of Montana
75	Roberts, Dar	Stanford University
76	Rock, Barry	JPL
77	Running, Steven W.	University of Montana
78	Ruzek, Martin	JPL

	Name	Representing
79	Samson, Scott A.	University of Nebraska, Lincoln
80	Satterwhite, Melvin	USAETL-RI
81	Schultz, Stan	JPL
82	Slater, Philip	University of Arizona
83	Sleigh, Bill	JPL
84	Solomon, Jerry	JPL
85	Spanner, Michael	Ames Research Center
86	Staenz, Karl	University of Zurich-Irchel
87	Stanich, Chuck	Daedalus Enterprises
88	Strahler, Alan	Hunter College
89	Taranik, James V.	University of Nevada, Reno
90	Tucker, Deanne	JPL
91	Ustin, Susan	University of California, Berkeley
92	Vane, Gregg	JPL
93	Vural, Kadri	Rockwell International Science Center
94	Walker, Richard	JPL
95	Walsh, Jerry	Great Falls, Virginia
96	Wickland, Diane E.	NASA Code EEL
97	Wood, Byron	Ames Reseach Center
98	Zak, Alex	JPL
99	Zall, Linda	Bethesda, Maryland
100	Zamudio, Joe	University of Colorado

APPENDIX 2

AGENDA OF THE
SECOND AIS DATA ANALYSIS WORKSHOP

MAY 6-8, 1986

The Second Airborne Imaging Spectrometer

Data Analysis Workshop

May 6, 7, and 8, 1986

Building 167 Conference Room
Jet Propulsion Laboratory
Pasadena, California

AGENDA

TUESDAY, MAY 6

8:00   Shuttle Bus Leaves Holiday Inn for JPL

8:30   Registration at JPL Visitor Control Center

9:00   WELCOMING REMARKS: Moustafa Chahine, JPL Chief Scientist

9:15   THE NASA HEADQUARTERS PERSPECTIVE ON IMAGING
        SPECTROMETRY: Diane Wickland, NASA Terrestrial Ecosystems
        Program Manager

9:30   THE SISEX/HIRIS PROJECT: OVERVIEW AND STATUS: Alex Goetz,
        University of Colorado

10:00   AVIRIS STATUS UPDATE: Gregg Vane, JPL

10:30   **BREAK**

11:00   AIS OPERATIONS IN 1985 AND PLANS FOR 1986: Gregg Vane, JPL

11:30   AIS DATA HANDLING AND ANALYSIS: Jerry Solomon, JPL

12:00   **LUNCH**

SESSION: CALIBRATION, THE ATMOSPHERE, DATA PROBLEMS AND TECHNIQUES

1:00   RADIOMETRIC CALIBRATION OF THE AIRBORNE IMAGING
        SPECTROMETER: Deanne Tucker and Gregg Vane, JPL

1:30   COMPARISON OF VARIOUS TECHNIQUES FOR CALIBRATION OF
        AIS DATA: Dar A. Roberts, Stanford University, Yasushi Yamaguchi,
        Geological Survey of Japan, and Ronald J. P. Lyon, Stanford University

2:00	ANALYSIS OF AIS RADIOMETRY WITH EMPHASIS ON DETERMINATION ATMOSPHERIC PROPERTIES AND SURFACE REFLECTANCE: J. E. Conel, S. Adams, R. E. Alley, G. Hoover, and S. Schultz, JPL
2:30	**BREAK**
3:00	AIRBORNE SPECTRORADIOMETRY: THE APPLICATION OF AIS DATA TO DETECTING OF SUBTLE MINERAL ABSORPTION FEATURES: Terry D. Cocks and Andy A. Green, CSIRO, Australia
3:30	ATMOSPHERIC WATER ABSORPTION FEATURES NEAR 2.2 um AND THEIR IMPORTANCE IN HIGH SPECTRAL RESOLUTION REMOTE SENSING: Fred A. Kruse and Roger N. Clark, USGS, Denver
4:00	LINEAR TRANSFORMS AND IMAGING SPECTROMETRY ANALYSIS: Jerry Solomon, JPL
4:30	DESTRIPING AIS DATA USING FOURIER FILTERING TECHNIQUES: Chris Hlavka, NASA/Ames Research Center
5:15	Shuttle Bus Returns to Holiday Inn
6:00	Workshop Reception at the Holiday Inn

WEDNESDAY, MAY 7

8:00	Shuttle Bus Leaves Holiday Inn for JPL

SESSION: GEOLOGICAL RESEARCH

9:00	ABUNDANCE AND DISTRIBUTION OF MINERAL COMPONENTS ASSOCIATED WITH MOSES ROCK (KIMBERLITE) DIATREME: John F. Mustard and Carle M. Pieters, Brown University
9:30	COMPARISON OF THE 1984 AND 1985 AIS DATA OVER THE SINGATSE RANGE (YERINGTON), NEVADA: R. J. P. Lyon, Stanford University
10:00	IDENTIFICATION OF HYDROTHERMAL ALTERATION ASSEMBLAGES USING AIRBORNE IMAGING SPECTROMETER DATA: Sandra C. Feldman and James V. Taranik, University of Nevada-Reno
10:30	**BREAK**
11:00	DETECTION OF HYDROTHERMAL ALTERATION AT VIRGINIA CITY, NEVADA, USING AIRBORNE IMAGING SPECTROMETRY: Amy Hutsinpiller and James V. Taranik, University of Nevada-Reno

SESSION: BOTANICAL AND GEOBOTANICAL RESEARCH

11:30   ANALYSIS OF AIS DATA OF THE BONANZA CREEK EXPERIMENTAL
          FOREST, ALASKA: Michael A. Spanner and David L. Peterson,
          NASA/Ames Research Center

12:00   **LUNCH**

1:00   SOIL TYPES AND FOREST CANOPY STRUCTURES IN SOUTHERN
          MISSOURI: A FIRST LOOK WITH AIS DATA: Glen M. Green and
          Raymond E. Arvidson, Washington University

1:30   GEOBOTANICAL STUDIES AT PILOT MOUNTAIN, NORTH CAROLINA,
          USING THE AIRBORNE IMAGING SPECTROMETER: N. M. Milton, P. A.
          Walsh, and T. L. Purdy, U. S. Geological Survey, Reston

2:00   TRACE ELEMENT-INDUCED STRESS IN FRESHWATER WETLAND
          VEGETATION: PRELIMINARY RESULTS: Byron L. Wood, NASA/Ames
          Research Center, and Louisa H. Beck, University of California - Berkeley

2:30   **BREAK**

3:00   PRELIMINARY ANALYSIS OF FLUORESCENCE LINE IMAGER (FLI)
          DATA ACQUIRED FOR FOREST DECLINE SITES IN VERMONT: Barry
          Rock, JPL

3:30   PATTERNS OF VEGETATION IN THE OWENS VALLEY, CALIFORNIA:
          Susan L. Ustin, University of California - Berkeley and University of
          California - Davis, Barrett N. Rock, JPL, and Roy A. Woodward, University
          of California - Berkeley and University of California - Davis

4:00   FURTHER OBSERVATIONS ON THE SUCCESS OF AIS DATA FOR THE
          GEOBOTANICAL DISCRIMINATION OF ROCK TYPES IN SOUTHWEST
          OREGON: David Mouat, University of Nevada

4:30   AIS SPECTRA OF DESERT SHRUB CANOPIES: RJay Murray, Milne
          Computer Center, Dennis L. Isaacson,William J. Ripple, Barry J. Schrumpf
          and Anthony J. Lewis, Oregon State University

5:15   Shuttle Bus Returns to Holiday Inn

THURSDAY, MAY 8

8:00   Shuttle Bus Leaves Holiday Inn for JPL

SESSION: GEOLOGICAL RESEARCH (RESUMED)

9:00 DELINEATION OF SOIL BOUNDARIES IN CENTRAL NEBRASKA: Scott Samson, University of Nebraska

9:30 PRELIMINARY GEOLOGICAL ANALYSIS OF AIS DATA AT MARY KATHLEEN, QUEENSLAND, AUSTRALIA: Jon F. Huntington, Andy A. Green, Maurice D. Craig and Terry D. Cocks, CSIRO, Australia

10:00 USE OF DIGITAL MUNSELL COLOR SPACE TO ASSIST INTERPRE-TATION OF IMAGING SPECTROMETRY DATA: GEOLOGIC EXAMPLES FROM THE NORTHERN GRAPEVINE MOUNTAINS, CALIFORNIA AND NEVADA: Fred A. Kruse, Daniel H. Knepper, Jr. and Roger N. Clark, USGS, Denver

10:30 **BREAK**

11:00 APPLICATION OF AIS DATA TO STRATIGRAPHIC STUDIES, WIND RIVER/BIGHORN BASIN, WYOMING: Harold Lang, Ernie Paylor, and Jim Conel, JPL

11:30 NEAR INFRARED DETECTION OF AMMONIUM MINERALS AT IVANHOE HOT SPRINGS, NEVADA: M. Dennis Krohn, USGS, Reston

12:00 **LUNCH**

1:00 SPAM Demonstrations at IPL

5:15 Shuttle Bus Returns to Holiday Inn

APPENDIX 3

CATALOG OF TEST SITES FLOWN WITH AIS
(FROM 12/82 THROUGH 4/86)

CATALOG OF TEST SITES FLOWN WITH AIS
(FROM 12/82 THROUGH 4/86)

DATE	SITE NAME	INVESTIGATOR
12/2/82	Mammoth, CA	Gillespie
	Long Valley, CA	Gillespie
	Mud Lake, NV	Goetz
to	Goldfield, NV	Goetz
	Cuprite, NV	Goetz
	Pico Anticline, CA	Rock
12/3/82	Mt. Pass, CA	Kahle
4/25/83	Mud Lake, NV	Goetz
	Cuprite, NV	Goetz
	Death Valley, CA	Kahle
	Mt. Pass, CA	Kahle
to	Silver Bell, AZ	Goetz
	Imperial Valley, CA	Rock
	Los River, W VA	Rock
	Klamath Forest, CA	Strahler
5/24/83	Josephine County, OR	Rock
8/5/83	Cuprite, NV	Goetz
	Boreal Forest, MN	Pitts
	Sleeping Bear Dunes, MI	Olson
	Saginaw Forest, MI	Olson
to	Konza Prairie, KS	Blad
	Lost River, W VA	Rock
	Washington N.F., VA	Labovitz
	Mineral, W VA	Labovitz
8/15/83	Klamath N. F., CA	Strahler
10/18/83	Slate Belt, NC	Wickland
10/20/83	Vermont, NH	Vogelmann
10/21/83	New Hampshire	Vogelmann
10/27/83	Virginia	Bell
10/27/83	Slate Belt, NC	Wickland
10/28/83	Virginia	Labovitz
10/28/83	Lost River, W VA	Rock
10/28/83	Virginia	Masuoka
10/30/83	Wind River, WY	Lang
4/25/84	Cuprite, NV	Goetz
4/25/84	Goldfield, NV	Adams
4/27/84	Death Valley, CA	Kahle
4/27/84	Jasper Ridge, CA	Mouat, Peterson
4/27/84	Stanford, CA	Mouat
5/05/84	Virginia	Bell

Date	Site Name	Investigator
5/05/84	Virginia	Masuoka
5/09/84	Slate Belt, NC	Wickland
5/11/84	Slate Belt, NC	Wickland
7/10/84	Cuprite, NV	Goetz
7/10/84	Owens Valley, CA	Rock
7/10/84	Death Valley, CA	Kahle
7/10/84	Sequoia, CA	Peterson
7/18/84	Boreal Forest, MN	Pitts, Star
7/19/84	Sleeping Bear, MI	Olson
7/20/84	Monument Valley, UT	Pieters
7/25/84	Ubehebe & Owlshead, NV	Raines
7/25/84	Hot Creek, NV	Feldman
7/25/84	Yerington, NV	Lyon
7/26/84	Oregon Transect	Peterson
7/26/84	Josephine Cty, OR	Mouat
7/26/84	Josephine Cty, OR	Gillespie
7/31/84	Stockton, CA	Wrigley
8/07/84	Sand Hill, NE	Blad
8/10/84	Purdue, IL	Vanderbilt
8/16/84	Delaware Bay, DL	Klemas
8/17/84	Vermont, NH	Rock-Vogelmann
9/07/84	Blackhawk Island, WI	Peterson
9/08/84	Vermont	Rock-Vogelmann
9/09/84	PowderRiver, WY	Dykstra, Segal
9/09/84	Wind River, WY	Lang
10/30/84	Owens Valley, CA	Rock, Ustin
10/30/84	Cuprite, NV	Goetz, Vane
10/31/84	Mono Lake, CA	Conel
10/31/84	Bridgeport Basin, CA	Gillespie
10/31/84	Sierra Nevada, CA	Gillespie
4/2/85	Owens Valley, CA	Rock, Ustin
4/2/85	Cuprite, NV	Goetz, Vane
5/22/85	Owens Valley, CA	Rock, Ustin
5/22/85	Jasper Ridge, CA	Mouat
5/23/85	Owens Valley, CA	Rock, Ustin
5/23/85	Cuprite, NV	Goetz, Vane
5/23/85	Grapevine, NV	Kruse
6/16/85	Cement, OK	Settle, McKeon
6/16/85	Sand Hills, NB	Blad

Date	Site Name	Investigator
6/18/85	Sand Hills, NB	Blad
7/2/85	Virginia Range, NV	Feldman
7/24/85	Ivanhoe, NV	Krohn
7/24/85	Carlin, NV	Podwysocki
7/25/85	Ruby Range, MT	Rowan
7/25/85	Little Falls, ID	Gillespie
7/26/85	Wind River, WY	Lang
7/27/85	Monument Valley, UT	Pieters
7/30/85	Marysvale, UT	Podwysocki
7/31/85	Lake City, CO	Lee
8/2/85	Ozark Mtns., MO	Arvidson
8/2/85	Purdue, IN	Vanderbilt
8/6/85	Blackhawk Island, WI	Peterson, Aber
8/9/85	Oak Ridge, TN	Balick
8/11/85	Pilot Mtn, NC	Milton
8/11/85	Ringwood, NC	Bell
8/12/85	Vermont	Rock
8/12//85	New Hampshire	Rock
8/13/85	Virginia	Masuoka
8/13/85	Central Virginia	Bell
8/23/85	Bonanza, Alaska	Peterson
8/28/85	Bonanza, Alaska	Peterson
8/28/85	Poker Caribou, Alaska	Peterson
8/30/85	Oregon Transect, OR	Peterson
8/30/85	Squaw Butte, Oregon	Schrumpf
9/23/85	Gustine, CA	Peterson
9/23/85	Sequoia, CA	Peterson
9/23/85	Cuprite, CA	Vane
9/23/85	Mono Lake, CA	Conel
9/23/85	Yerington, NV	Lyon
9/23/85	Virginia Range, NV	Feldman

AUSTRALIA

Date	Site Name	Investigator
10/1/85	Temora	Laughton
10/1/85	Junction Creek	Logan
10/1/85	Dicks Creek	Gallaway
10/1/85	Yarralaw	Williams
10/1/85	Braidwood	Atkinson
10/1/85	Goulburn	Kalma
10/2/85	Wycanna	Jupp
10/2/85	Inverell	Atkinson

Date	Site Name	Investigator
10/3/85	Puckapunyal	Morgan
10/3/85	Adelaide	Douglas
10/7/85	Loxton	Douglas
10/7/85	Broken Hill	O'Sullivan
10/7/85	Fowlers Gap	Milne
10/7/85	Wilkawillina	Huntington
10/7/85	Pine Creek	Hussey
10/8/85	Cascades	Houghton
10/8/85	Norseman	Burgess
10/8/85	St. Ives	Simpson
10/8/85	Yindarlgooda	Burgess
10/10/85	Murrin Murrin	Huntington
10/10/85	Agnew	Gregory
10/10/85	Skull Creek	Burgess
10/11/85	Dangin	Hick
10/11/85	York	Hick
10/11/85	Yalanbee	Hick
10/11/85	Dwellingup	Houghton
10/14/84	Jillawarra	Huntington
10/14/85	Port Hedland	Morgan
10/15/85	Sundown	Williams
10/15/85	Blina	Williams
10/15/85	Halls Creek	Otani
10/15/85	Ellendale B	O'Sullivan
10/15/85	Ellendale A	O'Sullivan
10/16/85	Munni Munni	Simpson
10/16/85	Coppins Gap	Huntington
10/16/85	Broadhurst	Swarbrick
10/19/85	Mount Isa	Simpson
10/19/85	Mary Kathleen	Huntington
10/19/85	Gorge Creek	Simpson
10/19/85	Phosphate Hill	Simpson
10/21/85	Palm Valley	Simpson
10/21/85	Stairway	Simpson
10/21/85	Allambi-Amadeus	Taylor
10/21/85	Riddock-Mordor	Horsfall
10/21/85	Hatches Creek	Horsfall

Date	Site Name	Investigator
10/22/85	Kidston	Logan
10/22/85	Bald Mountain	Gabell
10/22/85	Newcastle Range	Maffi
10/22/85	Chillagoe	Otani
10/22/85	Cairns	Kelly
10/24/85	Townsville	Morgan
10/24/85	Burdekin River	Pearce
10/26/85	Mt. Leyshon	Fraser
10/26/85	Burdekin River	Pearce
10/26/85	Bimurra	Maffi
10/26/85	Plateau	Munday/Swarbrick
10/26/85	Newcastle Range	Maffi
10/28/85	Mt. Leyshon	Fraser
10/28/85	Gregory	Gray
11/1/85	Hawaii	Kahle
11/2/85	Hawaii	Kahle
11/3/85	Hawaii	Kahle
11/7/85	Hawaii	Kahle
11/9/85	Kahoolawe, Hawaii	Elliot

APPENDIX 4

LIST OF SLIDES AND FIGURE TITLES

Slide No.

1. Cocks and Green, AIRBORNE SPECTRORADIOMETRY: THE APPLICATION
    OF AIS DATA TO DETECTING SUBTLE MINERAL ABSORPTION FEATURES
    (Figure 2, page 58) AIS Imagery in bands 11 and 29, showing
    horizontal striping.

2. Cocks and Green
    (Figure 5, page 60) Density-sliced radiance and log. residual
    spectra for a variety of processing conditions.

3. Mustard and Pieters, ABUNDANCE AND DISTRIBUTION OF MINERAL
    COMPONENTS ASSOCIATED WITH MOSES ROCK (KIMBERLITE) DIATREME
    (Figure 6, page 85) Deconvolution of AIS spectra into mineral
    abundance images (F-parameter for endmembers).

4. Mustard and Pieters
    (Figure 7, page 85) Deconvolution of AIS spectra into mineral
    abundance images (F-parameter for endmembers).

5. Huntington, Green, Craig, and Cocks
    PRELIMINARY GEOLOGICAL INVESTIGATION OF AIS DATA AT MARY
    KATHLEEN, QUEENSLAND, AUSTRALIA
    (Figure 10, page 128) Detail of "fanned" log residuals for the
    1.96 -2.4 micrometre window illustrating the CO2 bands at 2.00
    and 2.06 micrometres, and broad, intense absorption features
    at 2.28 micrometres (for example, between lines 667 and 943).

6. Kruse, Knepper, and Clark
    USE OF DIGITAL MUNSELL COLOR SPACE TO ASSIST INTERPRETATION
    OF IMAGING SPECTROMETER DATA--GEOLOGIC EXAMPLES FROM THE
    NORTHERN GRAPEVINE MOUNTAINS, CALIFORNIA AND NEVADA
    (Figure 3, page 135) Thematic mineralogical images (note that
    these images consist of two 32-pixel flightlines concatenated to
    form a single 64-pixel-wide image) and thematic map interpreted
    from the image and individual spectra. A, Overlay of pixels
    identified as carbonates (white) on a single band image;
    B, overlay of pixels identified as clay (white) on a single
    band image; C, Map interpreted from images A and B and
    individual spectra.

211

7.   Green and Arvidson
SOIL TYPES AND FOREST CANOPY STRUCTURES IN SOUTHERN
MISSOURI: A FIRST LOOK WITH AIS DATA
(Figure 2A, page 154) August, 1982, TM band 4 images of the
eastern half of the Rolla Quadrangle.

8.   Green and Arvidson
(Figure 3, page 156) August, 1985 band 4 image of the detailed
study area. (~25km wide) The white line marks the
AIS flightline.

9.   Ustin, Rock, and Woodward
PATTERNS OF VEGETATION IN THE OWENS VALLEY, CALIFORNIA
(Figure 2, page 182) Above, a 3-color composite of the scene in
Figure 1, after removal of most vertical striping. Below, the
8-band maximum likelihood classification map.

10.   Ustin, Rock, and Woodward
(Figure 4, page 184) Alluvial fan region depicting an
unsupervised 8-band maximum likelihood classification map before
destriping (top), a 3-band color composite (middle) after
removal of vertical striping, and the maximum likelihood
classification of the region before destriping (middle) and
after destriping (bottom).

11.   Murray, Isaacson, Schrumpf, Ripple, and Lewis
AIS SPECTRA OF DESERT SHRUB CANOPIES
(Figure 2, page 190) Equal-area normalized spectra for Papoose
Lake sites. Wavelength and wavenumber scales are approximate.

12.   Murray, Isaacson, Schrumpf, Ripple, and Lewis
(Figure 3, page 190) Original spectra for Papoose Lake sites.
Letters indicate general position of ground classes. Wavelength
and wavenumber scales are approximate.